# BULLETIN OF RUSSIAN STATE MEDICAL UNIVERSITY

## BIOMEDICAL JOURNAL OF PIROGOV RUSSIAN NATIONAL RESEARCH MEDICAL UNIVERSITY

Indexed in Scopus. CiteScore 2021: 0.5

Indexed in WoS. JCR 2021: 0.5

Five-year h-index is 8

**Scopus®**

**WEB OF SCIENCE™**

**Google** scholar

SCImago Journal & Country Rank 2020: 0.14

Listed in HAC 31.01.2020 (№ 507)

Open access to archive

**SJR**
Scimago Journal & Country Rank

ВЫСШАЯ АТТЕСТАЦИОННАЯ КОМИССИЯ (ВАК)

**CYBERLENINKA**

# ВЕСТНИК РОССИЙСКОГО ГОСУДАРСТВЕННОГО МЕДИЦИНСКОГО УНИВЕРСИТЕТА

## НАУЧНЫЙ МЕДИЦИНСКИЙ ЖУРНАЛ РНИМУ ИМ. Н. И. ПИРОГОВА

# BULLETIN OF RSMU   3, 2022

ВЕСТНИК РГМУ

## Contents
Содержание

# INLB PROTEIN SECRETED BY *LISTERIA MONOCYTOGENES* CONTROLS THE PATHOGEN INTERACTION WITH MACROPHAGES

Chalenko YM[1]✉, Abdulkadieva MM[2], Safarova PV[1,3], Kalinin EV[1], Slonova DA[4], Ermolaeva SA[1]

[1] Gamaleya Research Center of Epidemiology and Microbiology, Moscow, Russia

[2] Joint Institute for High Temperatures, Moscow, Russia

[3] Pirogov Russian National Research Medical University, Moscow, Russia

[4] Skolkovo Institute of Science and Technology, Moscow, Russia

The virulence of gram-positive bacterium *Listeria monocytogenes* depends on its capacity to infect non-professional phagocytes and proliferate inside them. *Listerias monocytogenes* captured by mononuclear phagocytic cells during the infectious process are resistant to lysosomal digestion and can proliferate inside macrophages. Internalin B (InlB), one of the key pathogenicity factors of *L. monocytogenes*, interacts with mammalian receptors c-Met and gC1q-R. For epithelial cells, such interactions with surface receptors promote activation of these receptors and cytoskeletal remodeling, which leads to massive bacterial invasion into non-professional phagocytes. For macrophages, by contrast, nothing is known about the role of InlB in their interactions with *L. monocytogenes* apart from the fact that both receptors are abundantly expressed by macrophages and participate in the determination of immune reactions. This study aimed at determination of the potential role of InlB in the interactions between *L. monocytogenes* and macrophages. We found that 1) InlB expression promoted a significant 3.5-fold increase in the rates of *L. monocytogenes* capture by macrophages; 2) the 24 h fold increase in bacterial number inside macrophages constituted $182.5 \pm 16.7$, $96 \pm 12$ and $13.3 \pm 3$ for EGDeΔinlB, EGDe and EGDeΔinlB::pInlB strains, respectively; 3) the EGDeΔinlB::pInlB strain, complemented with a plasmid copy of *inlB*, produced InlB at 3.3-fold higher rates than the type strain EGDe. We conclude that InlB negatively affects the survival of listeria inside macrophages. The results enable advanced understanding of the host-pathogen interactions for *L. monocytogenes*.

**Keywords:** listeriosis, *Listeria monocytogenes*, internalin B, innate immunity, human macrophages

✉ **Correspondence should be addressed:** Yaroslava M. Chalenko
Gamaleya, 18, Moscow, 123098, Russia; yaroslavazaka@yandex.ru

# БЕЛОК INLB, СЕКРЕТИРУЕМЫЙ *LISTERIA MONOCYTOGENES*, КОНТРОЛИРУЕТ ВЗАИМОДЕЙСТВИЕ ВОЗБУДИТЕЛЯ С МАКРОФАГАМИ

Я. М. Чаленко[1]✉, М. М. Абдулкадиева[2], П. В. Сафарова[1,3], Е. В. Калинин[1], Д. А. Слонова[4], С. А. Ермолаева[1]

[1] Национальный исследовательский центр эпидемиологии и микробиологии имени Н. Ф. Гамалеи, Москва, Россия

[2] Объединенный институт высоких температур, Москва, Россия

[3] Российский национальный исследовательский медицинский университет имени Н. И. Пирогова, Москва, Россия

[4] Автономная некоммерческая образовательная организация высшего профессионального образования «Сколковский институт науки и технологий», Москва, Россия

Способность инфицировать и размножаться в непрофессиональных фагоцитах лежит в основе вирулентности грамположительной бактерии *Listeria monocytogenes*. В процессе протекания инфекции захваченные клетками системы мононуклеарных фагоцитов листерии устойчивы к перевариванию и могут размножаться внутри макрофагов. Один из ключевых факторов патогенности *L. monocytogenes* белок интерналин В (InlB) взаимодействует с рецепторами клеток млекопитающих c-Met и gC1qR. При его взаимодействии с рецепторами, находящимися на поверхности эпителиальных клеток, происходит активация рецепторов, перестройки цитоскелета и, как результат, активная инвазия бактерий внутрь непрофессиональных фагоцитов. На сегодняшний день ничего неизвестно о влиянии InlB на взаимодействие *L. monocytogenes* с макрофагами, в то время как оба таргетных рецептора экспрессируются на поверхности макрофагов и вовлечены в развитие иммунных реакций. Целью работы было определить потенциальное влияние InlB на взаимодействие *L. monocytogenes* с макрофагами. Установлено, что 1) наличие InlB в 3,5 раза достоверно улучшает поглощение *L. monocytogenes* макрофагами; 2) через 24 ч штаммы EGDeΔinlB, EGDe и EGDeΔinlB::pInlB увеличили свою численность внутри макрофагов в $182,5 \pm 16,7$, $96 \pm 12$ и $13,3 \pm 3$ раз соответственно; 3) Штамм EGDeΔinlB::pInlB, комплементированный плазмидной копией гена *inlB,* продуцировал InlB в 3,3 раза лучше, чем штамм EGDe. Таким образом мы предполагаем, что InlB влияет на выживаемость листерий внутри макрофагов. Полученные результаты углубляют понимание процессов взаимодействия возбудителя с макрофагами.

**Ключевые слова:** листериоз, *Listeria monocytogenes*, интерналин В, врожденный иммунитет, макрофаги человека

✉ **Для корреспонденции:** Ярослава Михайловна Чаленко
ул. Гамалеи, д. 18, г. Москва, 123098, Россия; yaroslavazaka@yandex.ru

The earliest evidence on the existence of Listeria monocytogenes is dated back to 1926 and describes a lethal infection in rabbits accompanied by pronounced monocytosis [1]. The gram-positive bacterium *L. monocytogenes* causes listeriosis — a severe systemic disorder in animals and humans [2]. The main clinical symptoms of listeriosis in humans are sepsis, meningitis and meningoencephalitis [3]. Immune defense against *L. monocytogenes* is mainly ensured by innate and cellular adaptive immunity. The first-line effector cells are macrophages. Since *L. monocytogenes* is a facultative intracellular bacterium, it can survive the phagocytosis by mononuclear phagocytes and proliferate inside them.

The critical step in the infectious process is the invasion of *L. monocytogenes* into non professional phagocytes. This step is mediated by two cell surface proteins of *L. monocytogenes* — internalin A (InlA) and internalin B (InlB). The InlA protein is covalently bound to the bacterial surface, while its interaction with the host target protein E-cadherin mediates cytoskeletal remodeling and bacterial internalization [4]. The InlB protein exists in two forms: one of them is bacterial surface-bound and promotes active invasion of the bacteria into non-professional phagocytic cells; the second form (soluble) is thought to induce the non-specific activation of signaling pathways upon binding the target receptors. The functional role of soluble InlB is still uncertain. Eukaryotic proteins c-Met and gC1q-R have been identified as target receptors for InlB [5, 6]. c-Met is the high-affinity receptor for hepatocyte growth factor (HGF). c-Met activation triggers signaling pathways of cell proliferation and migration, as well as the control of immunity reactions in certain cell types [7]. c-Met is expressed by various epithelial cells and several immune cell lineages: macrophages, monocytes, dendritic cells and T cells [8]. c-Met has been also implicated in shifting macrophage polarization from M1 towards M2-like phenotypes [9].

The second target receptor of InlB is gC1q-R, a ubiquitously expressed protein initially identified as receptor for the globular heads of C1q [10] and subsequently characterized as a multifunctional protein interacting with a wide scope of ligands of endogenous and exogenous origin [11]. The InlB/gC1q-R binding facilitates the invasion of listeria into mammalian cells. Recent studies provide structural and functional details of InlB interactions with its receptors c-Met and gC1q-R and demonstrate the influence of these interactions on the phosphorylation dynamics of PI3K and MAPK signaling cascades in human epithelial cells [12–14]. Similarly with c-Met, gC1q-R is abundantly expressed on the surface of B lymphocytes and macrophages [15].

Thus, both mammalian receptors for InlB participate in multiple signaling pathways that mediate immune responses, which suggests a contribution of InlB to innate immunity through NF-κB activation and PI3K signaling in macrophages [16]. Indeed, the c-Met/InlB interaction enhanced the migratory capacity of certain immune cell lineages and positively regulated the production of pro-inflammatory cytokine IL6 by peritoneal dendritic cells [17]. However, no experimental evidence on the role of InlB in the interactions between *L. monocytogenes* and macrophages was published so far.

This study aimed to specify the functional role of InlB in the interactions of listeria with human macrophages.

METHODS

**Isolation of human macrophages from peripheral blood samples**

Human macrophages were differentiated from monocytes isolated from the mononuclear fraction of peripheral blood obtained from healthy donors. The isolation involved density gradient centrifugation with Ficoll-Paque Premium (HyClone; USA) followed by adhesion [18]. The monocytes were cultured at 37 °C and 5% $CO_2$ for 6 days in RPMI-1640 medium containing 2% inactivated human serum, 2 mM L-glutamine, 10 mM HEPES, 50 µM β- mercaptoethanol, 2 mM sodium piruvate and 2× MEM vitamin solution (HyClone; USA). On day 1, the medium was supplemented with GM-CSF to 50 ng/mL (SCI-Store; Russia). On day 4, the medium was replaced with a fresh portion and GM-CSF was added to 50 ng/mL. The cells were stained with fluorophore-conjugated primary antibodies to CD11b (APC-Cy7), CD80 (PE-Cy5), CD86 (BV421) and HLA-DR (PE-Cy7) and analyzed by flow cytometry (Beckman Coulter; USA).

**Bacterial strains and culture conditions**

The study used the following strains of *L. monocytogenes*: EGDe (type strain), EGDeΔinlB with chromosomal deletion of *inlB* and EGDeΔinlB::pInlB containing a plasmid copy of *inlB* complementing this deletion. The EGDeΔinlB strain was courtesy of Prof. J. Vazquez-Boland of the University of Edinburgh, UK. The InlB-encoding plasmid and the EGDeΔinlB::pInlB strain were described previously [14]. All strains of *L. monocytogenes* were grown in BHI broth (Becton, Dickinson and Company; USA) at 37 °C and 200 rpm continuous shaking. The strains transformed with InlB expression constructs (complemented) were grown with 10 µg/mL erythromycin in order to maintain the plasmid. To obtain infectious cultures, the bacteria were grown to the mid-logarithmic phase, ware washed three times with phosphate-buffered saline (PBS, Amresco; USA) and frozen in 100 µL aliquots in the presence of 10% glycerin (Sigma-Aldrich; USA).

**Assay of *L. monocytogenes* capture by macrophages**

The macrophages were grown in 24-well plates. The concentrations of bacterial cells in frozen cultures were determined by serial dilution method. The bacteria were added to the macrophages in growth medium at a MOI (multiplicity of infection) ratio of 1 : 100. After 1 h incubation at 37 °C and 5% $CO_2$ the cells were washed thrice with PBS and placed in DMEM (PanEco; Russia) containing 100 µg/mL gentamycin (Sigma-Aldrich; USA) to eliminate the extracellular bacteria. After 1 h incubation the cells were washed thoroughly with PBS to remove gentamycin and lysed with 1% Triton X-100 (Sigma-Aldrich; USA). The lysates were plated on BHI agar in serial dilutions. For the complemented strain, the solid medium was supplemented with 10 µg/mL erythromycin. The capture efficiency was evaluated by the ratio of the number of captured bacteria to the number of added bacteria.

**Assay of *L. monocytogenes* intracellular survival in macrophages**

After 1 h incubation at 37 °C and 5% $CO_2$ the cells were washed thrice with PBS and placed in DMEM (PanEco; Russia) containing 100 µg/mL gentamycin (Sigma-Aldrich; USA) to eliminate the extracellular bacteria. After 1 h incubation at the high gentamycin concentration the cells were washed and placed in fresh DMEM (PanEco; Russia) containing 20 µg/mL gentamycin (Sigma-Aldrich; USA) to prevent the survival of listerias outside macrophages. The plates were incubated for 24 h (since the start of infection) at 37 °C and 5% $CO_2$. The cells were then washed thrice with PBS) to remove gentamycin and
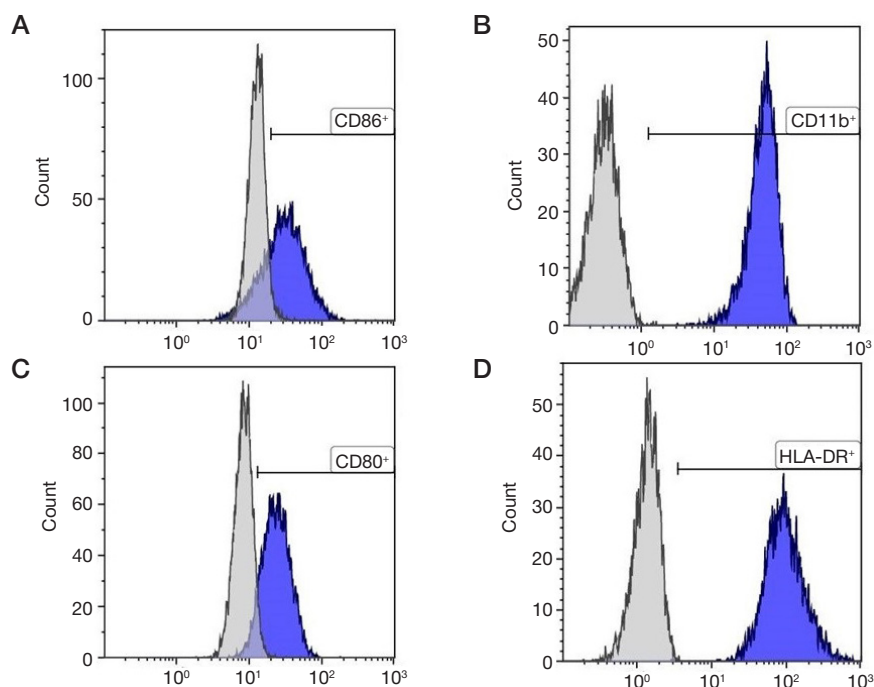
**Fig. 1.** Flow cytometry analysis of the macrophages obtained from peripheral blood monocytes of healthy donors. The macrophages were differentiated towards M1 phenotype; the plots show positivity for CD86 (**A**), CD11b (**B**), CD80 (**C**) and HLA-DR (**D**) markers

lysed by adding 100 μL of 1% Triton X-100. The lysates were subsequently diluted to 1 mL by adding 900 μL of PBS and plated on BHI agar in serial dilutions. For the complemented strain, the solid medium was supplemented with 10 μg/mL erythromycin. The survival efficiency was assessed by the ratio of the number of surviving bacteria to the number of introduced ELISA bacteria.

### Enzyme-linked immunosorbent assay (ELISA) test systems for InlB expression

The *L. monocytogenes* strains were grown in BHI for 18 h. The cells were separated from supernatant by centrifugation (4200 rpm, 15 min), washed thrice in PBS and resuspended in 500 μL of carbonate-bicarbonate buffer (pH 9.6). Cell surface expression levels for InlB were measured by direct ELISA. Briefly, a 96-well plate was loaded with sample aliquots, 100 μL per well, incubated overnight at +4 °C, washed with TTBS, three washes 250 μL each, filled with 200 μL of blocking buffer per well and incubated for 1 h at room temperature. The HRP-conjugated InlB-specific antibodies were used in 1 : 4000 dilution, 100 μL per well. After 1 h incubation at room temperature the wells were washed with TTBS, six washes 250 μL each, and the signal was developed with 100 μL of TMB (Thermo Fisher Scientific; USA) per well. The reactions were stopped by adding 100 μL of 2M $H_2SO_4$. The optical densities were measured at a wavelength of 450 nm on an iMark microplate absorbance reader (Bio-Rad; USA).

The levels of secreted InlB were measured by sandwich ELISA. Briefly, InlB-specific antibodies (4 μg/mL, diluted in carbonate-bicarbonate buffer pH 9.6) were added to fresh 96-well plate, 100 μL per well, and the plate was incubated overnight at +4 °C. The wells were washed with TTBS, three washes 250 μL each, filled with blocking buffer (2% BSA, 200 μL per well) and incubated for 1 h at room temperature. The blocking buffer was subsequently replaced with the sample and the plate was incubated for 1 h at room temperature. The wells were subsequently washed with TTBS, three washes 250 μL each, and the HRP-conjugated InlB-specific antibodies were added (1 : 4000, 100 μL per well). After 1 h incubation at room temperature the wells were washed with TTBS, six washes 250 μL each. The signal was developed with TMB (Thermo Fisher Scientific; USA), 100 μL per well; the reactions were stopped by adding 100 μL of 2M $H_2SO_4$. The optical densities were measured at 450 nm in iMark microplate absorbance reader (Bio-Rad; USA). The InlB concentration was determined with the use of calibration curve and recalculated for cell number in a sample.

### Statistical analysis

All experiments were carried out in three replicates and at least four repeats. The statistical analysis involved one-way ANOVA with post-hoc Tukey test (https://www.socscistatistics.com/tests/anova/default2.aspx). The differences were considered significant at $p < 0.05$ (see Supplementary 1 and 2).

RESULTS

### Characterization of differentiated macrophages

Macrophages play an important role in the innate immune responses and participate in stimulation of the immune effector cells differentiation. Macrophages are among the first cells to be infected and largely define the deployment of innate and adaptive immune reactions to *L. monocytogenes*. The macrophages differentiated from peripheral blood monocytes were analyzed by flow cytometry. The analysis revealed surface expression of CD11b, CD80, CD86 and HLA-DR markers characteristic of the pro-inflammatory M1 macrophage phenotypes [19] (Fig. 1). The cells contained large rounded nuclei with heterochromatin located beneath the nuclear membrane, formed numerous surface processes and were firmly adherent to the plastic (Fig. 2).

### Phagocytosis of *L. monocytogenes* by macrophages is InlB-dependent

The interaction of bacterial surface-bound InlB with c-Met expressed at the surface of non-professional phagocytes

mediates cytoskeletal remodeling within the target eukaryotic cells, leading to formation of phagocytic cup and subsequent internalization of the bacteria. At the same time, the contribution of InlB to *L. monocytogenes* interactions with professional phagocytes remains unknown. In the first experiment, we analyzed whether the presence of InlB affects the efficiency of *L. monocytogenes* capture by macrophages. The M1 macrophages were co-incubated with three different strains of *L. monocytogenes*: the wild-type EGDe, the EGDeΔinlB strain, derived from EGDe by inlB deletion (ΔInlB), and EGDeΔinlB::pInlB (ΔInlB complemented with inlB-containing plasmid). The data indicate that the presence of InlB improves the efficiency of *L. monocytogenes* capture by macrophages 3.5-fold (Fig. 3). No significant differences between the type strain EGDe and the complemented EGDeΔinlB::pInlB strains were observed in the experiments (Supplementary 1).

## Survival of *L. monocytogenes* inside macrophages is InlB-dependent

The effects of InlB on survival of the captured bacteria inside human macrophages were assessed after 24 h incubation, during which the EGDeΔinlB strain underwent 182.5 ± 16.7 fold increase in bacterial number, whereas for the type strain EGDe strain the rates were significantly lower (96 ± 12 fold increase in bacterial number). Remarkably, the EGDeΔinlB::pInlB strain complemented with a plasmid copy of inlB showed the lowest intracellular proliferation rates with a fold increase of 13.3 ± 3 only (Fig. 4; Supplementary 2). This effect possibly reflected complementation of the strain on the basis of a plasmid that consumed additional cell resources. The assumption was tested by infecting HEp-2 cells with EGDe and EGDeΔinlB::pInlB strains (similarly with the macrophage capture assay). Over 24 h, the numbers of EGDe and EGDeΔinlB::pInlB increased 515.8-fold and 508.9-fold respectively ($n = 3$), indicating similar intracellular proliferation rates for the type and plasmid-complemented strains of *L. monocytogenes* in HEp-2 cells.

In order to explain the differential survival of the type strain EGDe, its inlB-depleted derivative and plasmid-complemented strains in macrophages, we further hypothesized that the dramatically reduced survival of the complemented strain can be associated with the levels of InlB production. The analysis involved ELISA test systems capable of distinguishing between InlB exposed on the bacterial surface and InlB secreted to the culture medium. We found that EGDe and EGDeΔinlB::pInlB expressed similar levels of InlB associated with the cell surface. However, the levels of secreted InlB measured in supernatant for EGDeΔinlB::pInlB were 3.3-fold higher than for the type strain EGDe (Fig. 5). These results support our assumption that *L. monocytogenes* survival and/or proliferation in human macrophages are affected by InlB in a quantitative manner.

## DISCUSSION

In this study we show that interactions between *L. monocytogenes* and human macrophages are InlB-dependent: the presence of the pathogenicity factor InlB at the bacterial surface accelerates the capture of listerias by macrophages and interferes with their survival inside macrophages. Moreover, the InlB production levels negatively correlate with *L. monocytogenes* survival inside macrophages.

This finding is consistent with a recent study comparing inlB expression between non-clinical and clinical isolates and demonstrating significantly lower InlB production levels in the latter [20]. In addition, decreased production levels of InlB
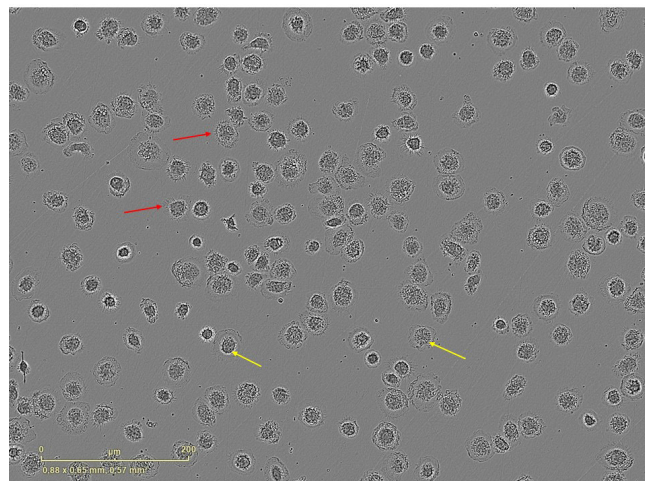


**Fig. 2.** Cell morphology of the M1 macrophages differentiated from peripheral blood monocytes of healthy donors. Red arrows indicate cell surface protrusions. Yellow arrows indicate large rounded nuclei. The images were acquired in an IncuCyte® S3 Live-Cell Imaging System (Sartorius; Göttingen, Germany)
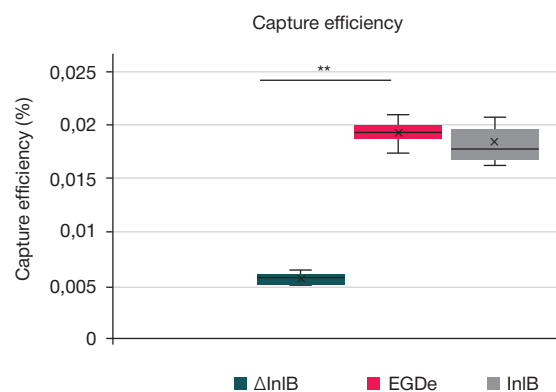


**Fig. 3.** Capture efficiency of *L. monocytogenes* ΔInlB strain, type strain EGDe and plasmid-complemented ΔInlB (InlB) strain by M1-like phenotype macrophages, **$p < 0.01$ ($n = 4$).
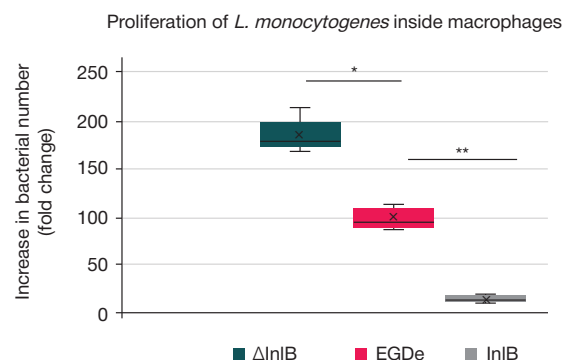


**Fig. 4.** Proliferation of *L. monocytogenes* ΔInlB strain, type strain EGDe and plasmid-complemented ΔInlB (InlB) strain inside M1-like phenotype macrophages over 24 h infection, * — $p < 0.05$, ** — $p < 0.01$ ($n = 4$).

were associated with decreased production of IL8 by non-professional phagocytes [20]. The authors suggest that the reduced IL8-inducing capacity of clinical strains may represent an immunity evasion mechanism that comes at a price of reduced efficiency of bacterial invasion into non-professional phagocytes [20]. This view is supported by our finding that higher levels of InlB production negatively affect the survival of listeria inside human macrophages.

Which of the two target receptors of InlB is responsible for this effect is still elusive. The activation of c-Met by its physiological ligand, HGF, promotes an M1-to-M2 shift in macrophage phenotypes [9]. The InlB/c-Met interaction

imitates the activity of HGF, leading to NF-κB activation and triggering of PI3K and MAPK pathways in various cell types including macrophages [14, 16]. The interaction of c-Met with InlB can enhance the motility of certain immune cell types. According to recent studies, this interaction facilitates secretion of the pro-inflammatory cytokine IL6 by peritoneal dendritic cells [16]. The dose-dependent effect of InlB on bacterial survival observed by us in the macrophage capture assay may indicate a contribution of intracellular receptors. A candidate intracellular receptor for InlB is gC1q-R, which has been attributed with both extra- and intracellular localization. The existence of other, as yet undescribed intracellular receptors for InlB cannot be excluded as well.

Overall, our results demonstrate a negative role of InlB in the innate immunity evasion by listerias. At the same time, InlB is required for the full-scale invasion of listerias into non-professional phagocytic cells. The balance of bacterial–host interactions between immune cells and principal target cells of the pathogen may define the degree of virulence for different strains of *L. monocytogenes*.

CONCLUSIONS

This study focused on the effects of InlB, the pathogenicity factor of *L. monocytogenes*, on the interactions of listerias with human macrophages. In our experiments, InlB significantly enhanced the capture of listerias by macrophages while inhibiting the survival/proliferation of listerias inside macrophages. Thus, we for the first time demonstrate a negative impact of InlB on the
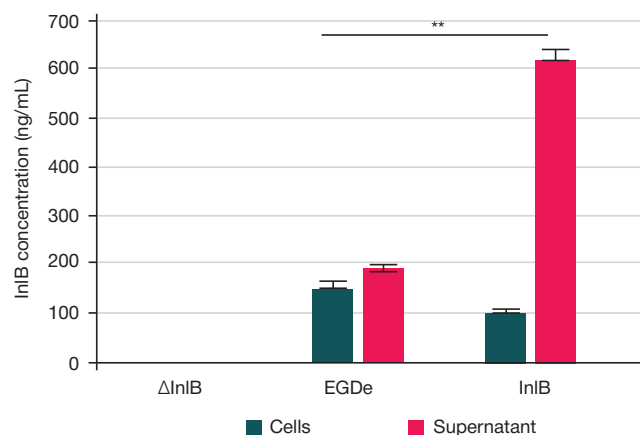


**Fig. 5.** Production levels of InlB protein in 18 h cultures of *L. monocytogenes*. The ΔInlB cultures contain no InlB protein; the type strain EGDe cultures contain 149.2 ± 13.3 ng/mL of InlB bound to the bacterial surface and 187.3 ± 9.8 ng/mL of InlB in the supernatant; the plasmid-complemented ΔInlB (InlB) cultures contain 100.7 ± 4.2 ng/mL of InlB bound to the bacterial surface and 614.6 ± 23 ng/mL of InlB in the supernatant, ** — $p < 0.01$ ($n = 3$)

innate immunity evasion by listerias. The balance between this newly observed effect of InlB and its decisive positive role in the infectivity of *L. monocytogenes* towards non-professional phagocytes, along with the mechanisms that evolved to maintain this balance, should be considered in detail in order to advance the understanding of pathogen-host interactions for different cell types of the body.

References

1. Murray E, Webb R, Swann M. A disease of rabbits characterized by a large mononuclear monocytosis, caused by a hitherto undescribed bacillus Bacterium monocytogenes. J Pathol Bacteriol. 1926; 29: 407–39.
2. Vázquez-boland J, Kuhn M, Berche P, Chakraborty T, Domi G, González-zorn B, et al. Listeria Pathogenesis and Molecular Virulence Determinants Listeria Pathogenesis and Molecular Virulence Determinants. Clin Microbiol Rev. 2001; 14: 584–640.
3. Allerberger F, Wagner M. Listeriosis: A resurgent foodborne infection. Clin Microbiol Infect. 2010; 16: 16–23.
4. Braun L, Cossart P. Interactions between Listeria monocytogenes and host mammalian cells. Microbes Infect. 2000; 2: 803–11.
5. Shen Y, Naujokas M, Park M, Ireton K. InlB-dependent internalization of Listeria is mediated by the Met receptor tyrosine kinase. Cell. 2000; 103: 501–10.
6. Cossart P. Met, the HGF-SF receptor: another receptor for Listeria monocytogenes. Trends Microbiol. 2001; 9: 105–7.
7. Organ S, Tsao M. An overview of the c-MET signaling pathway. Ther Adv Med Oncol. 2011; 3: 7–9.
8. Chen Q, DeFrances MC, Zarnegar R. Induction of Met proto-oncogene (hepatocyte growth factor receptor) expression during human monocyte-macrophage differentiation. Cell Growth Differ. 1996; 7: 821–32.
9. Nishikoba N, Kumagai K, Kanmura K, NakamuraY, Ono M, Eguchi H, et al. HGF-MET Signaling Shifts M1 Macrophages Toward an M2-Like Phenotype Through PI3K-Mediated Induction of Arginase-1 Expression. Front Immunol. 2020; 11: 1–10.
10. Ghebrehiwet B, Lim B, Peerschke E, Willis A, Reid K. Isolation, cDNA cloning, and overexpression of a 33-kDa cell surface glycoprotein that binds to the globular heads of C1q. J Exp Med. 1994; 179: 1809–21.
11. Ghebrehiwet B, Peerschke E. Structure and function of gC1q-R a multiligand binding membrane protein. Immunobiology. 1998; 199: 225–38.
12. Chalenko Y, Kalinin E, Marchenkov V, Sysolyatina E, Surin A,

Sobyanin K, et al. Phylogenetically Defined Isoforms of Listeria monocytogenes Invasion Factor InlB Differently Activate Intracellular Signaling Pathways and Interact with the Receptor gC1q-R. Int J Mol Sci. 2019; 20: 1–15.
13. ChalenkoY, Kolbasova O, Pivova E, Abdulkadieva M, Povolyaeva O, Kalinin E. Listeria monocytogenes Invasion Into Sheep Kidney Epithelial Cells Depends on InlB, and Invasion Efficiency Is Modulated by Phylogenetically Defined InlB Isoforms. Front Microbiol. 2022; 13: 1–14.
14. Sobyanin K, Sysolyatina E, Krivozubov M, Chalenko Y, Karyagina A, Ermolaeva S. Naturally occurring InlB variants that support intragastric Listeria monocytogenes infection in mice. FEMS Microbiol Lett. 2017: 1; 1–8.
15. Nepomuceno R, Tenner A. C1qRP, the C1q receptor that enhances phagocytosis, is detected specifically in human cells of myeloid lineage, endothelial cells, and platelets. J Immunol. 1998; 160: 1929–35.
16. Mansell A, Braun L, Cossart P, O'Neill L. A novel function of InlB from Listeria monocytogenes: activation of NF-kappaB in J774 macrophages. Cell Microbiol. 2000; 2: 127–36.
17. Calame D, Mueller-Ortiz S, Wetsel R. Innate and adaptive immunologic functions of complement in the host response to Listeria monocytogenes infection. Immunobiology. 2016; 221: 1407–17.
18. Fuss I, Kanof M, Smith P, Zola H. Isolation of whole mononuclear cells from peripheral blood and cord blood. Curr Protoc Immunol. 2009; 85: 1.1–7.1.8.
19. Huang X, Li Y, Fu M, Xin H. Polarizing Macrophages In Vitro. Germain Rousselet (ed.), Macrophages: Methods and Protocols. Methods in Molecular Biology. 2018; 1784: 119–26.
20. Werbrouck H, Grijspeerdt K, Botteldoorn N, Pamel E, Rijpens N, Damme J, et al. Differential inlA and inlB Expression and Interaction with Human Intestinal and Liver Cells by Listeria monocytogenes Strains of Different Origins. Appl Environ Microbiol. 2006; 72 (6): 3862–71.

## Литература

1.  Murray E, Webb R, Swann M. A disease of rabbits characterized by a large mononuclear monocytosis, caused by a hitherto undescribed bacillus Bacterium monocytogenes. J Pathol Bacteriol. 1926; 29: 407–39.
2.  Vázquez-boland J, Kuhn M, Berche P, Chakraborty T, Domi G, González-zorn B, et al. Listeria Pathogenesis and Molecular Virulence Determinants Listeria Pathogenesis and Molecular Virulence Determinants. Clin Microbiol Rev. 2001; 14: 584–640.
3.  Allerberger F, Wagner M. Listeriosis: A resurgent foodborne infection. Clin Microbiol Infect. 2010; 16: 16–23.
4.  Braun L, Cossart P. Interactions between Listeria monocytogenes and host mammalian cells. Microbes Infect. 2000; 2: 803–11.
5.  Shen Y, Naujokas M, Park M, Ireton K. InIB-dependent internalization of Listeria is mediated by the Met receptor tyrosine kinase. Cell. 2000; 103: 501–10.
6.  Cossart P. Met, the HGF-SF receptor: another receptor for Listeria monocytogenes. Trends Microbiol. 2001; 9: 105–7.
7.  Organ S, Tsao M. An overview of the c-MET signaling pathway. Ther Adv Med Oncol. 2011; 3: 7–9.
8.  Chen Q, DeFrances MC, Zarnegar R. Induction of Met proto-oncogene (hepatocyte growth factor receptor) expression during human monocyte-macrophage differentiation. Cell Growth Differ. 1996; 7: 821–32.
9.  Nishikoba N, Kumagai K, Kanmura K, NakamuraY, Ono M, Eguchi H, et al. HGF-MET Signaling Shifts M1 Macrophages Toward an M2-Like Phenotype Through PI3K-Mediated Induction of Arginase-1 Expression. Front Immunol. 2020; 11: 1–10.
10. Ghebrehiwet B, Lim B, Peerschke E, Willis A, Reid K. Isolation, cDNA cloning, and overexpression of a 33-kDa cell surface glycoprotein that binds to the globular heads of C1q. J Exp Med. 1994; 179: 1809–21.
11. Ghebrehiwet B, Peerschke E. Structure and function of gC1q-R a multiligand binding membrane protein. Immunobiology. 1998; 199: 225–38.
12. Chalenko Y, Kalinin E, Marchenkov V, Sysolyatina E, Surin A, Sobyanin K, et al. Phylogenetically Defined Isoforms of Listeria monocytogenes Invasion Factor InIB Differently Activate Intracellular Signaling Pathways and Interact with the Receptor gC1q-R. Int J Mol Sci. 2019; 20: 1–15.
13. ChalenkoY, Kolbasova O, Pivova E, Abdulkadieva M, Povolyaeva O, Kalinin E. Listeria monocytogenes Invasion Into Sheep Kidney Epithelial Cells Depends on InIB, and Invasion Efficiency Is Modulated by Phylogenetically Defined InIB Isoforms. Front Microbiol. 2022; 13: 1–14.
14. Sobyanin K, Sysolyatina E, Krivozubov M, Chalenko Y, Karyagina A, Ermolaeva S. Naturally occurring InIB variants that support intragastric Listeria monocytogenes infection in mice. FEMS Microbiol Lett. 2017: 1; 1–8.
15. Nepomuceno R, Tenner A. C1qRP, the C1q receptor that enhances phagocytosis, is detected specifically in human cells of myeloid lineage, endothelial cells, and platelets. J Immunol. 1998; 160: 1929–35.
16. Mansell A, Braun L, Cossart P, O'Neill L. A novel function of InIB from Listeria monocytogenes: activation of NF-kappaB in J774 macrophages. Cell Microbiol. 2000; 2: 127–36.
17. Calame D, Mueller-Ortiz S, Wetsel R. Innate and adaptive immunologic functions of complement in the host response to Listeria monocytogenes infection. Immunobiology. 2016; 221: 1407–17.
18. Fuss I, Kanof M, Smith P, Zola H. Isolation of whole mononuclear cells from peripheral blood and cord blood. Curr Protoc Immunol. 2009; 85: 1.1–7.1.8.
19. Huang X, Li Y, Fu M, Xin H. Polarizing Macrophages In Vitro. Germain Rousselet (ed.), Macrophages: Methods and Protocols. Methods in Molecular Biology. 2018; 1784: 119–26.
20. Werbrouck H, Grijspeerdt K, Botteldoorn N, Pamel E, Rijpens N, Damme J, et al. Differential inlA and inlB Expression and Interaction with Human Intestinal and Liver Cells by Listeria monocytogenes Strains of Different Origins. Appl Environ Microbiol. 2006; 72 (6): 3862–71.

# COMPARATIVE EFFICIENCY OF ACCESSIBLE TRANSFECTION METHODS IN MODEL CELL LINES FOR BIOTECHNOLOGICAL APPLICATIONS

Vorobyev PO[1], Kochetkov DV[1], Vasilenko KV[2], Lipatova AV[1] ✉

[1] Engelhardt Institute of Molecular Biology, Moscow, Russia

[2] Pirogov Russian National Research Medical University, Moscow, Russia

Transient gene expression is one of the most common methods in molecular biology, equally relevant for basic research projects and biotechnological industries. Despite the existence of commercial transfection systems, which afford high transfection efficiency and high expression levels of reporter genes, expanding such systems to industrial scales is often problematic due to high costs of the reagents. The well-described methods of cationic and calcium-phosphate transfection are accessible and ensure reproducible results at much lower costs. This study is aimed at comparative validation of calcium phosphate and cationic (polyethylenimine-based) transfection protocols along with the commercially available TurboFect reagent for mono- and cotransfections on a panel of commonly used cell lines including HEK293T, Huh7, BHK-21, CHO and MRC5. The efficiency of transfection with plasmid constructs encoding different fluorescent proteins was measured by flow cytometry. Of all the tested methods, calcium phosphate transfection afforded the highest efficiency of plasmid DNA delivery in all the cell lines except BHK21, for which the PEI method turned out to be more efficient than calcium phosphate transfection, and CHO, for which both methods showed comparable efficiency.

Keywords: calcium phosphate transfection, polyethylenimine, cotransfection, transfection, lentiviruses

✉ Correspondence should be addressed: Anastasia V. Lipatova
Vavilova, 32/1, Moscow, 119991, Russia; lipatovaanv@gmail.com

# СРАВНИТЕЛЬНЫЙ АНАЛИЗ ЭФФЕКТИВНОСТИ ОБЩЕДОСТУПНЫХ МЕТОДОВ ТРАНСФЕКЦИИ МОДЕЛЬНЫХ КЛЕТОЧНЫХ ЛИНИЙ ДЛЯ ЗАДАЧ БИОТЕХНОЛОГИИ

П. О. Воробьев[1], Д. В. Кочетков[1], К. В. Василенко[2], А. В. Липатова[1] ✉

[1] Институт молекулярной биологии имени В. А. Энгельгардта, Москва, Россия

[2] Российский национальный исследовательский медицинский университет имени Н. И. Пирогова, Москва, Россия

Краткосрочная экспрессия генов является одним из самых широко используемых методов в молекулярной биологии, как в исследовательских проектах, так и для решения задач биотехнологической промышленности. Несмотря на то что существующие коммерческие трансфекционные агенты позволяют добиться эффективной трансфекции и высокой экспрессии целевых генов в клетках, масштабирование производственного процесса часто затруднительно из-за высокой стоимости таких агентов. Хорошо описанные методы катионной или кальций-фосфатной трансфекции доступны и дают воспроизводимые результаты при значительно меньшей себестоимости. Целью исследования было проверить методы кальций-фосфатной трансфекции, катионной трансфекции (PEI) и коммерчески доступного реагента TurboFect на эффективность монотрансфекции и котрансфекции на панели широко используемых клеточных линий, таких как HEK293T, HUH7, BHK-21, CHO, MRC5. Эффективность трансфекции плазмидными конструкциями, несущими различные флуоресцентные белки, оценивали путем проведения проточной цитофлуориметрии. Среди всех методов кальций-фосфатная трансфекция позволяет добиться максимально эффективной доставки плазмидной ДНК во всех клеточных линиях, использованных в нашем исследовании, кроме BHK21 — для нее катионная трансфекция с использованием PEI оказалась эффективнее, и сопоставима по эффективности с кальций-фосфатным методом в клеточных линиях CHO.

Ключевые слова: кальций-фосфатная трансфекция, полоиэтиленимин, котрансфекция, трансфекция, лентивирусы

✉ Для корреспонденции: Анастасия Валерьевна Липатова
ул. Вавилова, д. 32/1, г. Москва, 119991, Россия; lipatovaanv@gmail.com

Transfection is the process of exogenous DNA or RNA delivery into eukaryotic cells [1], used for recombinant protein production [2], signal pathway investigation [3–6], etc. This group of methods has emerged in connection with the viral genome infectivity and its self-perpetuation research [7]. By now, transfection protocols are indispensable for the creation of recombinant viral strains, as well as for the production of viral vectors on the basis of lenti- and adeno-associated viruses [8, 9].

The 'chemical' transfection methods are classified by the type of the agent binding nucleic acid molecules to enable their introduction into a cell. Such agents include calcium phosphate, polyethylenimine (PEI) and other cationic polymers

(e.g. chitosan), liposomes and polyamidoamines [10]. Each agent has its own advantages and disadvantages; the choice should depend on the balance of cytotoxicity and transfection efficiency of the agent in a particular experimental setting [11]. Despite the extensive supply of ready-made commercial solutions including Lipofectamine 3000, TurboFect, SuperFect, and FuGENE HD [12], the accessible and well-studied calcium phosphate and cationic transfection methods are still actively used [10].

The calcium phosphate transfection (CPT) was firstly developed in 1973 [13] during studies on the adenoviral genome infectivity, but its mechanism had long remained incomprehensible. With the discovery of direct endosomal transport of CaPi–DNA precipitates to the nucleus in 1990 [14] the method became increasingly widespread. The classical protocol involves co-precipitation of calcium salts and DNA with the formation of hydroxyapatite complexes under precise physical and chemical conditions of oversaturated solution, within a defined range of temperatures and concentrations. The reproducible performance of this technique requires a certain amount of skill [15–18], although some recent modifications of the classical protocol effectively overcome this limitation [19, 20].

The cationic transfections with polyethylenimine (PEI) and its commercially available modifications (e.g. TurboFect™) are popular as well [10, 21]. The critical parameters in these protocols are DNA/PEI ratio and the molecular weight of PEI, a reduction in which hampers cytotoxicity. Commercial versions mostly use 25 kDa PEI [22]; another option is PEI "Max" — a chemically modified 40 kDa PEI with reduced cytotoxicity [10, 23]. The undoubted advantages of PEI include high efficiency, handling simplicity and universal applicability. The sensitivity of dry PEI to oxidation by atmospheric oxygen represents a certain drawback, fairly surmountable by dissolving the reagent in 0.2 M HCl for prolonged storage [24], whereas the cytotoxicity of the reagent can be reduced by using a lactate buffer as a medium for the transfection complexes formation.

The widely used transfection reagent Lipofectamine 3000 is extremely efficient and stable at a 4 °C storage temperature, but prohibitively expensive (50 USD for a single transfection experiment with 107 cells). This price tier of transfection reagents is beyond the scope of this article.

A simultaneous delivery of multiple genetic constructs to a cell is a widespread task often required for multimeric protein synthesis, design of recombinant viral strains [8, 9], lenti- and adeno-associated viral particle production and other biotechnological purposes, sometimes at industrial scales [25]. The use of ready-made commercial kits, whatever expedient and reliable, in large-scale transfections is hampered by high costs and also by logistical problems associated with the lack of domestically manufactured analogs. In this study, we compare the efficiencies of CPT, PEI and TurboFect methods in cotransfections with reporter plasmid constructs and quantitatively assess the effectivity by flow cytometry.

METHODS

## Cells

Cell lines HEK293T (ATCC #CRL-3216), BHK21 (ATCC #C-13), MRC5 (ATCC #CCL-171) and CHO K1 (ATCC #CCL-61) were purchased from ATCC (American Type Culture Collection; USA); cell lines CHO DG-44 и Huh7 were generously gifted by A.V. Ivanov (Laboratory of Biochemistry of Viral Infections at the Engelhardt Institute of Molecular Biology; Moscow, Russia). The cells were cultured in DMEM (Gibco; USA) supplemented with 10% fetal bovine serum (FBS, HyClone; USA) and antibiotics to

standard concentrations (penicillin 50 U/mL and streptomycin 50 µg/mL); CHO DG-44 cells were cultured in DMEM/F12 (PanEco; Russia) with 10% FBS and antibiotics.

## Plasmid constructs and transfection protocols

The coding sequences of Katushka, BFP and eGFP fluorescent proteins were cloned into the pL-CMV-PL4-Puro vector developed previously in the Laboratory of Cell Proliferation (Engelhardt Institute of Molecular Biology). After the verification of successful cloning by sequencing, the plasmids were propagated in the *E. coli* strain TOP-10 (New England Biolabs; USA) using 200 mL LB aliquots and purified with a Plasmid Midiprep 2.0 kit (Evrogen; Russia). The plasmid DNA extraction quality was controlled by spectrophotometry (NanoDrop 2000; ThermoFisher, USA) using the 260/280 nm absorbance ratio; all samples used in the experiments had A260/280 of 1.9 or higher.

The cells were plated in six-well plates 24 h prior to transfection, $1.5 \times 10^5$ cells in 4 mL of DMEM supplemented with 10% FBS, and maintained in an incubator at 37 °C, 5% $CO_2$ and high humidity until use.

The PEI transfection method was conducted as described previously [24]. The dry reagent (Cat# 23966 Polysciences, Inc.; USA) was dissolved in 0.2 M HCl to 5 µg/µL; this stock solution was aliquoted and stored long-term at –80 °C. The lactate buffer (20 mM sodium lactate, 150 mM NaCl, pH 4.0) was stored at 4 °C.

On the day of transfection, 3 µg of plasmid DNA were diluted with 150 µL of the lactate buffer. In a separate tube, 15 µg (3 µL) of PEI were diluted with 150 µL of the lactate buffer. The two mixtures were combined, mixed thoroughly, incubated at room temperature for 10–15 min and added drop-wise to the culture medium. In a modified version of this protocol, DNA and PEI were added to 300 µL of the lactate buffer, which preserved the transfection efficiency (data not shown). The fluorescence measurements were carried out 48 h post-transfection (after addition of DNA-containing complexes to cells).

Calcium phosphate transfections (CPT) were carried out in accordance with the previously published protocol [26]. The culture medium was replaced with DMEM (Gibco) supplemented with 10% FBS (HyClone), 2.25 mL per well, 1 h before the transfection. The DNA/$CaCl_2$/$dH_2O$ solution (125 µL) was prepared from 2M $CaCl_2$ diluted with other components to a final concentration of 148 mM; the total amount of DNA was 3 µg. The DNA/$CaCl_2$/$dH_2O$ solution was combined with the equal volume of 2× HBS buffer (HBS; Table 1) at thorough mixing. The transfection mixture was incubated at room temperature for 10–20 min and added drop-wise to the culture medium. The cultures were placed in an incubator; 6 h or 14 h post-transfection the culture medium was replaced with a fresh portion. The membrane shock procedure was carried out 14 h post-transfection: the culture medium was replaced with 1 mL of 10% DMSO in phosphate-buffered saline (PBS). After a 2.5 min-long incubation the cells were washed twice with 3 mL of PBS and covered with the fresh culture medium.

Transfections with TurboFect™ were carried out according to the manufacturer's recommendations. On the day of transfection, 4 µg of plasmid DNA were diluted with serum-free DMEM and combined with 6 µL of the TurboFect reagent. The mixture was incubated at room temperature for 20 min and added drop-wise to the culture medium.

## Cell viability assay

For a standard thiazolyl blue tetrazolium bromide (MTT) viability assay, the cells were transferred to 24-well plates. The tests

were carried out 24 h post-transfection as longer incubation times could blur the differential toxic effects. Dry MTT (Dia-M; Russia) was dissolved in PBS to obtain the solution (5 µg/mL) added directly to the wells. After a 3 h-long incubation, the culture medium was replaced with 300 µL of DMSO (PanEco; Russia). The controls were the corresponding non-transfected cultures. The detection was carried out in a CLARIOstar plate reader (BMG Labtech; USA) by measuring absorbance at 595 nm normalized to 490 nm.

### Flow cytometry assay and data processing

All the measurements were carried out in a BD LSRFortessa flow cytometer (Beckman Dickinson; USA) with detection in the PE (561/(586/15) nm — Katushka), FITC (488/(530/30) nm — eGFP) and Pacific Blue (405/(450/50) nm — tagBFP) channels. We used the preinstalled BD FACSDiva software for the compensation adjustment and primary processing of the data and the Flowing Software 2.0 (Perttu Terho, Turku Bioscience Centre; Finland) for the advanced analysis. All experiments were performed in three independent biological replicates.

### Lentiviral stock production and titration

Lentiviral component-encoding plasmids pREV, pGAG-pol, p-VSV-G and pL-CMV-eGFP-puro were constructed earlier in the Laboratory of Cell Proliferation (Engelhardt Institute of Molecular Biology). HEK293T cells were plated in Petri dishes to a 35% confluency; on the next day, the cells were transfected with a 2 : 1 : 1 : 4 mass ratio of the plasmids (in the listed order) [27]. After a 16 h-long incubation, the medium was replaced with DMEM containing 2% FBS. The harvesting of lentiviral particles was repeated twice daily, starting at 8 h since the first medium replacement. The titers of the pooled five consecutive viral stocks were evaluated on HEK293T cultures

**Table 1.** The 2× hepes buffer saline (HBS) composition

| NaCl | 280 mM |
|---|---|
| KCl | 10 mM |
| $Na_2HPO_4$ | 1.5 mM |
| Dextrose/glucose | 12 mM |
| HEPES pH 7.05 | 50 mM |

using a modified final dilution method. 10-fold serial dilutions of the viral stocks in serum-free DMEM were added to fresh cultures growing in 48-well cell culture plates at $1.5 \times 10^4$ cells per well. The medium was replaced with DMEM containing 2% FBS and the dilutions of lentiviral stocks were added. The experiment was conducted in four technical parallels. After 72 hours, fluorescent plaques were counted in wells with maximum viral dilutions.

### Statistical analysis

The data were analyzed using the GraphPad Prism 9.0 package (GraphPad Software, Inc.; La Jolla, CA, USA). The differences were validated using one-way ANOVA.

RESULTS

### Post-transfection cell viability assay

Fig. 1 shows the results of the MTT assay performed 24 h post-transfection.

The data indicate that over 80% cells survive the transfection procedure, independently of the cell line and protocol. MTT assays performed 48 h post-transfection are non-informative due to the effects of contact inhibition: in control wells, cells become 100% confluent, while transfected cells continue to proliferate.

Cell viability 24h post-transfection
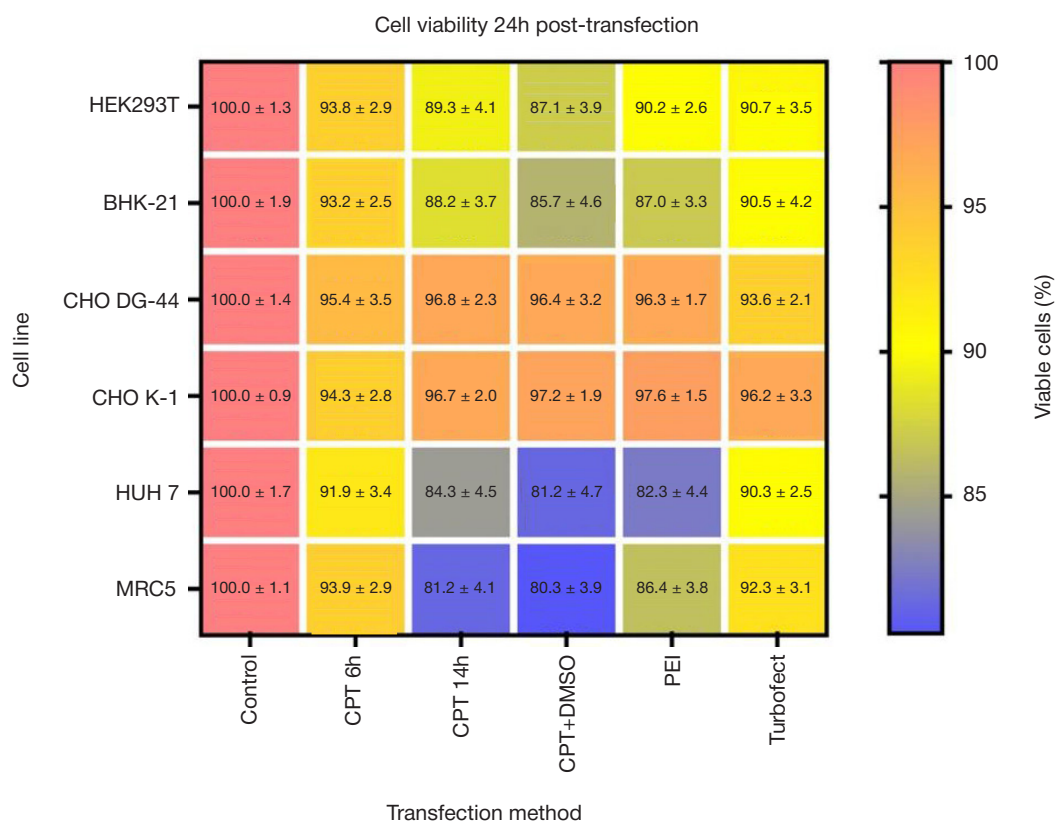


**Fig. 1.** The post-transfection MTT cell viability assay for PEI, TurboFect and CPT methods; Control — non-transfected cultures
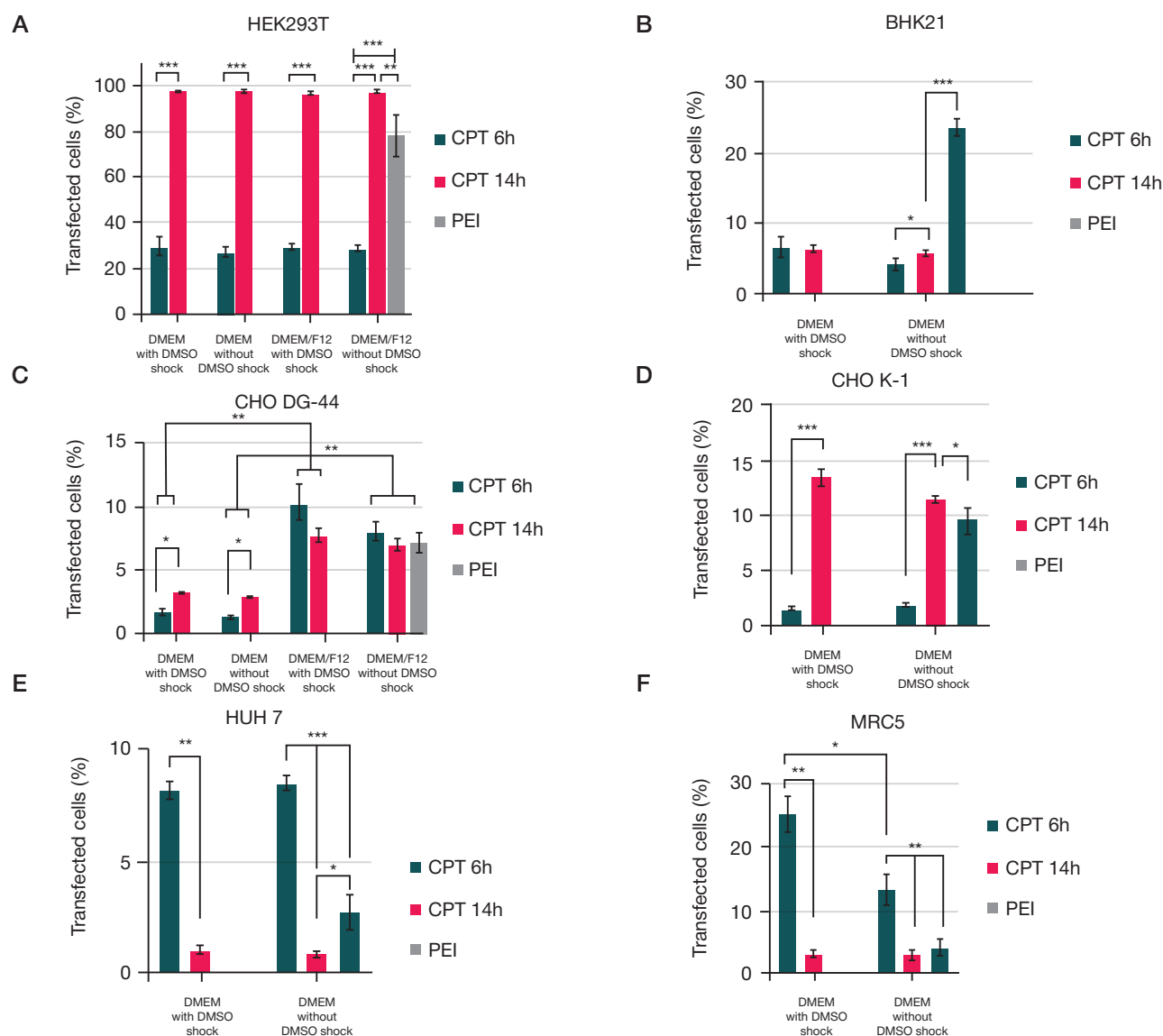
**Fig. 2.** Comparative efficiency of CPT and PEI monotransfections with Katushka expression plasmid (red fluorescence) in different model cell lines: HEK293T (**A**), BHK-21 (**B**), CHO DG-44 (**C**), CHO K-1 (**D**), Huh7 (**E**) and MRC5 (**F**). CPT 6 h — calcium phosphate transfection with 6 h incubation; CPT 14 h — calcium phosphate transfection with 14 h incubation

## Monotransfection efficiency assay

The comparative evaluation of the CPT and PEI methods in terms of the transfection efficiency involved the pL-CMV-Katushka-puro plasmid construct (Fig. 2).

The following conditions were varied for the optimization:

– the duration of incubation with the CaPi–DNA precipitate (6 h and 14 h);

– the impact of the membrane shock procedure (2.5 min exposure of 10% DMSO).

The increase of the incubation time with the CaPi–DNA precipitate from 6 h to 14 h dramatically enhanced the transfection efficiency for the HEK293T and CHO K 1 cell lines: the numbers of reporter-positive cells increased, respectively, from 27% to 97% for HEK293T ($p < 0.01$) and from 1.5% to 13% for CHO K-1 ($p < 0.01$). Importantly, the effect was cell line-dependent: the incubation time with the precipitate produced a drop in the transfection efficiency from 25% to 3% for MRC5 ($p < 0.01$) and from 8% to 1% for Huh7 ($p < 0.01$).

The introduction of the 10% DMSO treatment step (membrane shock) led to a significant increase in the transfection efficiency for the MRC5 cell line only ($p < 0.05$).

CPT showed the best results in all the cell lines except BHK-21. The PEI method was also efficient in most cell lines and produced comparable cytotoxic effects.

The influence of the cell culture medium on the CPT efficiency was tested using the HEK293T and CHO DG-44 cell lines (Figs. 2A and 2C). CHO DG-44 cells showed enhanced transfection efficiency in DMEM/F12 ($p < 0.01$). The use of the membrane shock (10% DMSO exposure) provided no significant enhancement in the transfection efficiency in these experiments.

*Cotransfection efficiency assay*

In the next series of experiments, we cotransfected the cells with plasmid constructs encoding eGFP and Katushka fluorescent proteins (Fig. 3A, Table 2). The highest cotransfection efficiency was observed in HEK293T cells. CPT worked significantly better than the PEI method for all the cell lines except BHK21 ($p < 0.001$). Transfections with TurboFect were the least efficient. Microphotographs of CPT in HEK293T are shown in Fig. 4.

The trends identified for double cotransfections were preserved in triple cotransfections, although the efficiencies (measured as the percentage of cells expressing all reporter

A

**eGFP/Katushka**



B
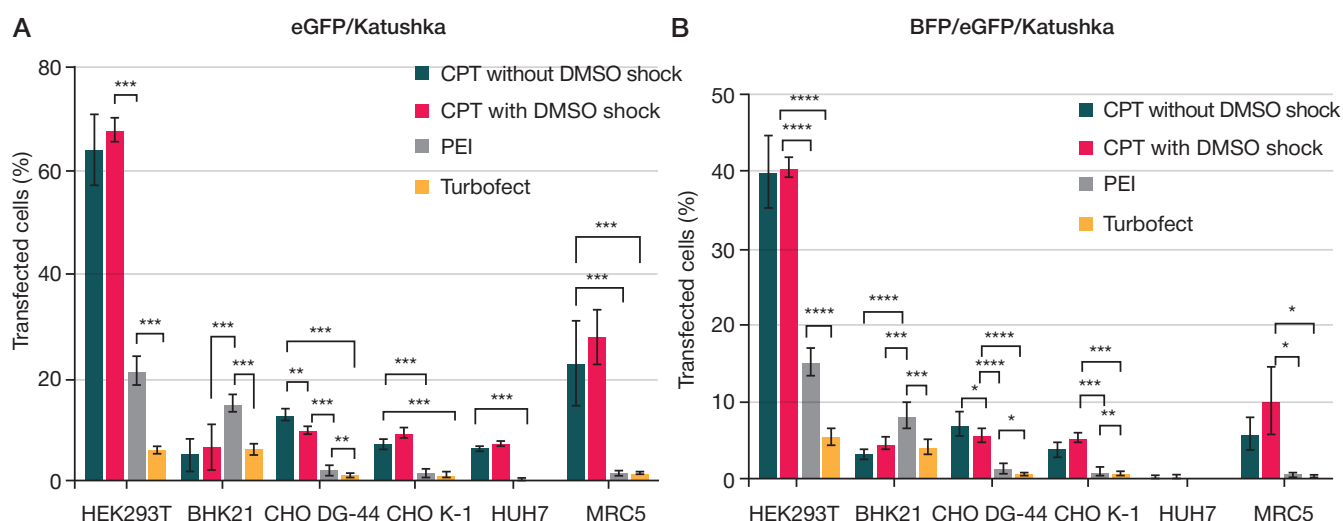
**BFP/eGFP/Katushka**



**Fig. 3.** Comparative efficiency of double cotransfections with eGFP and Katushka encoding plasmids (**A**) and triple cotransfections with BFP, eGFP and Katushka plasmids (**B**) in different model cell lines

proteins) were expectedly lower (Fig. 3B, Table 3). The flow cytometry data analysis for HEK293T and Huh7 is presented in Fig. 5; the positivity thresholds were set in accordance with the contour plots of autofluorescence for the non-transfected control cultures.

Overall, the results demonstrate excellent efficiency of the accessible chemical transfection methods in mono- and cotransfections, comparable with the efficiency of advanced commercially available systems exemplified by FuGENE HD and Lipofectamine 3000 [28].

### Assessment of the lentiviral particles' assembly efficiency

Lentiviral transduction is a standard tool for obtaining cell sublines stably expressing exogenous proteins, cell reprogramming and many other purposes in molecular and cell biology. To produce lentiviral stocks, the HEK293T packaging cell line is simultaneously transfected with 3–4 plasmid constructs encoding HIV-1 proteins and VSV-G glycoprotein, as well as a lentiviral genome plasmid carrying a reporter transgene. The yield of viral particles harvested with the supernatant depends

**Table 2.** Comparative efficiency of double cotransfections with eGFP and Katushka plasmids, measured 48 h post-transfection (best results in each row are highlighted)

| Cell line | Double-positive cells, % | | | |
|---|---|---|---|---|
| | CPT | CPT + DMSO | PEI | Turbofect |
| HEK293T | $64,27 \pm 6,85$ | $68,1 \pm 2,29$ ($p < 0,001$) | $21,33 \pm 2,78$ | $5,97 \pm 0,61$ |
| BHK21 | $5 \pm 3,11$ | $6.6 \pm 4.40$ | $15 \pm 1,85$ ($p < 0,001$) | $6,2 \pm 0,86$ |
| CHO DG-44 | $12,87 \pm 1,16$ ($p < 0,001$) | $9,85 \pm 0,75$ | $2,13 \pm 0,92$ | $1,05 \pm 0,47$ |
| CHO K-1 | $7,1 \pm 0,916$ | $9,43 \pm 0,93$ ($p < 0,001$) | $1,43 \pm 0,83$ | $1,13 \pm 0,51$ |
| HUH7 | $6,93 \pm 0,50$ | $7,23 \pm 0,55$ ($p < 0,001$) | $0,23 \pm 0,16$ | $0,09 \pm 0,06$ |
| MRC5 | $22,7 \pm 8,15$ | $27,93 \pm 5,25$ ($p < 0,001$) | $1,4 \pm 0,56$ | $1,55 \pm 0,25$ |

**Table 3.** Comparative efficiency of triple cotransfections with BFP, eGFP and Katushka encoding plasmids, measured 48 h post-transfection (best results in each row are highlighted)

| Cell line | Triple-positive cells, % | | | |
|---|---|---|---|---|
| | CPT | CPT + DMSO | PEI | Turbofect |
| HEK293T | $39,83 \pm 4,55$ | $40,47 \pm 1.27$ ($p < 0,001$) | $15,2 \pm 1,75$ | $5,57 \pm 0,98$ |
| BHK21 | $3,3 \pm 0,511$ | $4,63 \pm 0,80$ | $8,23 \pm 1,70$ ($p < 0,001$) | $4,16 \pm 0,92$ |
| CHO DG-44 | $7,2 \pm 1.52$ ($p < 0,001$) | $5,73 \pm 0,99$ | $1,33 \pm 0,72$ | $0,63 \pm 0,09$ |
| CHO K-1 | $3,8 \pm 0,92$ | $5,4 \pm 0,53$ ($p < 0,001$) | $0,93 \pm 0,41$ | $0,7 \pm 0,19$ |
| HUH7 | $0,13 \pm 0,06$ | $0,2 \pm 0,13$ (ns) | $0,09 \pm 0,06$ | $0,07 \pm 0,06$ |
| MRC5 | $5,8 \pm 2,02$ | $10,17 \pm 4,33$ ($p < 0,05$) | $0,43 \pm 0,15$ | $0,33 \pm 0,15$ |

**Note:** ns — not significant.

on the transfection efficiency and cell viability. Our choice of the CPT + DMSO, PEI and TurboFect protocols for this practical task was based on the preliminary optimization experiments.

Transfections were performed in a 10 cm Petri dish at a 70% confluency ($6 \times 10^6$ cells). The resulting viral titers evaluated by the final dilution method are presented in Fig. 6.

The highest viral particle production efficiency was achieved with CPT ($9 \times 10^5$ IFU/mL). The PEI and TurboFect protocols also produced satisfactory yields, albeit the titers were significantly lower ($10^5$ IFU/mL; $p < 0.05$, and $6 \times 10^4$ IFU/mL; $p < 0.01$, respectively).

DISCUSSION

The chemical transfection methods vary in toxicity and transfection efficiency depending on their chemical nature and DNA-to-agent ratio. Transfection efficiency is influenced by multiple parameters which are difficult to unify, as dedicated comparisons between studies are hindered by variability of experimental conditions [16, 24]. Here we report a comparative analysis of the efficiency for three transfection methods in several cell lines of a diverse origin.

HEK293T is one of the best-studied model cell lines, known for its high transfection capacity. These cells are ubiquitously used in the production of recombinant proteins and lentiviral stocks. CPT ensures excellent results in HEK293T cells (> 95% efficiency in monotransfections), with the length of incubation with the CaPi–DNA precipitate being a decisive factor. For the incubation times of 6 h and 14 h, the efficiency constituted 29% и 97%, respectively ($p < 0.01$), whereas the role of the membrane shock was negligible (no significant differences observed). In cotransfections, the efficiencies of the CPT and PEI methods constituted 68% and 21% for two-plasmid and 40% and 15% for three-plasmid systems, respectively ($p < 0.01$ in both cases). The corresponding efficiencies of the PEI and TurboFect methods constituted 21% and 5.9% for two-plasmid and 15% and 5% for three-plasmid transfections ($p < 0.01$).

We further tested the feasibility of multiple cotransfections with lentiviral component-encoding plasmids to produce viral particles encoding a reporter gene (eGFP) by these two methods. The tests involved titration of the harvested lentiviral stocks by the transduction assay with the reporter eGFP
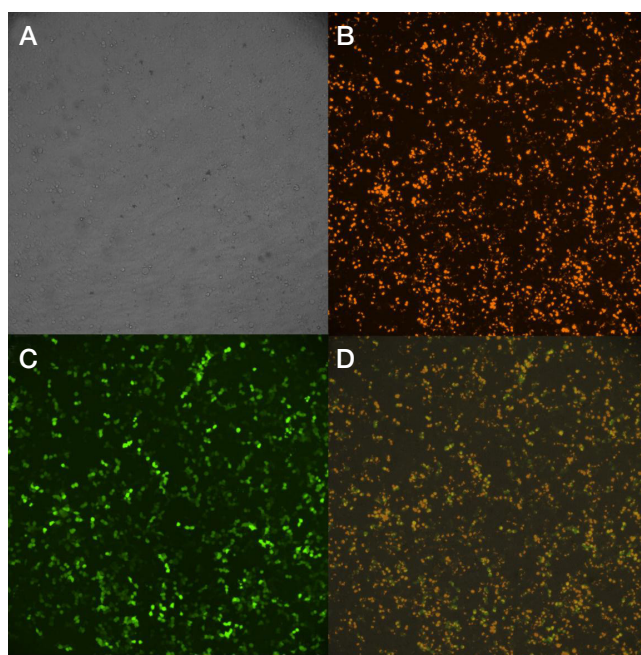
**Fig. 4.** Microphotographs of cell cultures cotransfected with genetic constructs encoding eGFP and Katushka fluorescent proteins. **A**. Light field. **B**. Katushka. **C**. eGFP. **D**. Merged image (magnification ×40)

fluorescence. In this series of experiments, the lentiviral stocks produced with CPT revealed the highest titers ($9 \times 10^5$ IFU/mL), whereas the titers produced with the PEI and TurboFect methods were significantly lower (105 IFU/mL and $6 \times 10^4$ IFU/mL, respectively; $p < 0.05$).

However, for the BHK-21 cell line, CPT proved to be significantly less efficient than the PEI method, yielding 6.6% vs 15% in double and 4.6% vs 8.3% in triple cotransfections ($p < 0.01$ for both); this result overlaps with the previously published data [24]. The discrepancy in the results can be explained by several critical factors, e.g., the PEI preparation method. The efficiency of the PEI method is compromised by the prolonged storage of the dry reagent, as its oxidation by atmospheric oxygen negatively affects the binding capacity [24]. The PEI method showed better efficiency than TurboFect in double and triple cotransfections (11% vs 6% and 8% vs 4%, respectively; $p < 0.01$
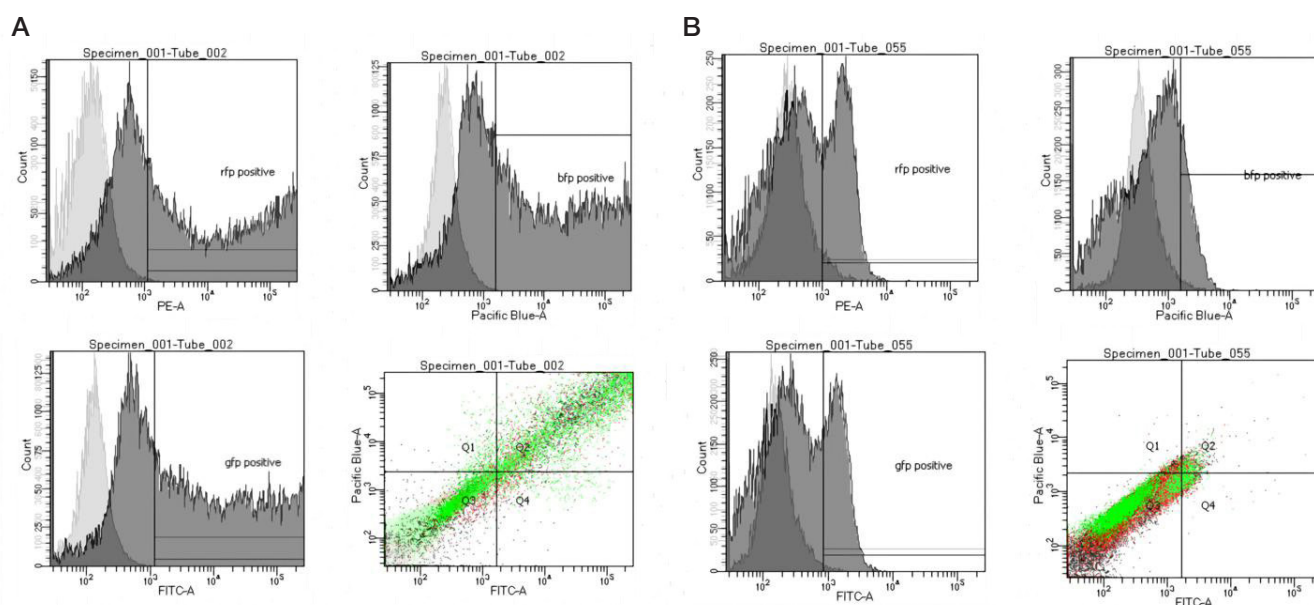
**Fig. 5.** Flow cytometry data for HEK293T and Huh7 cell lines (respectively, **A** and **B**); *light contour* — non-transfected control, *dark contour* — CPT. Populations single-positive for particular fluorescent proteins (eGFP, Katushka or BFP) or triple-positive (Q2) are indicated

in both cases). Of note, these results should be further verified by using a different batch of the TurboFect transfection reagent, which is highly sensitive to the storage temperature (should be stored at 2–8 °C).

Overall, CPT showed higher efficiency than PEI for most cell lines used in our study ($p < 0.001$ for HEK293T, Huh7, CHO DG-44 and CHO K-1, and $p < 0.05$ for MRC5). It should be noted that the use of the DMSO-induced membrane shock had small effects in both double and triple cotransfections of CHO-K1 ($p < 0.05$) and MRC5 cells. None of the protocols tested by us in this study ensured efficient cotransfections of Huh7; nevertheless, monotransfections of these cells by CPT with membrane shock afforded efficiencies as high as 7%.

One clear advantage of the PEI transfection method over CPT, although beyond the scope of our study, is the ease of use for suspension cell cultures. The Expi293 cell line, widely used for recombinant protein production, can be efficiently transfected using PEI instead of the expensive Expifectamine [29].

CONCLUSIONS

The calcium phosphate method ensures high transfection efficiency in a panel of cell lines widely used for research and biotechnological tasks. Despite its relative technical complexity, its efficiency cannot be affected with inappropriate storage conditions (a major liability in other protocols) and shows highly reproducible results. The use of the calcium phosphate method for the production of lentiviral stocks in HEK293T cells affords excellent yields ($9 \times 10^5$ IFU/mL without concentration, which is comparable with custom-made commercial supplies). The
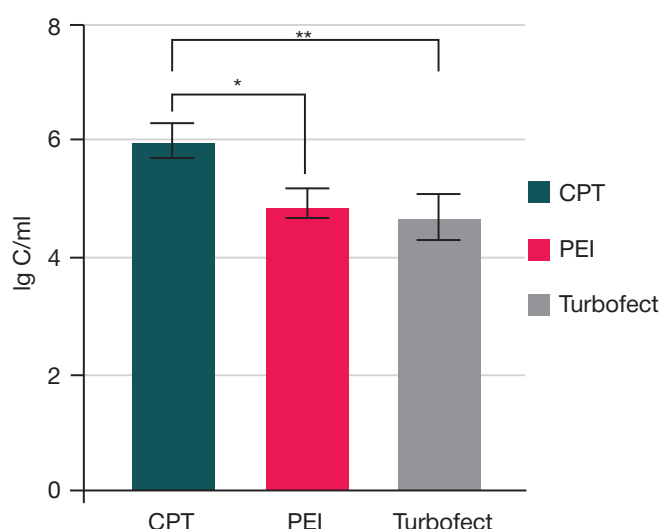


**Fig. 6.** Concentrations of lentiviral stocks produced with HEK293T cells using different transfection methods

cationic transfection with PEI also shows high efficiency in most cell lines, while its protocol is technically unburdened. Handling the reagents in compliance with the storage requirements makes the method easily scalable. The TurboFect protocol ensures acceptable results, although the transfection efficiency is lower; still, the protocol is technically simple and well suited for small research tasks. At the same time, high costs and lengthy delivery times make it an unlikely choice for large-scale projects.

References

1. Kim TK, Eberwine JH. Mammalian cell transfection: the present and the future. Analytical and Bioanalytical Chemistry. 2010; 397: 3173–8.
2. Teixeira AP, Stucheli P, Auslander S, Auslander D, Schonenberger P, Hurlemann S, et al. CelloSelect — A synthetic cellobiose metabolic pathway for selection of stable transgenic CHO cell lines. Metabolic Engineering. 2022; 70: 23–30.
3. Gu L, Kitamura M. Sensitive detection and monitoring of senescence-associated secretory phenotype by SASP-RAP assay. PLoS One. 2012; 7: e52305.
4. Miura M, Yuan J. Transient transfection assay of cell death genes. Methods in Enzymology. 2000; 322: 480–92.
5. Strebel A, Harr T, Bachmann F, Wernli M, Erb P. Green fluorescent protein as a novel tool to measure apoptosis and necrosis. Cytometry. 2001; 43: 126–33.
6. Boulaiz H, Prados J, Melguizo C, Garcia AM, Marchal JA, Ramos JL, et al. Inhibition of growth and induction of apoptosis in human breast cancer by transfection of gef gene. British Journal of Cancer. 2003; 89: 192–8.
7. Vaheri A, Pagano JS. Infectious poliovirus RNA: a sensitive method of assay. Virology. 1965; 27: 434–6.
8. Hoffmann E, Neumann G, Kawaoka Y, Hobom G, Webster RG. A DNA transfection system for generation of influenza A virus from eight plasmids. Proc Natl Acad Sci USA. 2000; 97: 6108–13.
9. Weber K, Bartsch U, Stocking C, Fehse B. A multicolor panel of novel lentiviral "gene ontology" (LeGO) vectors for functional gene analysis. Molecular Therapy. 2008; 16: 698–706.
10. Longo PA, Kavran JM, Kim MS, Leahy DJ. Transient mammalian cell transfection with polyethylenimine (PEI). Methods in Enzymology. 2013; 529: 227–40.
11. Jin L, Zeng X, Liu M, Deng Y, He N. Current progress in gene delivery technology based on chemical methods and nano-carriers. Theranostics. 2014; 4: 240–55.
12. Rahimi P, Mobarakeh VI, Kamalzare S, SajadianFard F, Vahabpour R, Zabihollahi R. Comparison of transfection efficiency of polymer-based and lipid-based transfection reagents. Bratisl Lek Listy. 2018; 119: 701–05.
13. Graham FL,van der Eb AJ. A new technique for the assay of infectivity of human adenovirus 5 DNA. Virology. 1973; 52: 456–67.
14. Orrantia E,Chang PL. Intracellular distribution of DNA internalized through calcium phosphate precipitation. Experimental Cell Research. 1990; 190: 170–4.
15. Kingston RE, Chen CA, Okayama H. Calcium phosphate transfection. Current protocols in immunology. 2001; 31: 1–9.
16. Olton D, Li J, Wilson ME, Rogers T, Close J, Huang L, et al. Nanostructured calcium phosphates (NanoCaPs) for non-viral gene delivery: influence of the synthesis parameters on transfection efficiency. Biomaterials. 2007; 28: 1267–79.
17. Pedraza CE, Bassett DC, McKee MD, Nelea V, Gbureck U, Barralet JE. The importance of particle size and DNA condensation salt for calcium phosphate nanoparticle transfection. Biomaterials. 2008; 29: 3384–92.
18. Sokolova VV, Radtke I, Heumann R, Epple M. Effective transfection of cells with multi-shell calcium phosphate-DNA nanoparticles. Biomaterials. 2006; 27: 3147–53.
19. Cao X, Deng W, Wei Y, Su W, Yang Y, Wei Y, et al. Encapsulation of plasmid DNA in calcium phosphate nanoparticles: stem cell uptake and gene transfer efficiency. Int J Nanomedicine. 2011; 6: 3335–49.
20. Nouri A, Castro R, Santos JL, Fernandes C, Rodrigues J, Tomas H. Calcium phosphate-mediated gene delivery using simulated body fluid (SBF). Int J Pharm. 2012; 434: 199–208.
21. Baker A, Saltik M, Lehrmann H, Killisch I, Mautner V, Lamm G, et al. Polyethylenimine (PEI) is a simple, inexpensive and effective reagent for condensing and linking plasmid DNA to adenovirus for gene delivery. Gene Therapy. 1997; 4: 773–82.
22. Moghimi SM, Symonds P, Murray JC, Hunter AC, Debska G, Szewczyk

A. A two-stage poly(ethylenimine)-mediated cytotoxicity: implications for gene transfer/therapy. Molecular Therapy. 2005; 11: 990–5.

23. Liu T, Yu X, Kan B, Guo Q, Wang X, Shi S, et al. Enhanced gene delivery using biodegradable poly(ester amine)s (PEAs) based on low-molecular-weight polyethylenimine and poly(epsilon-caprolactone)-pluronic-poly(epsilon-caprolactone). J Biomed Nanotechnol. 2010; 6: 351–9.

24. Fukumoto Y, Obata Y, Ishibashi K, Tamura N, Kikuchi I, Aoyama K, et al. Cost-effective gene transfection by DNA compaction at pH 4.0 using acidified, long shelf-life polyethylenimine. Cytotechnology. 2010; 62: 73–82.

25. Yahalom-Ronen Y, Tamir H, Melamed S, Politi B, Shifman O, Achdout H, et al. A single dose of recombinant VSV-G-spike vaccine provides protection against SARS-CoV-2 challenge. Nat Commun. 2020; 11: 6402.

26. Kwon M,Firestein BL. DNA transfection: calcium phosphate method. Methods Mol Biol. 2013; 1018: 107–10.

27. Chumakov SP, Kravchenko JE, Prassolov VS, Frolova EI, Chumakov PM. Efficient downregulation of multiple mRNA targets with a single shRNA-expressing lentiviral vector. Plasmid. 2010; 63: 143–9.

28. Hasan MM, Ragnarsson L, Cardoso FC, Lewis RJ. Transfection methods for high-throughput cellular assays of voltage-gated calcium and sodium channels involved in pain. PLoS One. 2021; 16: e0243645.

29. Fang XT, Sehlin D, Lannfelt L, Syvanen S, Hultqvist G. Efficient and inexpensive transient expression of multispecific multivalent antibodies in Expi293 cells. Biol Proced Online. 2017; 19: 11.

## Литература

1. Kim TK, Eberwine JH. Mammalian cell transfection: the present and the future. Analytical and Bioanalytical Chemistry. 2010; 397: 3173–8.

2. Teixeira AP, Stucheli P, Auslander S, Auslander D, Schonenberger P, Hurlemann S, et al. CelloSelect — A synthetic cellobiose metabolic pathway for selection of stable transgenic CHO cell lines. Metabolic Engineering. 2022; 70: 23–30.

3. Gu L, Kitamura M. Sensitive detection and monitoring of senescence-associated secretory phenotype by SASP-RAP assay. PLoS One. 2012; 7: e52305.

4. Miura M, Yuan J. Transient transfection assay of cell death genes. Methods in Enzymology. 2000; 322: 480–92.

5. Strebel A, Harr T, Bachmann F, Wernli M, Erb P. Green fluorescent protein as a novel tool to measure apoptosis and necrosis. Cytometry. 2001; 43: 126–33.

6. Boulaiz H, Prados J, Melguizo C, Garcia AM, Marchal JA, Ramos JL, et al. Inhibition of growth and induction of apoptosis in human breast cancer by transfection of gef gene. British Journal of Cancer. 2003; 89: 192–8.

7. Vaheri A, Pagano JS. Infectious poliovirus RNA: a sensitive method of assay. Virology. 1965; 27: 434–6.

8. Hoffmann E, Neumann G, Kawaoka Y, Hobom G, Webster RG. A DNA transfection system for generation of influenza A virus from eight plasmids. Proc Natl Acad Sci USA. 2000; 97: 6108–13.

9. Weber K, Bartsch U, Stocking C, Fehse B. A multicolor panel of novel lentiviral "gene ontology" (LeGO) vectors for functional gene analysis. Molecular Therapy. 2008; 16: 698–706.

10. Longo PA, Kavran JM, Kim MS, Leahy DJ. Transient mammalian cell transfection with polyethylenimine (PEI). Methods in Enzymology. 2013; 529: 227–40.

11. Jin L, Zeng X, Liu M, Deng Y, He N. Current progress in gene delivery technology based on chemical methods and nano-carriers. Theranostics. 2014; 4: 240–55.

12. Rahimi P, Mobarakeh VI, Kamalzare S, SajadianFard F, Vahabpour R, Zabihollahi R. Comparison of transfection efficiency of polymer-based and lipid-based transfection reagents. Bratisl Lek Listy. 2018; 119: 701–05.

13. Graham FL,van der Eb AJ. A new technique for the assay of infectivity of human adenovirus 5 DNA. Virology. 1973; 52: 456–67.

14. Orrantia E,Chang PL. Intracellular distribution of DNA internalized through calcium phosphate precipitation. Experimental Cell Research. 1990; 190: 170–4.

15. Kingston RE, Chen CA, Okayama H. Calcium phosphate transfection. Current protocols in immunology. 2001; 31: 1–9.

16. Olton D, Li J, Wilson ME, Rogers T, Close J, Huang L, et al. Nanostructured calcium phosphates (NanoCaPs) for non-viral gene delivery: influence of the synthesis parameters on transfection efficiency. Biomaterials. 2007; 28: 1267–79.

17. Pedraza CE, Bassett DC, McKee MD, Nelea V, Gbureck U, Barralet JE. The importance of particle size and DNA condensation salt for calcium phosphate nanoparticle transfection. Biomaterials. 2008; 29: 3384–92.

18. Sokolova VV, Radtke I, Heumann R, Epple M. Effective transfection of cells with multi-shell calcium phosphate-DNA nanoparticles. Biomaterials. 2006; 27: 3147–53.

19. Cao X, Deng W, Wei Y, Su W, Yang Y, Wei Y, et al. Encapsulation of plasmid DNA in calcium phosphate nanoparticles: stem cell uptake and gene transfer efficiency. Int J Nanomedicine. 2011; 6: 3335–49.

20. Nouri A, Castro R, Santos JL, Fernandes C, Rodrigues J, Tomas H. Calcium phosphate-mediated gene delivery using simulated body fluid (SBF). Int J Pharm. 2012; 434: 199–208.

21. Baker A, Saltik M, Lehrmann H, Killisch I, Mautner V, Lamm G, et al. Polyethylenimine (PEI) is a simple, inexpensive and effective reagent for condensing and linking plasmid DNA to adenovirus for gene delivery. Gene Therapy. 1997; 4: 773–82.

22. Moghimi SM, Symonds P, Murray JC, Hunter AC, Debska G, Szewczyk A. A two-stage poly(ethylenimine)-mediated cytotoxicity: implications for gene transfer/therapy. Molecular Therapy. 2005; 11: 990–5.

23. Liu T, Yu X, Kan B, Guo Q, Wang X, Shi S, et al. Enhanced gene delivery using biodegradable poly(ester amine)s (PEAs) based on low-molecular-weight polyethylenimine and poly(epsilon-caprolactone)-pluronic-poly(epsilon-caprolactone). J Biomed Nanotechnol. 2010; 6: 351–9.

24. Fukumoto Y, Obata Y, Ishibashi K, Tamura N, Kikuchi I, Aoyama K, et al. Cost-effective gene transfection by DNA compaction at pH 4.0 using acidified, long shelf-life polyethylenimine. Cytotechnology. 2010; 62: 73–82.

25. Yahalom-Ronen Y, Tamir H, Melamed S, Politi B, Shifman O, Achdout H, et al. A single dose of recombinant VSV-G-spike vaccine provides protection against SARS-CoV-2 challenge. Nat Commun. 2020; 11: 6402.

26. Kwon M,Firestein BL. DNA transfection: calcium phosphate method. Methods Mol Biol. 2013; 1018: 107–10.

27. Chumakov SP, Kravchenko JE, Prassolov VS, Frolova EI, Chumakov PM. Efficient downregulation of multiple mRNA targets with a single shRNA-expressing lentiviral vector. Plasmid. 2010; 63: 143–9.

28. Hasan MM, Ragnarsson L, Cardoso FC, Lewis RJ. Transfection methods for high-throughput cellular assays of voltage-gated calcium and sodium channels involved in pain. PLoS One. 2021; 16: e0243645.

29. Fang XT, Sehlin D, Lannfelt L, Syvanen S, Hultqvist G. Efficient and inexpensive transient expression of multispecific multivalent antibodies in Expi293 cells. Biol Proced Online. 2017; 19: 11.

# ISOFORMS OF MIR-148A AND MIR-203A ARE PUTATIVE SUPPRESSORS OF COLORECTAL CANCER

Nersisyan SA[1,2] ✉

[1] National Research University Higher School of Economics (HSE), Moscow, Russia

[2] Institute of Molecular Biology (IMB) of the National Academy of Sciences of the Republic of Armenia, Yerevan, Armenia

MicroRNAs are short non-coding molecules which regulate translation in a gene-specific manner. MicroRNA isoforms that differ by few extra or missing nucleotides at the 5'-terminus (5'-isomiR) show strikingly different target specificity. This study aimed to identify functional roles of 5'-isomiR in colorectal cancers. Transcriptomic targets of microRNA isoforms were predicted using bioinformatics tools miRDB and TargetScan. The sets of putative targets identified for 5'-isomiR were integrated with mRNA and microRNA sequencing data for primary colorectal tumors retrieved from The Cancer Genome Atlas Colon Adenocarcinoma (TCGA-COAD) database. The network of interactions among miRNA, their targets and transcription factors was built using the miRGTF-net algorithm. The results indicate that microRNA isoforms highly expressed in colorectal cancer and differing by a single nucleotide position at the 5'-terminus have ≤ 30% common targets. The regulatory network of interactions enables identification of the most engaged microRNA isoforms. Anti-correlated expression levels of canonical microRNA hsa-miR-148a-3p and its putative targets including *CSF1*, *ETS1*, *FLT1*, *ITGA5*, *MEIS1*, *MITF* and *RUNX2* proliferation regulators suggest an anti-tumor role for this molecule. The canonical microRNA hsa-miR-203a-3p|0 and its 5'-isoform bind different sets of anti-correlated putative targets, although both of them interact with genes involved in the epithelial-mesenchymal transition: *SNAI2* and *TNC*.

# ИЗОФОРМЫ микроРНК MIR-148A И MIR-203A ПРЕДПОЛОЖИТЕЛЬНО ИГРАЮТ РОЛЬ СУПРЕССОРОВ КОЛОРЕКТАЛЬНОГО РАКА

С. А. Нерсисян[1,2] ✉

[1] Национальный исследовательский университет «Высшая школа экономики», Москва, Россия

[2] Институт молекулярной биологии Национальной академии наук Республики Армения, Ереван, Армения

Изоформы микроРНК — класс коротких некодирующих РНК, осуществляющих регуляцию экспрессии генов. Изоформы микроРНК отличаются от канонических микроРНК несколькими нуклеотидами на концах молекулы, причем вариации с 5′-концов микроРНК изменяют множество генов-мишеней. Целью работы было провести анализ функциональной активности 5′-изоформ микроРНК в тканях колоректального рака. Мишени 5′-изоформ микроРНК были предсказаны с помощью биоинформатических программ miRDB и TargetScan. Полученные данные о мишенях 5′-изоформ микроРНК были интегрированы с данными секвенирования мРНК и изоформ микроРНК образцов первичных колоректальных опухолей проекта The Cancer Genome Atlas Colon Adenocarcinoma. Для построения сети взаимодействий изоформ микроРНК, их мишеней и транскрипционных факторов по интегрированным данным использовали алгоритм miRGTF-net. Показано, что высокоэкспрессированные при колоректальном раке изоформы микроРНК, различающиеся одним нуклеотидом на 5′-конце молекулы, имеют не более 30% общих мишеней. В регуляторной сети взаимодействий выявлены наиболее активные изоформы микроРНК. Уровни экспрессий канонической микроРНК hsa-miR-148a-3p и ее предсказанных мишеней, являющихся регуляторами клеточной пролиферации (*CSF1*, *ETS1*, *FLT1*, *ITGA5*, *MEIS1*, *MITF*, *RUNX2*), были значимо отрицательно коррелированы, откуда может следовать противоопухолевая роль данной молекулы. Каноническая микроРНК hsa-miR-203a-3p|0 и ее 5′-изоформа были антикоррелированы с различными генами-мишенями, но при этом обе потенциально подавляли экспрессию генов, вовлеченных в эпителиально-мезенхимный переход: *SNAI2* и *TNC*.

MicroRNAs are short non-coding RNA molecules which regulate gene expression at the post-transcriptional level [1]. Effective binding of microRNA to their target transcripts depends on perfect match between seed-region (nucleotides 2–7 counting from the 5′-terminus of microRNA) and its complementary site in mRNA [2]. The microRNA-mRNA binding inhibits translation and may also promote mRNA degradation provided a sufficient number of complementary bonds outside the seed-region [2]. Various microRNAs act as tumor suppressors and oncogenes in many cancers [3–5].

MicroRNA processing endonucleases Drosha and Dicer may cleave the long precursor molecules with certain imprecision, giving rise to microRNA isoforms with few extra or missing nucleotides at the termini [6]. Meanwhile, the exact positioning of

5′-terminus is pivotal for target specificity, as it defines the seed-region. MicroRNA 5'-isoforms (5'-isomiR) differing by a single extra or missing terminal nucleotide may target quite different sets of transcripts compared with the prototype canonical microRNA.

Colorectal cancer (CRC) is the third most common and the second most fatal cancer globally [7]. MicroRNAs have been widely implicated in the mechanisms of CRC progression and metastasis. For instance, miR-200 family has been shown to inhibit *ZEB1* and *ZEB2* genes that encode key transcription factors (TF) of the epithelial-mesenchymal transition (EMT) characteristic of CRC [8]. Accordingly, suppression of miR-200 at the level of transcription and/or processing facilitates EMT and metastasis [8]. MicroRNA expression profiles are actively employed as a source of putative CRC markers, both diagnostic and prognostic [9]. Contemporary research on the role of microRNA isoforms in CRC is focused on comparative evaluation of their expression levels in tumors and matching healthy tissues [10]. To the best of our knowledge, functional activity of 5'-isomiR in CRC has remained outside the focus.

A great diversity of microRNAs and at least an order of magnitude higher number of regulatory interactions they participate in (with about 200 targets per microRNA on average [1]) invoke the use of bioinformatic approaches. One of them is building and analysis of regulatory networks, with microRNA molecules and genes represented by graph's vertices and the interactions represented by edges between particular microRNAs and their targets [11]. The construction of regulatory networks is traditionally based on two sources: (1) knowledge databases of interactions between different types of molecules and (2) correlation analysis of mRNA and microRNA expression levels in clinical samples. We have previously developed an algorithm that allows integration of these two sources in a single network with the addition of TF as another class of major regulatory molecules [12]. The miRGTF-net algorithm affords complete and reliable description of intracellular interaction landscapes in cell/tissue types of interest.

This study aimed to identify functional roles of 5′-isomiR in CRC by integration of the gene expression profiles, sequence-based target prediction and TF activity data using the miRGTF-net algorithm.

METHODS

### Target prediction for microRNA isoforms

Pri-microRNA hairpin sequences and canonical Drosha and Dicer cleavage sites were retrieved from miRBase version 21 (https://www.mirbase.org). Designation of 5′-isomiR uses standard nomenclature: a digit after the vertical slash indicates a 5′ to 3′ shift in the cleavage position with regard to the canonical variant. For example, hsa-miR-10a-5p|+1 corresponds to the canonical hsa-miR-10a-5p devoid of the first nucleotide counting from the 5′-terminus.

For the target prediction, canonical microRNA and isomiR sequences were loaded in miRDB version 6.0 [13] and TargetScan version 7.2 [2]. For miRDB, putative targets with prediction scores ≥ 80 were qualified as valid in accordance with the developer's recommendations. The TargetScan predictions were tailored to the number of miRDB predictions by choosing the appropriate number of the strongest interactions for each microRNA isoform.

### Collection and analysis of sequencing data for mRNA and microRNA isoforms

The publicly available raw sequencing data for mRNA and miRNA isoforms were retrieved from The Cancer Genome Atlas Colon Adenocarcinoma (TCGA-COAD) project available at the Genomic Data Commons Data Portal (https://portal.gdc.cancer.gov/). The data were normalized in the edgeR package version 3.30.0 [14] using the Trimmed Mean of M-values (TMM) normalization algorithm yielding TMM-normalized Reads Per Kilobase of transcript per Million mapped reads (TMM-RPKM) matrices for mRNA expression and TMM-normalized Reads Per Million mapped reads (TMM-RPM) matrices for microRNA expression.

The 5'-isomiR expression matrices were sorted by total expression in the studied samples and the cumulative distribution functions were calculated. The minimal set of 5′-isomiR covering 95% of all sequencing reads were qualified as highly expressed and used in further analysis.

### Construction of a regulatory network of interactions among microRNA isoforms, their targets and transcription factors

The miRGTF-net algorithm [12] was applied to build a regulatory network of interactions among microRNA isoforms, their targets and transcription factors. A major advantage of the algorithm is the ability to integrate mRNA and miRNA isoform expression data retrieved from TCGA-COAD with biological knowledge databases including:

– TRRUST version 2 (https://www.grnpedia.org/trrust/): interactions between TF and genes;

– TransmiR version 2 (http://www.cuilab.cn/transmir): interactions between TF and microRNA;

– miRDB, TargetScan (see previous sections): interactions between microRNA isoforms and their targets;

– miRIAD (https://www.miriad-database.org): coexpression of host genes and their intronic microRNA.

The analysis involved a canonical sequence of steps of the miRGTF-net algorithm briefly described as follows. At first we built a network based on the interactions retrieved from databases. Then we calculated Spearman correlation coefficients based on the corresponding expression levels retrieved from TCGA-COAD. Edges connecting molecules with weakly correlated expression levels were eliminated (cutoff for the absolute value of Spearman's correlation was determined as the 0.9 quantile of the correlation distribution). Edges between microRNA isoforms and their putative targets showing positive correlations and edges between host genes and their intronic microRNA showing negative correlations were removed as well.

Next, we evaluated the strength of the linear relationships between expression of each vertex and its direct regulators. The corresponding linear models were built with the ridge regression method. Model quality was evaluated by the coefficient of determination ($R^2$) and strength and direction of regulation were evaluated using standardized regression coefficients (β-coefficients). The vertices and the edges were filtered using the default threshold values of miRGTF-net: β-coefficient absolute value ≥ 0.3 and 90% of the highest R2. Accordingly, the final network contained vertices corresponding to regulators of expression along with regulated entities (genes and microRNA isoforms).

The search of strongly connected components was carried out using the NetworkX package version 2.8 (https://networkx.org). The regulatory networks were visualized in Gephi (https://gephi.org) and yED Graph Editor (yWorks GmbH; Germany).

### Functional enrichment analysis

Functional annotation of gene sets (targets of microRNA isoforms) was carried out using DAVID web service version
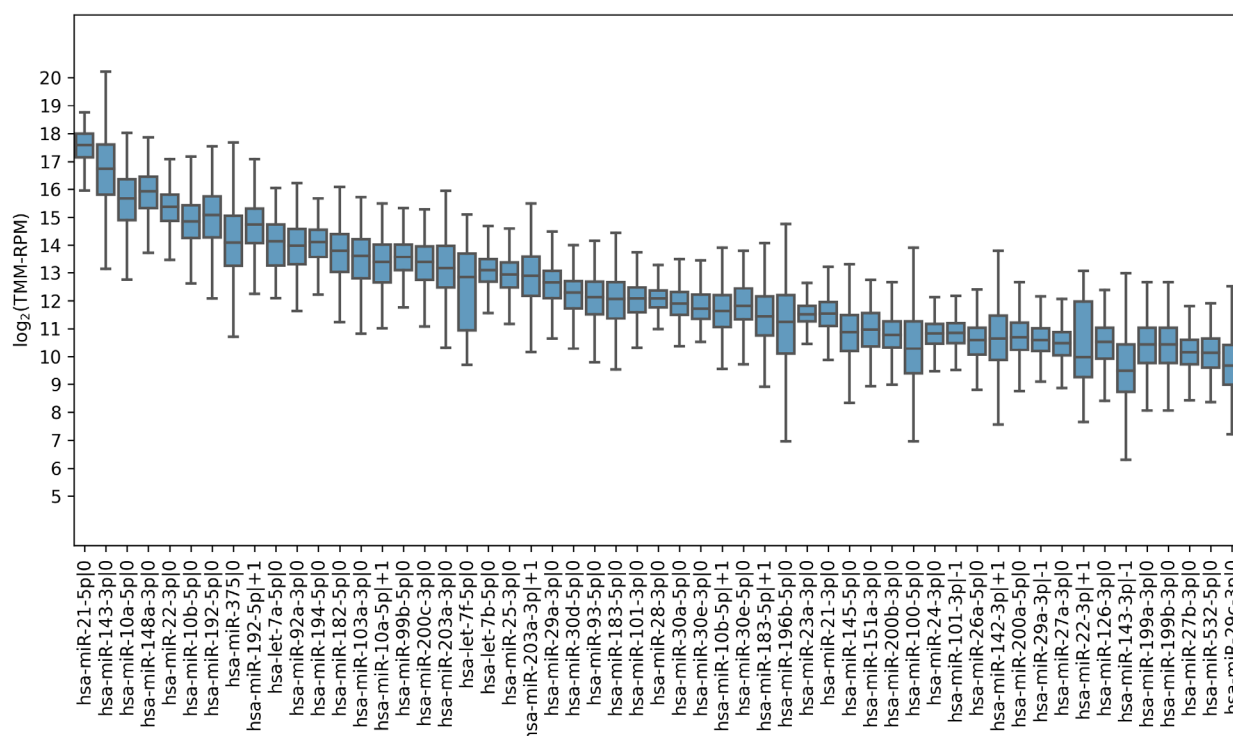
**Fig. 1.** Expression distributions for 55 most highly expressed microRNA 5'-isoforms in a sample of colorectal cancer tissues. Horizontal lines in the boxes are median values, box limits correspond to lower and upper quartiles, whisker termini correspond to minimal and maximal values

12/2021 [15] and Gene Ontology (GO) biological pathway descriptions [16].

RESULTS

**Expression of microRNA isoforms in CRC samples**

The analyzed TCGA-COAD dataset contained expression profiles of mRNA and 5′-isoforms of microRNA in a sample of 426 primary CRC tumor specimens. We identified a total of 55 highly expressed microRNA isoforms, 10 of them non-canonical (Fig. 1). Two of the identified non-canonical 5′-isomiR species accounted for over 1% of total microRNA expression each: hsa-miR-192-5p|+1 (2.4%) and hsa-miR-10a-5p|+1 (1.3%).

A shift of the 5′-terminus in microRNA results in altered seed-region of the mature molecule with a major effect on the putative target scope. Sequences of the identified canonical and non-canonical microRNA isoforms were used for biocomputational prediction of their targets. As expected, microRNA isoforms differing by a single extra nucleotide at the 5'-terminus had only slightly overlapping sets of targets. For example, the canonical hsa-miR-10a-5p and its 5′-isoform without one terminal nucleotide had only 11 common targets in a union of 267 (4,1%) (see Table). The maximal proportion of common targets was observed for hsa-miR-29a-3p and its longer isoform: 246 common targets in a union of 788 (31.2%).

**Regulatory network of interactions among microRNA isoforms, their targets and transcription factors**

At the next step of analysis, we constructed a regulatory network of interactions for CRC cells. The miRGTF-net algorithm enables the construction of such networks by integrating two types of data: (1) biologically substantiated interactions from biological knowledge databases and (2) mRNA and microRNA expression levels measured in tumor samples. The regulatory network contained four types of interactions:

– TF regulates protein-coding gene expression;
– TF regulates microRNA expression;
– microRNA isoform regulates protein-coding gene expression;
– protein-coding host gene is coexpressed with its intronic microRNA

The transcriptomic data for mRNA and microRNA isoforms retrieved from TCGA-COAD were used to look for interactions supported by significant correlations in the studied sample of tumor specimens.

The constructed network encompassed 333 molecules: 24 microRNA (5′-isoforms counted), 166 TF and 143 non-TF coding genes (Fig. 2). Of a total of 456 interactions, 42 represented inhibition of target genes by microRNA isoforms, 413 represented regulation of protein-coding and microRNA gene expression by TF and just a single interaction (between *HOXB3* and hsa-mir-10a) represented coexpression of a host gene and its intronic microRNA.

The highest number of negatively correlated targets (seven) was identified for the canonical hsa-miR-148a-3p. The list included known oncogenes including proliferation regulators and markers *(CSF1, ETS1, FLT1, MEIS1, MITF* and *RUNX2*; GO:0008284 — positive regulation of cell proliferation) and integrin-encoding gene *ITGA5* involved in regulation of cell proliferation, invasion and migration by transmitting signals into cells [17]. Importantly, hsa-miR-148a-3p was a member of the maximal strongly connected component of the regulatory network (i.e., a subgraph with a directed path between any two of the vertices) straightforwardly associated with EMT and estrogen signaling (Fig. 3). The plausible inhibition of protooncogenes by hsa-miR-148a-3p makes it a putative tumor suppressor in CRC.

A pair of canonical hsa-miR-203a-3p|0 and its 5′-isoform hsa-miR-203a-3p|+1 had the second highest number of putative targets. Amid the absence of negatively correlated common targets, both isoforms were likely to share an anti-tumor functionality by inhibiting expression of oncogenes. For example, expression of canonical hsa-miR-203a-3p|0
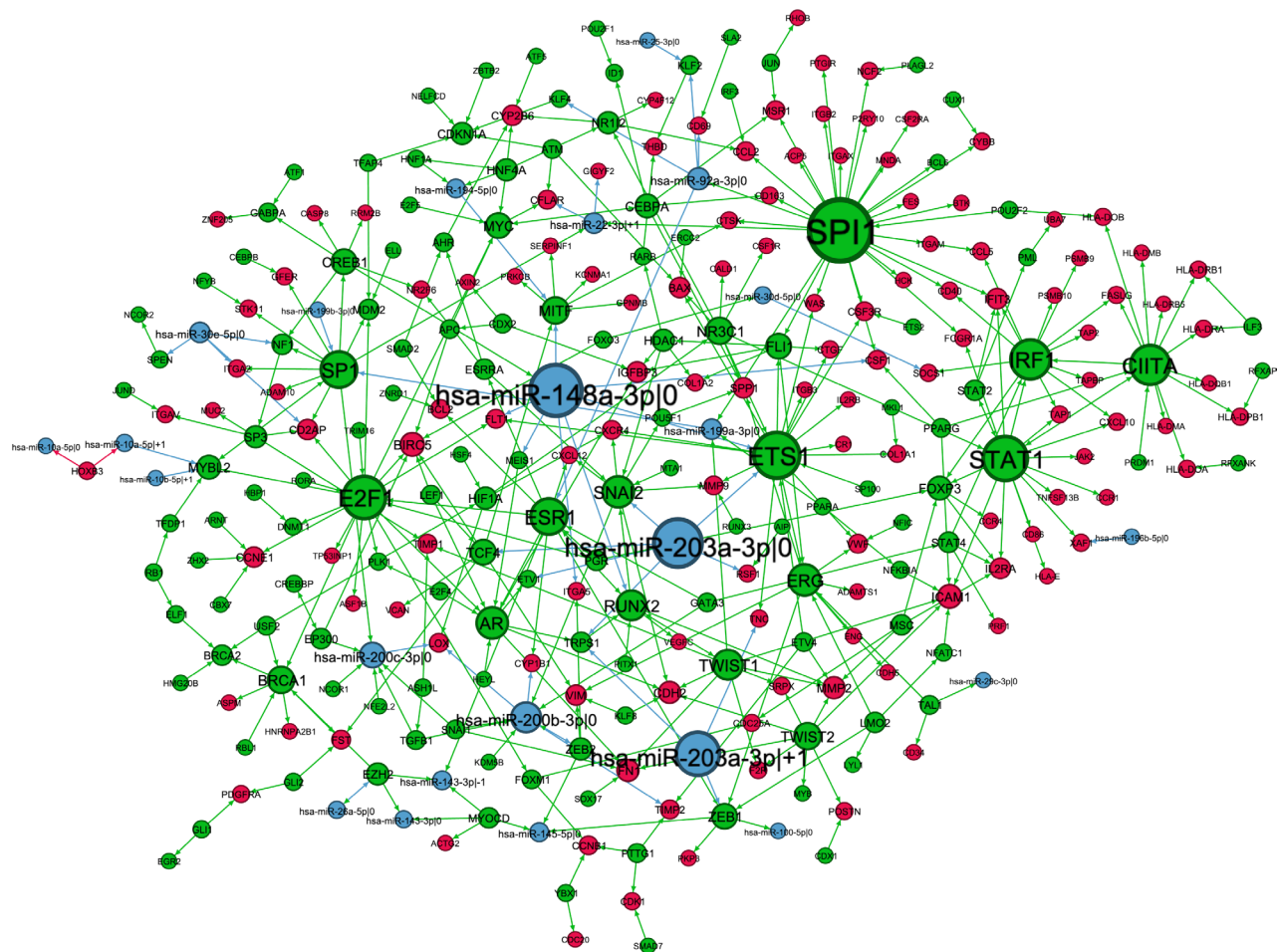
**Fig. 2.** Regulatory network of interactions among microRNA isoforms, their targets and transcription factors. *Blue*, *green* and *red* colors correspond to microRNA 5'-isoforms, transcription factors and target genes, respectively. The edges are colored in accordance with the type of regulator. The vertex sizes are linearly related to degrees

negatively correlated with expression of TF *SNAI2* known to be a prominent genetic driver in EMT [18], whereas its non-canonical 5′-isoform hsa-miR-203a-3p|+1 was characterized as a putative regulator of *TNC* — an extracellular matrix protein-encoding gene which also plays a key role in EMT characteristic of CRC [19].

DISCUSSION

The study applied bioinformatics analysis to assess the functional activity of 5′-isomiR in malignant colorectal tumors. The results indicate that microRNA isoforms differing by a single extra nucleotide at the 5'-terminus have limited number of common targets with a maximum overlap of 31.2%. The most active regulators identified among microRNA included hsa-miR-148a-3p (canonical) and two 5'-isoforms of hsa-miR-203a-3p: hsa-miR-203a-3p|0 (canonical) and hsa-miR-203a-3p|+1. Noteworthy, all three microRNAs were identified as putative inhibitors of pro-tumor gene expression, though the intersection of anti-correlated targets for canonical miR-203a and its 5′-isoform was empty.

The functional activity of 5′-isomiR was previously studied in the context of breast cancer. Two 5′-isoforms of hsa-miR-183-5p were shown to exert different transcriptomic effects in MDA-MB-231 cells; moreover, certain target genes of top clinical significance (*EGFR*, *NRAS*) were indirectly regulated by these isoforms with the effects being opposite [20]. To our knowledge, the current study is the first to deal with target scopes of 5′-isomiR in CRC.

Of seven putative targets of hsa-miR-148a-3p selected by us in this study, four genes have been experimentally validated *in vitro* — *CSF1*, *ITGA5* [21], *MITF* [22] and *RUNX2* [23]. In our own experimental setting, the hypoxia-induced inhibition of hsa-miR-148a-3p expression in CRC cell lines HT-29 and Caco-2 resulted in increased expression of the target gene *ITGA5* [24]. Other studies demonstrate the pro-apoptotic effect of miR-148a and the corresponding suppressive effects on proliferation, migration and invasiveness of CRC cells *in vitro* conferred through Bcl-2 [25], ErbB3 [26] and WNT10b [27] inhibition. Apart from CRC, the role of hsa-miR-148a-3p as a suppressor of tumor cell proliferation was confirmed in the contexts of breast, prostate and urothelial cancers [28]. Thus, our *in silico* findings on the anti-tumor role of miR-148a show good agreement with the published experimental evidence.

A similar picture is observed for the canonical form of miR-203a: the inferred interaction between miR-203a and *SNAI2* have been already validated *in vitro* [29], whereas overexpression of miR-203a in CRC cell lines has been shown to suppress migration and invasiveness [30]. Thus, the newly identified putative target scope of the non-canonical hsa-miR-203a-3p|+1 is consistent with the established functional profile of the canonical prototype microRNA.

CONCLUSIONS

Construction and analysis of regulatory networks of interactions by tailored bioinformatics tools provide a useful key to the functional activity of 5'-isomiR in colorectal cancer cells. We
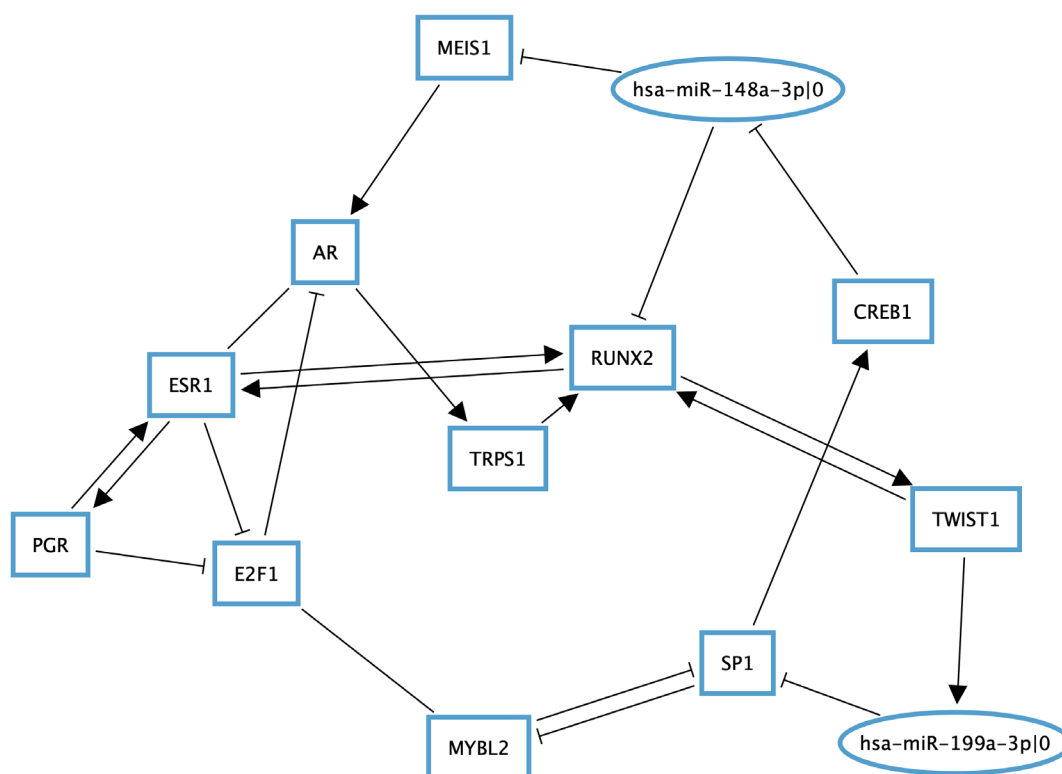
**Fig. 3.** Strongly connected subgraph of interactions between microRNA 5'-isoforms and transcription factors. *Ellipses* and *rectangles* denote microRNA isoforms and transcription factors, respectively. *Arrows* correspond to expression activation, *blunt*-end *lines* correspond to expression inhibition

demonstrate that 5′-isoforms of hsa-miR-203a-3p may exert similar anti-tumor effects by regulating completely different sets of target genes. Further experimental studies, e.g., overexpression of 5′-isoforms of hsa-miR-203a-3p and other microRNA *in vitro* and *in vivo*, will be required to understand molecular mechanisms of colorectal tumor development and progression.

**Table.** Numbers of putative targets for highly expressed canonical microRNAs and their 5'-isoforms

| Canonical microRNA | 5'-Isoform | Canonical microRNA, number of targets | 5'-Isoform, number of targets | Number of common targets |
|---|---|---|---|---|
| hsa-miR-10a-5p\|0 | hsa-miR-10a-5p\|+1 | 175 | 103 | 11 |
| hsa-miR-10b-5p\|0 | hsa-miR-10b-5p\|+1 | 173 | 102 | 12 |
| hsa-miR-22-3p\|0 | hsa-miR-22-3p\|+1 | 235 | 235 | 42 |
| hsa-miR-29a-3p\|0 | hsa-miR-29a-3p\|-1 | 671 | 363 | 246 |
| hsa-miR-101-3p\|0 | hsa-miR-101-3p\|-1 | 632 | 694 | 267 |
| hsa-miR-142-3p\|0 | hsa-miR-142-3p\|+1 | 254 | 359 | 33 |
| hsa-miR-143-3p\|0 | hsa-miR-143-3p\|-1 | 351 | 205 | 118 |
| hsa-miR-183-5p\|0 | hsa-miR-183-5p\|+1 | 366 | 396 | 63 |
| hsa-miR-192-5p\|0 | hsa-miR-192-5p\|+1 | 68 | 76 | 16 |
| hsa-miR-203a-3p\|0 | hsa-miR-203a-3p\|+1 | 573 | 676 | 256 |

### References

1. Lewis BP, Burge CB, Bartel DP. Conserved seed pairing, often flanked by adenosines, indicates that thousands of human genes are microRNA targets. Cell. 2005; 120 (1): 15–20. Available from: http://www.ncbi.nlm.nih.gov/pubmed/15652477.
2. Agarwal V, Bell GW, Nam J-W, Bartel DP. Predicting effective microRNA target sites in mammalian mRNAs. Elife. 2015; 4. Available from: http://www.ncbi.nlm.nih.gov/pubmed/26267216.
3. Garzon R, Calin GA, Croce CM. MicroRNAs in Cancer. Annu Rev Med. 2009; 60 (1): 167–79. Available from: http://www.ncbi.nlm.nih.gov/pubmed/19630570.
4. Nersisyan S, Shkurnikov M, Poloznikov A, Turchinovich A, Burwinkel B, Anisimov N, et al. Post-Processing Algorithm for miRNA Microarray Data. Int J Mol Sci. 2020; 21 (4). Available

from: http://www.ncbi.nlm.nih.gov/pubmed/32059403.
5. Turchinovich A, Tonevitsky AG, Cho WC, Burwinkel B. Check and mate to exosomal extracellular miRNA: new lesson from a new approach. Front Mol Biosci. 2015; 2 (APR): 11. Available from: http://www.ncbi.nlm.nih.gov/pubmed/25988178.
6. Zhiyanov A, Nersisyan S, Tonevitsky A. Hairpin sequence and structure is associated with features of isomiR biogenesis. RNA Biol. 2021; 18 (sup1): 430–8. Available from: http://www.ncbi.nlm.nih.gov/pubmed/34286662.
7. Sung H, Ferlay J, Siegel RL, Laversanne M, Soerjomataram I, Jemal A, et al. Global Cancer Statistics 2020: GLOBOCAN Estimates of Incidence and Mortality Worldwide for 36 Cancers in 185 Countries. CA Cancer J Clin. 2021; 71 (3): 209–49. Available

from: http://www.ncbi.nlm.nih.gov/pubmed/33538338.

8.  Hill L, Browne G, Tulchinsky E. ZEB/miR-200 feedback loop: at the crossroads of signal transduction in cancer. Int J cancer. 2013; 132 (4): 745–54. Available from: http://www.ncbi.nlm.nih.gov/pubmed/22753312.

9.  Chen B, Xia Z, Deng Y-N, Yang Y, Zhang P, Zhu H, et al. Emerging microRNA biomarkers for colorectal cancer diagnosis and prognosis. Open Biol. 2019; 9 (1): 180212. Available from: http://www.ncbi.nlm.nih.gov/pubmed/30958116.

10. Zelli V, Compagnoni C, Capelli R, Corrente A, Cornice J, Vecchiotti D, et al. Emerging Role of isomiRs in Cancer: State of the Art and Recent Advances. Genes (Basel) 2021; 12 (9). Available from: http://www.ncbi.nlm.nih.gov/pubmed/34573429.

11. Galatenko VV, Galatenko AV, Samatov TR, Turchinovich AA, Shkurnikov MY, Makarova JA, et al. Comprehensive network of miRNA-induced intergenic interactions and a biological role of its core in cancer. Sci Rep. 2018; 8 (1): 2418. Available from: http://www.ncbi.nlm.nih.gov/pubmed/29402894.

12. Nersisyan S, Galatenko A, Galatenko V, Shkurnikov M, Tonevitsky A. miRGTF-net: Integrative miRNA-gene-TF network analysis reveals key drivers of breast cancer recurrence. PLoS One. 2021; 16 (4): e0249424. Available from: http://www.ncbi.nlm.nih.gov/pubmed/33852600.

13. Chen Y, Wang X. miRDB: an online database for prediction of functional microRNA targets. Nucleic Acids Res. 2020; 48 (D1): D127–31. Available from: http://www.ncbi.nlm.nih.gov/pubmed/31504780.

14. Robinson MD, McCarthy DJ, Smyth GK. edgeR: a Bioconductor package for differential expression analysis of digital gene expression data. Bioinformatics. 2010; 26 (1): 139–40. Available from: http://www.ncbi.nlm.nih.gov/pubmed/19910308.

15. Sherman BT, Hao M, Qiu J, Jiao X, Baseler MW, Lane HC, et al. DAVID: a web server for functional enrichment analysis and functional annotation of gene lists (2021 update). Nucleic Acids Res. 2022. Available from: http://www.ncbi.nlm.nih.gov/pubmed/35325185.

16. Gene Ontology Consortium. The Gene Ontology resource: enriching a GOld mine. Nucleic Acids Res. 2021; 49 (D1): D325–34. Available from: http://www.ncbi.nlm.nih.gov/pubmed/33290552.

17. Hamidi H, Ivaska J. Every step of the way: integrins in cancer progression and metastasis. Nat Rev Cancer. 2018; 18 (9): 533–48. Available from: http://www.ncbi.nlm.nih.gov/pubmed/30002479.

18. Dudas J, Ladanyi A, Ingruber J, Steinbichler TB, Riechelmann H. Epithelial to Mesenchymal Transition: A Mechanism that Fuels Cancer Radio/Chemoresistance. Cells. 2020; 9 (2). Available from: http://www.ncbi.nlm.nih.gov/pubmed/32059478.

19. Takahashi Y, Sawada G, Kurashige J, Matsumura T, Uchi R, Ueo H, et al. Tumor-derived tenascin-C promotes the epithelial-mesenchymal transition in colorectal cancer cells. Anticancer Res. 2013; 33 (5): 1927–34. Available from: http://www.ncbi.nlm.nih.

20. Telonis AG, Loher P, Jing Y, Londin E, Rigoutsos I. Beyond the one-locus-one-miRNA paradigm: microRNA isoforms enable deeper insights into breast cancer heterogeneity. Nucleic Acids Res. 2015; 43 (19): 9158–75. Available from: http://www.ncbi.nlm.nih.gov/pubmed/26400174.

21. Cimino D, De Pittà C, Orso F, Zampini M, Casara S, Penna E, et al. miR148b is a major coordinator of breast cancer progression in a relapse-associated microRNA signature by targeting ITGA5, ROCK1, PIK3CA, NRAS, and CSF1. FASEB J. 2013; 27 (3): 1223–35. Available from: http://www.ncbi.nlm.nih.gov/pubmed/23233531.

22. Haflidadóttir BS, Bergsteinsdóttir K, Praetorius C, Steingrímsson E. miR-148 regulates Mitf in melanoma cells. PLoS One. 2010; 5 (7): e11574. Available from: http://www.ncbi.nlm.nih.gov/pubmed/20644734.

23. Liu H, Su H, Wang X, Hao W. MiR-148a regulates bone marrow mesenchymal stem cells-mediated fracture healing by targeting insulin-like growth factor 1. J Cell Biochem. 2018. Available from: http://www.ncbi.nlm.nih.gov/pubmed/30335895.

24. Nersisyan S, Galatenko A, Chekova M, Tonevitsky A. Hypoxia-Induced miR-148a Downregulation Contributes to Poor Survival in Colorectal Cancer. Front Genet. 2021; 12: 662468. Available from: http://www.ncbi.nlm.nih.gov/pubmed/34135940.

25. Zhang H, Li Y, Huang Q, Ren X, Hu H, Sheng H, et al. MiR-148a promotes apoptosis by targeting Bcl-2 in colorectal cancer. Cell Death Differ. 2011; 18 (11): 1702–10. Available from: http://www.ncbi.nlm.nih.gov/pubmed/21455217.

26. Zhao W, Zheng J, Wei G, Yang K, Wang G, Sun X. miR-148a inhibits cell proliferation and migration through targeting ErbB3 in colorectal cancer. Oncol Lett. 2019; 18 (3): 2530–6. Available from: http://www.ncbi.nlm.nih.gov/pubmed/31402949.

27. Shi L, Xi J, Xu X, Peng B, Zhang B. MiR-148a suppressed cell invasion and migration via targeting WNT10b and modulating β-catenin signaling in cisplatin-resistant colorectal cancer cells. Biomed Pharmacother. 2019; 109: 902–9. Available from: http://www.ncbi.nlm.nih.gov/pubmed/30551544.

28. Li Y, Deng X, Zeng X, Peng X. The Role of Mir-148a in Cancer. J Cancer. 2016; 7 (10): 1233–41. Available from: http://www.ncbi.nlm.nih.gov/pubmed/27390598.

29. Ma X, Li L, Jia T, Chen M, Liu G, Li C, et al. miR-203a controls keratinocyte proliferation and differentiation via targeting the stemness-associated factor ΔNp63 and establishing a regulatory circuit with SNAI2. Biochem Biophys Res Commun. 2017; 491 (2): 241–9. Available from: http://www.ncbi.nlm.nih.gov/pubmed/28754589.

30. Qian Z, Gong L, Mou Y, Han Y, Zheng S. MicroRNA-203a-3p is a candidate tumor suppressor that targets thrombospondin 2 in colorectal carcinoma. Oncol Rep. 2019; 42 (5): 1825–32. Available from: http://www.ncbi.nlm.nih.gov/pubmed/31545460.

## Литература

1.  Lewis BP, Burge CB, Bartel DP. Conserved seed pairing, often flanked by adenosines, indicates that thousands of human genes are microRNA targets. Cell. 2005; 120 (1): 15–20. Available from: http://www.ncbi.nlm.nih.gov/pubmed/15652477.

2.  Agarwal V, Bell GW, Nam J-W, Bartel DP. Predicting effective microRNA target sites in mammalian mRNAs. Elife. 2015; 4. Available from: http://www.ncbi.nlm.nih.gov/pubmed/26267216.

3.  Garzon R, Calin GA, Croce CM. MicroRNAs in Cancer. Annu Rev Med. 2009; 60 (1): 167–79. Available from: http://www.ncbi.nlm.nih.gov/pubmed/19630570.

4.  Nersisyan S, Shkurnikov M, Poloznikov A, Turchinovich A, Burwinkel B, Anisimov N, et al. Post-Processing Algorithm for miRNA Microarray Data. Int J Mol Sci. 2020; 21 (4). Available from: http://www.ncbi.nlm.nih.gov/pubmed/32059403.

5.  Turchinovich A, Tonevitsky AG, Cho WC, Burwinkel B. Check and mate to exosomal extracellular miRNA: new lesson from a new approach. Front Mol Biosci. 2015; 2 (APR): 11. Available from: http://www.ncbi.nlm.nih.gov/pubmed/25988178.

6.  Zhiyanov A, Nersisyan S, Tonevitsky A. Hairpin sequence and structure is associated with features of isomiR biogenesis. RNA Biol. 2021; 18 (sup1): 430–8. Available from: http://www.ncbi.nlm.nih.gov/pubmed/34286662.

7.  Sung H, Ferlay J, Siegel RL, Laversanne M, Soerjomataram I, Jemal A, et al. Global Cancer Statistics 2020: GLOBOCAN Estimates of Incidence and Mortality Worldwide for 36 Cancers in 185 Countries. CA Cancer J Clin. 2021; 71 (3): 209–49. Available from: http://www.ncbi.nlm.nih.gov/pubmed/33538338.

8.  Hill L, Browne G, Tulchinsky E. ZEB/miR-200 feedback loop: at the crossroads of signal transduction in cancer. Int J cancer. 2013; 132 (4): 745–54. Available from: http://www.ncbi.nlm.nih.gov/pubmed/22753312.

9.  Chen B, Xia Z, Deng Y-N, Yang Y, Zhang P, Zhu H, et al. Emerging microRNA biomarkers for colorectal cancer diagnosis and prognosis. Open Biol. 2019; 9 (1): 180212. Available from: http://www.ncbi.nlm.nih.gov/pubmed/30958116.

10. Zelli V, Compagnoni C, Capelli R, Corrente A, Cornice J, Vecchiotti D, et al. Emerging Role of isomiRs in Cancer: State of the Art and Recent Advances. Genes (Basel) 2021; 12 (9). Available from:

http://www.ncbi.nlm.nih.gov/pubmed/34573429.

11. Galatenko VV, Galatenko AV, Samatov TR, Turchinovich AA, Shkurnikov MY, Makarova JA, et al. Comprehensive network of miRNA-induced intergenic interactions and a biological role of its core in cancer. Sci Rep. 2018; 8 (1): 2418. Available from: http://www.ncbi.nlm.nih.gov/pubmed/29402894.

12. Nersisyan S, Galatenko A, Galatenko V, Shkurnikov M, Tonevitsky A. miRGTF-net: Integrative miRNA-gene-TF network analysis reveals key drivers of breast cancer recurrence. PLoS One. 2021; 16 (4): e0249424. Available from: http://www.ncbi.nlm.nih.gov/pubmed/33852600.

13. Chen Y, Wang X. miRDB: an online database for prediction of functional microRNA targets. Nucleic Acids Res. 2020; 48 (D1): D127–31. Available from: http://www.ncbi.nlm.nih.gov/pubmed/31504780.

14. Robinson MD, McCarthy DJ, Smyth GK. edgeR: a Bioconductor package for differential expression analysis of digital gene expression data. Bioinformatics. 2010; 26 (1): 139–40. Available from: http://www.ncbi.nlm.nih.gov/pubmed/19910308.

15. Sherman BT, Hao M, Qiu J, Jiao X, Baseler MW, Lane HC, et al. DAVID: a web server for functional enrichment analysis and functional annotation of gene lists (2021 update). Nucleic Acids Res. 2022. Available from: http://www.ncbi.nlm.nih.gov/pubmed/35325185.

16. Gene Ontology Consortium. The Gene Ontology resource: enriching a GOld mine. Nucleic Acids Res. 2021; 49 (D1): D325–34. Available from: http://www.ncbi.nlm.nih.gov/pubmed/33290552.

17. Hamidi H, Ivaska J. Every step of the way: integrins in cancer progression and metastasis. Nat Rev Cancer. 2018; 18 (9): 533–48. Available from: http://www.ncbi.nlm.nih.gov/pubmed/30002479.

18. Dudas J, Ladanyi A, Ingruber J, Steinbichler TB, Riechelmann H. Epithelial to Mesenchymal Transition: A Mechanism that Fuels Cancer Radio/Chemoresistance. Cells. 2020; 9 (2). Available from: http://www.ncbi.nlm.nih.gov/pubmed/32059478.

19. Takahashi Y, Sawada G, Kurashige J, Matsumura T, Uchi R, Ueo H, et al. Tumor-derived tenascin-C promotes the epithelial-mesenchymal transition in colorectal cancer cells. Anticancer Res. 2013; 33 (5): 1927–34. Available from: http://www.ncbi.nlm.nih.gov/pubmed/23645740.

20. Telonis AG, Loher P, Jing Y, Londin E, Rigoutsos I. Beyond the one-locus-one-miRNA paradigm: microRNA isoforms enable deeper insights into breast cancer heterogeneity. Nucleic Acids Res. 2015; 43 (19): 9158–75. Available from: http://www.ncbi.nlm.nih.gov/pubmed/26400174.

21. Cimino D, De Pittà C, Orso F, Zampini M, Casara S, Penna E, et al. miR148b is a major coordinator of breast cancer progression in a relapse-associated microRNA signature by targeting ITGA5, ROCK1, PIK3CA, NRAS, and CSF1. FASEB J. 2013; 27 (3): 1223–35. Available from: http://www.ncbi.nlm.nih.gov/pubmed/23233531.

22. Haflidadóttir BS, Bergsteinsdóttir K, Praetorius C, Steingrímsson E. miR-148 regulates Mitf in melanoma cells. PLoS One. 2010; 5 (7): e11574. Available from: http://www.ncbi.nlm.nih.gov/pubmed/20644734.

23. Liu H, Su H, Wang X, Hao W. MiR-148a regulates bone marrow mesenchymal stem cells-mediated fracture healing by targeting insulin-like growth factor 1. J Cell Biochem. 2018. Available from: http://www.ncbi.nlm.nih.gov/pubmed/30335895.

24. Nersisyan S, Galatenko A, Chekova M, Tonevitsky A. Hypoxia-Induced miR-148a Downregulation Contributes to Poor Survival in Colorectal Cancer. Front Genet. 2021; 12: 662468. Available from: http://www.ncbi.nlm.nih.gov/pubmed/34135940.

25. Zhang H, Li Y, Huang Q, Ren X, Hu H, Sheng H, et al. MiR-148a promotes apoptosis by targeting Bcl-2 in colorectal cancer. Cell Death Differ. 2011; 18 (11): 1702–10. Available from: http://www.ncbi.nlm.nih.gov/pubmed/21455217.

26. Zhao W, Zheng J, Wei G, Yang K, Wang G, Sun X. miR-148a inhibits cell proliferation and migration through targeting ErbB3 in colorectal cancer. Oncol Lett. 2019; 18 (3): 2530–6. Available from: http://www.ncbi.nlm.nih.gov/pubmed/31402949.

27. Shi L, Xi J, Xu X, Peng B, Zhang B. MiR-148a suppressed cell invasion and migration via targeting WNT10b and modulating β-catenin signaling in cisplatin-resistant colorectal cancer cells. Biomed Pharmacother. 2019; 109: 902–9. Available from: http://www.ncbi.nlm.nih.gov/pubmed/30551544.

28. Li Y, Deng X, Zeng X, Peng X. The Role of Mir-148a in Cancer. J Cancer. 2016; 7 (10): 1233–41. Available from: http://www.ncbi.nlm.nih.gov/pubmed/27390598.

29. Ma X, Li L, Jia T, Chen M, Liu G, Li C, et al. miR-203a controls keratinocyte proliferation and differentiation via targeting the stemness-associated factor ΔNp63 and establishing a regulatory circuit with SNAI2. Biochem Biophys Res Commun. 2017; 491 (2): 241–9. Available from: http://www.ncbi.nlm.nih.gov/pubmed/28754589.

30. Qian Z, Gong L, Mou Y, Han Y, Zheng S. MicroRNA-203a-3p is a candidate tumor suppressor that targets thrombospondin 2 in colorectal carcinoma. Oncol Rep. 2019; 42 (5): 1825–32. Available from: http://www.ncbi.nlm.nih.gov/pubmed/31545460.

# TRANSCRIPTIONAL PROFILING OF *MYCOBACTERIUM SMEGMATIS* EXPOSED TO SUBINHIBITORY CONCENTRATIONS OF G4-STABILIZING LIGANDS

Zaychikova MV, Bespiatykh DA, Malakhova MV, Bodoev IN, Vedekhina TS, Veselovsky VA, Klimina KM, Varizhuk AM, Shitikov EA ✉

Federal Research and Clinical Center of Physical-Chemical Medicine, Moscow, Russia

The spread of *Mycobacterium tuberculosis* drug resistance accentuates the demand for anti-tuberculosis drugs with a fundamentally new mechanism of action without conferring cross-resistance. G-quadruplexes (G4, non-canonical DNA structures) are plausible new drug targets. Although G4-stabilizing ligands have been shown to inhibit mycobacterial growth, the exact mechanism of their action is uncertain. The aim of this study was to assess a possible correlation between putative G4 elements in a model mycobacterial strain *M. smegmatis* MC2155 and transcriptomic changes under the action of subinhibitory concentrations of G4 ligands BRACO-19 and TMPyP4. We also planned to compare the results with corresponding data previously obtained by us using higher, inhibitory concentrations of these ligands. For BRACO-19, we identified 589 (316↑; 273↓) and 865 (555↑; 310↓) differentially expressed genes at 5 μM and 10 μM, respectively. For TMPyP4, we observed the opposite trend, the number of differentially expressed genes decreased at higher concentration of the ligand: 754 (337↑; 417↓) and 702 (359↑; 343↓) for 2 μM and 4 μM, respectively. Statistical analysis revealed no correlation between ligand-induced transcriptomic changes and genomic localization of the putative quadruplex-forming sequences. At the same time, the data indicate certain functional specificity of the ligand-mediated transcriptomic effects, with TMPyP4 significantly affecting expression levels of transcription factors and arginine biosynthesis genes and BRACO-19 significantly affecting expression levels of iron metabolism and replication and reparation system genes.

**Keywords:** G-quadruplexes, transcriptomic analysis, *Mycobacterium smegmatis*, *Mycobacterium tuberculosis*, BRACO-19, TMPyP4, antimicrobial therapy

✉ **Correspondence should be addressed:** Egor A. Shitikov
Malaya Pirogovskaya, 1a, Moscow, 119435, Russia; eshitikov@mail.ru

# ВЛИЯНИЕ СУБИНГИБИРУЮЩИХ КОНЦЕНТРАЦИЙ G4-СТАБИЛИЗИРУЮЩИХ ЛИГАНДОВ НА ТРАНСКРИПТОМНЫЙ ПРОФИЛЬ *MYCOBACTERIUM SMEGMATIS*

М. В. Зайчикова, Д. А. Беспятых, М. В. Малахова, И. Н. Бодоев, Т. С. Ведехина, В. А. Веселовский, К. М. Климина, А. М. Варижук, Е. А. Шитиков ✉

Федеральный научно-клинический центр физико-химической медицины Федерального медико-биологического агентства, Москва, Россия

В связи с широким распространением лекарственной устойчивости у *Mycobacterium tuberculosis* особое значение приобретает поиск противотуберкулезных препаратов с принципиально новым механизмом действия, исключающим развитие перекрестной устойчивости. В этом отношении определенный интерес представляют G-квадруплексы (G4) — неканонические структуры ДНК, участвующие в регуляции и поддержании стабильности генома. Показано, что G4-стабилизирующие соединения, лиганды, оказывают ингибирующий эффект на рост микроорганизма, но точный механизм их действия неизвестен. Целью исследования было выявить связь между наличием потенциальных G4 в геноме модельного микроорганизма *M. smegmatis* mc2 155 и изменением транскриптомного профиля под действием субингибирующих концентраций лигандов BRACO-19 и TMPyP4, а также провести сравнительный анализ результатов с данными, полученными нами ранее для ингибирующих концентраций указанных лигандов. Под действием BRACO-19 было идентифицировано 589 (316↑; 273↓) и 865 (555↑; 310↓) дифференциально экспрессированных генов, для 5 и 10 мкМ соответственно. Напротив, в случае с TMPyP4 обнаружено снижение числа дифференциально экспрессированных генов с 754 (337↑; 417↓) до 702 (359↑; 343↓) для концентраций 2 и 4 мкМ соответственно. Статистический анализ не выявил связи между изменением уровня экспрессии генов под действием лигандов и наличием потенциальных квадруплекс-формирующих последовательностей, вне зависимости от локализации G4. Тем не менее было установлено, что TMPyP4 вызывает значительные изменения в экспрессии факторов транскрипции и генах биосинтеза аргинина, а BRACO-19 — в генах метаболизма железа, а также в генах систем репликации и репарации.

**Ключевые слова:** G-квадруплексы, транскриптомный анализ, *Mycobacterium smegmatis*, *Mycobacterium tuberculosis*, BRACO-19, TMPyP4, антимикробная терапия

✉ **Для корреспонденции:** Егор Александрович Шитиков
ул. Малая Пироговская, д. 1а, г. Москва, 119435, Россия; eshitikov@mail.ru

Tuberculosis, caused by *Mycobacterium tuberculosis* complex, is a global problem for modern healthcare. According to WHO expert estimates, in 2020 the number of deaths caused by the disease increased by 100,000 people compared to 2019 and amounted to 1.3 million. The negative trend is expected to continue in the coming years, reflecting a reduction in funding for tuberculosis diagnostics and treatment amid the overall strain on global healthcare due to the COVID-19 pandemic [1].

Despite the use of anti-tuberculosis therapy, the treatment success rate for drug-resistant cases does not exceed 60%. The ubiquitously emerging resistance of mycobacterial strains to new drugs such as linezolid, bedaquiline, clophosamine, etc. [2] accentuates the demand for new anti-tuberculosis drugs with a fundamentally different mechanism of action, as well as new targets for anti-tuberculosis therapy.

One plausible new target is represented by G-quadruplexes (G4) — non-canonical secondary structures formed by guanine-rich DNA and RNA sequences under physiological conditions. Each structural unit of G4 — G-quartet — consists of four guanine bases. The G-quartets are held together by ϖ-ϖ-stacking interactions and additionally stabilized by metal cations [3].

In eukaryotes, such non-canonical nucleic acid structures are fairly well studied and play an important role in genome stability regulation and maintenance [4]. In the 2000s, putative quadruplex sequences (PQS) were discovered in genomes of many bacteria and archaea, but their functional role requires further investigation [5]. G4 are possibly involved in various aspects of bacterial physiology, including survival in adverse environments, pathogenic bacteria interactions with the host, antigenic variation, etc. [6].

G4 ligands, typically compounds with low-molecular weight, bind the quadruplexes and affect their thermal stability, which may displace or reestablish certain protein factors and enzymes functionally associated with DNA or RNA and ultimately interfere with transcription and translation. The best known G4 ligands include acridine derivative BRACO-19 and cationic porphyrin TMPyP4 (Fig. 1). Potential use of G4-ligands as antimicrobials has been demonstrated for *Vibrio cholerae*, *Klebsiella pneumoniae*, *Streptococcus pneumoniae* and *Mycobacterium tuberculosis* [6].

Tuberculosis mycobacteria, with their high GC content and considerable PQS density, represent a promising target for antimicrobial action of G4-stabilizing ligands. Inhibition of their growth by micromolar concentrations of known G4-ligands c-exNDI-2, BRACO-19 and TMPyP4 has been previously demonstrated. In these experiments, c-exNDI-2 and BRACO-19 exerted stabilizing effects on particular G-quadruplex elements located in promoter regions [7].

Similarly, TMPyP4 exerted a stabilizing effect on quadruplexes located in virulence-associated genes [8].

It should be emphasized that all the aforementioned studies were focused on quadruplex-forming sequences at particular genomic locations; notably, the presence of G4 was invariably associated with inhibited expression of the corresponding gene under the action of ligand. In our previous study, we analyzed the transcriptomic response to inhibitory concentrations of TMPyP4 (4 μM) and BRACO-19 (10 μM) in a model Mycobacterium smegmatis MC2155 strain. We found that 10% and 12% genes of the bacterium changed their expression under the action of TMPyP4 and BRACO-19, respectively. However, we found no statistically significant correlation between differential expression and the presence of PQS [9].

In this study, we aimed to assess the influence of subinhibitory concentrations of G4 ligands TMPyP4 (2 μM) and BRACO-19 (5 μM) on gene expression profiles in *M. smegmatis* MC²155 and interpret the results in connection with the previously obtained data.

METHODS

### Bacterial strain and cultivation conditions

In this study *Mycobacterium smegmatis* MC²155 model strain was used in all experiments. The cultivation was carried out at 37 °C in a humid atmosphere containing 5% $CO_2$ using Middlebrook 7H9 broth (HiMedia; India) or Middlebrook 7H11 agar (HiMedia) with addition of 0.5% glycerol and 10% Middlebrook OADC growth supplement (HiMedia). Cryopreserved bacteria from a certified collection were seeded on agar plates and grown for 24 h before inoculation to a liquid medium.

Cultivation of *M. smegmatis* for the transcriptomic analysis was carried out in accordance with the previous publication [9]. Bacterial cells were grown to 0.47 optical density measured at 570 nm, corresponding to the mid-exponential phase, and transferred to 5 mL tubes (NUOVA APTACA; Italy). G4-stabilizing agents were added to the cultures in final concentrations corresponding to a half of minimal inhibitory concentration (5 μM for BRACO-19 and 2 μM for TMPyP4). The cells were incubated for 4 h (cell division time described previously [10]) at 37 °C in a humid atmosphere containing 5% $CO_2$ in a thermal shaker (250 rpm). All experiments were carried out in three biological replicates.

### RNA extraction and transcriptomic analysis

RNA extraction and transcriptomic assay were carried out using previously described protocols [9]. Bacterial cells were

**BRACO-19**

**TMPyP4**



9808666

135398505
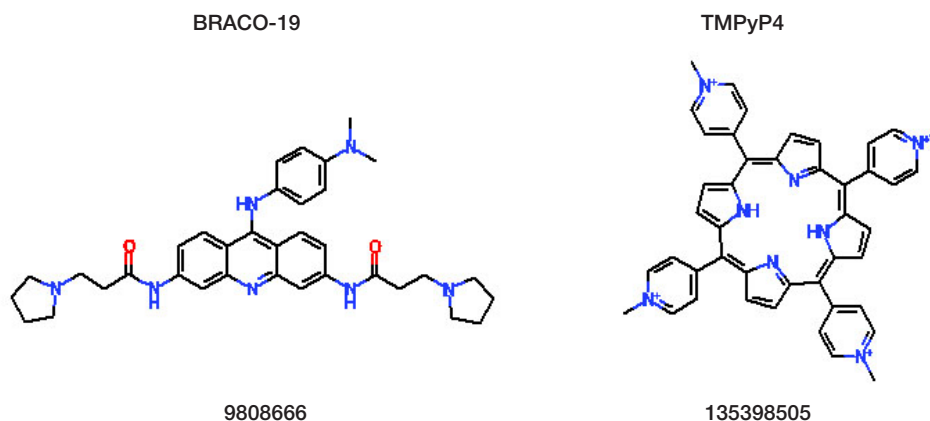
**Fig. 1.** Structural formulas of the BRACO-19 and TMPyP4 ligands
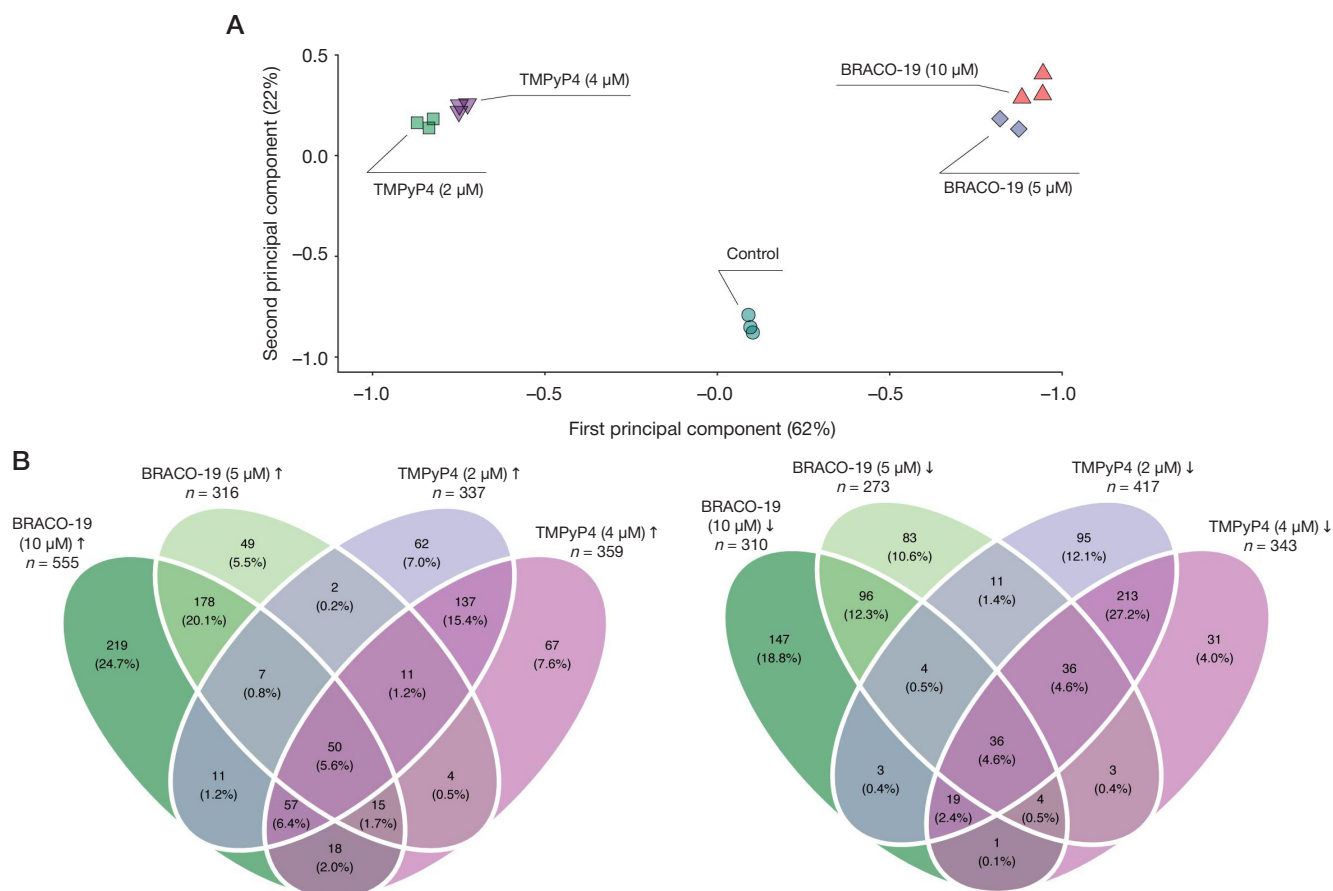
**Fig. 2.** Transcriptomic differences revealed in *Mycobacterium smegmatis* treated with different concentrations of BRACO-19 and TMPyP4. **A**. The principal components analysis shows correlations of gene expression levels under five sets of conditions (designated by *colors*). **B**. Venn diagrams show intersections among the sets of genes regulated by exposure to BRACO-19 and TMPyP4 in different concentrations

collected by centrifugation (8000 g, 10 min, 4 °C); the pellet was washed with phosphate buffered saline and mixed with RNAprotect Bacteria Reagent (Qiagen; USA) to stabilize RNA. The cells were lyzed in Lysing Matrix B 2 mL tubes placed in a MagNA Lyzer instrument (Roche; Switzerland) for 30 s. The lyzates were processed in a KingFisher automated station (Thermo Fisher Scientific; USA) using MagMAX mirVana Total RNA Isolation Kit (Thermo Fisher Scientific) in accordance with the manufacturer's protocol. The isolated total RNA was treated with TURBO DNA-free kit (Thermo Fisher Scientific) in a 50 µL volume. Additional RNA purification was performed with Agencourt RNA Clean XP kit (Beckman Coulter; USA).

The libraries were prepared starting from 300 ng of total RNA. The ribosomal RNA was removed by Ribo-Zero Plus rRNA Depletion Kit (Illumina; USA) in accordance with the manufacturer's protocol. The transcriptomic libraries were prepared using NEBNext Ultra II Directional RNA Library Prep Kit (NEB; USA). The libraries were pooled in equimolar amounts, diluted to a 12 pM final concentration and high-throughput sequenced on HiSeq 2500 Illumina platform using HiSeq Rapid SBS Kit v2 (50 cycles) and HiSeq SR Rapid Cluster Kit v2 with 1% Phix (Illumina) added as control. The sequencing data are deposited in NCBI (Accession: PRJNA765512).

### Bioinformatics analysis

The sequencing reads were mapped to *M. smegmatis* MC$^2$155 genome (CP000480.1) using HISAT2 [11]. The sorting of SAM files, their conversion to BAM files and subsequent indexing were carried out in SAMtools software [12]. The mapping quality and gene coverage were assessed using QualiMap [13];

the reports were aggregated by MultiQC [14]. The mapped reads were assigned to specific genes using featureCounts [15]. Differential gene expression analysis was performed with edgeR package [16] for R. Genes with false discovery rate (FDR) less than 0.05 and a fold change (log2FC) threshold of |1| (i.e. ≥ |2|-fold change) were considered differentially expressed. For intersample comparisons the counts were normalized using the gene length corrected trimmed mean of M-values [17]. Subsequent analysis of functional enrichment for GO terms (categories) and KEGG pathways involving differentially expressed genes was performed with clusterProfiler package [18]; the categories were considered enriched at FDR ≤ 0.05.

### RESULTS

### Transcriptomic influence of G4-stabilizing ligands BRACO-19 and TMPyP4 in *M. smegmatis* MC$^2$155

To assess the influence of G4 ligands on transcriptomic profiles of *M. smegmatis*, the bacteria were exposed to subinhibitory concentrations of BRACO-19 and TMPyP4 (5 µM and 2 µM, respectively) for 4 h. The results of RNA sequencing for the ligand-treated bacterial cultures were compared mutually as well as against previously obtained data for higher, inhibitory concentrations of the ligands (10 µM and 4 µM, respectively).

The principal components analysis revealed clusterization of the replicates in every experiment as well as pronounced effects of both ligands compared with the control (Fig. 2A). At the same time, the analysis revealed close similarity of the effects for different concentrations of the same ligand.
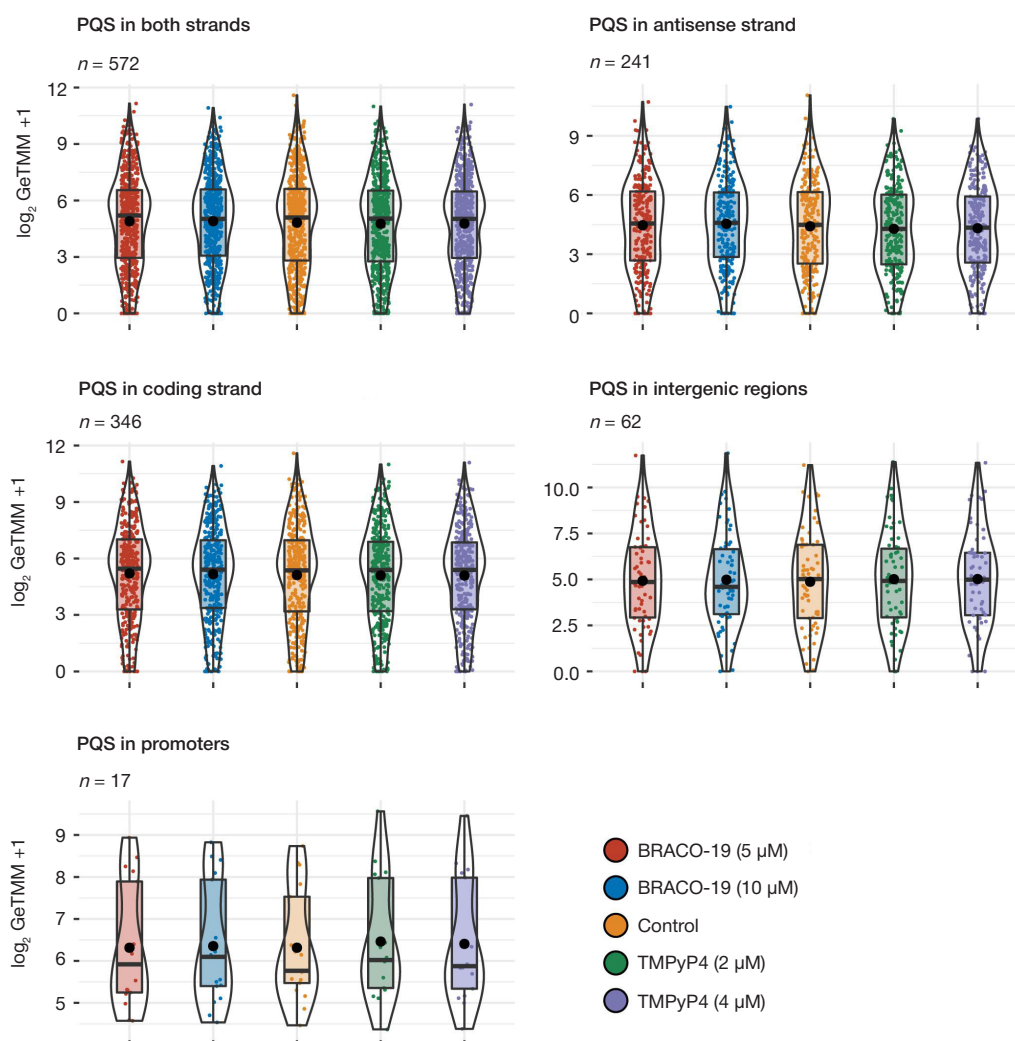
**Fig. 3.** Boxplot showing differential expression of PQS-containing genes in *Mycobacterium smegmatis* exposed to different concentrations of BRACO-19 and TMPyP4. The number of genes with PQS (n) excludes genes with low CPM (Counts Per Million); for PQS in intergenic regions, both flanking genes are included. Box limits correspond to lower and upper quartiles; horizontal line inside the box indicates the median and *black dot* indicates the mean value. Games-Howell post hoc test was applied to calculate *p* values

For BRACO-19, we identified 589 (316↑; 273↓) and 865 (555↑; 310↓) differentially expressed genes at 5 μM and 10 μM, respectively (Fig. 2B). For TMPyP4, we observed the opposite trend with decreased number of differentially expressed genes at higher concentration of the ligand: 754 (337↑; 417↓) and 702 (359↑; 343↓) for 2 μM and 4 μM, respectively.

### Ligand-induced changes in expression of genes associated with putative quadruplex-forming sequences

Correlations of the ligand sensitivity with the presence of putative quadruplex-forming sequences were assessed for the following groups of genes identified previously: PQS in both DNA strands (615 genes of $n = 665$), PQS in coding strand (255 genes of $n = 267$), PQS in antisense (template) strand (360 genes of $n = 398$), PQS in intergenic regions (two flanking genes for 14 elements of $n = 53$) and PQS in promoter regions (17 genes of $n = 17$) [9]. Both ligands revealed no statistically significant differences with control samples for all groups of genes regardless of concentration (Games-Howell post-hoc test $p_{adj}$. >> 0.05; Fig. 3).

Interestingly, the number of differentially expressed quadruplex-associated genes increased as 58 → 75 with increasing concentration of BRACO-19 (5 μM → 10 μM),

but decreased as 72 → 59 with increasing concentration of TMPyP4 (2 μM → 4 μM) (Fig. 4).

### Ligand-induced changes in expression of genes of the replication and repair system

Comparative analysis of RNA sequencing data for BRACO-19 and TMPyP4 revealed their differential influence on the replication and repair system of *M. smegmatis* at transcriptional level (see Table). The effects of BRACO-19 included elevated expression levels for DNA gyrases, translesion synthesis DNA polymerases, DNA and RNA helicases and DNA repair system proteins. Translesion synthesis DNA polymerases are SOS response proteins involved in active recovery of the bacterial chromosome integrity [19]. DNA gyrases (type II topoisomerases) participate in DNA synthesis by introducing negative supercoils [20], whereas methyltransferase Ogt and DNA glycosylase AlkA prevent DNA damage during alkylation [21]. It should be noted that the use of BRACO-19 in subinhibitory concentration (5 μM) affected expression of fewer genes compared with the inhibitory concentration (10 μM). A > 2-fold increase in expression upon switching the dose of BRACO-19 from subinhibitory to inhibitory, observed for *ogt* and *alkA* genes only, may indicate a specific dose-dependent effect of the given ligand on these genes.
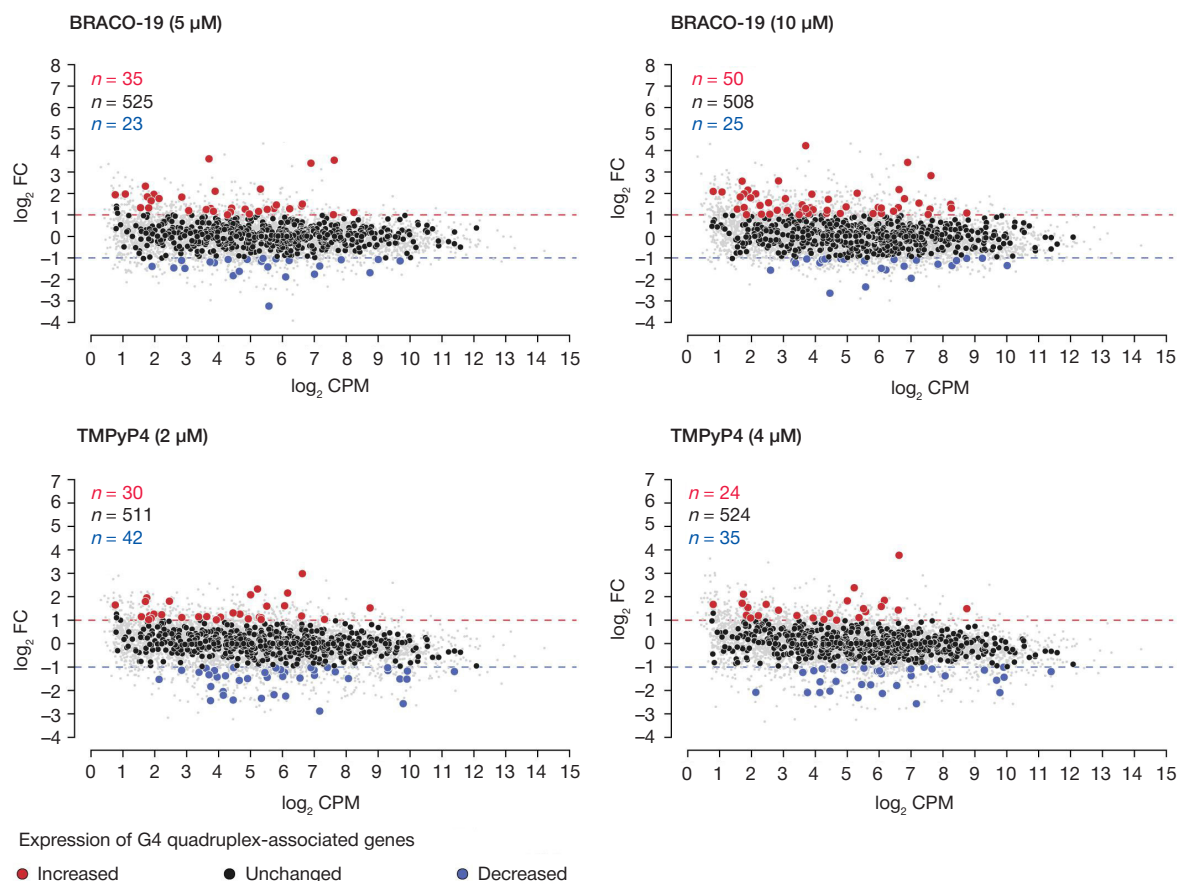
**Fig. 4.** Mean-difference plots (MD-plots) of fold changes ($\log_2$ FC) versus average expression levels ($\log_2$ CPM) for the putative quadruplex-associated genes

For TMPyP4, the only gene with an increased expression level of the repair system was *ssbb*. This gene encodes a protein which participates in replication and recombination repair processes through binding to single-stranded DNA to keep it from rehybridization. Expression level of the DNA helicase gene RecQ was increased by both ligands.

### Ligand-induced changes in metabolic pathways of *M. smegmatis* MC²155

The analysis of GO terms and KEGG pathways revealed significant enrichments (FDR < 0.05; Fig. 5) for the transcription (GO:0006351), arginine biosynthesis (GO:0006526), transport (GO:0006810), sulfur metabolism (msm00920), siderophore group nonribosomal peptide biosynthesis (msm01053) and ABC transporter (msm02010) functionalities.

Similarly, with the use of BRACO-19 in inhibitory concentrations, the exposure to subinhibitory levels of the same compound affected the only metabolic pathway associated with iron metabolism. The analysis identified elevated expression of genes involved in siderophore biosynthesis, transport, and reuptake. By contrast, genes involved in iron storage showed reduced expression. It is important to note that, judging by the level of enrichment, the response of the bacterial cell to subinhibitory concentrations of the ligand was stronger.

The use of TMPyP4 stimulated expression of transcription factor-encoding genes (GO:0006351) and genes involved in sulfur metabolism (msm00920) associated with the enrichment of cellular transport systems observed at different concentrations of the ligand: the majority of GO:0006810, msm02010 and msm00920 genes were common between these groups. By contrast, genes involved in arginine biosynthesis (GO:0006526) showed reduced expression at both concentrations of the ligand.

## DISCUSSION

This study continues our previous research on the transcriptomic response of *M. smegmatis* to inhibitory concentrations of G4-stabilizing compounds BRACO-19 and TMPyP4 [9]. In this work, we used subinhibitory concentrations of the ligands for more refined specification of the links between PQS and gene expression, as well as identification of primary responders among metabolic pathways.

The bioinformatics analysis revealed extensive transcriptomic alterations induced by subinhibitory concentrations of G4 ligands (Fig. 2). The influence of ligand concentration on the extent of transcriptomic effect depended on the ligand: increasing the ligand concentration to inhibitory led to either increase or decrease in the number of differentially expressed genes (for BRACO-19 and TMPyP4, respectively). Further analysis of the data revealed no significant regulation of PQS-associated genes by G4 ligands or concentration-dependent ligand-mediated G4 stabilization (Fig. 3). We also analyzed common effects of the two ligands by focusing on particular genes reacting similarly to both ligands by either up- or downregulation. However, even for genes selected on this basis, we failed to find specific evidence of the ligand-mediated G4 stabilization or dose-dependent effects. Stabilization of the quadruplex structures previously described in *M. tuberculosis* could not be confirmed, given significant genomic divergence between *M. tuberculosis* and *M. smegmatis*.

The analysis of KEGG pathways and GO categories also revealed no signs of dose dependency. All transcriptomic effects exerted by subinhibitory concentrations of the ligands were consistent with the previously published results obtained by using inhibitory concentrations of these ligands [9] (Fig. 5). The only interesting exception is transcriptomic representation

**Table.** Changes in the replication and repair system gene expression in *M. smegmatis* under the action of BRACO-19 and TMPyP4

| Locus | Gene | Product | Expression levels under the action of BRACO-19 compared with the control | | Expression levels under the action of TMPyP4 compared with the control | |
| --- | --- | --- | --- | --- | --- | --- |
| | | | 5 μM | 10 μM | 2 μM | 4 μM |
| MSMEG_0005 | *gyrB* | DNA gyrase subunit B | **2.485372\*** | **2.304708** | −1.79363 | −1.70249 |
| MSMEG_0006 | *gyrA* | DNA gyrase subunit A | **2.152993** | **2.316561** | **−2.34404** | −1.84273 |
| MSMEG_1327 | *recB* | Exodeoxyribonuclease subunit B | 1.158257 | 1.240121 | −2.16073 | −2.2508 |
| MSMEG_1620 | *imuA′* | Hypothetical protein | 1.957144 | **2.865713** | 1.419836 | −1.08999 |
| MSMEG_1622 | *imuB* | Repair DNA polymerase | 1.867917 | **2.435738** | 1.721681 | 1.944552 |
| MSMEG_1633 | *dnaE2* | Translesion synthesis DNA polymerase | 1.855874 | **2.529669** | 1.720836 | 1.865113 |
| MSMEG_2442 | *RNaseH2 (rnhB)* | Ribonuclease HII | 1.845015 | **2.135989** | 1.353681 | 1.362699 |
| MSMEG_3172 | *dinB1* | DNA polymerase IV | 2.069791 | **2.304246** | 1.066778 | 1.130623 |
| MSMEG_3885 | *helY* | DEAD/DEAH family RNA helicase | 2.540092 | **3.424716** | −1.17839 | −1.13342 |
| MSMEG_4701 | *ssbb* | Single-stranded DNA-binding protein | 1.509562 | 1.910513 | **2.236647** | **2.367929** |
| MSMEG_4925 | *alkA* | Transcription regulator, Ada family protein/ DNA-3-methyladenine glycosylase II | **3.608202** | **8.892216** | 1.477495 | 1.539172 |
| MSMEG_4928 | *ogt* | Cysteine methyltransferase | **4.145998** | **9.941453** | 1.106208 | 1.357626 |
| MSMEG_5397 | *recQ* | ATP-dependent DNA helicase RecQ | **3.156958** | **4.455866** | **2.107502** | **2.911045** |
| MSMEG_5422 | *mazG* | Pyrophosphohydrolase | 1.754292 | 1.586085 | **−2.46206** | **−2.19913** |
| MSMEG_6443 | *dinB3* | DNA polymerase IV | **2.077001** | **2.867936** | 1.164152 | 1.261415 |
| MSMEG_6896 | *ssba* | Single-stranded DNA-binding protein | −1.70995 | **−2.71083** | −1.27025 | −1.32274 |

**Note:** \* — bold typed are entries complying with the following criteria: more than 2-fold change and FDR < 0.05.

of the iron metabolism system, which reacted to BRACO-1 with higher enrichment at subinhibitory concentrations of the ligand. This cellular system becomes activated under conditions of iron deficiency, with oxidative or nitrosative stress, as well as under increased demand for metalloproteins involved in DNA replication and repair [22]. The use of BRACO-19 in subinhibitory concentrations led to overrepresentation of the siderophore nonribosomal peptide biosynthesis pathway

(msm01053) including the mycobactin synthesis genes. Other systems of the pathway revealed a gradual increase in gene expression levels at higher concentrations of the ligand.

Among the replication and repair system genes of *M. smegmatis*, the only gene activated by subinhibitory concentrations of BRACO-19 and TMPyP4 was *recQ*. The ability of RecQ helicase to resolve the quadruplex structures has been demonstrated for *E. coli*; however, RecQ of
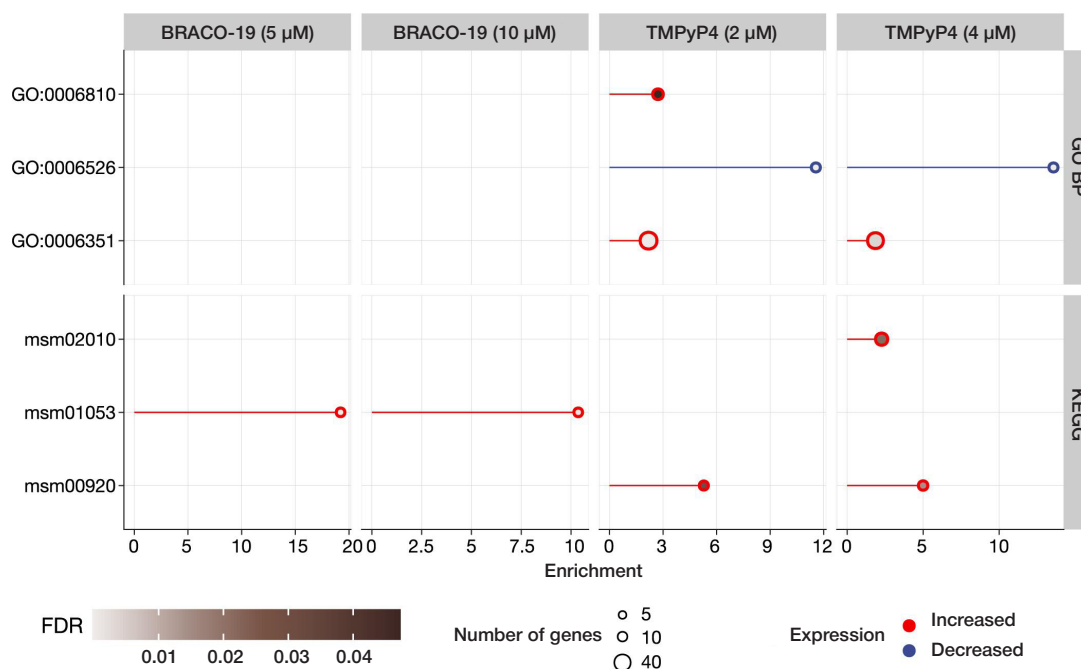


**Fig. 5.** GO categories and KEGG pathways showing enrichment under exposure to BRACO-19 and TMPyP4 in different concentrations: GO:0006810 — Transport; GO:0006526 — Arginine biosynthesis; GO:0006351 — DNA-dependent transcription; msm02010 — ABC transporters; msm01053 — Biosynthesis of siderophore group nonribosomal peptides; msm00920 — Sulfur metabolism

*M. smegmatis* is not homologous to the eponymous protein of *E. coli*; moreover, RecQ is absent in *M. tuberculosis* [23]. This point questions the ability of RecQ protein of *M. smegmatis* to resolve G4 structures and subjects it to further scrutiny.

It should be recognized that transcriptional response in bacteria is a complex phenomenon modulated by multiple factors, including subtle genetic differences, environmental exposures, etc. Recent findings indicate that quadruplexes, apart from their inhibitory effect, can act as transcriptional activators depending on the conditions. In eukaryotes, quadruplexes may provide structural cores for transcription factor binding and promote functional changes in chromatin architecture, R-loop stabilization, etc. [24]. In bacteria, the quadruplex stabilization by naphthalene diimide derivatives has been shown to inhibit gene expression in Gram-negative strains while enhancing it in Gram-positive strains, which supports the bidirectional nature of the quadruplex-mediated regulation [25]. The regulatory role of RNA quadruplexes in bacteria should not be ignored, as their functional presence in prokaryotes has been proved experimentally [26]. The use of advanced techniques for quadruplex detection and verification, including proteomic experiments, will ensure further progress in our understanding of the role of particular G4 elements in genomic regulation.

CONCLUSIONS

Guanine quadruplexes, described in the majority of microorganisms, represent an important element of functional genomic regulation. The current study, however, secures no direct relationship between stabilization of the putative quadruplex structures and expression of genes associated with these structures. Both quadruplex-stabilizing ligands tested in this study exerted diverse transcriptomic effects, encompassing numerous genes and several metabolic pathways. The changes observed for the transcription factor-encoding genes and the replication and repair system genes under the action of these ligands indicate their potential involvement at the RNA/DNA level, consistently with the current concept of quadruplex-mediated genomic regulation. The enhanced transcription of RecQ DNA helicase gene observed in the studied systems positions its product as a plausible candidate enzyme participating in the resolution of quadruplex structures.

## References

1. Global Tuberculosis Report 2021 [cited 2022 Apr 7]. Available from: https://www.who.int/teams/global-tuberculosis-programme/tb-reports/global-tuberculosis-report-2021.
2. Kadura S, King N, Nakhoul M, Zhu H, Theron G, Köser CU, et al. Systematic review of mutations associated with resistance to the new and repurposed Mycobacterium tuberculosis drugs bedaquiline, clofazimine, linezolid, delamanid and pretomanid. Journal of Antimicrobial Chemotherapy. 2020; 75 (8): 2031.
3. Spiegel J, Adhikari S, Balasubramanian S. The structure and function of DNA G-quadruplexes. Trends Chem. 2020; 2 (2): 123–36.
4. Masai H, Tanaka T. G-quadruplex DNA and RNA: Their roles in regulation of DNA replication and other biological functions. Biochemical and Biophysical Research Communications. 2020; 531 (1): 25–38.
5. Bartas M, Cutová M, Brázda V, Kaura P, Šť'Astný J, Kolomazník J, et al. The presence and localization of G-quadruplex forming sequences in the domain of bacteria. Molecules. 2019; 24 (9).
6. Yadav P, Kim N, Kumari M, Verma S, Sharma TK, Yadav V, et al. G-quadruplex structures in bacteria: biological relevance and potential as an antimicrobial target. Journal of Bacteriology. 2021; 203 (13).
7. Perrone R, Lavezzo E, Riello E, Manganelli R, Palù G, Toppo S, et al. Mapping and characterization of G-quadruplexes in Mycobacterium tuberculosis gene promoter regions. Sci Rep. 2017; 7 (1).
8. Mishra SK, Shankar U, Jain N, Sikri K, Tyagi JS, Sharma TK, et al. Characterization of G-quadruplex motifs in espB, espK, and cyp51 genes of mycobacterium tuberculosis aspotential drug targets. Mol Ther Nucleic Acids. 2019; 16: 698–706.
9. Shitikov E, Bespiatykh D, Malakhova M, Bespyatykh J, Bodoev I, Vedekhina T, et al. Genome-wide tanscriptional response of mycobacterium smegmatis MC 2 155 to G-quadruplex ligands BRACO-19 and TMPyP4. Front Microbiol. 2022; 13.
10. Logsdon MM, Aldridge BB. Stable regulation of cell cycle events in mycobacteria: insights from Inherently heterogeneous bacterial populations. Front Microbiol. 2018; 9 (MAR).
11. Kim D, Langmead B, Salzberg SL. HISAT: a fast spliced aligner with low memory requirements. Nat Methods. 2015; 12 (4): 357–60.
12. Li H, Handsaker B, Wysoker A, Fennell T, Ruan J, Homer N, et al. The sequence alignment/map format and SAMtools. Bioinformatics. 2009; 25 (16): 2078–9.
13. Okonechnikov K, Conesa A, García-Alcalde F. Qualimap 2: advanced multi-sample quality control for high-throughput sequencing data. Bioinformatics. 2016; 32 (2): 292–4.
14. Ewels P, Magnusson M, Lundin S, Käller M. MultiQC: summarize analysis results for multiple tools and samples in a single report. Bioinformatics. 2016; 32 (19): 3047–8.
15. Liao Y, Smyth GK, Shi W. featureCounts: an efficient general purpose program for assigning sequence reads to genomic features. Bioinformatics. 2014; 30 (7): 923–30.
16. Robinson MD, McCarthy DJ, Smyth GK. edgeR: a Bioconductor package for differential expression analysis of digital gene expression data. Bioinformatics. 2010; 26 (1): 139–40.
17. Smid M, Coebergh van den Braak RRJ, van de Werken HJG, van Riet J, van Galen A, de Weerd V, et al. Gene length corrected trimmed mean of M-values (GeTMM) processing of RNA-seq data performs similarly in intersample analyses while improving intrasample comparisons. BMC Bioinformatics. 2018; 19 (1).
18. Yu G, Wang LG, Han Y, He QY. clusterProfiler: an R package for comparing biological themes among gene clusters. OMICS. 2012; 16 (5): 284–7.
19. W Yang, Y Gao. Translesion and repair DNA polymerases: diverse structure and mechanism. Annu Rev Biochem. 2018; 87: 239–61.
20. Mdluli K, Ma Z. Mycobacterium tuberculosis DNA gyrase as a target for drug discovery. Infect Disord Drug Targets. 2007; 7 (2): 159–68.
21. Yang M, Aamodt RM, Dalhus B, Balasingham S, Helle I, Andersen P, et al. The ada operon of Mycobacterium tuberculosis encodes two DNA methyltransferases for inducible repair of DNA alkylation damage. DNA Repair. 2011; 10 (6): 595–602.
22. Namouchi A, Gómez-Muñoz M, Frye SA, Moen LV, Rognes T, Tønjum T, et al. The Mycobacterium tuberculosis transcriptional landscape under genotoxic stress. BMC Genomics. 2016; 17 (1): 1–13.
23. Wu X, Maizels N. Substrate-specific inhibition of RecQ helicase. Nucleic Acids Research. 2001; 29 (8): 1765–71.
24. Robinson J, Raguseo F, Nuccio SP, Liano D, di Antonio M. DNA G-quadruplex structures: more than simple roadblocks to transcription? Nucleic Acids Res. 2021; 49 (15): 8419–31.
25. Cebrián R, Belmonte-Reche E, Pirota V, de Jong A, Morales JC, Freccero M, et al. G-quadruplex DNA as a target in pathogenic bacteria: efficacy of an extended naphthalene diimide ligand and Its mode of action. Journal of Medicinal Chemistry. 2021.
26. Shao X, Zhang W, Umar MI, Wong HY, Seng Z, Xie Y, et al. RNA G-quadruplex structures mediate gene regulation in bacteria. mBio. 2020; 11 (1).

## Литература

1. Global Tuberculosis Report 2021 [cited 2022 Apr 7]. Available from: https://www.who.int/teams/global-tuberculosis-programme/tb-reports/global-tuberculosis-report-2021.
2. Kadura S, King N, Nakhoul M, Zhu H, Theron G, Köser CU, et al. Systematic review of mutations associated with resistance to the new and repurposed Mycobacterium tuberculosis drugs bedaquiline, clofazimine, linezolid, delamanid and pretomanid. Journal of Antimicrobial Chemotherapy. 2020; 75 (8): 2031.
3. Spiegel J, Adhikari S, Balasubramanian S. The structure and function of DNA G-quadruplexes. Trends Chem. 2020; 2 (2): 123–36.
4. Masai H, Tanaka T. G-quadruplex DNA and RNA: Their roles in regulation of DNA replication and other biological functions. Biochemical and Biophysical Research Communications. 2020; 531 (1): 25–38.
5. Bartas M, Cutová M, Brázda V, Kaura P, Šťastný J, Kolomazník J, et al. The presence and localization of G-quadruplex forming sequences in the domain of bacteria. Molecules. 2019; 24 (9).
6. Yadav P, Kim N, Kumari M, Verma S, Sharma TK, Yadav V, et al. G-quadruplex structures in bacteria: biological relevance and potential as an antimicrobial target. Journal of Bacteriology. 2021; 203 (13).
7. Perrone R, Lavezzo E, Riello E, Manganelli R, Palù G, Toppo S, et al. Mapping and characterization of G-quadruplexes in Mycobacterium tuberculosis gene promoter regions. Sci Rep. 2017; 7 (1).
8. Mishra SK, Shankar U, Jain N, Sikri K, Tyagi JS, Sharma TK, et al. Characterization of G-quadruplex motifs in espB, espK, and cyp51 genes of mycobacterium tuberculosis aspotential drug targets. Mol Ther Nucleic Acids. 2019; 16: 698–706.
9. Shitikov E, Bespiatykh D, Malakhova M, Bespyatykh J, Bodoev I, Vedekhina T, et al. Genome-wide tanscriptional response of mycobacterium smegmatis MC 2 155 to G-quadruplex ligands BRACO-19 and TMPyP4. Front Microbiol. 2022; 13.
10. Logsdon MM, Aldridge BB. Stable regulation of cell cycle events in mycobacteria: insights from Inherently heterogeneous bacterial populations. Front Microbiol. 2018; 9 (MAR).
11. Kim D, Langmead B, Salzberg SL. HISAT: a fast spliced aligner with low memory requirements. Nat Methods. 2015; 12 (4): 357–60.
12. Li H, Handsaker B, Wysoker A, Fennell T, Ruan J, Homer N, et al. The sequence alignment/map format and SAMtools. Bioinformatics. 2009; 25 (16): 2078–9.
13. Okonechnikov K, Conesa A, García-Alcalde F. Qualimap 2: advanced multi-sample quality control for high-throughput sequencing data. Bioinformatics. 2016; 32 (2): 292–4.
14. Ewels P, Magnusson M, Lundin S, Käller M. MultiQC: summarize analysis results for multiple tools and samples in a single report. Bioinformatics. 2016; 32 (19): 3047–8.
15. Liao Y, Smyth GK, Shi W. featureCounts: an efficient general purpose program for assigning sequence reads to genomic features. Bioinformatics. 2014; 30 (7): 923–30.
16. Robinson MD, McCarthy DJ, Smyth GK. edgeR: a Bioconductor package for differential expression analysis of digital gene expression data. Bioinformatics. 2010; 26 (1): 139–40.
17. Smid M, Coebergh van den Braak RRJ, van de Werken HJG, van Riet J, van Galen A, de Weerd V, et al. Gene length corrected trimmed mean of M-values (GeTMM) processing of RNA-seq data performs similarly in intersample analyses while improving intrasample comparisons. BMC Bioinformatics. 2018; 19 (1).
18. Yu G, Wang LG, Han Y, He QY. clusterProfiler: an R package for comparing biological themes among gene clusters. OMICS. 2012; 16 (5): 284–7.
19. W Yang, Y Gao. Translesion and repair DNA polymerases: diverse structure and mechanism. Annu Rev Biochem. 2018; 87: 239–61.
20. Mdluli K, Ma Z. Mycobacterium tuberculosis DNA gyrase as a target for drug discovery. Infect Disord Drug Targets. 2007; 7 (2): 159–68.
21. Yang M, Aamodt RM, Dalhus B, Balasingham S, Helle I, Andersen P, et al. The ada operon of Mycobacterium tuberculosis encodes two DNA methyltransferases for inducible repair of DNA alkylation damage. DNA Repair. 2011; 10 (6): 595–602.
22. Namouchi A, Gómez-Muñoz M, Frye SA, Moen LV, Rognes T, Tønjum T, et al. The Mycobacterium tuberculosis transcriptional landscape under genotoxic stress. BMC Genomics. 2016; 17 (1): 1–13.
23. Wu X, Maizels N. Substrate-specific inhibition of RecQ helicase. Nucleic Acids Research. 2001; 29 (8): 1765–71.
24. Robinson J, Raguseo F, Nuccio SP, Liano D, di Antonio M. DNA G-quadruplex structures: more than simple roadblocks to transcription? Nucleic Acids Res. 2021; 49 (15): 8419–31.
25. Cebrián R, Belmonte-Reche E, Pirota V, de Jong A, Morales JC, Freccero M, et al. G-quadruplex DNA as a target in pathogenic bacteria: efficacy of an extended naphthalene diimide ligand and Its mode of action. Journal of Medicinal Chemistry. 2021.
26. Shao X, Zhang W, Umar MI, Wong HY, Seng Z, Xie Y, et al. RNA G-quadruplex structures mediate gene regulation in bacteria. mBio. 2020; 11 (1).

# THE ROLE OF GENETIC FACTORS IN FAMILIAL CASE OF ACNE

Demina OM[1]✉, Rumyantsev AG[1,2], Potekaev NN[1]

[1] Pirogov Russian National Research Medical University, Moscow, Russia

[2] Dmitry Rogachev National Medical Research Center of Pediatric Hematology, Oncology and Immunology, Moscow, Russia

Acne is one of the most common dermatoses. A prominent genetic component for this disease has been reported and the manifestation in first-line relatives is considered an important risk factor. Here we present a clinical case illustrating the relevance of particular genetic polymorphisms mapped to *NCF1*, *CD3E*, *ORAI1*, *IGHM* and *TAZ* in patients with severe forms and burdened family history of the disease. Genetic examination identified the same allelic variants in five candidate target genes (*NCF1*, *CD3E*, *ORAI1*, *IGHM* and *TAZ*) in two closely related patients (father and son) with severe acne. The identified genetic configuration may interfere with the oxidase activity and promote defects in mitochondrial function along with reduced T cell proliferation and imbalanced immunoglobulin production. The findings may provide an important reference point for further clinical investigation and treatment of severe torpid dermatoses.

**Keywords:** acne, genetic variant, oxidase system

✉ Correspondence should be addressed: Olga M. Demina
Ostrovityanova, 1, Moscow, 117997, Russia; demina.om@mail.ru

## РОЛЬ ГЕНЕТИЧЕСКИХ ФАКТОРОВ ПРИ СЕМЕЙНОМ СЛУЧАЕ АКНЕ

О. М. Демина[1]✉, А. Г. Румянцев[1,2], Н. Н. Потекаев[1]

[1] Российский национальный исследовательский медицинский университет имени Н. И. Пирогова, Москва, Россия

[2] Национальный медицинский исследовательский центр детской гематологии, онкологии и иммунологии имени Дмитрия Рогачева, Москва, Россия

В настоящее время акне относится к наиболее распространенным дерматозам. Сообщается о роли генетической предрасположенности к развитию заболевания. Показано, что фактором риска развития дерматоза может быть наличие болезни у родственников первой линии родства. Представлен случай идентификации и определения значимости полиморфизма генов *NCF1*, *CD3E*, *ORAI1*, *IGHM*, *TAZ* у больных тяжелыми формами заболевания с отягощенным семейным анамнезом. Проведенные исследования позволили выявить идентичные аллельные варианты в пяти генах: *NCF1*, *CD3E*, *ORAI1*, *IGHM*, *TAZ* у двух близкородственных пациентов (отец и сын) с акне тяжелой степени. Полиморфизмы изученных генов, вероятно, влияют на развитие дисбаланса системы оксидаз, работу митохондрий, сниженной пролиферации Т-клеток, а также формирования дисбаланса секреции иммуноглобулинов. Полученные данные могут быть факторами торпидного течения тяжелой формы дерматоза, что определяет необходимость дальнейших исследований.

**Ключевые слова:** акне, полиморфизм генов, молекулярно-генетические исследования

✉ Для корреспонденции: Ольга Михайловна Демина
ул. Островитянова, д. 1, г. Москва, 117997, Россия; demina.om@mail.ru

Acne is a prevalent skin disorder with an estimated 35–90% cases arising in adolescents. The age at onset typically spans from 14 years to the beginning of the third decade of life, but clinical symptoms of the disease may persist or develop *de novo* in adulthood. The up-to-date WHO criteria for the definition of chronic diseases classify acne as a chronic dermatosis. Its multifactorial pathogenesis involves the excessive influence of androgens on sebaceous follicles, sebum hypersecretion, abnormal follicular keratinization, *Cutibacterium acnes* colonization and the inflammatory reaction development [1–3]. Gender-based epidemiological studies indicate higher prevalence of acne in women, whereas men in general present with more severe course of the disease [1].

The role of genetic predisposition in acne has been extensively studied. Manifestation of the disease in first-line relatives is considered one of the main risk factors for acne. Familial cases display not only higher incidence of the disease, but also its more severe course. A likely additive effect of maternal and paternal components for this disease has been demonstrated — a history of dermatosis in both parents significantly intensifies the risk of acne in their offspring [4, 5].

The heritable nature of familial acne and its tendency towards aggravated course, especially in boys and men, necessitates the search for molecular markers and putative drug targets in patients with this pathology.

## Clinical case description

In 2019–2020, we consulted two patients with severe acne: a father P. 45 years old and his son K. 17 years old. Both patients sought medical attention simultaneously, with similar complaints of skin rashes on face, chest and back.

The first patient (father) had lived with acne for 10 years, i.e. the disease manifested in adulthood without a pubertal history.

The rashes presented as multiple comedones, papules and pustules, initially on the face and spreading to chest and back within 6–7 months. The recurrent and gradually aggravating skin lesions clearly indicated a transition from moderate to severe course: deep pustules and nodules formed confluent conglomerates which resolved to atrophic scars. The patient consulted a local dermatovenerologist and received several treatments including oral antibacterials (doxycycline 100 mg twice a day for 14–21 days; three courses at 1.5–3 month intervals) and external therapy (clindamycin phosphate gel 1%, on clean and dry skin of the affected area in thin layer twice a day for 1 month, in combination with adapalene gel 0.1% on clean and dry skin of the affected area nightly, extended to five months) with a temporary positive effect.

The second patient (son) initially presented with the disease at the age of 14, with multiple comedones, papules, pustules and nodules developing on his face, chest and back. The rashes proceeded to recurrent disease, accompanied by formation of deep nodules that resolved into atrophic scars. The patient also consulted a local doctor and received treatments including oral antibacterials (doxycycline 100 mg twice a day for 14–21 days; four courses at 2–4 month intervals) and external therapy (clindamycin phosphate gel 1%, on clean and dry skin of the affected area in thin layer twice a day for 1 month in combination with adapalene gel 0.1% on clean and dry skin of the affected area nightly, extended to five months, followed by the use of azelaic acid, 15% gel, twice a day mornings and evenings for 6 months). Similarly with the father, the son experienced a temporary curative effect. In addition, the patients had a family burden of cancer: father of the first patient (accordingly, paternal grandfather to the second patient) had rectal cancer.

To assess the contribution of genetic factors to the onset and course of acne in the studied clinical case, we performed molecular genetic examination by high-throughput DNA sequencing (next-generation sequencing, NGS). Genomic DNA was extracted from whole blood samples donated by the patients using CellSep Advanced Kit (DiaSorin Ireland Ltd.; Ireland) in accordance with the manufacturer's protocol. The construction of adapter-ligated DNA libraries was carried out using NebNext Ultra II DNA Library Prep Kit for Illumina (New England Biolabs; USA). The hybridization-based enrichment with coding sequences of target genes was implemented using a custom probe panel (Roche; Switzerland) in accordance with the SeqCap EZ target enrichment protocol for Illumina NGS systems recommended by the manufacturer. The obtained DNA libraries were sequenced on MiSeq platform (Illumina; USA) in a paired-end mode (115×2) with an average depth of 143× and 99% coverage of the target region with a minimal depth of 10×. The sequencing data were processed using a customized automated bioinformatics pipeline.

Population frequencies for the identified variants were estimated using reference datasets of the Genome Aggregation Database (gnomAD) international project — gnomAD Exomes (ExAC) for exonic variants and gnomAD Genomes for intronic variants. Computational assessment of clinical value for the identified missense variants used *SIFT*, *PolyPhen-2*, *PROVEAN* and *UMD Predictor* pathogenicity prediction algorithms for amino acid substitutions. Computational assessment for the identified variants mapping to splice sites or regions adjacent to splice sites used *MutationTaster*, *Human Splicing Finder* and *NNSplice* software.

## Discussion

The molecular genetic study identified identical allelic variants in five candidate target genes *NCF1*, *CD3E*, *ORAI1*, *IGHM* and *TAZ* of the two patients (Table). In four of these genes (*NCF1*, *CD3E*, *ORAI1* and *TAZ*), the identified variants mapped to exons. For *IGHM*, two allelic variants were identified, corresponding to single-nucleotide polymorphisms rs1059216 and rs1136534 and mapping to intergenic region: non-synonymous C>T and synonymous A>G, respectively.

The analysis of zygosity status for the identified allelic variants revealed homozygosity for rs707410 in *NCF1*, homozygosity for rs1059216 in *IGHM*, heterozygosity for rs1136534 in *IGHM* and homozygosity for rs62617809 in *TAZ*. The heterozygous *CD3E* (c.353-16A>C) and homozygous *ORAI1* (*GGCCCC>G*) variants have not been previously associated with any disease.

The population frequency analysis for the identified *NCF1*, *CD3E*, *ORAI1*, *IGHM* and *TAZ* allelic variants using the gnomAD Exomes (ExAC) reference datasets also revealed no pathological links.

The representations of identified allelic variants of five candidate genes in two closely related patients were identical. For heterozygous *CD3E* (c.353-16A>C) and homozygous *ORAI1* (GGCCCC>G), no pathological associations have been described prior to this report.

*NCF1* (neutrophil cytosolic factor 1) encodes a 47 kDa cytosolic protein subunit of NADPH-oxidase in neutrophils. An important biological indicator of immunity-related significance for these enzymes is their localization in the macrophage plasma membrane and participation in antimicrobial defense. Autosomal-recessive *NCF1* variants have been described in chronic granulomatosis [6]. The rs201802880 polymorphism in *NCF1-339* has been preliminary associated with systemic lupus erythematosus [7].

The identified allelic variant *rs707410* in *NCF1*, homozygous in both patients, may promote imbalance in the oxidase system and interfere with the phagocytic activity of immune cells, thus prolonging the inflammation and contributing to severe clinical symptoms of acne.

*CD3E* gene encodes ε subunit of T cell co-receptor CD3 (CD3E). Along with γ, δ and ζ subunits of CD3, CD3E forms a complex with T cell receptor and participates in the antigen-specific T cell activation. CD3E is a transmembrane protein that regulates both the clonal T cell development and the adaptive immune response [8]. Mutated *CD3E* has been implicated in the severe combined immunodeficiency [9].

The identified allelic variant *CD3E* (c.353-16A>C), heterozygous in both patients, may interfere with proliferative capacity of T cells and thus mediate a failure of adaptive immunity.

*ORAI1* (Orai calcium release-activated calcium modulator 1) encodes a calcium channel activated upon release of calcium ions from internal depots. Such channels provide a principal route for the calcium influx in T cells and their activation [10]. Mutations in *ORAI1* may lead to severe combined immunodeficiency [11]. The ORAI1 calcium channels have been preliminary implicated in allergic dermatoses, albeit by yet unknown mechanism [12]. *De novo* mutations in *ORAI1* have been shown to reduce the counts of NK and $T_{reg}$ cells thus promoting immunodeficiencies and autoimmune inflammatory reactions. Such mutations have been reported in the anhydrotic ectodermal dysplasia [13].

The identified allelic variant *ORAI1* (GGCCCC>G), homozygous in both patients, may contribute to secondary immunodeficiencies.

*IGHM* (immunoglobulin heavy <constant> mu) encodes a constant region of immunoglobulin heavy chains. During the effector phase of humoral immune response, the antigen-stimulated B cells produce immunoglobulins to ensure the antigen clearance. Mutations in *IGHM* have been implicated in the autosomal recessive agammaglobulinemia [14].

**Table.** Characterization of *NCF1*, *CD3E*, *ORAI1*, *IGHM* and *TAZ* allelic variants in the patients with severe acne

| Locus | *NCF1* | *CD3E* | *ORAI1* | *IGHM* | *TAZ* |
|---|---|---|---|---|---|
| Chromosome | 7 | 11 | 12 | 14 | X |
| Chromosome coordinates | 74777361 | 118313691 | 121626865- 121626870 | 105855558, 105855808 | 154412069 |
| Allelic variant ID | *rs707410* | previously undescribed | previously undescribed | *rs1059216, rs1136534* | *rs62617809* |
| Location in gene | exon 2, splice site | exon 7, splice site | exon 1, splice site | intergenic region | exon 2 |
| Description | c.153+14T>C | c.353-16A>C | GGCCCC> G | C>T (non-synonymous); A>G (synonymous) | c.110-17T>C |
| Zygocity | Homozygous | Heterozygous | Homozygous | Homozygous | Homozygous |

In addition, both patients presented with identical allelic variants in *IGHM*: homozygous rs1059216 and heterozygous rs1136534. Of these two variants, the homozygous non-synonymous rs1059216 is more likely to interfere with the balanced immunoglobulin synthesis and thus contribute to severe torpid acne.

The X-linked predisposition patterns in dermatoses are of particular clinical interest. *TAZ* gene is located on X chromosome (Xq18) and contains 11 exons; its product, tafazzin, participates in metabolism of cardiolipin incorporated in the inner mitochondrial membrane. The reduced levels of energy metabolism in leukocytes may interfere with their differentiation, with a negative effect on systemic and local immunity. Mutations in *TAZ* are causative for Barth syndrome [15].

The identified allelic variant rs62617809 of *TAZ*, homozygous in both patients, may negatively affect mitochondrial functionalities in multiple cell types including the cellular wing of immunity.

CONCLUSION

Extensive molecular genetic analysis for a selection of candidate genes in two first-line relatives (father and son) with highly similar clinical picture of severe acne identified six allelic variants in five candidate genes. Exonic variants were identified in *NCF1*, *CD3E*, *ORAI1* and *TAZ*; two of them, heterozygous *CD3E* (c.353-16A>C) and homozygous *ORAI1* (GGCCCC>G), are reported for the first time. For the fifth gene, *IGHM*, we identified two previously described allelic variants, rs1059216 and rs1136534, located intergenically and representing single-nucleotide substitutions: C>T (non-synonymous) and A>G (synonymous). All identified genetic variants had the same zygosity status in both patients.

The *NCF1*, *CD3E*, *ORAI1*, *IGHM* and *TAZ* genes participate in the oxidase system activity and play a regulatory role in the rates of T cell proliferation and immunoglobulin production. Specific etiological contributions to severe torpid acne for the identified genetic variants have yet to be determined.

References

1. Heng AS, Chew FT. Systematic review of the epidemiology of acne vulgaris. Sci Rep. 2020; 10 (1): 5754. PubMed PMID: 32238884  DOI: 10.1038/s41598-020-62715-3.

2. Cong TX, Hao D, Wen X, Li XH, He G, Jiang X. From pathogenesis of acne vulgaris to anti-acne agents. Arch Dermatol Res. 2019; 311 (5): 337–49. PubMed PMID: 30859308 DOI: 10.1007/s00403-019-01908-x.

3. Lichtenberger R, Simpson MA, Smith C, Barker J, Navani AA. Genetic architecture of acne vulgaris. J Eur Acad Dermatol Venereol. 2017; 31: 1978–90. PubMed PMID: 28593717 DOI: 10.1111/jdv.14385.

4. Xu SX, Wang HL, Fan X, Sun LD, Yahg S, Wang PG, et al. The familial risk of acne vulgaris in Chinese Hans – a case–control study. J Eur Acad Dermatol Venereol. 2007; 21: 602–5. PubMed PMID:17447973 DOI: 10.1111/j.1468-3083.2006.02022.x.

5. Abo El-Fetoh NM, Alenezi NG, Alshamari NG, Alenezi OG. Epidemiology of acne vulgaris in adolescent male students in Arar, Kingdom of Saudi Arabia. J Egypt Public Health Assoc. 2016; 91 (3): 144–9. PubMed PMID: 27749646 DOI: 10.1097/01.EPX.0000492401.39250.62.

6. Kuhns DB, Hsu AP, Sun D, Lau K, Fink D, Griffith P, et al. NCF1 (p47phox)-deficient chronic granulomatous disease: comprehensive genetic and flow cytometric analysis. Blood Adv. 2019; 3 (2): 136–47. PubMed PMID: 30651282 DOI: 10.1182/bloodadvances.2018023184.

7. Linge P, Arve S, Olsson LM, Leonard D, Sjöwall C, Frodlund M, et al. NCF1-339 polymorphism is associated with altered formation of neutrophil extracellular traps, high serum interferon activity and antiphospholipid syndrome in systemic lupus erythematosus. Ann Rheum Dis. 2020; 79 (2): 254–61. PubMed PMID: 31704719 DOI: 10.1136/annrheumdis-2019-215820.

8. Li L, Guo X, Shi X, Li C, Wu W, Yan C, et al. Ionic CD3-Lck interaction regulates the initiation of T-cell receptor signaling. Proc Natl Acad Sci USA. 2017; 114 (29): E5891–9. PubMed PMID: 28659468 DOI: 10.1073/pnas.1701990114.

9. Firtina S, Ng YY, Ng OH, Nepesov S, Yesilbas O, Kilercik M, et al. A novel pathogenic frameshift variant of CD3E gene in two T-B+ NK+ SCID patients from Turkey.Immunogenetics. 2017; 69 (10): 653–9. PubMed PMID: 28597365 DOI: 10.1007/s00251-017-1005-7.

10. Bhardway R, Hediger M, Demaurex N. Redox modulation of Stim-Orai signaling. Cell Calcium. 2016; 60: 142–52. PubMed PMID:27041216 DOI: 10.1016/j.ceca.2016.03.006.

11. Thompson JL, Mignen O, Shuttleworth TJ. The Orai1 severe combined immune deficiency mutation and calcium release-activated Ca2+ channel function in the heterozygous condition. J Biol Chem. 2009; 284 (11): 6620–6. PubMed PMID: 19075015 DOI: 10.1074/jbc.M808346200.

12. Yan S, Chen W, Zhang Y, Li J, Chen X. Calcium release-activated calcium modulator 1 as a therapeutic target in allergic skin diseases. Life Sci. 2019; 228: 152–7. PubMed PMID: 31055088 DOI: 10.1016/j.lfs.2019.05.001.

13. Lian J, Cuk M, Kahlfuss S, Kozhaya L, Vaeth M, Rieux-Laucat F, et al. ORAI1 mutations abolishing store-operated Ca2+ entry cause anhidrotic ectodermal dysplasia with immunodeficiency. J Allergy Clin Immunol. 2018; 142 (4): 1297–310. PubMed PMID: 29155098 DOI: 10.1016/j.jaci.2017.10.031.

14. Silva P, Justicia A, Regueiro A, Fariña S, Couselo JM, Loidi L. Autosomal recessive agammaglobulinemia due to defect in µ heavy chain caused by a novel mutation in the IGHM gene. Genes Immun. 2017; 18 (3): 197–9. DOI: 28769069 10.1038/gene.2017.14.

15. Zapała B, Płatek T, Wybrańska I. A novel TAZ gene mutation and mosaicism in a Polish family with Barth syndrome. Ann Hum Genet. 2015; 79 (3): 218–24. PubMed PMID: 25776009 DOI: 10.1111/ahg.12108.

## Литература

1. Heng AS, Chew FT. Systematic review of the epidemiology of acne vulgaris. Sci Rep. 2020; 10 (1): 5754. PubMed PMID: 32238884 DOI: 10.1038/s41598-020-62715-3.

2. Cong TX, Hao D, Wen X, Li XH, He G, Jiang X. From pathogenesis of acne vulgaris to anti-acne agents. Arch Dermatol Res. 2019; 311 (5): 337–49. PubMed PMID: 30859308 DOI: 10.1007/s00403-019-01908-x.

3. Lichtenberger R, Simpson MA, Smith C, Barker J, Navani AA. Genetic architecture of acne vulgaris. J Eur Acad Dermatol Venereol. 2017; 31: 1978–90. PubMed PMID: 28593717 DOI: 10.1111/jdv.14385.

4. Xu SX, Wang HL, Fan X, Sun LD, Yahg S, Wang PG, et al. The familial risk of acne vulgaris in Chinese Hans – a case–control study. J Eur Acad Dermatol Venereol. 2007; 21: 602–5. PubMed PMID:17447973 DOI: 10.1111/j.1468-3083.2006.02022.x.

5. Abo El-Fetoh NM, Alenezi NG, Alshamari NG, Alenezi OG. Epidemiology of acne vulgaris in adolescent male students in Arar, Kingdom of Saudi Arabia. J Egypt Public Health Assoc. 2016; 91 (3): 144–9. PubMed PMID: 27749646 DOI: 10.1097/01. EPX.0000492401.39250.62.

6. Kuhns DB, Hsu AP, Sun D, Lau K, Fink D, Griffith P, et al. NCF1 (p47phox)-deficient chronic granulomatous disease: comprehensive genetic and flow cytometric analysis. Blood Adv. 2019; 3 (2): 136–47. PubMed PMID: 30651282 DOI: 10.1182/bloodadvances.2018023184.

7. Linge P, Arve S, Olsson LM, Leonard D, Sjöwall C, Frodlund M, et al. NCF1-339 polymorphism is associated with altered formation of neutrophil extracellular traps, high serum interferon activity and antiphospholipid syndrome in systemic lupus erythematosus. Ann Rheum Dis. 2020; 79 (2): 254–61. PubMed PMID: 31704719 DOI: 10.1136/annrheumdis-2019-215820.

8. Li L, Guo X, Shi X, Li C, Wu W, Yan C, et al. Ionic CD3-Lck interaction regulates the initiation of T-cell receptor signaling. Proc Natl Acad Sci USA. 2017; 114 (29): E5891–9. PubMed PMID: 28659468 DOI: 10.1073/pnas.1701990114.

9. Firtina S, Ng YY, Ng OH, Nepesov S, Yesilbas O, Kilercik M, et al. A novel pathogenic frameshift variant of CD3E gene in two T-B+ NK+ SCID patients from Turkey.Immunogenetics. 2017; 69 (10): 653–9. PubMed PMID: 28597365 DOI: 10.1007/s00251-017-1005-7.

10. Bhardway R, Hediger M, Demaurex N. Redox modulation of Stim-Orai signaling. Cell Calcium. 2016; 60: 142–52. PubMed PMID:27041216 DOI:10.1016/j.ceca.2016.03.006.

11. Thompson JL, Mignen O, Shuttleworth TJ. The Orai1 severe combined immune deficiency mutation and calcium release-activated Ca2+ channel function in the heterozygous condition. J Biol Chem. 2009; 284 (11): 6620–6. PubMed PMID: 19075015 DOI: 10.1074/jbc.M808346200.

12. Yan S, Chen W, Zhang Y, Li J, Chen X. Calcium release-activated calcium modulator 1 as a therapeutic target in allergic skin diseases. Life Sci. 2019; 228: 152–7. PubMed PMID: 31055088 DOI: 10.1016/j.lfs.2019.05.001.

13. Lian J, Cuk M, Kahlfuss S, Kozhaya L, Vaeth M, Rieux-Laucat F, et al. ORAI1 mutations abolishing store-operated Ca2+ entry cause anhidrotic ectodermal dysplasia with immunodeficiency. J Allergy Clin Immunol. 2018; 142 (4): 1297–310. PubMed PMID: 29155098 DOI: 10.1016/j.jaci.2017.10.031.

14. Silva P, Justicia A, Regueiro A, Fariňa S, Couselo JM, Loidi L. Autosomal recessive agammaglobulinemia due to defect in μ heavy chain caused by a novel mutation in the IGHM gene. Genes Immun. 2017; 18 (3): 197–9. DOI: 28769069 10.1038/gene.2017.14.

15. Zapała B, Płatek T, Wybrańska I. A novel TAZ gene mutation and mosaicism in a Polish family with Barth syndrome. Ann Hum Genet. 2015; 79 (3): 218–24. PubMed PMID: 25776009 DOI: 10.1111/ahg.12108.

# INTERMEMBRANE OLIGOMERIZATION OF SARS-COV-2 M-PROTEIN: POSSIBLE ROLE IN VIRAL BUDDING

Sokolinskaya EL, Putlyaeva LV, Gorshkova AA, Lukyanov KA ✉

Center for Molecular and Cellular Biology, Skolkovo Institute of Science and Technology, Moscow, Russia

Despite the extensive research spurred by the catastrophic effects of COVID-19 pandemic, precise molecular mechanisms of some stages in SARS-CoV-2 life cycle remain elusive. One of such stages is the detachment of viral particles during budding. Using confocal fluorescence microscopy, we observed formation of specific structures by endoplasmic reticulum in human cells expressing SARS-CoV-2 M-protein, implicating oligomerization of M-protein across parallel membranes. In our opinion, such intermembrane oligomerization may provide a driving force for pinching off the viral particles during SARS-CoV-2 budding.

# МЕЖМЕМБРАННАЯ ОЛИГОМЕРИЗАЦИЯ М-БЕЛКА КОРОНАВИРУСА SARS-COV-2: ВОЗМОЖНАЯ РОЛЬ В ПОЧКОВАНИИ ВИРУСА

Е. Л. Соколинская, Л. В. Путляева, А. А. Горшкова, К. А. Лукьянов ✉

Центр молекулярной и клеточной биологии, Сколковский институт науки и технологий, Москва, Россия

Несмотря на интенсивные исследования, стимулированные катастрофическими последствиями пандемии COVID-19, точные молекулярные механизмы некоторых стадий жизненного цикла коронавируса SARS-CoV-2, в частности, отрыва вирусных частиц при почковании, остаются неизвестными. При экспрессии М-белка SARS-CoV-2 в клетках человека мы наблюдали образование специфических структур эндоплазматического ретикулума, появление которых свидетельствует о способности М-белка к олигомеризации в составе параллельных мембран. На наш взгляд, такая межмембранная олигомеризация М-белка может быть движущей силой для сближения и слияния мембран при отшнуровывании вирусных частиц SARS-CoV-2.

The ongoing SARS-CoV-2 pandemic constantly reminds us that our current means of dealing with life-threatening zoonotic viral infections are critically limited. The combined administration of drugs targeting diverse molecular entities appears a promising strategy of preventing 'quick' resistance. In this regard, the development of screening platforms and the search for inhibitors with novel mechanisms of action are highly relevant.

A mature SARS-CoV-2 virion carries single-stranded RNA genome (coding strand) and four structural proteins designated N, M, S and E [1, 2]. The soluble nucleocapsid protein (N) ensures binding and compactization of the viral RNA. The rest structural proteins are integral membrane polypeptides. The homotrimeric spike protein (S) ensures specific binding of the particle with ACE2 receptor at the cell surface and subsequent internalization of the complex by fusion of viral and host cell membranes. S-protein is large (1272 amino acid residues, a.a.r.) and has a prominent extracellular N-terminal portion followed by transmembrane helix and small cytoplasmic C-terminal domain. M-protein, the highest-copied, is thought to coordinate the viral particle assembly through interactions with N-protein (and accordingly with the viral genome) and other structural proteins. M-protein (222 a.a.r.) consists of short extracellular N-terminal portion, three transmembrane segments and cytoplasmic C-terminal domain; its structure

has not been determined experimentally but relies on available models for homologous proteins. E-protein of SARS-CoV-2 is small (75 a.a.r.), low-copied (few molecules per virion) and forms homopentamers. Its N-terminus exposed to extracellular space is followed by a single transmembrane segment and small cytoplasmic C-terminal domain. E-protein has been implicated in the viral particle assembly and viroporin ion channel functionalities.

Despite the most diligent research efforts of the last two years, some steps in the SARS-CoV-2 life cycle are still poorly understood. For instance, exact molecular mechanisms of the viral budding remain elusive. The release of membrane-enveloped viral particles involves two principal steps: formation of spherical protrusions at the membrane and subsequent detachment of the enveloped particles from the host membrane [3]. Many viral proteins reveal a capacity of deforming the membrane to initiate budding, but only few of them can mediate membrane fission for the final detachment. Most enveloped viruses use the host cell 'endosomal sorting complex required for transport' (ESCRT) apparatus to promote the membrane scission [4]. However, in certain taxa including coronaviruses this stage involves viral proteins only [5, 6].

A recent computational modeling study has demonstrated that E-protein can both sense and induce the membrane curvature, as its cytoplasmic C-terminus 'prefers' convex
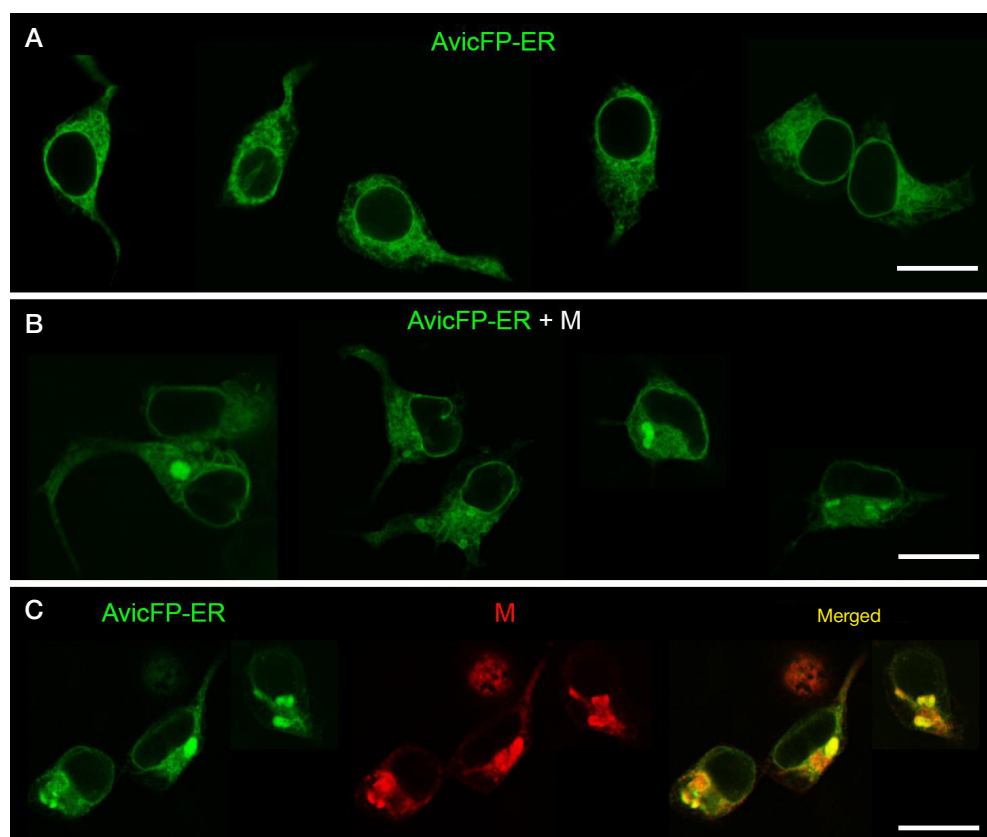
**Fig. 1.** Confocal fluorescence microscopy of HEK293T cells transfected with expression constructs. Scale bars, 20 μm. **A**. Transfection with plasmid encoding fluorescent protein AvicFP-ER localized to ER (*green* channel). **B**. Cotransfection with plasmids encoding AvicFP-ER (*green* channel) and M-protein. **C**. Cotransfection with plasmids encoding AvicFP-ER (*green* channel) and M-protein with subsequent immunostaining for M-protein (*red* channel; a merged channel image is shown on the *right*). The images are collages of four (**A**), four (**B**) and two (**C**) fields of view, showing representative results of each experiment.

regions of the membrane [7]. Apart from a circular convex region (neck) which connects the budding virion with the host cell membrane, the inside of the budding particles is concave. The curvature-induced segregation effect may explain the fewness of E-protein molecules in the virion; importantly, it also suggests active participation of E-protein in the neck formation and scission [8].

In this study, we used fluorescence microscopy of human cells expressing SARS-CoV-2 M-protein. Compared with the full-fledged viral infections of cell cultures, transfection models have certain advantages. Firstly, a particular target protein can be studied as a separate entity uninfluenced by other viral components, which affords a reduction in research complexity and a higher degree of accuracy. Secondly, the absence of infectious agent eliminates the safety concerns and allows making research in a conventional laboratory. Thirdly, such single-component experimental systems can be readily transformed into safe and straightforwardly scalable screening platforms for corresponding inhibitors. On the other hand, the reductionist models based on individual viral genes have serious limitations and all findings obtained with such models require verification in more sophisticated settings.

HEK293T cells were transfected with expression vector encoding SARS-CoV-2 M-protein (pGBW-m4134547, AddGene plasmid #152583) and green fluorescent protein mAvicFP1 with endoplasmic reticulum (ER) localization signal (mAvicFP1-ER) to enable ER visualization [9]. The confocal microscopy observations were carried out with Leica DMIRE2 TCS SP2 inverted microscope (Leica; Germany) in green (excitation 488 nm, detection 500–535 nm) and red (excitation 543 nm, detection 560–660 nm) channels. Preliminary control transfections with mAvicFP1-ER produced the expected patterns of cytoplasmic

fluorescence shaped as a delicate network morphologically corresponding to ER (Fig. 1A). However, in cotransfections with the M-protein-encoding construct, the mAvicFP1-ER signal looked different. The network was preserved, but the majority of cells presented with bright rounded structures 1–5 μm in size (Fig. 1B). Immunostaining with anti-M-protein antibody (polyclonal rabbit IgG, ABIN6952906; antibodies-online Inc., USA) topped with goat secondary antibodies conjugated to Alexa Fluor 594 red-fluorescent dye (A-11012; Invitrogen, USA) revealed colocalization of M-protein and mAvicFP1-ER (Fig. 1C). Apparently, M-protein was associated with ER membranes and somehow promoted their agglomeration.

Similar structures were previously described in cells expressing certain proteins anchored in ER membranes and prone to oligomerization. The effect was explained by interactions of protein subunits across ER membranes resulting in agglomeration of the membranes into multishaped multilayered arrays — the so-called 'organised smooth endoplasmic reticulum' (OSER) structures [9, 10] (Fig. 2A).

SARS-CoV-2 M-protein is known to be capable of dimerization within a membrane [11]. Our findings indicate that M-protein is also prone to oligomerization across two membranes. The interaction is likely to involve C-terminal domains protruding into cytosol.

Effective scission of a membranous vesicle requires membrane convergence to a 1–5 nm distance [12]. As C-terminal domain in M-protein extends by 3 nm from the membrane surface [11], intermembrane interactions between C-terminal domains can bring the opposite membranes as close as 3–6 nm. Therefore, intermembrane oligomerization of M-protein may provide a driving force for the membrane convergence, which enables scission of SARS-CoV-2 particles during budding (Fig. 2B).
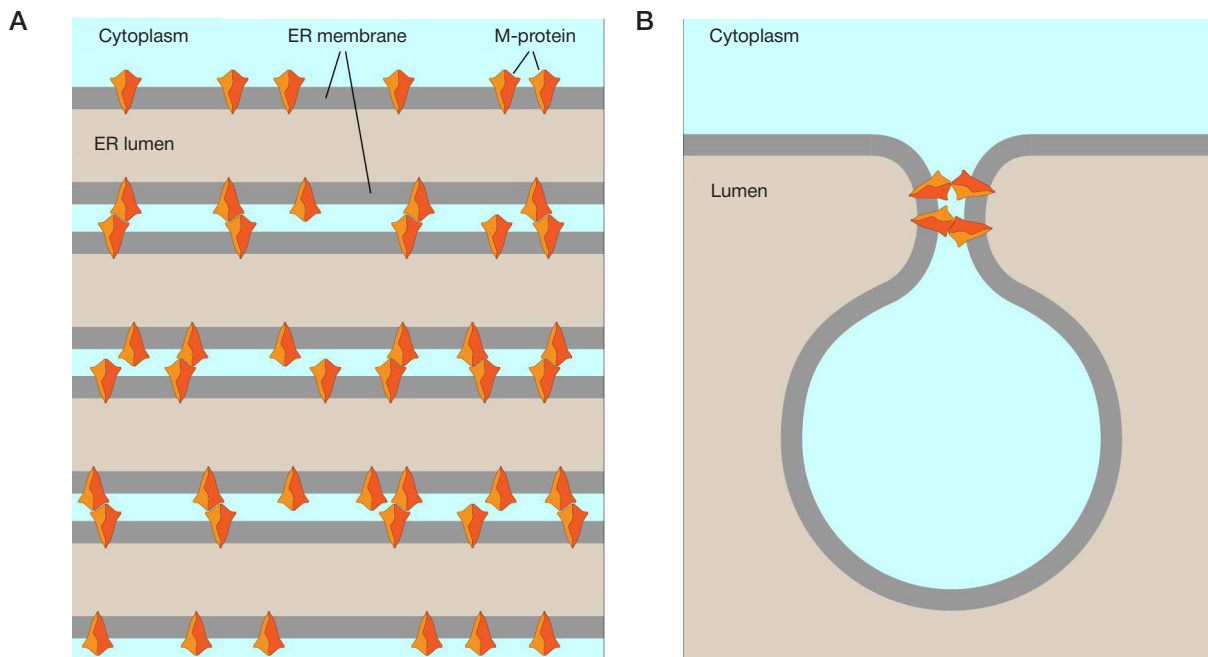
**Fig. 2.** A scheme of SARS-CoV-2 M-protein intermembrane oligomerization. **A**. Stacking of ER membranes into OSER structure through interactions of M-protein dimers in adjacent membranes. **B**. Hypothetical participation of the M-protein intermembrane oligomers in the neck formation during budding (M-protein molecules at other locations are omitted for clearance).

This hypothesis can be tested by mutagenesis of M-protein at the putative intermembrane interaction interfaces (the external amino acid positions of C-terminal domain unengaged in dimerization). The developed test for OSER structures may provide a simple means to assess the influence of particular amino acid substitutions on the intermembrane oligomerization capacity. In the case of confirmed functional significance, visualization of OSER structures in M-protein-expressing cells can be used as a safe functional assay in high-throughput screenings of the candidate inhibitors.

CONCLUSION

Here we describe the formation of OSER structures in human cells expressing SARS-CoV-2 M-protein. The confocal microscopy observations indicate effective oligomerization of M-protein subunits across adjacent ER membranes. We believe that such interactions may promote membrane convergence and ultimately facilitate the detachment of viral particles during budding. If true, the developed test for OSER structures can be used in high-throughput screenings of M-protein oligomerization inhibitors.

References

1. Yan W, Zheng Y, Zeng X, He B, Cheng W. Structural biology of SARS-CoV-2: open the door for novel therapies. Signal Transduct Target Ther. 2022; 7: 26.
2. Putlyaeva LV, Lukyanov KA. Studying SARS-CoV-2 with Fluorescence Microscopy. Int J Mol Sci. 2021; 22.
3. Rossman JS, Lamb RA. Viral membrane scission. Annu Rev Cell Dev Biol. 2013; 29: 551–69.
4. Barnes J, Wilson DW. Seeking Closure: How Do Herpesviruses Recruit the Cellular ESCRT Apparatus? J Virol. 2019; 93.
5. Rossman JS, Jing X, Leser GP, Lamb RA. Influenza virus M2 protein mediates ESCRT-independent membrane scission. Cell. 2010; 142: 902–13.
6. J Alsaadi EA, Jones IM. Membrane binding proteins of coronaviruses. Future Virol. 2019; 14: 275–86.
7. Kuzmin A, Orekhov P, Astashkin R, Gordeliy V, Gushchin I. Structure and dynamics of the SARS-CoV-2 envelope protein

monomer. Proteins. 2022; 90: 1102–14.
8. Venkatagopalan P, Daskalova SM, Lopez LA, Dolezal KA, Hogue BG. Coronavirus envelope (E) protein remains at the site of assembly. Virology. 2015; 478: 75–85.
9. Costantini LM, Fossati M, Francolini M, Snapp EL. Assessing the tendency of fluorescent proteins to oligomerize under physiologic conditions. Traffic. 2012; 13: 643–9.
10. Snapp EL, Hegde RS, Francolini M, Lombardo F, Colombo S, Pedrazzini E, et al. Formation of stacked ER cisternae by low affinity protein interactions. J Cell Biol. 2003; 163: 257–69.
11. Monje-Galvan V, Voth GA. Molecular interactions of the M and E integral membrane proteins of SARS-CoV-2. Faraday Discuss. 2021; 232: 49–67.
12. Campelo F, Malhotra V. Membrane fission: the biogenesis of transport carriers. Annu Rev Biochem. 2012; 81: 407–27.

Литература

1. Yan W, Zheng Y, Zeng X, He B, Cheng W. Structural biology of SARS-CoV-2: open the door for novel therapies. Signal Transduct Target Ther. 2022; 7: 26.
2. Putlyaeva LV, Lukyanov KA. Studying SARS-CoV-2 with Fluorescence Microscopy. Int J Mol Sci. 2021; 22.
3. Rossman JS, Lamb RA. Viral membrane scission. Annu Rev Cell

Dev Biol. 2013; 29: 551–69.
4. Barnes J, Wilson DW. Seeking Closure: How Do Herpesviruses Recruit the Cellular ESCRT Apparatus? J Virol. 2019; 93.
5. Rossman JS, Jing X, Leser GP, Lamb RA. Influenza virus M2 protein mediates ESCRT-independent membrane scission. Cell. 2010; 142: 902–13.

6.  J Alsaadi EA, Jones IM. Membrane binding proteins of coronaviruses. Future Virol. 2019; 14: 275–86.
7.  Kuzmin A, Orekhov P, Astashkin R, Gordeliy V, Gushchin I. Structure and dynamics of the SARS-CoV-2 envelope protein monomer. Proteins. 2022; 90: 1102–14.
8.  Venkatagopalan P, Daskalova SM, Lopez LA, Dolezal KA, Hogue BG. Coronavirus envelope (E) protein remains at the site of assembly. Virology. 2015; 478: 75–85.
9.  Costantini LM, Fossati M, Francolini M, Snapp EL. Assessing the tendency of fluorescent proteins to oligomerize under physiologic conditions. Traffic. 2012; 13: 643–9.
10. Snapp EL, Hegde RS, Francolini M, Lombardo F, Colombo S, Pedrazzini E, et al. Formation of stacked ER cisternae by low affinity protein interactions. J Cell Biol. 2003; 163: 257–69.
11. Monje-Galvan V, Voth GA. Molecular interactions of the M and E integral membrane proteins of SARS-CoV-2. Faraday Discuss. 2021; 232: 49–67.
12. Campelo F, Malhotra V. Membrane fission: the biogenesis of transport carriers. Annu Rev Biochem. 2012; 81: 407–27.

# A NEW STRATEGY IN SELECTION OF HORMONE THERAPY FOR ENDOMETRIAL PROLIFERATIVE PROCESS IN POSTMENOPAUSAL PATIENTS

Savelyeva GM, Breusenko VG, Kareva EN, Golukhov GN, Gutorova DS ✉, Ovchinnikova AV, Ivanovskaya TN,  Shcherbatyuk KV

Pirogov Russian National Research Medical University, Moscow, Russia

The limited efficacy of hormone therapy for endometrial proliferative process (EPP) in postmenopausal patients and its side effects on the immune system functionalities have not been studied in detail. Here we assess the feasibility of hormone therapy for EPP in postmenopausal patients through evaluation of estradiol and progesterone receptor gene expression in endometrial tissue and peripheral blood mononuclear cells (PBMC). The study enrolled 92 postmenopausal patients with EPP, including 37 pts with glandular-fibrous polyps, 7 pts with non-atypical endometrial hyperplasia (EH), 8 pts with atypical endometrial hyperplasia (AEH), 31 pts with moderately differentiated adenocarcinoma and 9 pts with highly differentiated adenocarcinoma. The PBMC isolates and endometrial samples were tested for ERα, ERβ, mER, PRA, PRB, mPR and PGRmC1 expression by reverse real time polymerase chain reaction (RT–PCR). Differential changes in PBMC receptor profiles upon in vitro exposure to progesterone or mifepristone were determined for patients with endometrial polyps and healthy women. The results indicate elevated expression of ERα, ERβ, PRA, PRB, mPR and PGRmC1 by endometrial tissues in EH and elevated expression of mER, ERα and PRA by PBMC in AEH, apparently reflecting suppressed functionalities of monocytes, macrophages, T-cells and natural killer cells. Unaltered expression of the studied genes by PBMC in endometrial adenocarcinoma may reflect the incrementing tumor autonomy. In vitro, mifepristone inhibited ERα, ERβ, mPR, PGRmC1, PRA and PRB expression in PBMC isolated from patients with endometrial polyps. We suppose that such effects can mitigate the negative influence of sex steroid hormones on immunocompetent cells.

**Keywords:** endometrial proliferative process, endometrial hyperplasia, postmenopause, hormonal therapy, ERα, ERβ, mER, PRA, PRB, mPR, PGRmC1

# НОВАЯ СТРАТЕГИЯ ПОИСКА ГОРМОНАЛЬНОЙ ТЕРАПИИ ПРОЛИФЕРАТИВНЫХ ПРОЦЕССОВ ЭНДОМЕТРИЯ У ПАЦИЕНТОК В ПОСТМЕНОПАУЗЕ

Г. М. Савельева, В. Г. Бреусенко, Е. Н. Карева, Г. Н. Голухов, Д. С. Гуторова ✉, А. В. Овчинникова, Т. Н. Ивановская, К. В. Щербатюк

Российский национальный исследовательский медицинский университет имени Н. И. Пирогова, Москва, Россия

Причины неэффективности гормональной терапии пролиферативных процессов эндометрия (ППЭ) в постменопаузе остаются неясными. Влияние гормональной терапии ППЭ на активность иммунной системы достаточно не изучено. Целью работы было на основании результатов исследования экспрессии генов рецепторов эстрадиола и прогестерона в ткани эндометрия, клетках мононуклеарной фракции периферической крови (МНФК) определить целесообразность и возможность назначения гормональной терапии ППЭ у пациенток в постменопаузе. Обследовали 92 пациентки в постменопаузе с ППЭ: с железисто-фиброзными полипами — 37; с гиперплазией без атипии (ГЭ) — 7; атипической гиперплазией (АГЭ) — 8; умереннодифференцированной аденокарциномой — 31; высокодифференцированной аденокарциномой — 9. В МНФК и образцах ткани эндометрия исследовали экспрессию ERα, ERß, mER, PRA, PRB, mPR, PGRmC1 методом РТ-ПЦР. В эксперименте определяли изменение рецепторного профиля МНФК после инкубации клеток с прогестероном и мифепристоном у пациенток с полипами эндометрия и здоровых женщин. При анализе результатов в ткани ГЭ обнаружен высокий уровень ERα, ERβ, PRA, PRB, mPR, PGRmC1. В МНФК при АГЭ выявлен высокий уровень mER, ERα, PRA. Это может свидетельствовать о подавлении функции моноцитов, макрофагов, Т-лимфоцитов и натуральных киллеров. При аденокарциноме эндометрия рецепторный транскриптом в МНФК не нарушен, что может означать развитие автономности опухоли. В исследовании in vitro мифепристон снижает экспрессию ERα, ERß, mPR, PGRmC1, PRA, PRB в МНФК у пациенток с полипами эндометрия. На наш взгляд, это нивелирует негативное действие половых стероидных гормонов на иммунокомпетентные клетки.

**Ключевые слова:** пролиферативные процессы эндометрия, гиперплазия эндометрия, постменопауза, гормональная терапия, ERα, ERß, mER, PRA, PRB, mPR, PGRmC1

Endometrial cancer occupies a prominent place in the epidemiological structure of malignant tumours [1]. The morbidity peaks at 65–69 years, constituting 98.1 cases per 100,000 women of this age group. Endometrial adenocarcinoma is the most prevalent type of uterine cancer. This hormone-dependent tumor often develops against the clinical background of endometrial proliferative process (EPP) [2]. The hormone therapy options show limited efficacy for endometrial tumours and are indicated exclusively in young patients with early stages of low-grade uterine cancer. In cases of atypical endometrial hyperplasia (AEH), surgical treatment is usually recommended first-line due to the high risks (40–60%) of concomitant endometrial adenocarcinoma [3]. For non-atypical endometrial hyperplasia (EH), hormone therapy may be 100% efficacious; however, to achieve this level, the progestogens must act directly and sustainably on the endometrium (e.g. by means of levonorgestrel-containing intrauterine system) [4, 5]. With the use of oral forms, the efficacy constitutes 50–69% [6]. The higher rates of response achieved with intrauterine delivery systems can be attributed to their low systemic influence.

Personalized prediction of response to hormone therapy in EPP is highly relevant. The candidate prognostic factors include expression of pro- and antiapoptotic proteins and overall endometrial receptivity, as well as differential expression of hormone receptors in endometrial glands and stroma [7–11]. However, no convincing results at the tissue level have been obtained so far. Even with the high sensitivity of tissue to hormonal influence, systemic effects of the treatment were often disregarded. In particular, data on the immunity-related side effects of hormone therapy for EPP are missing, despite its alleged principal significance. Despite the lack of significant correlation between the type of endometrial pathology and composition of immunocompetent cells, the corresponding functional relationships have not been assessed [12].

According to recent evidence, hormone substances (both endogenous and pharmaceutical) affect immunocompetent cell functionalities as they bind corresponding receptors abundantly expressed by these cells [13], and the outcomes may be complex, as different cell types and subpopulations of the immune system express specific hormone receptor signatures [13]. It should be noted, however, that these preliminary data were collected in healthy donors without proper accounting for the age group.

The aim of this study was to assess the feasibility and advisability of hormone therapy for EPP in postmenopausal patients on personalised basis, by studying differential expression of estradiol and progesterone receptor genes in endometrial tissue and peripheral blood mononuclear cells (PBMC) collected from the patients. In addition, we applied in vitro tests of the hormone drug effects on PBMC receptor profiles as a sensitivity assay.

METHODS

The study was carried out in 2012–2021 at the City Clinical Hospital № 31, Moscow, the clinical base for the Obstetrics and Gynecology Chair of the Pirogov Medical University. Part of the material was accessed in the Oncogynecology Department of the Oncology Dispensary № 1, Moscow. The study enrolled 92 hospitalized patients with EPP, postmenopausal, assigned to either main or comparison group based on histological diagnosis. The main group included 55 pts with different forms of high-rate EPP: 7 pts with non-atypical endometrial hyperplasia (EH), 8 pts with atypical endometrial hyperplasia (AEH) and 40 pts with endometrial adenocarcinoma (31 pts

with moderately differentiated adenocarcinoma (G1) and 9 pts with highly differentiated adenocarcinoma (G2)). The comparison group included 37 pts with histologically verified glandular-fibrous endometrial polyps qualified as a low-rate form of EPP. The study of hormone receptor gene expression in PBMC involved a control group of 10 healthy women in postmenopause without gynecological pathology. This group consisted of staff members at the Pirogov Medical University and City Clinical Hospital № 31 without clinical manifestations of EPP. The absence of endometrial pathology and other gynecological diseases was confirmed by pelvic ultrasound scans. The control group donated blood samples.

Inclusion criteria for main and comparison groups were as follows: the presence of pathomorphologically verified endometrial pathology; post-menopause. The histological specimens were classified in accordance with the 2014 World Health Organization (WHO) classification criteria as non-atypical endometrial hyperplasia, atypical endometrial hyperplasia, endometrial adenocarcinoma (either moderately or highly differentiated) or endometrial polyp (glandular-fibrous variant).

Exclusion from the study (main, comparison and control groups) was based on the following unified criteria: taking hormonal medications (estrogens, gestagens, gonadotropin-releasing hormone agonists, hormone replacement therapy and/or tamoxifen) within 6 months prior to the study, gynaecological diseases (uterine fibroids of size exceeding a 6–7 weeks pregnant uterus, ovarian tumors) and inflammatory processes of any localisation at the time of sampling.

The age of participants enrolled in the study varied within the total range of 53–80 years constituting 64.2 ± 6.27 years on average. The time since menopause varied and depended on the age of participants.

The reasons for hospitalisation included endometrial pathology confirmed by pelvic ultrasound examination in 60 pts (65.22%) and genital tract bleeding in 32 pts (34.78%).

The gynaecological comorbidities were dominated by small uterine fibroids (5- to 6-week pregnancy and at the stage of regression) in 63.04%. In addition, 28.26% of the patients had a history of endometrial pathology (polyps, non-atypical endometrial hyperplasia) at various times in their lives.

The non-gynecological comorbidities were dominated by chronic hypertension, ischemic heart disease and variable degree of obesity (diagnosed in 80.43%, 72.82% and 90.2% of the patients, respectively).

All patients underwent standard examination including routine ultrasound scans with a Logiq E9 apparatus (GE; USA) equipped with a 4–10 MHz intracavitary microconvex transducer. All patients presented with increased endometrial thickness exceeding 4 mm, accompanied by echostructure heterogeneity and hyperechoic foci.

Hysteroscopy with dilation and curettage was performed in 55 (59.78%) pts, 16 of which underwent resection or ablation of the endometrium. Total hysterectomy was performed in 37 (40.22%) pts by laparotomy in 30 pts, laparoscopy in 6 pts and vaginal access in 1 pt.

Blood samples were collected from the patients before the surgery. PBMC were isolated from peripheral blood as described by Bouman et al. [14]. The endometrial biopsies were dissected midway into identical halves: one for gene expression assay and one for histological examination. The tissues were placed into labeled Thermo Scientific™ Nunc™ 1.5 mL cryogenic vials and frozen in liquid nitrogen to preserve mRNA, subsequently isolated with RIBO-prep kits (InterLabService; Russia) and handled in accordance with manufacturer's protocols.
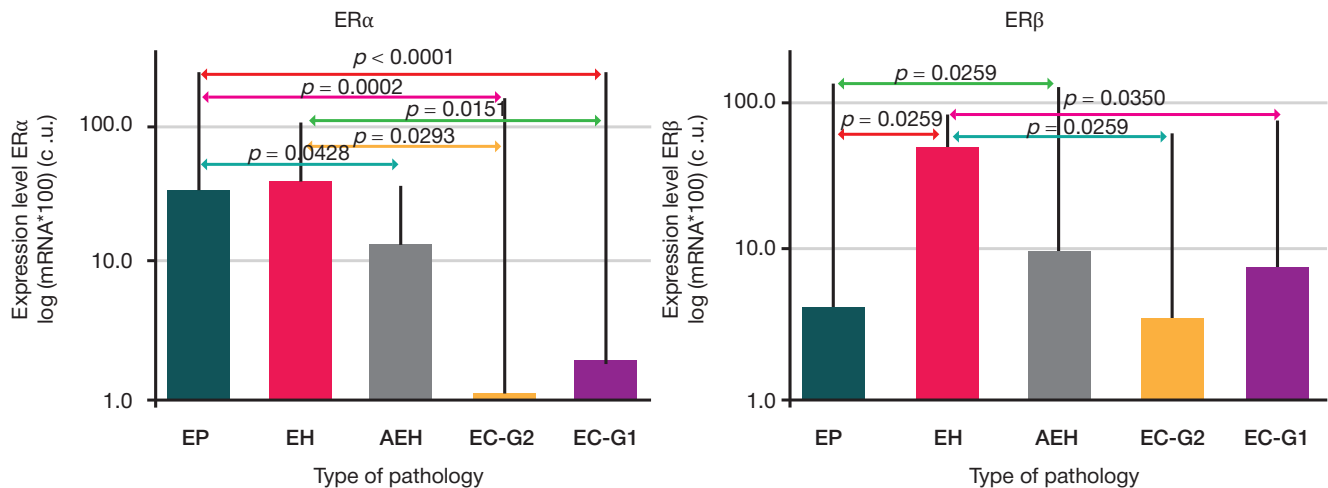
**Fig. 1.** Expression of estradiol nuclear receptor genes in endometrial tissue of postmenopausal patients with endometrial proliferative process. Vertical axis: lg mRNA level $(1/2-\Delta Ct) \times 10^2$, reference gene GAPDH; horizontal axis: EP — endometrial polyp (glandular-fibrous), EH — non-atypical endometrial hyperplasia, AEH — atypical endometrial hyperplasia, EC-G1 — highly differentiated (G1) endometrial carcinoma, EC-G2 — moderately differentiated (G2) endometrial carcinoma

Expression levels of estradiol and progesterone receptor-encoding genes (respectively ERα, ERβ and mER, and PRA, PRB, mPR and PGRmC1) in endometrial biopsies and PBMC were assessed by real time polymerase chain reaction method (RT–PCR). mRNA isolation, reverse transcription and DNA quantitation were carried out by standard protocols; gene expression levels were assessed by PCR using iCycler iQ™ Real Time PCR system (BioRad; Germany) against GAPDH as a reference transcript. The relative abundancies of specific transcripts were calculated by ΔCt method using $(1/2)^{\wedge}\Delta Ct$ and $2^{\wedge}(-\Delta\Delta Ct)$ equations, where $\Delta Ct = Ct(mER) - Ct(GAPDH)$ and $\Delta\Delta Ct = \Delta Ct$ (pathology) $- \Delta Ct$ (control).

In addition, we conducted in vitro experiments to assess the effects of gestagen exposure on estradiol and progesterone receptor gene expression in PBMC isolated from blood samples of the patients with endometrial polyps and matching healthy individuals. The cells were exposed to progesterone or mifepristone added to $10^{-8}$ M final concentrations in the incubation medium to be compared with no-hormone-added control incubations. Following the exposure, the cells were subject to estradiol and progesterone receptor gene expression measurements as described in the previous paragraph.

PBMC viability *in vitro* was measured by MTT test [15] following the exposure.

Patient database for the study was constructed on the basis of individual clinical histories, with the use of standard program packages Microsoft Excel 7.0 (Microsoft; USA) for Windows 2007 (Microsoft; USA) and Numbers version 4.3 (5046) (Apple; USA) for MacBook Pro 2013 (Apple; USA). The analysis involved comparative evaluation of qualitative and quantitative indicators for the groups. Statistical processing and visualisation of the data was carried out in GraphPad Prism version 5.0 (GraphPad Software; USA) and STATISTICA 8 (StatSoftInc; USA) program packages. The comparisons were made using Fisher and Mann–Whitney tests; differences qualified as non-random with at least 95% probability ($p < 0.05$) were considered statistically significant.

RESULTS

The results indicate that expression of estradiol and progesterone receptor genes in endometrial tissue depends on the types of endometrial pathology. Consistently with previous findings [16], high expression levels of estradiol receptors ERα and ERβ were observed in EH and low in adenocarcinoma (Fig. 1).

For progesterone nuclear receptor genes [16], we revealed high expression levels in EH and AEH (Fig. 2). The PRA and PRB expression levels, although similar between the groups, differed in a more specialised comparison between patients with adenocarcinoma and AEH. Consistently with other studies, we observed a sharp decrease in expression for PRA and a less pronounced effect for PRB in adenocarcinoma compared with AEH.
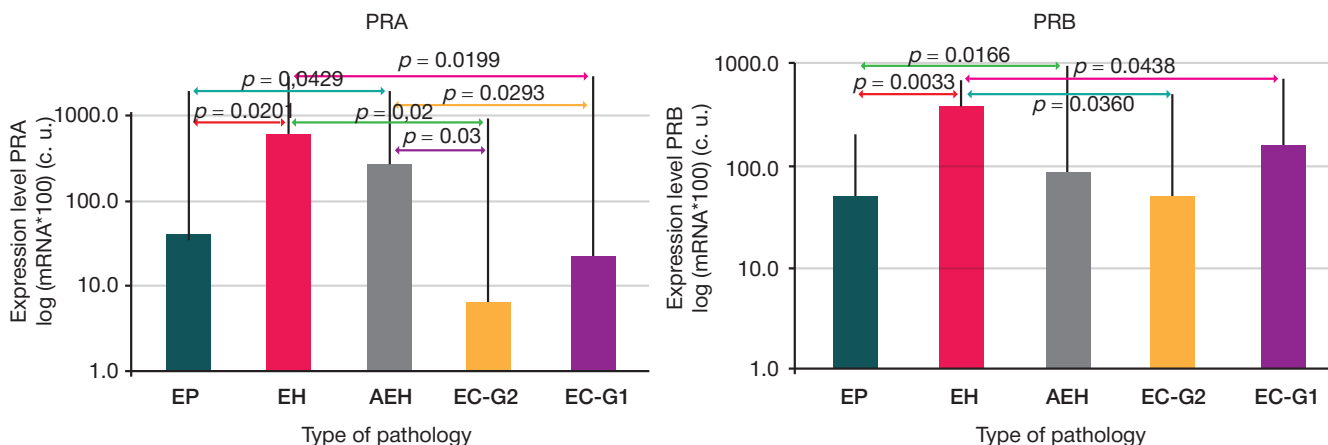


**Fig. 2.** Expression of progesterone nuclear receptor genes in endometrial tissue of postmenopausal patients with endometrial proliferative process. Vertical axis: lg mRNA level $(1/2-\Delta Ct) \times 10^2$, reference gene GAPDH; horizontal axis: EP — endometrial polyp (glandular-fibrous), EH — non-atypical endometrial hyperplasia, AEH — atypical endometrial hyperplasia, EC-G1 — highly differentiated (G1) endometrial carcinoma, EC-G2 — moderately differentiated (G2) endometrial carcinoma
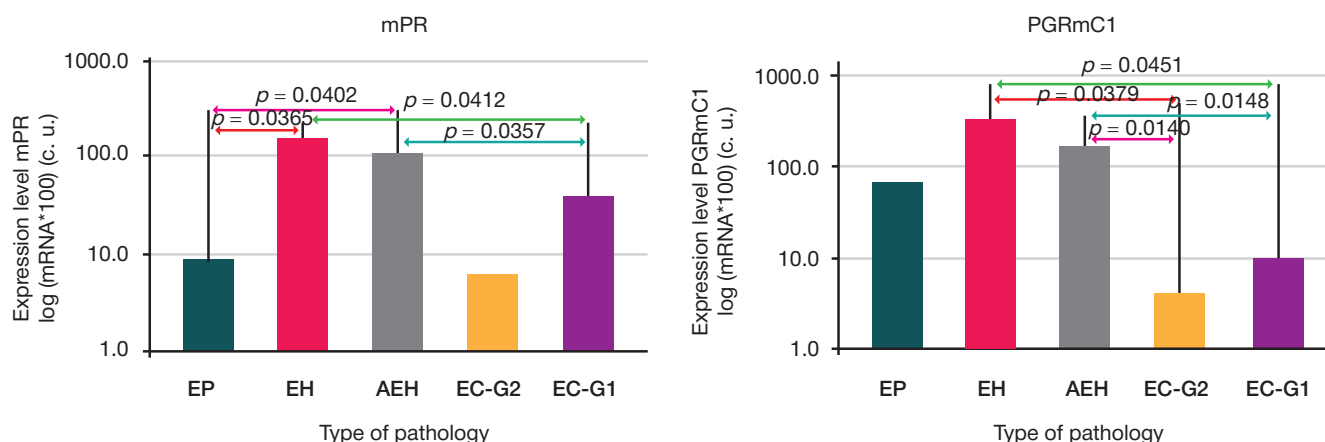
**Fig. 3.** Expression of progesterone membrane receptor genes in endometrial tissue of postmenopausal patients with endometrial proliferative process. Vertical axis: lg mRNA level $(1/2–\Delta Ct) \times 10^2$, reference gene GAPDH; horizontal axis: EP — endometrial polyp (glandular-fibrous), EH — non-atypical endometrial hyperplasia, AEH — atypical endometrial hyperplasia, EC-G1 — highly differentiated (G1) endometrial carcinoma, EC-G2 — moderately differentiated (G2) endometrial carcinoma

We also observed elevated expression of mPR in EH and AEH (Fig. 3), whereas PGRmC1 expression levels were specifically reduced in adenocarcinoma (Fig. 3).

Consistently with previous reports [17], PBMC isolated from patients with AEH expressed higher levels of mER, ERα and PRA compared with the cells derived from healthy women (Fig. 4). In addition, PBMC isolated from patients with endometrial adenocarcinoma expressed significantly lower levels of ERβ compared with the control group.

Comparison of estradiol and progesterone receptor gene expression levels between endometrial tissue and PBMC revealed matching profiles for ERα and PRA (Figs. 1, 2, 4).

In vitro exposure of PBMC derived from healthy women to either mifepristone or progesterone stimulated the expression of both estradiol and progesterone receptor genes (Figs. 5, 6).

A similar exposure of PBMC derived from patients with endometrial polyps to progesterone resulted in elevated expression of mER, mPR and PGRmC1, whereas exposure of these cells to mifepristone resulted in decreased expression of ERα, ERβ, mPR, PGRmC1, PRA and PRB.

*In vitro* study of mifepristone effects on PBMC viability using MTT test revealed a decrease in the number of viable proliferating cytokine-producing immunocompetent cells ($p < 0.05$).

DISCUSSION

The proper, patient-oriented selection of hormone therapy in postmenopausal patients with EPP requires accounting for the steroid receptor status of endometrial tissue. With low
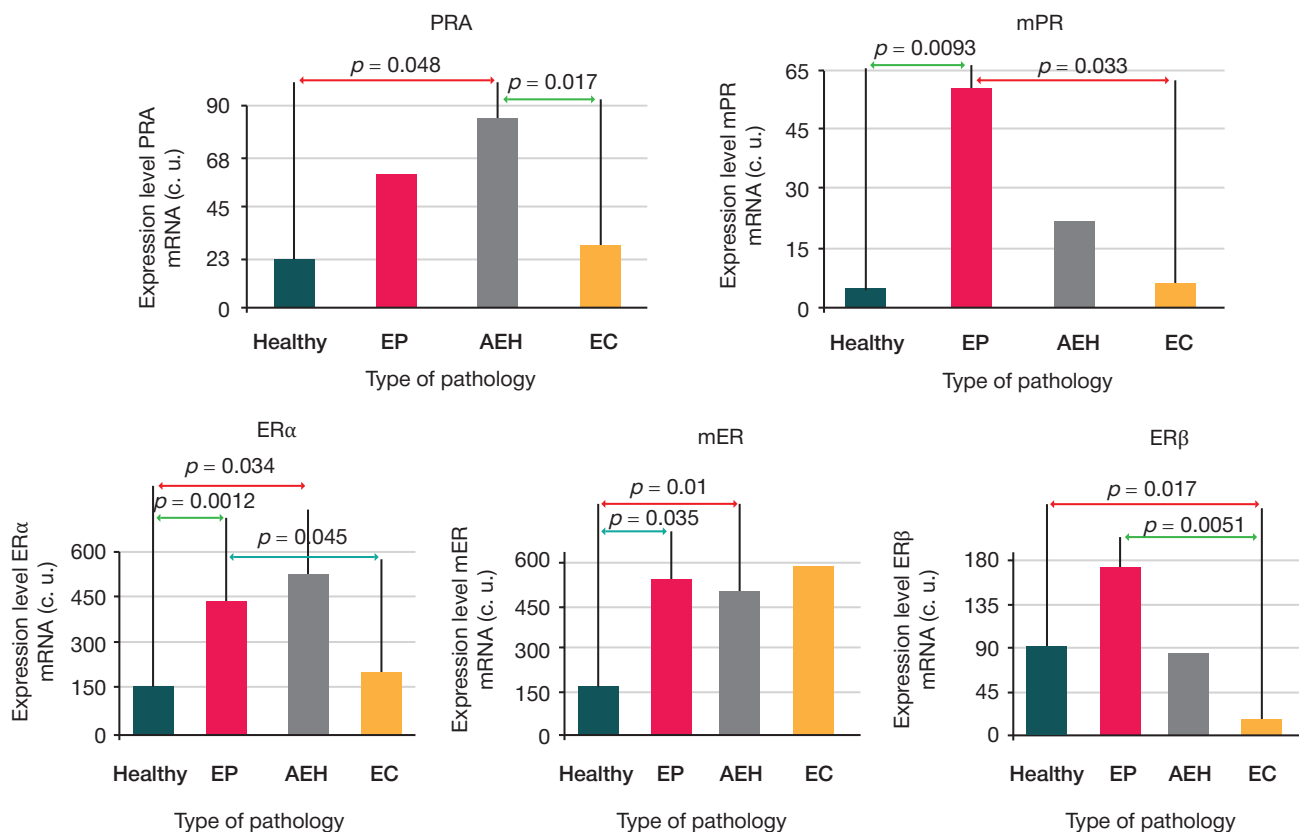


**Fig. 4.** Expression of estradiol and progesterone receptor genes in peripheral blood mononuclear cells of postmenopausal patients with endometrial proliferative process. Vertical axis: lg mRNA level $(1/2–\Delta Ct) \times 10^4$, reference gene GAPDH; horizontal axis: Healthy — matching healthy donors; EP — endometrial polyp (glandular-fibrous), AEH — atypical endometrial hyperplasia, EC— endometrial carcinoma; $p$ — level of significance
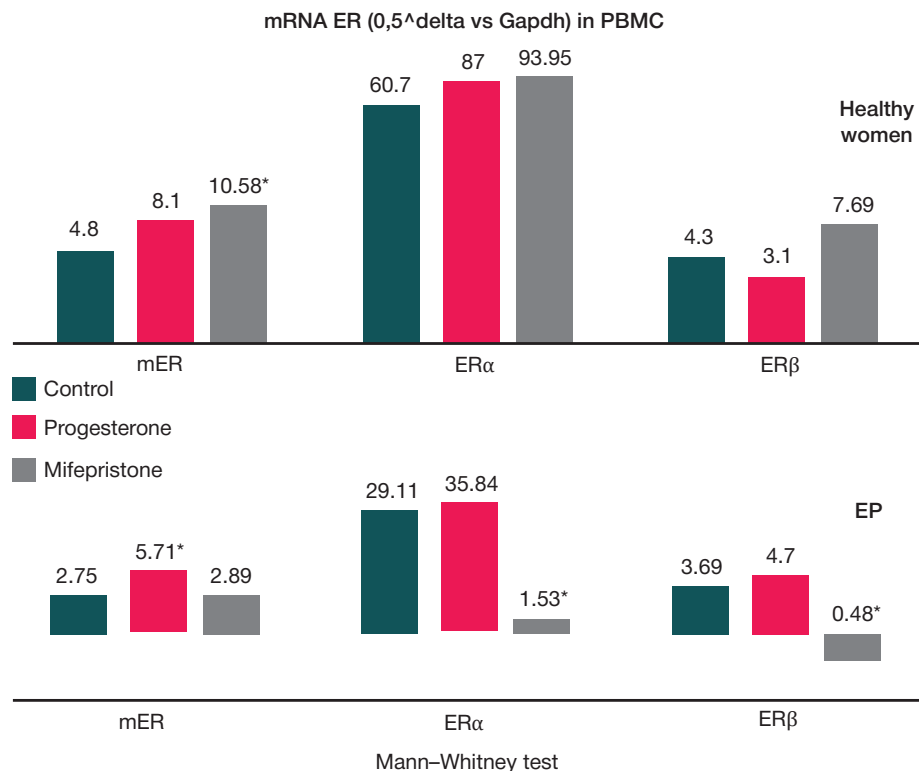
**Fig. 5.** Expression of estradiol receptor genes in peripheral blood mononuclear cells after *in vitro* exposure to progesterone and mifepristone. Vertical axis: mRNA level (1/2–ΔCt) × 100, reference gene GAPDH; horizontal axis: receptor type; EP — endometrial polyp (glandular-fibrous); * — $p \leq 0.05$

receptor availability, the local response to hormone exposure may not reach therapeutic values [4, 6, 7]. However, some postmenopausal patients with EPP show resistance to hormone therapy and develop relapses despite the availability of hormone receptors in the endometrial tissue. Such clinical situations are mechanistically unclear and require further investigation.

ERα and ERβ are main receptors that mediate proliferative action of estrogens on the endometrial tissue [18], with the major role played by ERα. The high expression of ERα and ERβ

observed by us in EH and AEH (Fig. 1) may indicate potential efficacy of aromatase inhibitors (estrogen synthesis blockers) in postmenopausal patients with this condition.

The elevated expression levels of ERβ in EH and AEH (Fig. 1) indicate its involvement in EPP pathogenesis. ERβ is known to mediate both proliferative and anti-proliferative estrogen signaling, which makes it a plausible drug target and justifies the screenings for its selective ligands. A correlation of higher ERβ expression levels with more aggressive forms of endometrial adenocarcinoma, demonstrated by comparative analysis
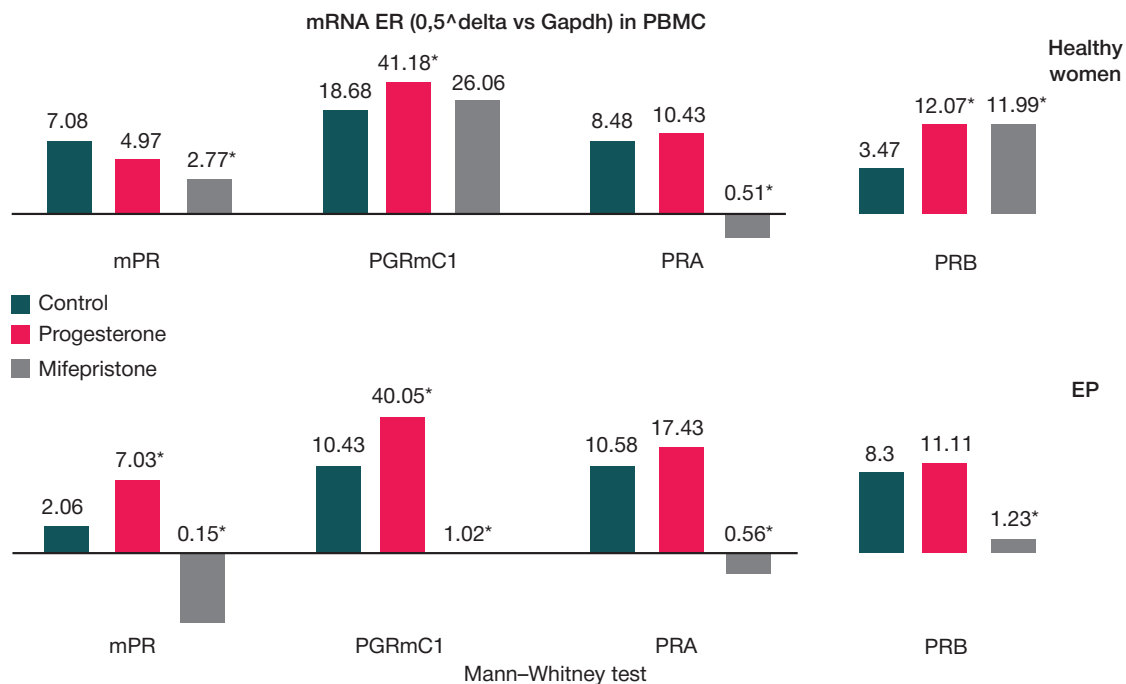


**Fig. 6.** Expression of progesterone receptor genes in peripheral blood mononuclear cells after *in vitro* exposure to progesterone and mifepristone. Vertical axis: mRNA level (1/2–ΔCt) × 100, reference gene GAPDH; horizontal axis: receptor type; EP — endometrial polyp (glandular-fibrous); * — $p \leq 0.05$

of ERα and ERβ expression in endometrial adenocarcinoma tissues [18], corroborates our hypothesis on a prominent role of ERβ in EPP pathogenesis. Other authors report high expression of estradiol nuclear receptors in EH tissues revealed by immunohistochemistry [19] albeit in mixed-age cohorts.

High expression levels of progesterone nuclear receptors in EH and AEH observed by us in this study (Fig. 2) may represent a compensatory counter-proliferative mechanism, possibly indicating a shortage of endogenous gestagens and justifying the prescription of synthetic gestagens as a pathogenetic treatment in this form of endometrial pathology. At the same time, in adenocarcinoma, PRB shows no sharp decrease in expression (by contrast with PRA), and is expressed at a level comparable with AEH, which may reflect unequal contributions of PRA and PRB to the pathogenesis consistently with other reports on this subject [20]. For instance, in the absence of PRA, PRB can support proliferation [21]. In this regard, given the predominance of PRB expression in endometrial tissue under conditions of EH, it would be reasonable to expect the lack of inhibitory effect from progesterone. In such cases, the gestagen-based regimens are likely to fail and even promote disease progression. These considerations indicate the need for personalised profiling of steroid receptors in endometrial biopsies or curettage material prior to synthetic gestagen prescription. At high PRA expression levels the gestagen therapy administration can be justified, whereas at high PRB expression levels its benefits should be doubted.

The membrane progesterone receptor mPR can potentiate the PRB-mediated signal transmission and significantly contribute to the progression of endometrial adenocarcinoma [22]. mPR and PRB jointly mediate the gestagen-induced proliferative signaling in target cells. Accordingly, the observed high expression level of mPR in EH and AEH (Fig. 3) may represent an adverse factor along with high expression of PRB.

Decreased expression of PRA, mPR and PGRmC1 in endometrial adenocarcinoma tissue indicates its compromised receptivity to progesterone and explains the low efficacy of hormone therapy for these patients, consistently with the common opinion that prescriptions of hormone therapy for endometrial adenocarcinoma should involve hormone receptor gene expression profiling administered on personalized basis [11].

Proliferative processes are known to be controlled by the immune system. Under compromised immune surveillance, these processes may become uncontrollable and lead to malignant transformation of the tissue. The receptor-mediated influence of sex steroids on immunocompetent cells is a proven fact [13]. However, to the best of our knowledge, no explicit data on the expression of estradiol and progesterone receptors by PBMC in EPP are available as yet.

In this study we observed impaired sensitivity of PBMC to steroids in EPP, indicative of their altered functionalities, given the reportedly unaltered leukocyte formula in EPP [12]. The unique receptor signatures expressed by different types of mononuclear cells [13] help explain the differential changes in their functionalities under the action of hormones.

ERα is the dominant type of estradiol receptors in monocytes/macrophages and T-helpers. Estradiol suppresses the monocyte-macrophageal responses while stimulating T-helper immunity [23, 24]. The high expression of ERα by PBMC in AEH observed by us in this study (Fig. 4) indicates increased sensitivity of the cells to the inhibitory action of estradiol on the monocyte-macrophageal compartment along with the opposite, stimulating effect on T-helper immunity. On the other hand, such stimulation of T-cell responses is known to activate macrophages and promote the release of pro-inflammatory cytokines by these cells second-hand

[23, 24], which explains the persistence of chronic inflammatory processes as one of pathogenetic components in malignant tumorigenesis.

T-killers, known to be heavily engaged at early stages of the anti-tumor response, are almost entirely devoid of nuclear receptors to estradiol; meanwhile, estrogens effectively suppress the activity of T-killers [24]. These findings implicate the membrane receptor mER as a cornerstone of estrogen signaling in T-killers. Accordingly, the increase in mononuclear cell sensitivity observed by us for AEH (Fig. 4) may favor the clonal preservation of atypical cells in endometrial tissue.

PRA has been shown to mediate the inhibition of cytokine release by progesterone [25]; among PBMC, this receptor is expressed by natural killers only. The high expression level of PRA observed by us in natural killer cells (Fig. 4) apparently potentiates the AEH progression.

Thus, in AEH, the monocyte, macrophage, T-cell and natural killer cell functionalities are inhibited. The explanation runs as follows: hyperexpression of receptors enhances the sensitivity of mononuclear cells to hormones (endogenous and pharmaceutical), which ultimately leads to the inhibition of immunocompetent cell functionalities. The uncontrollable nature of this process may support AEH malignisation, hence the low efficacy (and occasionally the overall adverse effect) of hormone therapy in postmenopausal patients with AEH.

In contrast to AEH, expression levels of ERα, PRA, mPR by PBMC in adenocarcinoma are similar to those of healthy women (Fig. 4), which is rather unexpected given the progressive deterioration of immunity characteristic of cancers. The dominance of ERα and PRA in PBMC has been already mentioned. According to the published evidence, mPR is a major steroid receptor in T-cells and monocytes/macrophages [26]. In combination with our data, this means that corresponding transcriptomic signatures of monocytes, macrophages, T cells and normal killer cells in postmenopausal patients with endometrial adenocarcinoma stay unaltered. This feature may be considered as a sign of escape of the malignant tumor from the immune surveillance.

Unexpected disease-related expression dynamics in PBMC was revealed for ERβ (Fig. 4). This receptor is the principal member of estrogen signaling pathway in B-cells [27]. Our data reveal a sharp decrease in its expression for endometrial adenocarcinoma compared to the control group (Fig. 4). In our opinion, this indicates hardly a loss of tumor sensitivity to external signals (since in such case the receptor expression levels would be closer to normal), but rather a second-hand suppression of B-cell immunity by the tumor.

Comparative analysis of hormone receptor gene expression in endometrial tissue and PBMC revealed matching ERα and PRA profiles. For endometrial adenocarcinoma, the trend may indicate masking of the tumor from direct effects of hormones as well as the immune system. Accordingly, prescription of hormone therapy to postmenopausal patients with endometrial adenocarcinoma is unjustified.

The high expression of PRA by endometrial tissue and mononuclear cells in AEH (Figs. 2, 4) indicates their increased sensitivity to gestagens; in PBMC, this feature is conducive to the atypical clone preservation.

Thus, pharmacological strategies for EPP in postmenopausal patients should account for the immunity-related side effects involving PBMC. The hormone drugs should be prescribed with caution due to their possible negative effect on immunocompetent cells.

To determine a synthetic drug with the mildest effect on the immune system, we comparatively analysed the binding

activity of progesterone receptors in PBMC with gestagens (P4 = 100%) and observed a 2-times weaker PBMC binding affinity for the so-called strong gestagens (medroxyprogesterone acetate and norethisterone, commonly prescribed in EPP) compared to progesterone ($p < 0.05$). As these drugs have been shown to effectively side-target immunocompetent cells and thus reduce their anti-proliferative activity, our experimental study engaged the anti-gestagenic drug mifepristone chosen as a model candidate medication to gain control over these processes.

Mifepristone, which actively and effectively binds progesterone receptors in mononuclear cells, is widely featured in clinical studies of treatments for hormone-dependent pathologies [28]. We used the 'canonical' mifepriston rather than more recent formulations because of its antitumor activity and lack of hepatotoxicity [29], which is particularly important in postmenopausal patients.

Progesterone exposure of PBMC derived from healthy women and patients with endometrial polyps promoted an increase in estradiol and progesterone receptor gene expression in both sample types (Figs. 5, 6), indicating increase sensitivity to the adverse impact of sex steroid hormones on PBMC functionalities. The differential influence of varying progesterone concentrations on cytokine synthesis has been demonstrated by other authors [30]; our findings (we used progesterone in nanomolar concentrations) do not contradict the published evidence.

Mifepristone exposure of PBMC revealed a beneficial effect of this drug on cells derived from patients with endometrial polyps, in the form of decreased expression of ERα, ERβ, mPR, PGRmC1, PRA and PRB receptors in PBMC (Figs. 5, 6), possibly counteracting the negative effect of sex steroids on immunocompetent cells. This observation justifies the prescription of this drug to patients with endometrial pathology, aimed at mitigation of PBMC sensitivity to suppressive action of sex hormones and thus promoting normalisation of the immune status. The data requires further validation on clinical cohorts.

The suppressive effect of mifepristone on the mononuclear cell viability observed by us in this study requires further investigation in order to screen for related substances most sparing towards the immunocompetent cells, but at the same time reducing the increased expression of estradiol and progesterone receptors by PBMC.

CONCLUSIONS

Selection of pathogenetic hormone therapy for endometrial proliferative process in postmenopausal patients requires accurate assessment of receptor status in the endometrial tissue and also in peripheral blood mononuclear cells. Hormone receptor gene expression data are highly relevant for predicting the response of endometrial tissue to hormone therapy in combination with its effect on immunocompetent cells. According to the results, high levels of PRA mRNA in endometrial hyperplasia sample can be used as a predictor of efficacy for anti-relapse gestagens therapy. Most notably, at high expression levels of PRB, its can be dangerous — leading to unpredictable tissue response and progressive proliferation. The cause of non-efficacy of the standard gestagen therapy for endometrial proliferative process is partially due to its underestimated inhibitory influence on the immune system. The effects of hormone drugs on functional profiles of PBMC and neutralisation of the adverse side effects of sex steroid hormones on immunocompetent cells without reducing their viability are relevant subjects of further investigation.

References

1. Kaprin AD, Starinskij VV, Shaxzadova AO, redaktory. Sostoyanie onkologicheskoĭ pomoshhi naseleniyu Rossii v 2020 godu. M.: MNIOI im. P.A. Gercena, 2021; 239 s. Russian.
2. Kurcer MA, Breusenko VG, Goluxov GN, Golova YuA, Esipova IA, Ovchinnikova AV, et al. Diagnostika i lechenie dobrokachestvennyx vnutrimatochnyx zabolevaniĭ u pacientok v postmenopauze. Voprosy ginekologii, akusherstva i perinatologii. 2019; 18 (3): 71–79. Russian.
3. Vetter MH, Smith B, Benedict J, Hade EM, Bixel K, Copeland LJ, et al. Preoperative predictors of endometrial cancer at time of hysterectomy for endometrial intraepithelial neoplasia or complex atypical hyperplasia. Am J Obstet Gynecol. 2020; 222 (1).
4. Dumanovskaya MR, Chernuxa GE, Tabeeva GI, Asaturova AV. Giperplaziya ehndometriya: poisk optimal'nyx resheniĭ i strategiĭ. Akusherstvo i ginekologiya. 2021; 4: 23–31. Russian.
5. Mittermeier T. Levonorgestrel-releasing intrauterine system for endometrial hyperplasia. Mittermeier T, Farrant C, Wise MR. Cochrane Database Syst Rev. 2020; 9 (9): CD012658. DOI:10.1002/14651858.CD012658.pub2.
6. Dolapcioglu K, Boz A, Baloglu A. The efficacy of intrauterine versus oral progestin for the treatment of endometrial hyperplasia. A prospective randomized comparative study. Clin Exp Obstet Gynecol. 2013; 40: 122–6.
7. Ashrafyan LA, Antonova IB, Ivashina SV, Babaeva NA, Aleshikova AI, Baranov II. Optimizaciya diagnosticheskoĭ taktiki u pacientok s anomal'nymi matochnymi krovotecheniami v periody peri- i postmenopauzy. Akusherstvo i ginekologiya: Novosti. Mneniya. Obucheniya, 2019; 1 (23). Dostupno po ssylke (data obrashheniya: 07.06.2021): https://cyberleninka.ru/article/n/optimizatsiya-diagnosticheskoy-taktiki-u-patsientok-s-anomalnymi-matochnymi-krovotecheniya-v-periody-peri-i-

8. Russo M, Newell JM, Budurlean L, Houser KR, Sheldon K, Kesterson J, et al. Mutational profile of endometrial hyperplasia and risk of progression to endometrioid adenocarcinoma. Cancer. 2020; 126 (12): 2775–83. DOI: 10.1002/cncr.32822.
9. Unanyan AL, Sidorova IS, Kogan EA, Baburin DV. Kliniko-patogeneticheskie osobennosti giperplasticheskix processov ehndometriya u zhenshhin perimenopauzal'nogo vozrasta. RMZh «Medicinskoe obozrenie». 2018; 1 (I): 67–71. Russian.
10. Patel MV, Shen Z, Rodriguez-Garcia M, Usherwood EJ, Tafe LJ, Wira CR. Endometrial Cancer Suppresses CD8+ T Cell-Mediated Cytotoxicity in Postmenopausal Women. Front Immunol. 2021. Available from: https://DOI.org/10.3389/fimmu.2021.657326.
11. Wang C, Tran DA, Fu MZ, Chen W, Fu SW, Li X. Estrogen Receptor, Progesterone Receptor, and HER2 Receptor Markers in Endometrial Cancer. J Cancer. 2020; 11 (7): 1693–701. DOI: 10.7150/jca.41943.
12. Kadagidze Z. G. Subpopulyacii limfocitov pri zlokachestvennom roste. Vopr. onkologii. 1984; 1: 90–97.
13. Dama A, Baggio C, Boscaro C, Albiero M, Cignarella A. Estrogen Receptor Functions and Pathways at the Vascular Immune Interface. Int J Mol Sci. 2021; 22 (8): 4254. Available from: https://doi.org/10.3390/ ijms22084254.
14. Bouman A, Schipper M, Heineman MJ, Faas M. 17beta-estradiol and progesterone do not influence the production of cytokines from lipopolysaccharide-stimulated monocytes in humans. Fertil Steril. 2004; 82 (Suppl 3): 1212–9.
15. Fisenko VP, redaktor. Rukovodstvo po ehksperimental'nomu (doklinicheskomu) izucheniyu novyx farmakologicheskix veshhestv. M.: Remedium, 2000; 398 s. Russian.
16. Saveleva GM, Breusenko VG, Kareva EN, i dr. Izuchenie roli

ehkspressii genov receptorov ehstrogenov i progesterona v vozniknovenii proliferativnyx processov v ehndometrii dlya resheniya voprosa o taktike vedeniya bol'nyx s ukazannymi patologicheskimi izmeneniyami ehndometriya. Rossijskij vestnik akushera-ginekologa. 2018; 18 (6): 17–24. DOI: 10.17116/rosakush20181806117. Russian.

17. Savelyeva GM, Breusenko VG, Kareva EN, Ivanovskaya TN, Tikhonov DA, Gutorova DS. Steroid-receptor profile of the peripheral blood mononuclear cells in postmenopausal patients with endometrial proliferative processes. Vopr. ginekol. akus. perinatol. (Gynecology, Obstetrics and Perinatology). 2019;18 (3): 80–86. DOI: 10.20953/1726-1678-2019-3-80-86. Russian.

18. Obata T, Nakamura M, Mizumoto Y, Iizuka T, Ono M, Terakawa J, et al. Dual expression of immunoreactive estrogen receptor — and p53 is a potential predictor of regional lymph node metastasis and postoperative recurrence in endometrial endometrioid carcinoma. PLoS ONE; 12 (11): 2017: e0188641. Available from: https://doi.org/10.1371/journal.pone.0188641.

19. Singh P, Chaurasia A, Dhingra V, Misra V. Expression of ERα and PR in Various Morphological Patterns of Abnormal Uterine Bleeding-Endometrial causes in Reproductive Age Group. J Clin Diagn Res. 2016;10 (8): EC06-EC9. DOI: 10.7860/JCDR/2016/19565.829.

20. Swasti. Estrogen and progesterone receptors in endometrial cancer: where are we today? Gynecol Obstet. 2018; 8: 2. DOI: 10.4172/2161-0932.1000e127.

21. Greca A, Bellora N, Dily F, Jara R, Nacht AS, Oliete JQ, et al. Chromatin topology defines estradiol-primed progesterone receptor and PAX2 binding in endometrial cancer cells. 2022; eLife. 11: e66034. Available from: https://doi.org/10.7554/eLife.66034.

22. Sinreih M, Knific T, Thomas P, Frković Grazio S, Rižner TL. Membrane progesterone receptors — and — have potential as prognostic biomarkers of endometrial cancer. J Steroid Biochem Mol Biol. 2018; 178: 303–11. DOI: 10.1016/j.jsbm.2018.01.011. PMID: 29353001.

23. Trenti A, Tedesco S, Boscaro C, Trevisi L, Bolego C, Cignarella A. Estrogen, Angiogenesis, Immunity and Cell Metabolism: Solving the Puzzle. Int J Mol Sci. 2018; 19 (3): 859. DOI: 10.3390/ijms19030859. PMID: 29543707. PMCID: PMC5877720.

24. Navarro FC. Herrnreiter C, Nowak L, Watkins SK. Estrogen Regulation of T-Cell Function and Its Impact on the Tumor Microenvironment. Gender and the Genome. 2018; 2 (3): 81–91. DOI: 10.1177/2470289718801379 journals.sagepub.com/home/gng.

25. Arruvito L, et al. NK Cells Expressing a Progesterone Receptor Are Susceptible to Progesterone-Induced Apoptosis. J Immunol. 2008; 180 (8): 5746–5753. DOI: https://doi.org/10.4049/jimmunol.180.8.5746.

26. Polikarpova AV, Levina IS, Sigai NV, Zavarzin IV, Morozov IA, Rubtsov PM, Guseva AA, Smirnova OV, Shchelkunova TA. Immunomodulatory effects of progesterone and selective ligands of membrane progesterone receptors. Steroids. 2019; 145: 5–18. DOI: 10.1016/j.steroids.2019.02.009. Epub 2019 Feb 10. PMID: 30753845.

27. Hasni MS, Yakimchuk K. Expression and effects of ligand-activated estrogen receptors in chronic lymphocytic leukemia. Anticancer research. 2019; 39: 167–172. DOI: 10.21873/anticanres.13093.

28. Shen Q, Zou S, Sheng B, Zhao M, Sun LZ, Zhu X. Mifepristone inhibits IGF-1 signaling pathway in the treatment of uterine leiomyomas. Drug Des Devel Ther. 2019; 13: 3161–70. DOI: 10.2147/DDDT.S212157. PMID: 31564832. PMCID: PMC6731989.

29. Lukovic J, Milosavljević Z, Zečević Luković T, Mitrović M, Andjelković M, et al. Antitumor effect of mifepristone on human endometrial stromal cell line. Vojnosanitetski Pregled. 2021; 78 (6).

30. Kırıcı P, Tanrıverdi E. Effects of different progesterone doses on the concentrations of proinflammatory and anti-inflammatory cytokines in pregnant women with threatened abortion. 2021; 13 (11): e19333. DOI: 10.7759/cureus.19333.

## Литература

1. Каприн А. Д., Старинский В. В., Шахзадова А. О., редакторы. Состояние онкологической помощи населению России в 2020 году. М.: МНИОИ им. П.А. Герцена, 2021; 239 с.

2. Курцер М. А., Бреусенко В. Г., Голухов Г. Н., Голова Ю. А., Есипова И. А., Овчинникова А. В., Ляфишева Д. М. Диагностика и лечение доброкачественных внутриматочных заболеваний у пациенток в постменопаузе. Вопросы гинекологии, акушерства и перинатологии. 2019; 18 (3): 71–79.

3. Vetter MH, Smith B, Benedict J, Hade EM, Bixel K, Copeland LJ, et al. Preoperative predictors of endometrial cancer at time of hysterectomy for endometrial intraepithelial neoplasia or complex atypical hyperplasia. Am J Obstet Gynecol. 2020; 222 (1).

4. Думановская М. Р., Чернуха Г. Е., Табеева Г. И., Асатурова А. В. Гиперплазия эндометрия: поиск оптимальных решений и стратегий. Акушерство и гинекология. 2021; 4: 23–31.

5. Mittermeier T. Levonorgestrel-releasing intrauterine system for endometrial hyperplasia. Mittermeier T, Farrant C, Wise MR. Cochrane Database Syst Rev. 2020; 9 (9): CD012658. DOI:10.1002/14651858.CD012658.pub2.

6. Dolapcioglu K, Boz A, Baloglu A. The efficacy of intrauterine versus oral progestin for the treatment of endometrial hyperplasia. A prospective randomized comparative study. Clin Exp Obstet Gynecol. 2013; 40: 122–6.

7. Ашрафян Л. А., Антонова И. Б., Ивашина С. В., Бабаева Н. А., Алешикова А. И., Баранов И. И. Оптимизация диагностической тактики у пациенток с аномальными маточными кровотечениями в периоды пери- и постменопаузы. Акушерство и гинекология: Новости. Мнения. Обучения, 2019; 1 (23). Доступно по ссылке (дата обращения: 07.06.2021): https://cyberleninka.ru/article/n/optimizatsiya-diagnosticheskoy-taktiki-u-patsientok-s- anomalnymi-matochnymi-krovotecheniya-v-periody-peri-i-postmenopauzy.

8. Russo M, Newell JM, Budurlean L, Houser KR, Sheldon K, Kesterson J, et al. Mutational profile of endometrial hyperplasia and risk of progression to endometrioid adenocarcinoma. Cancer. 2020; 126 (12): 2775–83. DOI: 10.1002/cncr.32822.

9. Унанян А. Л., Сидорова И. С., Коган Е. А., Бабурин Д. В. Клинико-патогенетические особенности гиперпластических процессов эндометрия у женщин перименопаузального возраста. РМЖ «Медицинское обозрение». 2018; 1 (I): 67–71.

10. Patel MV, Shen Z, Rodriguez-Garcia M, Usherwood EJ, Tafe LJ, Wira CR. Endometrial Cancer Suppresses CD8+ T Cell-Mediated Cytotoxicity in Postmenopausal Women. Front Immunol. 2021. Available from: https://DOI.org/10.3389/fimmu.2021.657326.

11. Wang C, Tran DA, Fu MZ, Chen W, Fu SW, Li X. Estrogen Receptor, Progesterone Receptor, and HER2 Receptor Markers in Endometrial Cancer. J Cancer. 2020; 11 (7): 1693–701. DOI: 10.7150/jca.41943.

12. Кадагидзе З. Г. Субпопуляции лимфоцитов при злокачественном росте. Вопр. онкологии. 1984; 1: 90–97.

13. Dama A, Baggio C, Boscaro C, Albiero M, Cignarella A. Estrogen Receptor Functions and Pathways at the Vascular Immune Interface. Int J Mol Sci. 2021; 22 (8): 4254. Available from: https://doi.org/10.3390/ ijms22084254.

14. Bouman A, Schipper M, Heineman MJ, Faas M. 17beta-estradiol and progesterone do not influence the production of cytokines from lipopolysaccharide-stimulated monocytes in humans. Fertil Steril. 2004; 82 (Suppl 3): 1212–9.

15. Фисенко В. П., редактор. Руководство по экспериментальному (доклиническому) изучению новых фармакологических веществ. М.: Ремедиум, 2000; 398 с.

16. Савельева Г. М., Бреусенко В. Г., Карева Е. Н., и др. Изучение роли экспрессии генов рецепторов эстрогенов и прогестерона в возникновении пролиферативных процессов в эндометрии для решения вопроса о тактике ведения больных с указанными патологическими изменениями эндометрия. Российский вестник акушера-гинеколога. 2018; 18 (6): 17–24. DOI: 10.17116/rosakush20181806117.

17. Савельева Г. М., Бреусенко В. Г., Карева Е. Н., Ивановская Т. Н., Тихонов Д. А., Гуторова Д. С. Стероидно-рецепторный профиль мононуклеаров периферической крови у пациенток в постменопаузе с пролиферативными процессами эндометрия. Вопросы гинекологии, акушерства и перинатологии. 2019; 18 (3): 80–86.

18. Obata T, Nakamura M, Mizumoto Y, Iizuka T, Ono M, Terakawa J, et al. Dual expression of immunoreactive estrogen receptor — and p53 is a potential predictor of regional lymph node metastasis and postoperative recurrence in endometrial endometrioid carcinoma. PLoS ONE; 12 (11): 2017: e0188641. Available from: https://doi.org/10.1371/journal.pone.0188641.

19. Singh P, Chaurasia A, Dhingra V, Misra V. Expression of ERα and PR in Various Morphological Patterns of Abnormal Uterine Bleeding-Endometrial causes in Reproductive Age Group. J Clin Diagn Res. 2016;10 (8): EC06-EC9. DOI: 10.7860/JCDR/2016/19565.829.

20. Swasti. Estrogen and progesterone receptors in endometrial cancer: where are we today? Gynecol Obstet. 2018; 8: 2. DOI: 10.4172/2161-0932.1000e127.

21. Greca A, Bellora N, Dily F, Jara R, Nacht AS, Oliete JQ, et al. Chromatin topology defines estradiol-primed progesterone receptor and PAX2 binding in endometrial cancer cells. 2022; eLife. 11: e66034. Available from: https://doi.org/10.7554/eLife.66034.

22. Sinreih M, Knific T, Thomas P, Frković Grazio S, Rižner TL. Membrane progesterone receptors — and — have potential as prognostic biomarkers of endometrial cancer. J Steroid Biochem Mol Biol. 2018; 178: 303–11. DOI: 10.1016/j.jsbmb.2018.01.011. PMID: 29353001.

23. Trenti A, Tedesco S, Boscaro C, Trevisi L, Bolego C, Cignarella A. Estrogen, Angiogenesis, Immunity and Cell Metabolism: Solving the Puzzle. Int J Mol Sci. 2018; 19 (3): 859. DOI: 10.3390/ijms19030859. PMID: 29543707. PMCID: PMC5877720.

24. Navarro FC. Herrnreiter C, Nowak L, Watkins SK. Estrogen Regulation of T-Cell Function and Its Impact on the Tumor Microenvironment. Gender and the Genome. 2018; 2 (3): 81–91. DOI: 10.1177/2470289718801379 journals.sagepub.com/home/gng.

25. Arruvito L, et al. NK Cells Expressing a Progesterone Receptor Are Susceptible to Progesterone-Induced Apoptosis. J Immunol. 2008; 180 (8): 5746–5753. DOI: https://doi.org/10.4049/jimmunol.180.8.5746.

26. Polikarpova AV, Levina IS, Sigai NV, Zavarzin IV, Morozov IA, Rubtsov PM, Guseva AA, Smirnova OV, Shchelkunova TA. Immunomodulatory effects of progesterone and selective ligands of membrane progesterone receptors. Steroids. 2019; 145: 5–18. DOI: 10.1016/j.steroids.2019.02.009. Epub 2019 Feb 10. PMID: 30753845.

27. Hasni MS, Yakimchuk K. Expression and effects of ligand-activated estrogen receptors in chronic lymphocytic leukemia. Anticancer research. 2019; 39: 167–172. DOI: 10.21873/anticanres.13093.

28. Shen Q, Zou S, Sheng B, Zhao M, Sun LZ, Zhu X. Mifepristone inhibits IGF-1 signaling pathway in the treatment of uterine leiomyomas. Drug Des Devel Ther. 2019; 13: 3161–70. DOI: 10.2147/DDDT.S212157. PMID: 31564832. PMCID: PMC6731989.

29. Lukovic J, Milosavljević Z, Zečević Luković T, Mitrović M, Andjelković M, et al. Antitumor effect of mifepristone on human endometrial stromal cell line. Vojnosanitetski Pregled. 2021; 78 (6).

30. Kırıcı P, Tanrıverdi E. Effects of different progesterone doses on the concentrations of proinflammatory and anti-inflammatory cytokines in pregnant women with threatened abortion. 2021; 13 (11): e19333. DOI: 10.7759/cureus.19333.

# ALTERED AMINO ACID PROFILES OF THE "MOTHER–FETUS" SYSTEM IN COVID-19

Lomova NA ✉, Chagovets VV, Dolgopolova EL, Novoselova AV, Petrova UL, Shmakov RG, Frankevich VE

Kulakov National Medical Research Center for Obstetrics, Gynecology and Perinatology, Moscow, Russia

Systemic nature of the human body response to SARS-CoV-2 requires dedicated analysis at the molecular level. COVID-19 during pregnancy affects maternal health and may entail complications in the early neonatal period and possibly long-term consequences for the offspring. The aim of the study was to assess the impact of COVID-19 on amino acid profiles in maternal venous blood, amniotic fluid and umbilical cord blood in order to develop a diagnostic panel accounting for possible consequences. The main group included 29 pregnant patients with a confirmed diagnosis of COVID-19 and the control group included 17 somatically healthy pregnant women. Amino acid profiles of the biological fluids were measured by high-performance liquid chromatography combined to mass spectrometry (HPLC-MS) and assessed in logistic regression models. The analysis revealed altered content of certain amino acids, their biosynthetic precursors and metabolites in the biological fluids collected from patients with COVID-19 possibly reflecting the development of systemic inflammatory reaction and associated changes in gene expression profiles. These findings may guide further research into health outcomes for neonates born from mothers infected with SARS-CoV-2 during pregnancy. The study may help to develop advanced recommendations and differential care protocols for pregnant women and newborns diagnosed with COVID-19.

**Keywords:** COVID-19, amino acids, mass spectrometry, blood plasma, umbilical cord blood, venous blood, amniotic fluid, clinical neonatal markers, metabolic pathways

✉ **Correspondence should be addressed:** Natalia A. Lomova
Oparina, 4, Moscow, 117997, Russia; natasha-lomova@yandex.ru

# ИЗМЕНЕНИЕ АМИНОКИСЛОТНОГО ПРОФИЛЯ В СИСТЕМЕ «МАТЬ–ПЛОД» ПРИ COVID-19

Н. А. Ломова ✉, В. В. Чаговец, Е. Л. Долгополова, А. В. Новоселова, У. Л. Петрова, Р. Г. Шмаков, В. Е. Франкевич

Национальный медицинский исследовательский центр акушерства, гинекологии и перинатологии имени В. И. Кулакова, Москва, Россия

Вирус SARS-CoV-2 оказывает значительное влияние на организм человека, и актуален вопрос о характере этого воздействия на молекулярном уровне. COVID-19 не только оказывает влияние на мать в период беременности, но и повышает риск осложнений в раннем неонатальном периоде и может иметь отдаленные последствия для здоровья новорожденного. Целью исследования было определить влияние COVID-19 на аминокислотный состав венозной крови беременных, амниотической жидкости и плазмы пуповинной крови для разработки диагностической панели, а также провести анализ возможных последствий для состояния новорожденного. Основную группу составили 29 пациенток с подтвержденным диагнозом COVID-19; контрольную группу — 17 соматически здоровых женщин. На первом этапе работы был проведен анализ аминокислотного профиля. Обнаруженные различия в содержании аминокислот в различных биологических жидкостях позволили разработать модели логистической регрессии. По данным математического анализа задействованности метаболических путей маркеров-аминокислот в венозной и пуповинной плазме крови матерей и новорожденных в группе с COVID-19 обнаружено статистически значимое изменение биосинтеза и путей метаболизма ряда аминокислот, задействованных в реализации воспалительной реакции, изменений энергетического метаболизма, нарушений регуляции экспрессии и транскрипции белковых молекул и пр. Эти результаты могут быть использованы для выбора направления дальнейших исследований возможных последствий для здоровья новорожденных от матерей, перенесших COVID-19, и определения требований к лечению и медицинской помощи беременным женщинам и новорожденным после постановки диагноза COVID-19.

**Ключевые слова:** COVID-19, аминокислоты, масс-спектрометрия, плазма, пуповинная кровь, венозная кровь, амниотическая жидкость, маркеры состояния новорожденного, метаболические пути

✉ **Для корреспонденции:** Наталья Анатольевна Ломова
ул. Академика Опарина, д. 4, г. Москва, 117997, Россия; natasha-lomova@yandex.ru

The past 50 years encountered over 300 outbreaks of new or long-forgotten infections, including three coronavirus infections in 2002, 2012, and 2019. These viral outbreaks, ignited by direct contacts between old and new host species of the virus, reflect the lack of compliance with sanitary and hygienic requirements typical for Asian marketplaces. Coronaviruses make up an extensive family of 40 viruses, seven of which have been implicated in human diseases. Their emergence results from the continuous biological evolution: certain viral strains that prosper in animals gradually evolve the capability to infect humans. The infamous connection between SARS-CoV-2 and humanity was likely initiated at a large animal and seafood wholesale market in Wuhan. The severe acute respiratory syndrome outbreak caused by this virus in China rapidly escalated to global pandemic challenging healthcare systems with the unpreceded demand for intensive care.

A number of studies indicate higher severity of COVID-19 in pregnant women compared to age-matched non-pregnant controls [1]. In addition, COVID-19 during pregnancy has been associated with increased risks of premature labor [1, 2]. Advanced maternal age, excessive body weight, and comorbidities such as hypertension or diabetes increase the risks of COVID-19 pregnancy complications [3].

The isolated reported cases of vertical transmission of the virus, as well as serious maternal complications in the antenatal period might need advanced verification [4–7]. According to the WHO, all studied samples of amniotic fluid and breast milk were SARS-CoV-2-negative. The ability of the active virus to be transmitted from mother to fetus or newborn during pregnancy and childbirth has not been characterized thoroughly. At the same time, newborns from SARS-CoV-2 infected mothers may be at higher risks of early neonatal complications and long-term health consequences.

Omics studies, metabolomics in particular, represent a promising direction of medical research. The high-throughput approaches help to identify candidate markers for secure diagnostics, patient management optimization and prognosis. A 2020 study correlated 204 metabolites in blood plasma of patients with the severity of COVID-19 [8]. Amino acids, an integral part of the metabolome, are pivotal markers of physiological status. Optimal levels of amino acids in the body ensure metabolic equilibrium and smooth functioning of organ systems, whereas amino acid imbalances indicate the opposite. Altered amino acid concentrations have been observed in cardiovascular disease [9], H1N1 influenza virus-associated pneumonia [10] and chronic obstructive pulmonary disease [11]. Certain neonatal pathologies, notably the storage diseases, can be diagnosed by measuring the amino acid content in dried blood spots [12]. The disease-related changes of metabolic profiles in biological fluids of the human body provide valuable diagnostic substratum for a number of pathological conditions. For example, altered amino acid profiles in patients with COVID-19 have been associated with compromised oxygen homeostasis [13]. Another study on amino acid profiles in adults and children with COVID-19 identified changes plausibly associated with endothelial and T cell dysfunctions [14, 15].

In our previously published article, we searched for COVID-19 predictive markers in amniotic fluid and cord blood [16]. In the current study, we analyze amino acid composition of maternal venous blood, amniotic fluid and umbilical cord blood as metabolomic projection of the "mother–fetus" system in order to provide a relevant description of affected metabolic pathways and account for potential clinical significance and long-term consequences of COVID-19 in pregnancy.

## METHODS

Patient enrollment and clinical data and sample collection were carried out in March–May 2020 at the National Medical Research Center for Obstetrics, Gynecology and Perinatology named after Academician V. I. Kulakov, its First Infectious Unit refurbished into "red zone" for patients diagnosed with COVID-19 including those pregnant.

The study enrolled 46 pregnant women admitted for observation and delivery at the National Medical Research Center for Obstetrics, Gynecology and Perinatology named after Academician V. I. Kulakov. The main group included 29 patients with confirmed diagnosis of COVID-19 and the control group included 17 somatically healthy women without pregnancy complications. The diagnosis of COVID-19 was verified by PCR test (DNA Technology LLC; Russia). The enrollment was carried out on recourse. Inclusion in the main group was based on positive PCR test for COVID-19. Inclusion in the control group was based on the lack of clinical symptoms and negative PCR test for COVID-19. Exclusion criteria for the study encompassed multifetal pregnancy, rhesus- and AB0-isoimmunizations, as well as chromosome aberrations, genetic mutations and congenital malformations in the fetus.

Samples of venous blood plasma from pregnant participants, umbilical cord blood plasma from their newborns and amniotic fluid were collected for the analysis. Sample transportation was carried out within the premises of the National Medical Research Center for Obstetrics, Gynecology and Perinatology named after Academician V.I. Kulakov for subsequent analysis in lab spaces certified for biosafety level II. We measured 31 amino acids in physiological fluids by high-performance liquid chromatography-combined mass spectrometry (HPLC-MS) using standard kits and a protocol from the manufacturer (JASEM; Turkey). The samples were analyzed in a 1260 Infinity II LC system (Agilent; USA) with MS detection in a 6460 Triple Quad instrument (Agilent; USA). The transitions from parent ions to daughter fragments for the analyzed amino acids, corresponding chromatographic retention times, internal standard concentrations, as well as sensitivity and reproducibility parameters for the analysis are described in the JASEM manual.

### Statistical analysis of the data

Statistical processing of the data was carried out using R scripts (R Core Team; Austria) in RStudio integrated environment (RStudio, Inc.; USA). The normality of quantitative data distributions was assessed by Shapiro–Wilk test. Normal distributions were described by means and standard deviations. Distributions other than normal were described by medians with lower and upper quartiles in the Me (Q1; Q3) format. The comparisons involved parametric Student's t-test for the data complying with normal distributions and nonparametric Mann–Whitney test for distributions other than normal. The threshold $p$-value was accepted 0.05; $p$-values smaller than 0.001 were underspecified as $p < 0.001$. The feasibility of patient stratification of the basis of amino acid profiles was assessed by logistic regression method. The initial set of logistic regression models were built using all possible combinations of amino acids as independent variables possibly reflecting affiliation of the patient with particular group of the study (dependent variable). These first-round models were subjected to receiver operating characteristic (ROC) analysis and candidate models with the highest area-under-the-curve (AUC) values were selected for subsequent validation. Each model was characterized

**Table 1.** Clinical characterization of the main group (patients with COVID-19 while pregnant)

| Clinical characteristics | COVID-19, $n$ = 29 (%) |
|---|---|
| Clearly symptomatic | 21 (71.41) |
| Elevated body temperature (> 37 °C) | 12 (41.38) |
| Anosmia | 7 (24.14) |
| Sore throat | 3 (10.34) |
| Dyspnea | 4 (13.79) |
| Cough | 12 (41.38) |
| Fatigue | 4 (13.79) |
| Mild symptoms | 22 (75.86) |
| Moderate symptoms | 6 (20.69) |
| Severe symptoms | 1 (3.45) |

by Wald's test with corresponding 95% confidence interval (CI) and odds ratio (OR) with CI. The quality assessment for the developed models involved determination of sensitivity and specificity by ROC analysis. Metabolomic implications of the identified between-the-group differences were assessed using MetaboAnalyst version 5.0 tool (https://www.metaboanalyst. ca/) connected to the KEGG compound and pathway database (Kyoto Encyclopedia of Genes and Genomes). Statistical significance for a metabolic pathway influence was determined by hypergeometric test controlled with Benjamini–Hochberg procedure. The assessment of individual marker contributions involved topological analysis and relative mediation effect. Associations with the disease were considered significant at false discovery rates below the level of significance (FDR < 0.05).

RESULTS

The study enrolled 46 pregnant participants: 29 inpatients with confirmed diagnosis of COVID-19 (main group) and 17 conditionally healthy inpatients (control group). Clinical characterization for the main group (patients with COVID-19 while pregnant) is given in Table 1; clinical characterization for the entire cohort (both groups) is given in Table 2.

None of the newborns had COVID-19. All newborns were tested for SARS-CoV-2 immediately after birth, and repeatedly on days 3 and 10 of life. The negative test results may indicate the lack of vertical transmission. No perinatal deaths occurred in the studied cohort.

The laboratory assay used commercial reagent kits for targeted quantitative measurement of 31 amino acids in biological samples of maternal venous blood plasma, amniotic fluid and umbilical cord blood plasma by HPLC-MS.

At the first stage of the analysis we measured amino acid content of the maternal venous blood plasma for the two groups of the study. Statistical analysis of HPLC-MS data identified five

amino acids with concentrations differing significantly between the groups: 1-methylhistidine, lysine, cystine, glutamic acid and glutamine (Table S1, Fig. 1).

The identified differences inspired the search for a mathematical model that would enable distinguishing between SARS-CoV-2-positive pregnant patients and matched controls on the basis of amino acid content of the venous blood plasma. The corresponding HPLC-MS measurements were used as a basis for logistic regression models. The first round of modeling employed all possible combinations of amino acids. All developed models were subject to ROC analysis and four models with the highest AUC values were selected for subsequent validation (Fig. S1, Table S2).

The maximal AUC of 0.78 was shown by a model involving methylhistidine and cystine, characterized by 0.93 sensitivity and 0.94 specificity (Table S3).

A similar HPLC-MS profiling of 31 amino acids in the amniotic fluid and statistical analysis of the data revealed eight amino acids with concentrations differing significantly between the groups: 1-methylhistidine, 3-methylhistidine, arginine, cystathionine, cystine, glutamine, histidine and trans-4-hydroxyproline (Fig. 2, Table S4).

A search for the means of metabolomic differentiation between SARS-CoV-2-positive pregnant patients and matched controls was subsequently carried out for the amniotic fluid samples; the results are given in Fig. S2 and Tables S5 and S6. Construction of logistic regression models for amino acid profiles in amniotic fluid followed the same algorithm as for the venous blood plasma. In this series, the maximal AUC of 0.89 was shown by a model that involved arginine, cystine, histidine and trans-4-hydroxyproline, characterized by 0.84 sensitivity and 0.93 specificity (Table S6). Somewhat higher levels of sensitivity and specificity (0.84 and 1, respectively) were shown by a model that involved 1-methylhistidine, cysteine and trans-4-hydroxyproline (Table S6).

**Table 2.** Clinical characterization of the two groups of the study

| Parameter | COVID-19, $n$ = 29 | Control group, $n$ = 17 | $p$-value |
|---|---|---|---|
| Age | 29.9 (± 5.03) | 32.0 (± 5.03) | 0.16 |
| Height | 166.62 (± 7.37) | 165.76 (± 7.34) | 0.71 |
| Weight | 77.64 (± 11.58) | 71.87 (± 9.75) | 0.10 |
| BMI | 27.85 (± 4.52) | 26.12 (± 3.16) | 0.18 |
| Term at delivery | 38 (± 1.52) | 39.42 (± 1.14) | 0.001 |
| Weight at birth | 3332 (± 484) | 3585 (± 424) | 0.08 |
| Height at birth | 52.4 (± 2.66) | 53.1 (± 2.29) | 0.35 |
| Apgar score at 1 min | 8 (8; 8) | 9 (9; 9) | 0.69 |
| Apgar score at 5 min | 8 (8; 8) | 9 (9; 9) | 0.83 |
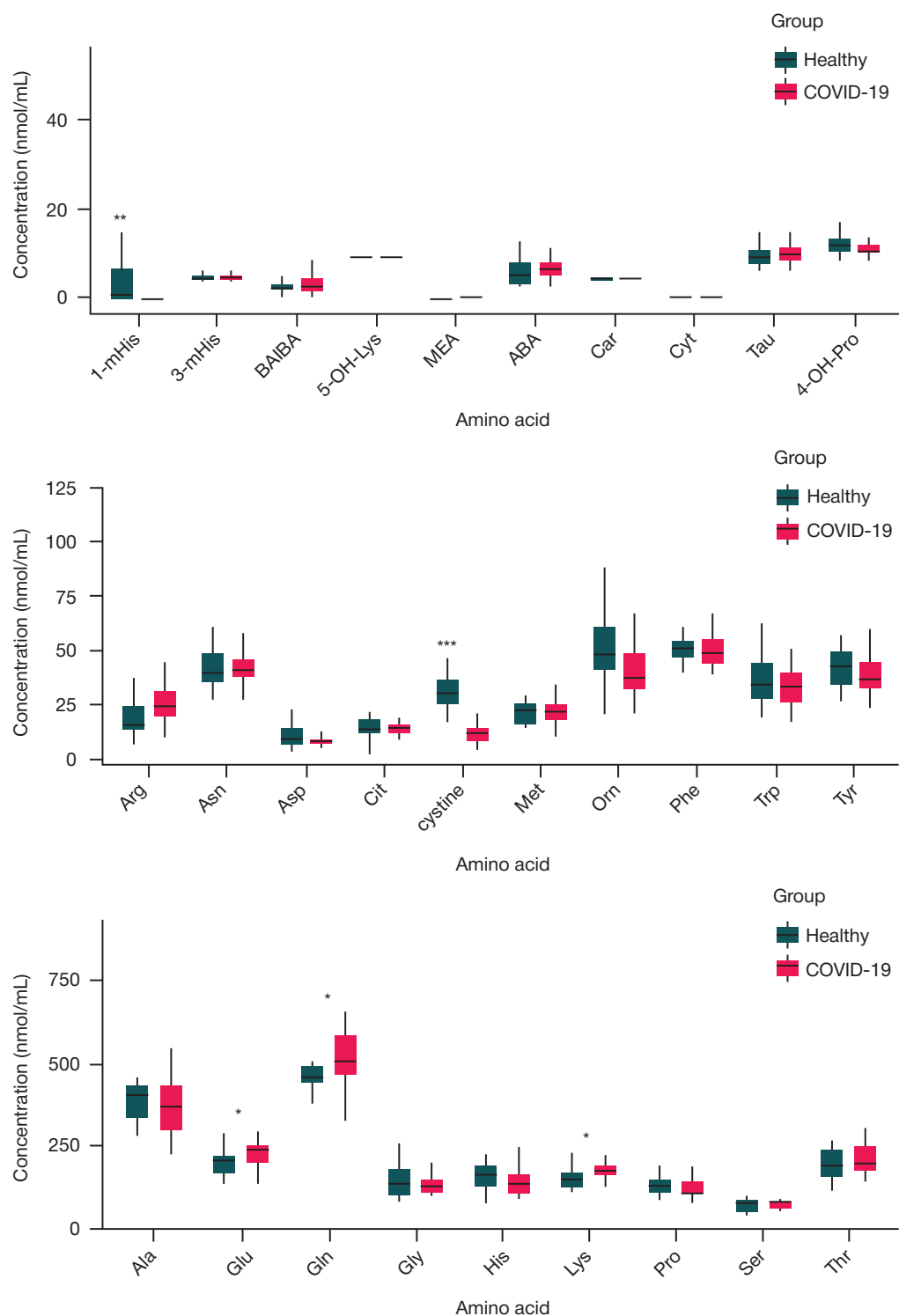
**Fig. 1.** Boxplots of amino acid concentrations in the maternal venous blood plasma for the two groups of the study. Box limits represent lower and upper quartiles (respectively, Q1 and Q3); box heights are interquartile ranges (IQR); horizontal lines in the boxes are medians (Q2); the whisker termini are within Q3+1.5 IQR (upper) and Q1-1.5 IQR (lower); * — p-value ≤ 0.05; ** — p-value ≤ 0.01; *** — p-value ≤ 0.001. 1-mHis — 1-methyl-L-histidine; 3-mHis — 3-methyl-L-histidine; bAla — β-alanine; BAIBA — 3-aminoisobutyric acid; 5-OH-Lys — DL-5-hydroxylysine; MEA — ethanolamine; ABA — L-2-aminobutyric acid; AAD — L-2-aminoadipic acid; Ala — L-alanine; Arg — L-arginine; Asn — L-asparagine; Asp — L-aspartic acid; Car — L-carnosine; Cit — L-citrulline; Cyt — L-cystathionine; cystine — L-cystine; Glu — L-glutamic acid; Gln — L-glutamine; Gly — L-glycine; His — L-histidine; Lys — L-lysine; Met — L-methionine; Orn — L-ornithine; Phe — L-phenylalanine; Pro — L-proline; Ser — L-serine; Thr — L-threonine; Trp — L- tryptophan; Tyr — L-tyrosine; Val — L-valine; Tau — taurine; 4-OH-Pro — *trans*-4-hydroxy-L-proline

A similar analytical scheme was applied to the umbilical cord blood plasma samples. Statistical analysis of the spectral data revealed four candidate amino acids with concentrations differing significantly between the groups: 1-methylhistidine, β-alanine, cysteine and histidine (Fig. 3, Table S7).

Construction of logistic regression models for amino acid profiles of the umbilical cord blood plasma was carried out similarly with other sample types; the results are given in Fig. S3 and Tables S8 and S9. All successful regression models built in this series involved cystine, which showed the most pronounced between-the-group differences. All models obtained in this series had AUC = 1 at sensitivity and specificity of 1 (Table S9).

The three types of studied biological samples (amniotic fluid, maternal venous blood and umbilical cord blood plasma)
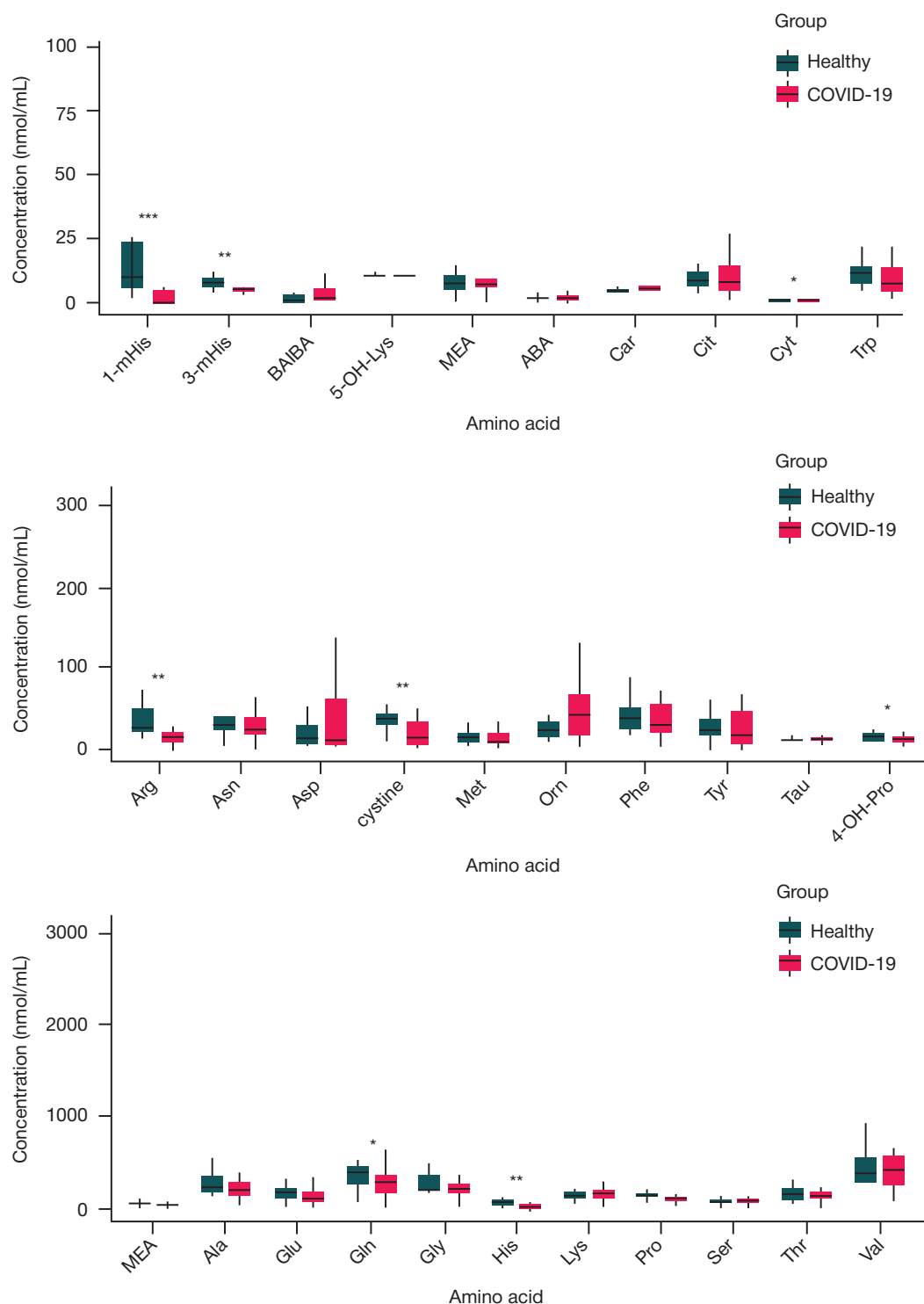
**Fig. 2.** Boxplots of amino acid concentrations in the amniotic fluid for the two groups of the study. Box limits represent lower and upper quartiles (respectively, Q1 and Q3); box heights are interquartile ranges (IQR); horizontal lines in the boxes are medians (Q2); the whisker termini are within Q3+1.5 IQR (upper) and Q1-1.5 IQR (lower); * — *p*-value ≤ 0.05; ** — *p*-value ≤ 0.01; *** — *p*-value ≤ 0.001. 1-mHis — 1-methyl-L-histidine; 3-mHis — 3-methyl-L-histidine; BAIBA — 3-aminoisobutyric acid; 5-OH-Lys — DL-5-hydroxylysine; MEA — ethanolamine; ABA — L-2-aminobutyric acid; AAD — L-2-aminoadipic acid; Car — L-carnosine; Cit — L-citrulline; Cyt — L-cystathionine; 4-OH-Pro — *trans*-4-hydroxy-L-proline

had certain matches among the amino acids with significant between-the-group concentration differences. Concentrations of 1-methylhistidine and cystine showed COVID-19-related differences in all three types of biological samples thus most consistently reflecting the metabolome of the mother–fetus system. L-Histidine, a coded amino acid and precursor of 1-methylhistidine, showed differential content in both maternal and fetal plasma, but not in amniotic fluid. Another marker, glutamine, 'responded' to COVID-19 in maternal venous blood

plasma and amniotic fluid, but not in umbilical cord blood plasma (Table S10).

The identification of recurring statistically significant changes for the content of certain amino acids in three biological media of the mother–fetus complex during SARS-CoV-2 infections required advanced interpretation. In this regard, we analyzed participation of these amino acids in key metabolic pathways and their possible clinical significance for the mother and the fetus, including potential long-term consequences. The
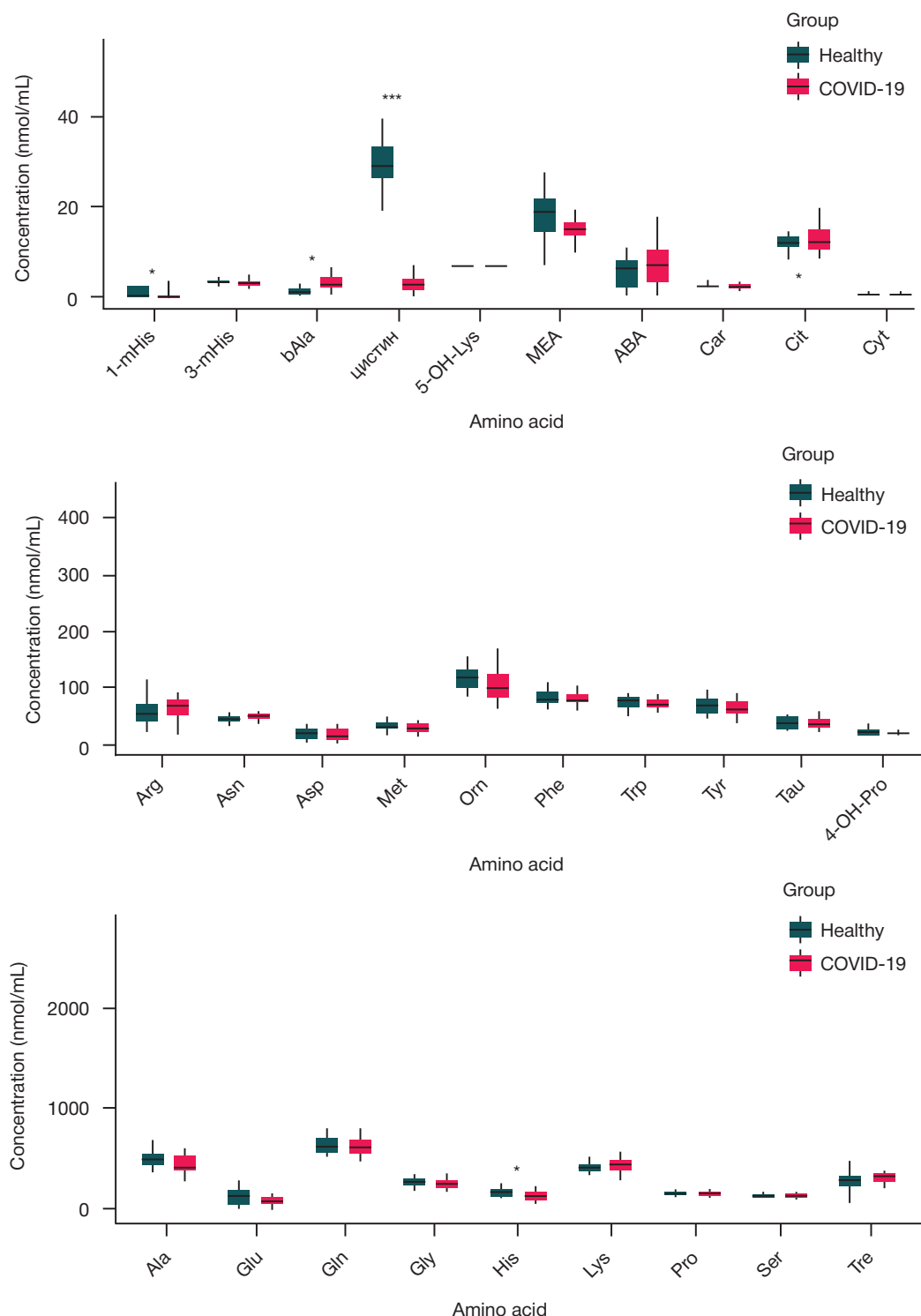
**Fig. 3.** Boxplots of amino acid concentrations in the umbilical cord blood plasma for the two groups of the study. Box limits represent lower and upper quartiles (respectively, Q1 and Q3); box heights are interquartile ranges (IQR); horizontal lines in the boxes are medians (Q2); the whisker termini are within Q3+1.5 IQR (upper) and Q1-1.5 IQR (lower); * — $p$-value ≤ 0.05; ** — $p$-value ≤ 0.01; *** — $p$-value ≤ 0.001. 1-mHis — 1-methyl-L-histidine; 3-mHis — 3-methyl-L-histidine; bAla — β-alanine; BAIBA — 3-aminoisobutyric acid; 5-OH-Lys — DL-5-hydroxylysine; MEA — ethanolamine; ABA — L-2-aminobutyric acid; AAD — L-2-aminoadipic acid; Ala — L-alanine; Arg — L-arginine; Asn — L-asparagine; Asp — L-aspartic acid; Car — L-carnosine; Cit — L-citrulline; Cyt — L-cystathionine; 4-OH-Pro — *trans*-4-hydroxy-L-proline

analysis employed MetaboAnalyst version 5.0 tool (https://www.metaboanalyst.ca/) connected to the KEGG database (Kyoto Encyclopedia of Genes and Genomes).

For amniotic fluid, the identified COVID-19-associated changes in amino acid profiles revealed no significant matches with specific metabolic pathways (Fig. 4A, Table S11). For umbilical cord blood plasma, the observed changes implicated histidine and β-alanine metabolism imbalances (Fig. 4B, Table S12). For maternal venous blood plasma, the plausibly affected

pathways included D-glutamine and D-glutamate metabolism, arginine biosynthesis and alanine, aspartate and glutamate metabolism (Fig. 4C, Table S13).

DISCUSSION

The obtained results indicate significant differences in concentrations of certain amino acids in biological fluids of pregnant patients with and without COVID-19, including eight
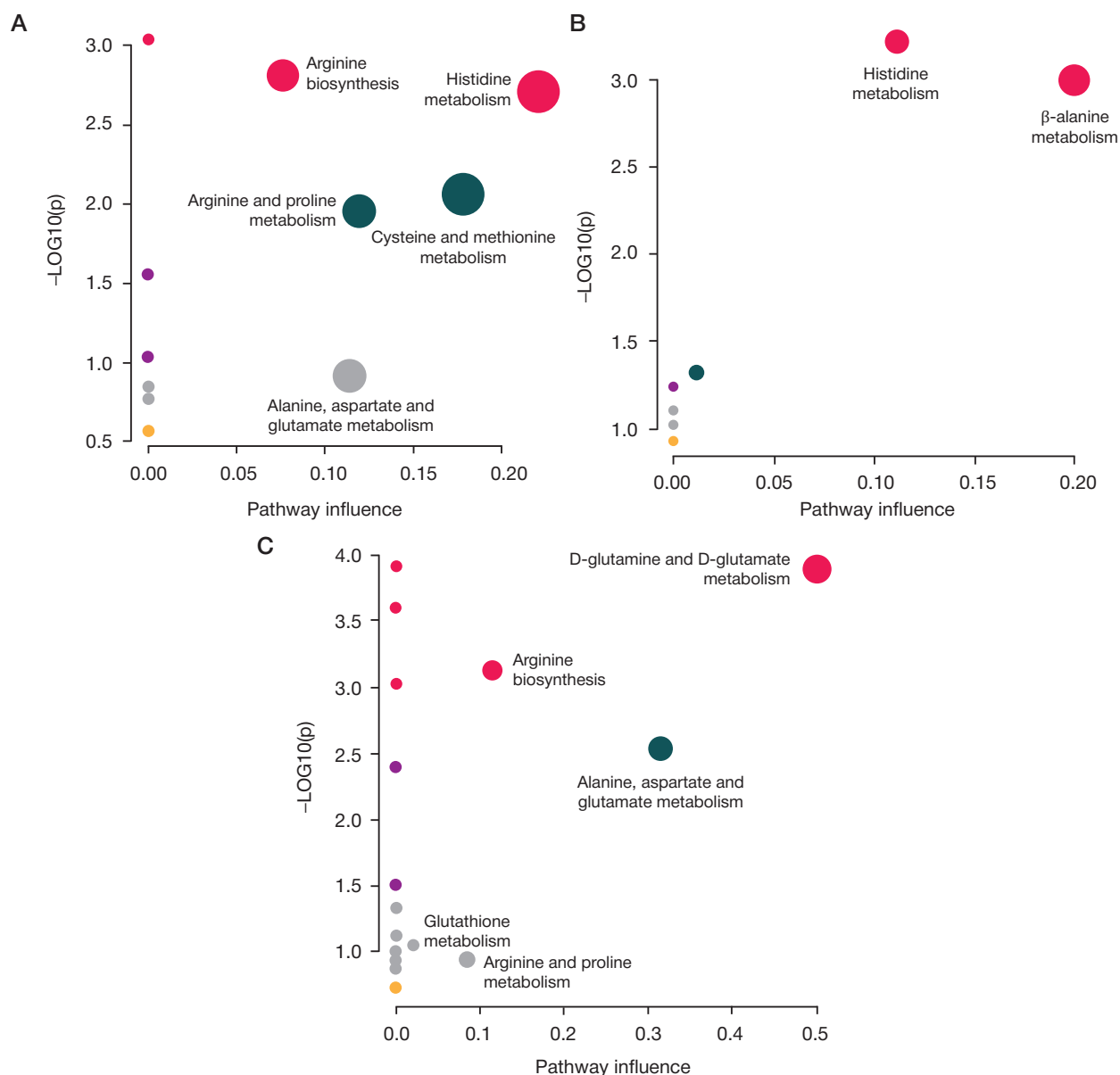
**Fig. 4.** Charts of the metabolic pathway influence for amino acid markers in the studied biological samples: amniotic fluid (**A**); cord blood plasma (**B**); venous blood plasma (maternal, **C**)

amino acids in amniotic fluid, five amino acids in maternal venous blood plasma and four amino acids in umbilical cord blood plasma. Of those, eight amino acids, notably arginine, had reduced concentrations in the biological fluids of patients with COVID-19. Similar changes in plasma levels of arginine and its metabolites in COVID-19 observed by other authors [14] may reflect endothelial dysfunction implicated in the development of COVID-19 lung injury [17, 18]. Low bioavailability of arginine has been associated with dysregulated endothelial and T cell functionalities [19, 20] among other pathophysiological consequences [21]. Apart from the reduced arginine levels, patients with COVID-19 presented with significantly altered systemic concentrations of citrulline, glutamine, alanine, glycine, histidine, proline and several other amino acids, though the mechanisms and pathophysiological interpretation of these changes are elusive [14]. Reduced systemic levels of amino acids are typical for other pathological conditions as well [9, 11, 12, 14, 22, 23]. In our setting, COVID-19-related changes in amino acid profiles of the maternal venous blood plasma revealed statistically supported associations with D-glutamine and D-glutamate metabolism, as well as alanine, aspartate and

glutamate metabolism and notably the arginine biosynthesis pathways.

The semi-essential or conditionally essential amino acid arginine is one of the most metabolically versatile amino acids serving as a precursor for the synthesis of urea, nitric oxide, polyamines, proline, glutamate, creatine and agmatine. Arginine is metabolized via a complex and tightly regulated set of pathways which remain understudied at both cellular and systemic levels. A decrease in arginine concentration resulting from altered arginase activity may selectively affect expression of specific genes [24]. The arginine deficiency-associated abnormal protein expression in cell cultures has been studied for over 40 years [25]. Arginine is a prominent small-molecule regulator of gene expression [26–29].

Amino acids showing synchronous concentration dynamics in amniotic fluid, umbilical cord blood and maternal venous blood in 'response' to COVID-19 are particularly interesting. Significant concentration differences in all three studied biological media were revealed for two amino acids, 1-methylhistidine and cystine, with particularly high differentiating significance demonstrated for the latter — a non-coded amino acid derived

from oxidative dimerization of cysteine. L-Cystine represents a key biochemical module in creation and maintenance of the tertiary structure of proteins and peptides, indispensable for their biological activity. For example, peptide hormones vasopressin, oxytocin, insulin and somatostatin acquire their biological activity through formation of intramolecular disulfide bridges.

Synchronous COVID-19-associated dynamics in maternal and fetal blood plasma was observed for L-histidine (a substrate of protein synthesis and precursor for 1-methylhistidine).

The altered content of amino acid markers observed by us in umbilical cord blood plasma implicated histidine and β-alanine metabolism imbalances.

The naturally occurring beta-amino acid β-alanine is formed through dihydrouracil and carnosine degradation. Carnosyl β-alanine and related dipeptides represent a water-soluble component of the cellular anti-oxidant protection system, complementing the fat-soluble membrane-anchored anti-oxidative agents. These dipeptides alleviate toxic effects of reactive oxygen species and unsaturated aldehydes through prevention of protein cross-linking [30]. The reported proliferative effect of β-alanine and related molecules is apparently confined to muscle and nervous tissues, characterized by low proliferative capacity and extremely strong oxidative metabolism. It can be assumed that, apart from the anti-oxidant activity in muscle tissue, these amino acids may contribute to regenerative response and stimulate proliferation of normal (non-tumor) human cells.

The implication of amino acid markers in histidine metabolism may link COVID-19 with disruption of histidine decarboxylation and histamine production pathways during pregnancy.

A coding heterocyclic α-amino acid L-histidine is one of the two conditionally essential amino acids (along with arginine), initially considered essential in children only. Histidine residues with their unique electronic properties are encountered in catalytically active centers of many enzymes. Histidine is an important precursor in histamine biosynthesis known to play a central role in inflammatory response and certain allergic reactions. Histidine is known to facilitate tissue growth and repair, nerve fiber myelination and hematopoiesis. Histidine deficiency has been shown to promote hearing loss and neurodegeneration.

Overall, the obtained results indicate that SARS-CoV-2 infections may have significant metabolomic effects reflected by altered profiles of marker amino acids in amniotic fluid and umbilical cord blood, as well as in maternal circulation. Considering the vital significance of proteinogenic amino acids, these alterations may affect protein production machinery at all levels of the mother–fetus system even in the absence of COVID-19 symptoms during parturition. Long-term effects of intrauterine exposure to COVID-19 remain a high priority clinical issue. Assessment of metabolic profiles in relation to viral replication, host inflammatory response and altered energy metabolism lays the foundation for future research in this direction.

## CONCLUSIONS

In this study, we used the targeted metabolomics approaches to identify changes in systemic levels of amino acids in pregnant patients infected with SARS-CoV-2 at the time of admission to inpatient facilities. Statistically significant differences in concentrations between the control group of conditionally healthy pregnant women and the matched group of patients with COVID-19 were revealed for eight amino acids in the amniotic fluid (1-methylhistidine, 3-methylhistidine, arginine, cystathionine, cystine, glutamine, histidine and trans-4-hydroxiproline), five amino acids in the maternal venous blood plasma (1-methylhistidine, lysine, cystine, glutamic acid and glutamine) and four amino acids in the umbilical cord blood plasma (1-methylhistidine, β-alanine, cystine and histidine). Metabolic disorders involving the identified amino acids have been described in a number of pathological conditions including acute respiratory distress syndrome in severe sepsis, H1N1 influenza-associated pneumonia, bacterial pneumonia, sickle cell anemia, thalassemia, malaria, acute asthma, cystic fibrosis, pulmonary hypertension, cardiovascular diseases and certain cancers. Analysis of amino acid markers in representative biological fluids of the mother–fetus system revealed significant COVID-19-associated changes in the biosynthesis and catabolism of amino acids involved in inflammatory reactions and altered metabolic patterns with corresponding changes in gene and protein expression. These results may help investigate health outcomes of COVID-19 in newborns and their mothers, which may include endocrine, nervous, allergic and other components, in order to adjust clinical recommendations for COVID-19 in pregnancy.

### References

1. Chiu-Lin Wang, Yi-Yin liu, Chin-Hu Wu, Chun-Yu Wang, Chun-Hung Wang, Cheng-Yu Long. Impact of COVID-19 on Pregnancy. International Journal of Medical Sciences. 2021; 18 (3): 763–7. DOI: 10.7150/ijms.49923.

2. Schwartz DA, Graham AL. Potential Maternal and Infant Outcomes from (Wuhan) Coronavirus 2019-nCoV Infecting Pregnant Women: Lessons from SARS, MERS, and Other Human Coronavirus Infections. Viruses. 2020; 12 (4): 194.

3. Zaigham M, Andersson O. Maternal and perinatal outcomes with COVID–19:A systematic review of 108 pregnancies. Acta Obstet Gynecol Scand. 2020; 99 (7): 823–9.

4. Chen H, Guo J, Wang C, Luo F, Yu X, Zhang W, et al. Clinical characteristics and intrauterine vertical transmission potential of COVID-19 infection in nine pregnant women: a retrospective review of medical records. Lancet. 2020; 395 (10226): 809–15.

5. Sukhikh G, Petrova U, Prikhodko A, Starodubtseva N, Chingin K, Chen H, et al. Vertical Transmission of SARS-CoV-2 in Second Trimester Associated with Severe Neonatal Pathology. Viruses.

2021; 13 (3). DOI:10.3390/v13030447.

6. Ellington S, Strid P, Tong VT, Woodworth K, Galang RR, Zambrano LD, et al. Characteristics of women of reproductive age with laboratory-confirmed SARS-COV-2 infection by pregnancy status — United States, January 22-June 7, 2020. Morb Mortal Wkly Rep. 2020; 69 (25): 769–5.

7. Vivanti AJ, Vauloup-Fellous C, Prevot S, Zupan V, Suffee C, Do Cao J, et al. Transplacental transmission of SARS-CoV-2 infection. Nat Commun. 2020; 11 (1). DOI: 10.1038/s41467020-17436-6.

8. Shen B, Yi X, Sun Y, Bi X, Du J, Zhang C, et al. Proteomic and Metabolomic Characterization of COVID-19 Patient Sera. Cell. 2020; 182 (1): 59–72.

9. McGarrah RW, Crown SB, Zhang G, Shah SH, M.H.S., Newgard CB. Cardiovascular Metabolomics. Circ Res. 2018; 122 (9): 1238–58. DOI: 10.1161/CIRCRESAHA.117.311002.

10. Banoei MM, Vogel HJ, Weljie AM, Kumar A, Yende S, Angus DC, et al. Plasma metabolomics for the diagnosis and prognosis of

H1N1 influenza pneumonia. 2017; 1–15.

11. Inoue S, Ikeda H. Differences in plasma amino acid levels in patients with and without bacterial infection during the early stage of acute exacerbation of COPD. Int J COPD. 2019; 14: 575–83.

12. Moat SJ, George RS, Carling RS. Use of Dried Blood Spot Specimens to Monitor Patients with Inherited Metabolic Disorders. Int J Neonatal Screen. 2020; 6 (2): 1–17.

13. Páez-Franco JC, Torres-Ruiz J, Sosa-Hernández VA, Cervantes-Díaz R, Romero-Ramírez S, Pérez-Fragoso A, et al. Metabolomics analysis reveals a modified amino acid metabolism that correlates with altered oxygen homeostasis in COVID-19 patients. Sci Rep. 2021; 11 (1). DOI: 10.1038/s41598-021-85788-0.

14. Rees CA, Rostad CA, Mantus G, Anderson EJ, Chahroudi A, Jaggi P. Altered amino acid profile in patients with SARS-CoV-2 infection. 2021; 118 (25): 4–6.

15. Hirschel J, Vogel M, Baber R, Garten A, Beuchel C, Dietz Y, et al. Relation of whole blood amino acid and acylcarnitine metabolome to age, sex, BMI, puberty, and metabolic markers in children and adolescents. Metabolites. 2020; 10 (4). DOI: 10.3390/metabo10040149.

16. Lomova NA, Chagovets VV, Dolgopolova EL, Novoselova AV, Petrova UL, Shmakov RG, et al. Changes in amino acid profile of cord blood plasma and amniotic fluid of mothers with COVID-19. Bulletin of Russian State Medical University. 2021; (3): 12–22. DOI: 10.24075/BRSMU.2021.032

17. Diorio C, McNerney KO, Lambert M, Paessler M, Anderson EM, Henrickson SE, et al. Evidence of thrombotic microangiopathy in children with SARS-CoV-2 across the spectrum of clinical presentations. Blood Adv. 2020; 4 (23): 6051–63.

18. Tay MZ, Poh CM, Rénia L, MacAry PA, Ng LFP. The trinity of COVID-19: immunity, inflammation and intervention. Nature Reviews Immunology. 2020; 20 (6): 363–74.

19. Gambardella J, Khondkar W, Morelli MB, Wang X, Santulli G, Trimarco V. Arginine and endothelial function. Biomedicines. 2020; 8 (8): 277.

20. Rodríguez PC, Ochoa AC. Arginine regulation by myeloid derived

21. Morris CR, Hamilton-Reeves J, Martindale RG, Sarav M, Ochoa Gautier JB. Acquired Amino Acid Deficiencies: A Focus on Arginine and Glutamine. In: Nutrition in Clinical Practice. SAGE Publications Inc., 2017; 30S–47S.

suppressor cells and tolerance in cancer: Mechanisms and therapeutic perspectives. Immunological Reviews. 2008; 222 (1): 180–91.

22. IKEDA H. Plasma amino acid levels in individuals with bacterial pneumonia and healthy controls. 2020; 1–17.

23. Ware LB, Magarik JA, Wickersham N, Cunningham G, Rice TW, Christman BW, et al. Low plasma citrulline levels are associated with acute respiratory distress syndrome in patients with severe sepsis. Crit Care. 2013; 17 (1): 1–8.

24. Morris SM Jr. Arginine: beyond protein. Am J Clin Nutr. 2006; 83: 508S–12S.

25. Schimke RT. Repression of enzymes of arginine biosynthesis in mammalian tissue culture. Biochim Biophys Acta. 1962; 62: 599–601.

26. Jackson MJ, Allen SJ, Beaudet AL, O'Brien WE. Metabolite regulation of argininosuccinate synthetase in cultured human cells. J Biol Chem. 1988; 263: 16388–94.

27. Lee J, Ryu H, Ferrante RJ, Morris SM Jr, Ratan RR. Translational control of inducible nitric oxide synthase expression by arginine can explain the arginine paradox. Proc Natl Acad Sci USA. 2003; 100: 4843–8.

28. Taheri F, Ochoa JB, Faghiri Z, Culotta K, Park HJ, Lan MS, et al. L-Arginine regulates the expression of the T-cell receptor zeta chain (CD3zeta) in Jurkat cells. Clin Cancer Res. 2001; 7: 958s–65s.

29. Fernandez J, Lopez AB, Wang C, Mishra R, Zhou L, Yaman I, et al. Transcriptional control of the arginine/lysine transporter, cat-1, by physiological stress. J Biol Chem. 2003; 278: 50000–9.

30. Cheng J, Wang F, Yu DF, Wu PF, Chen JG. The cytotoxic mechanism of malondialdehyde and protective effect of carnosine via protein cross-linking/mitochondrial dysfunction/reactive oxygen species/MAPK pathway in neurons. European Journal of Pharmacology. 2011; 650, 184–94.

## Литература

1. Chiu-Lin Wang, Yi-Yin liu, Chin-Hu Wu, Chun-Yu Wang, Chun-Hung Wang, Cheng-Yu Long. Impact of COVID-19 on Pregnancy. International Journal of Medical Sciences. 2021; 18 (3): 763–7. DOI: 10.7150/ijms.49923.

2. Schwartz DA, Graham AL. Potential Maternal and Infant Outcomes from (Wuhan) Coronavirus 2019-nCoV Infecting Pregnant Women: Lessons from SARS, MERS, and Other Human Coronavirus Infections. Viruses. 2020; 12 (4): 194.

3. Zaigham M, Andersson O. Maternal and perinatal outcomes with COVID–19:A systematic review of 108 pregnancies. Acta Obstet Gynecol Scand. 2020; 99 (7): 823–9.

4. Chen H, Guo J, Wang C, Luo F, Yu X, Zhang W, et al. Clinical characteristics and intrauterine vertical transmission potential of COVID-19 infection in nine pregnant women: a retrospective review of medical records. Lancet. 2020; 395 (10226): 809–15.

5. Sukhikh G, Petrova U, Prikhodko A, Starodubtseva N, Chingin K, Chen H, et al. Vertical Transmission of SARS-CoV-2 in Second Trimester Associated with Severe Neonatal Pathology. Viruses. 2021; 13 (3). DOI:10.3390/v13030447.

6. Ellington S, Strid P, Tong VT, Woodworth K, Galang RR, Zambrano LD, et al. Characteristics of women of reproductive age with laboratory-confirmed SARS-COV-2 infection by pregnancy status — United States, January 22-June 7, 2020. Morb Mortal Wkly Rep. 2020; 69 (25): 769–5.

7. Vivanti AJ, Vauloup-Fellous C, Prevot S, Zupan V, Suffee C, Do Cao J, et al. Transplacental transmission of SARS-CoV-2 infection. Nat Commun. 2020; 11 (1). DOI: 10.1038/s41467020-17436-6.

8. Shen B, Yi X, Sun Y, Bi X, Du J, Zhang C, et al. Proteomic and Metabolomic Characterization of COVID-19 Patient Sera. Cell. 2020; 182 (1): 59–72.

9. McGarrah RW, Crown SB, Zhang G, Shah SH, M.H.S., Newgard CB.

Cardiovascular Metabolomics. Circ Res. 2018; 122 (9): 1238–58. DOI: 10.1161/CIRCRESAHA.117.311002.

10. Banoei MM, Vogel HJ, Weljie AM, Kumar A, Yende S, Angus DC, et al. Plasma metabolomics for the diagnosis and prognosis of H1N1 influenza pneumonia. 2017; 1–15.

11. Inoue S, Ikeda H. Differences in plasma amino acid levels in patients with and without bacterial infection during the early stage of acute exacerbation of COPD. Int J COPD. 2019; 14: 575–83.

12. Moat SJ, George RS, Carling RS. Use of Dried Blood Spot Specimens to Monitor Patients with Inherited Metabolic Disorders. Int J Neonatal Screen. 2020; 6 (2): 1–17.

13. Páez-Franco JC, Torres-Ruiz J, Sosa-Hernández VA, Cervantes-Díaz R, Romero-Ramírez S, Pérez-Fragoso A, et al. Metabolomics analysis reveals a modified amino acid metabolism that correlates with altered oxygen homeostasis in COVID-19 patients. Sci Rep. 2021; 11 (1). DOI: 10.1038/s41598-021-85788-0.

14. Rees CA, Rostad CA, Mantus G, Anderson EJ, Chahroudi A, Jaggi P. Altered amino acid profile in patients with SARS-CoV-2 infection. 2021; 118 (25): 4–6.

15. Hirschel J, Vogel M, Baber R, Garten A, Beuchel C, Dietz Y, et al. Relation of whole blood amino acid and acylcarnitine metabolome to age, sex, BMI, puberty, and metabolic markers in children and adolescents. Metabolites. 2020; 10 (4). DOI: 10.3390/metabo10040149.

16. Lomova NA, Chagovets VV, Dolgopolova EL, Novoselova AV, Petrova UL, Shmakov RG, et al. Changes in amino acid profile of cord blood plasma and amniotic fluid of mothers with COVID-19. Bulletin of Russian State Medical University. 2021; (3): 12–22. DOI: 10.24075/BRSMU.2021.032

17. Diorio C, McNerney KO, Lambert M, Paessler M, Anderson EM, Henrickson SE, et al. Evidence of thrombotic microangiopathy in children with SARS-CoV-2 across the spectrum of clinical

presentations. Blood Adv. 2020; 4 (23): 6051–63.

18. Tay MZ, Poh CM, Rénia L, MacAry PA, Ng LFP. The trinity of COVID-19: immunity, inflammation and intervention. Nature Reviews Immunology. 2020; 20 (6): 363–74.

19. Gambardella J, Khondkar W, Morelli MB, Wang X, Santulli G, Trimarco V. Arginine and endothelial function. Biomedicines. 2020; 8 (8): 277.

20. Rodríguez PC, Ochoa AC. Arginine regulation by myeloid derived suppressor cells and tolerance in cancer: Mechanisms and therapeutic perspectives. Immunological Reviews. 2008; 222 (1): 180–91.

21. Morris CR, Hamilton-Reeves J, Martindale RG, Sarav M, Ochoa Gautier JB. Acquired Amino Acid Deficiencies: A Focus on Arginine and Glutamine. In: Nutrition in Clinical Practice. SAGE Publications Inc., 2017; 30S–47S.

22. IKEDA H. Plasma amino acid levels in individuals with bacterial pneumonia and healthy controls. 2020; 1–17.

23. Ware LB, Magarik JA, Wickersham N, Cunningham G, Rice TW, Christman BW, et al. Low plasma citrulline levels are associated with acute respiratory distress syndrome in patients with severe sepsis. Crit Care. 2013; 17 (1): 1–8.

24. Morris SM Jr. Arginine: beyond protein. Am J Clin Nutr. 2006; 83: 508S–12S.

25. Schimke RT. Repression of enzymes of arginine biosynthesis in mammalian tissue culture. Biochim Biophys Acta. 1962; 62: 599–601.

26. Jackson MJ, Allen SJ, Beaudet AL, O'Brien WE. Metabolite regulation of argininosuccinate synthetase in cultured human cells. J Biol Chem. 1988; 263: 16388–94.

27. Lee J, Ryu H, Ferrante RJ, Morris SM Jr, Ratan RR. Translational control of inducible nitric oxide synthase expression by arginine can explain the arginine paradox. Proc Natl Acad Sci USA. 2003; 100: 4843–8.

28. Taheri F, Ochoa JB, Faghiri Z, Culotta K, Park HJ, Lan MS, et al. L-Arginine regulates the expression of the T-cell receptor zeta chain (CD3zeta) in Jurkat cells. Clin Cancer Res. 2001; 7: 958s–65s.

29. Fernandez J, Lopez AB, Wang C, Mishra R, Zhou L, Yaman I, et al. Transcriptional control of the arginine/lysine transporter, cat-1, by physiological stress. J Biol Chem. 2003; 278: 50000–9.

30. Cheng J, Wang F, Yu DF, Wu PF, Chen JG. The cytotoxic mechanism of malondialdehyde and protective effect of carnosine via protein cross-linking/mitochondrial dysfunction/reactive oxygen species/MAPK pathway in neurons. European Journal of Pharmacology. 2011; 650, 184–94.

# PREDICTING PRETERM BIRTH BASED ON VAGINAL MICROBIOTA ASSESSMENT BY REAL-TIME PCR IN THE FIRST TRIMESTER

Voroshilina ES[1,2] ✉, Khautin LV[2], Kudryavtseva EV[1], Kovalev VV[1], Plotko EE[2]

[1] Ural State Medical University, Yekaterinburg, Russia

[2] "Garmonia" Medical Center, Yekaterinburg, Russia

Detecting high risk of preterm birth (PB) early makes its prevention possible. The aim of the work was to develop a mathematical predictive model for assessing the risk of preterm birth based on a quantitative analysis of the vaginal microbiota in the first trimester of pregnancy. The study included 199 pregnant women, i.e. 41 pregnancies that ended in preterm birth, and 158 — in term birth. Vaginal microbiota was analyzed in all patients in the 1st trimester of pregnancy by quantitative real-time PCR (qPCR). The method of dicriminant analysis was used to develop a predictive model. A method for predicting PB was developed with the calculation of the PRIMA prognostic index (Premature Birth. Index Of Microbiological Analysis). If the value of PRIMA > 0 – the risk of premature birth is low, if PRIMA < 0 – the risk is high. The sensitivity and specificity of the method are respectively 70.7% and 79.75%, the effectiveness is 77.89%. Evaluation of vaginal microbiota in the 1st trimester makes it possible to identify a high-risk group of PB and perform timely preventive measures.

## ПРОГНОЗИРОВАНИЕ ПРЕЖДЕВРЕМЕННЫХ РОДОВ НА ОСНОВАНИИ ИССЛЕДОВАНИЯ МИКРОБИОТЫ ВЛАГАЛИЩА МЕТОДОМ ПЦР В РЕАЛЬНОМ ВРЕМЕНИ В ПЕРВОМ ТРИМЕСТРЕ БЕРЕМЕННОСТИ

Е. С. Ворошилина[1,2] ✉, Л. В. Хаютин[2], Е. В. Кудрявцева[1], В. В. Ковалев[1], Е. Э. Плотко[2]

[1] Уральский государственный медицинский университет, Екатеринбург, Россия

[2] Медицинский центр «Гармония», Екатеринбург, Россия

Раннее выявление высокого риска развития преждевременных родов (ПР) дает возможность их предупреждения. Целью работы было разработать математическую прогностическую модель для оценки риска преждевременных родов на основании количественного анализа микробиоты влагалища в первом триместре беременности. В исследование было включено 199 беременных, из которых у 41-й беременность закончилась преждевременными родами, у 158 — срочными родами. Всем участницам проводили исследование микробиоты влагалища методом ПЦР в реальном времени (ПЦР-РВ). Для разработки прогностической модели использовали метод дискриминантного анализа. Был разработан способ прогнозирования ПР с расчетом прогностического индекса ПРИМА (сокр. от «Преждевременные роды. Индекс микробиологического анализа»). Если значение ПРИМА > 0, риск ПР низкий, если ПРИМА < 0, риск высокий. Чувствительность и специфичность метода составляют соответственно 70,7 и 79,75%, эффективность — 77,89%. Оценка микробиоты влагалища в первом триместре дает возможность определения группы высокого риска ПР и проведения своевременных профилактических мероприятий.

Prevention and early diagnosis of gestational complications are crucial for reducing maternal and neonatal mortality rates, as well as for reducing morbidity throughout the rest of their lives [1]. Preterm birth (PB) accounts for estimated 70% of neonatal mortality and 36% of child mortality. Long-term consequences of PB take the form of neurological disorders in children in 25–50% of cases [2], and therefore, it represents not only a medical, but also a social problem worldwide.

Preterm birth occurs during 22nd to 36th weeks of pregnancy [2]. PB is one of the great obstetrical syndromes, which are characterized by a long preclinical stage [1, 2, 3, 4]. The prevalence of PB in Russia is about 6% of the total number of births [2]. Moreover, in 70–80% of PB cases, the labor occurs spontaneously, and only 20–30% of the cases manifest with early signs from mother and/or fetus [2, 3].

In recent years, a number of the most significant complications of pregnancy (premature birth, placental insufficiency, fetal growth retardation syndrome, and preeclampsia) are increasingly considered as a single group called "the great obstetrical syndromes" [4, 5].

These pathological conditions are based on placental disorders in the early stages of pregnancy, associated with defects in the gestational transformation of spiral arteries, which in turn can be caused by a number of etiological factors (luteal insufficiency, disorders in the formation of immunological tolerance, acquired or congenital thrombophilia, direct or indirect effects of infectious agents) [6, 7]. In clinical practice, as a rule, there is a complex combination of several etiological factors and pathogenetic mechanisms.

The 2020 clinical recommendations on preterm birth management emphasize the scientifically proven relationship between PB and genital tract infections (GTIs). The course of GTIs in most cases is asymptomatic [2, 8]. A change in the microbiota of the genital tract leads to an increase in the contractile activity of the myometrium and degradation of the extracellular matrix with the remodeling of the cervix and amniotic membrane [2, 8, 9].

The structure of genital infections in pregnant women is dominated by vaginal microbiota disorders. More than half of women have at least one episode of genital pathology associated with dysbiotic disorders during pregnancy [10]. At the same time, pregnancy itself is a risk factor for the development of a pathology caused by opportunistic microbiota and microorganisms with weak virulence and aggression factors [11].

Vaginal dysbiosis is caused by an imbalance between the opportunistic and physiological microflora, the extreme degree of which is pronounced dysbiosis, which definitely requires treatment [12, 13, 14]. The state of vaginal microbiocenosis, where the proportion of lactobacilli is in the range of 20–80% of the total bacterial load (TBL), is regarded as moderate dysbiosis [15]. Whether this option is normal or requires treatment to date remains unclear.

The emergence of quantitative molecular based methods has significantly expanded our understanding of the quantitative and qualitative vaginal microbiota composition in normal and pathological conditions, including pregnancy [16].

Given the long preclinical stage of PB, development of new prognostic models for this state is crucial. Vaginal microbiota analysis and timely treatment in high-risk women may lead to a decrease in the preterm birth rates and thus improve the perinatal outcomes.

The aim of the work was to develop a mathematical predictive model for assessing the risk of preterm birth based on a quantitative analysis of the vaginal microbiota in the first trimester of pregnancy.

METHODS

### Research design

A single-center cohort retrospective comparative study included 199 patients who received prenatal care at the Garmonia Medical Center (Yekaterinburg) in the period from 2012 to 2021. The study was conducted on the basis of the laboratory department of the "Garmonia" Medical Center.

### Inclusion and exclusion criteria

Inclusion criteria for the main group: age from 20 to 42 years, spontaneous preterm birth (28–36 weeks gestation), consent to participate in the study.

Inclusion criteria for the control group: age from 20 to 42 years, term birth, consent to participate in the study.

Exclusion criteria for the main group: severe endocrine diseases; arterial hypertension of 2nd–3rd degrees; thyroid diseases in the decompensation stage; coagulopathy; antiphospholipid syndrome; intrauterine infectious processes during pregnancy; severe chronic diseases (kidneys, liver, respiratory organs, cardiovascular system, central nervous system); mental illnesses; present or history of oncological diseases; chronic alcohol or nicotine intoxication, substances abuse; uterine malformations.

Exclusion criteria for the control group: refusal to participate in the study, indications for induced preterm birth or preterm surgical delivery, infections of the genital tract caused by obligate pathogens.

### Groups of patients

The main group (group 1) included patients with PB ($n$ = 41), the control group (group 2) consisted of women with successful full-term delivery ($n$ = 158).

### Research methods

All participants of the study underwent a clinical and laboratory examination, in accordance with the current standards.

All patients underwent vaginal microbiota analysis by qPCR at 6–12 weeks of gestation (I trimester). The material for the study was collected in an Eppendorf tube containing 1 ml of sterile saline solution from the posterolateral vaginal wall. DNA was extracted using the PREP GS PLUS reagent kit (DNA Technology LLC; Russia), was performed using Femoflor ® 16 REAL-TIME PCR Detection Kit (DNA Technology LLC; Russia) according to the manufacturer's instructions. 16 groups of bacteria were typed and quantified. According to the test results, each vaginal sample was automatically characterized using the software provided by the manufacturer.

### Ethical aspects

The design of the study was reviewed and approved by the local ethics committee of the Federal State Budgetary Educational Institution of the Ministry of Health of the Russian Federation, Protocol No. 7 of 28.03.2011. All participants of the study were informed about the methods and nature of the study, the inclusion of the survey results in the scientific study and signed a voluntary informed consent.

### Methods of statistical analysis

Statistical processing of the study results was carried out using computer programs Statistica 7.0 (StatSoft Inc.; USA), Microsoft Excel 2016 and StatPlus:mac 8.0.3 (AnalystSoft; USA). The normality of the distribution was checked using the Kolmogorov–Smirnov criterion. The distribution was not normal. For quantitative indicators, the median value (Me) and the interquartile range ($Q_1$–$Q_3$) were indicated, and the nonparametric Mann–Whitney criterion was used to assess the statistical significance of the differences. Absolute and relative values (%) were presented for qualitative indicators, the statistical significance of the differences was determined using the criterion $\chi^2$. The strength of the association of the obtained values was estimated in the values of the odds ratio indicator (OR) with a 95% confidence interval (95% CI). The differences were considered statistically significant at $p < 0.05$. To form the regression equation, which formed the basis of the predictive model, the method of discriminant analysis with the calculation of canonical coefficients of the discriminant function (CCDF) was used. ROC analysis was applied to evaluate the effectiveness of the proposed predictive model.

RESULTS

### Clinical and anamnesis characteristics of the examined patients

Initially, the groups were compared according to their medical history parameters. The data of somatic and obstetric-gynecological history of the patients were taken into account. The average age of the examined patients was 29.04 ± 4.62 years for the main group and 28.53 ± 4.03 years for the control group ($p > 0.05$). In terms of weight and height parameters, the differences were not significant ($p > 0.05$). The frequency of detection of somatic pathologies (diseases of the cardiovascular, urinary, respiratory, nervous systems, endocrinopathies, pathology of the gastrointestinal tract and autoimmune diseases) also did not differ between the groups ($p > 0.05$). Thus, the groups were clinically comparable.

### Vaginal microbiota analysis

Vaginal microbiota composition was assessed by qPCR. In accordance with the previously proposed criteria [16], 4 variants of vaginal microbiocenosis were distinguished, the frequency of detection of which differed in pregnant women of the analyzed groups (Fig. 1).

In the main group, dysbiosis of varying severity was determined in 16 (39.0%) patients, in the control group it was determined in 18 (11.39%) patients ($\chi^2 = 17.457$; $p < 0.001$ [2.9E-5]). The detection rates of *Ureaplasma spp* in an amount of more than $10^4$ genomequivalents in ml (GE/ml) differed significantly: 18 (43.9%) in the main group, 39 (24.7%) in the control group ($\chi^2 = 5.853$; $p = 0.016$). Moreover, in group 1 dysbiosis in combination with *Ureaplasma spp.* in an amount of more than $10^4$ GE/ml was detected in 11 (26.8%) women, and in the control group — in 6 (3.8%) pregnant women ($\chi^2 = 21.991$; $p < 0.001$ [2.7E-6]). At the same time, detection rates of conditional normocenosis associated with *Ureaplasma spp.* in the amount of more than $10^4$ GE/ml, did not differ between the groups. Also, there were no statistically significant differences in the detection rates of absolute normocenosis and conditional normocenosis associated with *Candida spp*.

### Discriminant analysis

For the convenience of assessing the risk of PB and the distribution of pregnant women into low- or high-risk groups, based on the results of vaginal microbiota analysis by using qPCR, we have developed a prognostic method with the calculation of the prognostic index PRIMA (Preterm birth. Index of Microbiological Analysis). To develop a prognostic index a discriminant analysis was carried out in the obtained matrices of laboratory parameters for patients of the analyzed groups.



**Fig. 1.** The structure of vaginal microbiocenosis in the examined groups of pregnant women ($\chi^2 = 19.066$; $p < 0.001$ [1.2E-5])

*Lactobacillus spp.*, *Staphylococcus spp.*, *Sneathia spp.* / *Leptotrichia spp.* / *Fusobacterium spp.*, *Gardnerella vaginalis* / *Prevotella bivia* / *Porphyromonas spp.*, *Eubacterium spp.*, *Lachnobacterium spp.* / *Clostridium spp.*, *Mobiluncus spp.* / *Corynebacterium spp.*, *Ureaplasma spp* were the most significant in predicting the risk of PB. The total bacterial load (TBL) was also taken into account. The data were determined in the Lg GE/ml format.

CCDF are presented in Table 1.

The PRIMA index is calculated by the following formula:

$$PRIMA = 0.25 - 0.49 \times X_1 + 0.74 \times X_2 - 0.16 \times X_3 - 0.22 \times X_4 - 0.04 \times X_5 - 0.22 \times X_6 - 0.03 \times X_7 - 0.03 \times X_8 + 0.3 \times X_9,$$ where

$X_1$ is TBL, Lg GE/ml;

$X_2$ is *Lactobacillus spp.*, Lg GE/ml;

$X_3$ is *Gardnerella vaginalis* / *Prevotella bivia* / *Porphyromonas spp.*, Lg GE/ml;

$X_4$ is *Lactobacillus spp.*, Lg GE/ml;

$X_5$ is *Sneathia spp.* / *Leptotrichia spp.* / *Fusobacterium spp.*, Lg GE/ml;

$X_6$ is *Lachnobacterium spp.* / *Clostridium spp.*, Lg GE/ml;

$X_7$ is *Mobiluncus spp.* / *Corynebacterium spp.*, Lg GE/ml;

$X_8$ is *Ureaplasma spp.*, Lg GE/ml;

$X_9$ is *Staphylococcus spp.*, Lg GE/ml;

If the value of PRIMA > 0 — the risk of preterm birth is low, if PRIMA < 0 — the risk is high.

The average PRIMA value in groups 1 and 2 was –0.39 (–1.43 –0) and 0.33 (–0.15 –0.84) respectively. The differences were statistically significant ($p < 0.001$). Graphically, the value of the PRIMA index is represented by Fig. 2.

To assess the effectiveness of the presented predictive model, ROC analysis was performed. The ROC curve for the PRIMA index is represented by Fig. 3. The area under the curve (area under curve, AUC) was 0.76 (95% CI 0.68–0.84), which corresponds to the good quality of the predictive model.

**Table 1.** CCDF when calculating the PRIMA index

| Parameter, Lg GE/ml | Non-standardized CCDF | Standardized CCDF |
|---|---|---|
| TBL | 0.46 | 0.33 |
| *Lactobacillus spp.* | –0.69 | –0.76 |
| *Staphylococcus spp.* | –0.28 | –0.44 |
| *Sneathia spp.* + *Leptotrichia spp.* + *Fusobacterium spp.*, | 0.04 | 0.07 |
| *Gardnerella vaginalis* + *Prevotella bivia* + *Porphyromonas spp.* | 0.15 | 0.29 |
| *Eubacterium spp.* | 0.2 | 0.36 |
| *Lachnobacterium spp.* + *Clostridium spp.* | 0.21 | 0.36 |
| *Mobiluncus spp.* + *Corynebacterium spp.* | 0.03 | 0.04 |
| *Ureaplasma spp.* | 0.03 | 0.06 |

To determine the sensitivity and specificity of the presented prognostic method, a holdout sample was used. The sensitivity and specificity parameters were respectively 70.7% and 79.75%, the effectiveness of the method was 77.89% (Table 2).

Sensitivity and specificity at different values of the PRIMA index are shown in Fig. 4.

DISCUSSION

According to previous studies, the lactobacilli-dominated type of the vaginal microbiota, which is established by the beginning of the second trimester, is the most favorable for the successful course and timely completion of pregnancy [17]. Normal microbiota in such pregnant women, as a rule, persists in the second and third trimesters [18]. In our study, we did not find statistically significant differences in the incidence of absolute and relative normocenosis in the 1st trimester of pregnancy, however, it was shown that severe dysbiosis is a risk factor for preterm birth: in group 1, it was significantly more common.

The presence of various opportunistic microorganisms, especially those associated with bacterial vaginosis, in the vaginal microbiota is prognostically unfavorable [17]. At the same time, treatment of bacterial vaginosis during pregnancy is often unsuccessful, and the proven elimination of *G. vaginalis* does not reduce the risk of PB due to the presence of other obligate anaerobes with a reduced proportion of lactobacilli [12]. Earlier studies have shown that the presence of *Ureaplasma spp* in a high titer is a risk factor for PB [19]. In our work, we confirmed these data — in the main group, *Ureaplasma spp*. in the amount of more than $10^4$ GE/ml was detected significantly more often. Moreover, in group 1, dysbiosis in combination with *Ureaplasma spp*. in an amount of more than $10^4$ GE/ml was detected in 11 (26.8%) women, and in the control group — in 6 (3.8%) women ($x^2 = 21.991$; $p < 0.001$). At the same time, detection rates of conditional normocenosis associated with *Ureaplasma spp*. in the amount of more than $10^4$ GE/ml, did not differ between the groups. Probably *Ureaplasma spp*. has the greatest significance in patients with dysbiosis.

Other opportunistic microorganisms have no independent significance, however, together they can form the type of vaginal microbiota, which increases or, conversely, reduces the risk of PB. To effectively predict this condition, a comprehensive assessment is necessary.

Previously, an attempt was made to develop a prognostic model for assessing the risk of PB based on the results of vaginal microbiota evaluation [17]. However, the authors of the proposed method used the NGS sequencing method (the target site of the bacterial genome is the 16S rRNA gene). Despite high informativeness, this approach has a number of disadvantages: complex sample preparation, difficulty in controlling the collection of material, long duration of analysis, difficulty in interpreting the results, high cost of equipment and reagents for research. These disadvantages make it almost impossible to use NGS sequencing in routine medical practice. For this purpose, real-time PCR method is much more convenient.

On this basis, we have developed a method for predicting preterm birth, taking into account data on the qualitative and quantitative composition of the vaginal microbiota of pregnant women obtained using qPCR. The novelty of the proposed method is that for the first time, a highly effective prediction of preterm birth is carried out solely on the basis of the qualitative and quantitative composition of vaginal microbiota. The proposed prognostic PRIMA index takes into account the role of 8 out of 16 determined parameters in the complex vaginal microbial
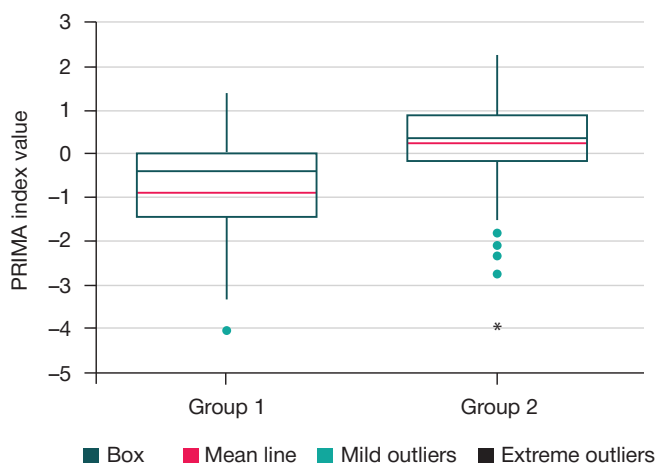


Fig. 2. The value of the PRIMA index in the analyzed groups
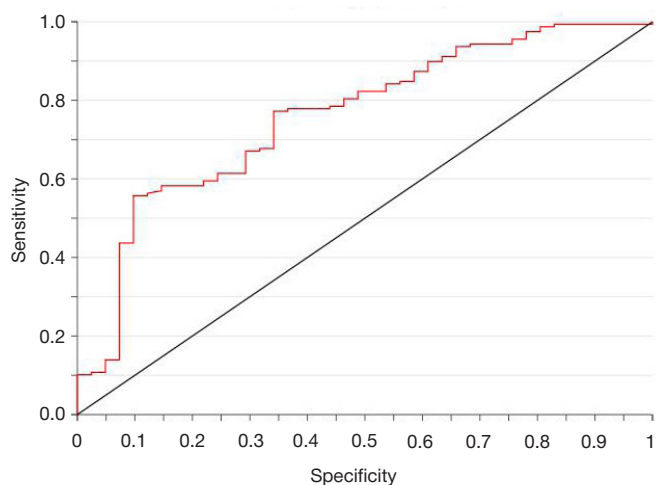


Fig. 3. ROC curve of the PRIMA index
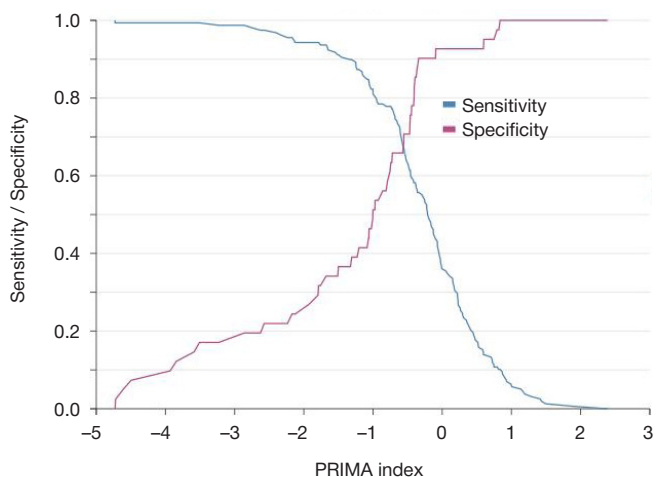


Fig. 4. Sensitivity and specificity at different values of the PRIMA index

community. It is noteworthy that in addition to *G. vaginalis*, which is traditionally associated with an increased risk of PB [17], 4 other groups of obligate anaerobes were significant in the formation of the prognostic index. This fact emphasizes the expediency of a comprehensive analysis of vaginal microbiota with an assessment of the significance of all potentially present microorganisms.

The limitation of this study is the exclusion of clinical and medical history data, as well as the results of other analyses from the number of parameters used to compile a prognostic index. We understand that preterm births cannot be entirely attributed to vaginal microbiota disorders. Therefore, it is possible to increase

**Table 2.** Sensitivity and specificity of the PRIMA index

| Group / Prognosis | 1 | 2 | Total | % correct |
|---|---|---|---|---|
| 1 | 29 | 12 | 41 | 70.7 |
| 2 | 32 | 126 | 158 | 79.75 |
| Total | 61 | 138 | 199 | 77.89 |

the sensitivity and specificity of the predictive model by including additional markers.

CONCLUSIONS

The predictive model developed by us makes it possible to detect pregnant women at risk of PB early on the basis of a comprehensive assessment of the vaginal microbiota by real-time PCR in the first trimester of pregnancy. The use of the proposed prognostic PRIMA index justifies the need to treat vaginal dysbiosis already in the first trimester of pregnancy to reduce the risks of preterm birth and, consequently, reduce perinatal morbidity and mortality. Distinguishing patients at risk for preterm birth based on the PRIMA index creates prerequisites for the use of already known preventive methods, for example, vaginal micronized progesterone from 22 to 34 weeks of pregnancy. The proposed prognostic method can be widely used in clinical practice, does not require significant additional costs.

### References

1. Kudryavtseva EV «Bol'shie akusherskie sindromy»: patogenez, prognozirovanie, taktika [dissertaciya]. M., 2020. Russian.
2. Prezhdevremennye rody. Klinicheskie rekomendacii. M.: Ministerstvo zdravooxraneniya RSFSR, 2020; 66 s. Russian.
3. Ananth CV, Vintzileos AM. Medically indicated preterm birth: recognizing the importance of the problem. Clin Perinatol. 2008; 35 (1): 53–67.
4. Romero R. Prenatal medicine: The child is the father of the man. J Matern Fetal Neonatal Med. 2009; 22 ( 8): 636–9.
5. Di Renzo GC. The great obstetrical syndromes. J Matern Fetal Neonatal Med. 2009; 22: 633–5.
6. Tosto V, Giardina I, Tsibizova V, Di Renzo GC. Preterm Birth, from the biological knowledges to the prevention: an overview, maternal-fetal medicine. 2020; 2 (3): 162–71. DOI: 10.1097/FM9.0000000000000054.
7. Tantengco OAG, Menon R. Breaking down the barrier: the role of cervical infection and inflammation in preterm birth. Front Glob Womens Health. 2022; 2: 777643. DOI: 10.3389/fgwh.2021.777643.
8. Kemp MW. Preterm birth, intrauterine infection, and fetal inflammation. Front Immunol. 2014; 5: 574.
9. Keelan JA. Intrauterine inflammatory activation, functional progesterone withdrawal, and the timing of term and preterm birth. J Reprod Immunol. 2018; 125: 89–99.
10. Khautin LV, Plotko EEh, Voroshilina ES. Anaehrobnyj disbioz vlagalishha vo vremya beremennosti: osobennosti techeniya i vozmozhnosti korrekcii. Ural'skij medicinskij zhurnal. 2016; 2 (135): 55–60.
11. Strizhakov AN, Budanov PV. Sostoyanie mikrocenoza vlagalishha i sposoby korrekcii ego narushenij vo vremya beremennosti. Voprosy ginekologii, akusherstva i perinatologii. 2007; 5: 37–43. Russian.

12. Shimaoka M, Yo Y, Doh K, Kotani Y, Suzuki A, Tsuji I, et al. Association between preterm delivery and bacterial vaginosis with or without treatment. Sci Rep. 2019; 9 (1): 509. DOI: 10.1038/s41598-018-36964-2.
13. Han Y, Liu Z, Chen T. Role of Vaginal Microbiota Dysbiosis in Gynecological Diseases and the Potential Interventions. Front Microbiol. 2021; 12: 643422. DOI: 10.3389/fmicb.2021.643422.
14. Klinicheskie rekomendacii po diagnostike i lecheniyu zabolevanij, soprovozhdayushhixsya patologicheskimi vydeleniyami iz polovyx putej zhenshhin. Rossijskoe obshhestvo akusherov-ginekologov. M., 2019; 57 s. Russian.
15. Voroshilina ES, Plotko EEh, Khautin LV, Tishhenko NA, Zornikov DL. Preobladanie Lactobacillus iners v mikrobiocenoze vlagalishha zhenshhin s umerennym disbiozom associirovano s nalichiem klinicheskix priznakov infekcionno-vospalitel'noj patologii vlagalishha. Vestnik RGMU. 2017; 2: 47–51. Russian.
16. Voroshilina ES, Tumbinskaya LV, Donnikov AE, Plotko EEh, Khautin LV. Biocenoz vlagalishha s tochki zreniya kolichestvennoj polimeraznoj cepnoj reakcii: chto est' norma? Akusherstvo i ginekologiya. 2011; 1: 57–65. Russian.
17. Fettweis JM, Serrano MG, Brooks JP, Edwards DJ, Girerd PH, Parikh HI et al. The vaginal microbiome and preterm birth. Nat Med. 2019; 25: 1012–21.
18. Voroshilina ES, Tumbinskaya LV, Donnikov AE, Plotko EEh, Khautin LV. Biocenoz vlagalishha s tochki zreniya kolichestvennoj PCR: izmeneniya i korrekciya vo vremya beremennosti . Ural'skij medicinskij zhurnal. 2010; 3 (68): 105–12. Russian.
19. Kikhney J, von Schöning D, Steding I, Schulze J, Petrich A, Hiergeist A, et al. Is Ureaplasma spp. the leading causative agent of acute chorioamnionitis in women with preterm birth? Clinical Microbiology and Infection. 2017; 23 (2): 119.e1–119.e7.

### Литература

1. Кудрявцева Е. В. «Большие акушерские синдромы»: патогенез, прогнозирование, тактика [диссертация]. М., 2020.
2. Преждевременные роды. Клинические рекомендации. М.: Министерство здравоохранения РСФСР, 2020; 66 с.
3. Ananth CV, Vintzileos AM. Medically indicated preterm birth: recognizing the importance of the problem. Clin Perinatol. 2008; 35 (1): 53–67.
4. Romero R. Prenatal medicine: The child is the father of the man. J Matern Fetal Neonatal Med. 2009; 22 ( 8): 636–9.
5. Di Renzo GC. The great obstetrical syndromes. J Matern Fetal Neonatal Med. 2009; 22: 633–5.
6. Tosto V, Giardina I, Tsibizova V, Di Renzo GC. Preterm Birth, from the biological knowledges to the prevention: an overview, maternal-fetal medicine. 2020; 2 (3): 162–71. DOI: 10.1097/FM9.0000000000000054.
7. Tantengco OAG, Menon R. Breaking down the barrier: the role of cervical infection and inflammation in preterm birth. Front Glob Womens Health. 2022; 2: 777643. DOI: 10.3389/fgwh.2021.777643.
8. Kemp MW. Preterm birth, intrauterine infection, and fetal inflammation. Front Immunol. 2014; 5: 574.
9. Keelan JA. Intrauterine inflammatory activation, functional progesterone withdrawal, and the timing of term and preterm birth. J Reprod Immunol. 2018; 125: 89–99.
10. Хаютин ЛВ, Плотко ЕЭ, Ворошилина ЕС. Анаэробный дисбиоз влагалища во время беременности: особенности течения и возможности коррекции. Уральский медицинский

журнал. 2016; 2 (135): 55–60.

11. Стрижаков А. Н., Буданов П. В. Состояние микроценоза влагалища и способы коррекции его нарушений во время беременности. Вопросы гинекологии, акушерства и перинатологии. 2007; 5: 37–43.

12. Shimaoka M, Yo Y, Doh K, Kotani Y, Suzuki A, Tsuji I, et al. Association between preterm delivery and bacterial vaginosis with or without treatment. Sci Rep. 2019; 9 (1): 509. DOI: 10.1038/s41598-018-36964-2.

13. Han Y, Liu Z, Chen T. Role of Vaginal Microbiota Dysbiosis in Gynecological Diseases and the Potential Interventions. Front Microbiol. 2021; 12: 643422. DOI: 10.3389/fmicb.2021.643422.

14. Клинические рекомендации по диагностике и лечению заболеваний, сопровождающихся патологическими выделениями из половых путей женщин. Российское общество акушеров-гинекологов. М., 2019; 57 с.

15. Ворошилина Е. С., Плотко Е. Э., Хаютин Л. В., Тищенко Н. А., Зорников Д. Л. Преобладание Lactobacillus iners в микробиоценозе влагалища женщин с умеренным дисбиозом ассоциировано

с наличием клинических признаков инфекционно-воспалительной патологии влагалища. Вестник РГМУ. 2017; 2: 47–51.

16. Ворошилина Е. С., Тумбинская Л. В., Донников А. Е., Плотко Е. Э., Хаютин Л. В. Биоценоз влагалища с точки зрения количественной полимеразной цепной реакции: что есть норма? Акушерство и гинекология. 2011; 1: 57–65.

17. Fettweis JM, Serrano MG, Brooks JP, Edwards DJ, Girerd PH, Parikh HI et al. The vaginal microbiome and preterm birth. Nat Med. 2019; 25: 1012–21.

18. Ворошилина Е. С., Тумбинская Л. В., Донников А. Е., Плотко Е. Э., Хаютин Л. В. Биоценоз влагалища с точки зрения количественной ПЦР: изменения и коррекция во время беременности . Уральский медицинский журнал. 2010; 3 (68): 105–12.

19. Kikhney J, von Schöning D, Steding I, Schulze J, Petrich A, Hiergeist A, et al. Is Ureaplasma spp. the leading causative agent of acute chorioamnionitis in women with preterm birth? Clinical Microbiology and Infection. 2017; 23 (2): 119.e1–119.e7.

# CLINICAL AND MORPHOLOGICAL FEATURES OF NON-SMALL CELL LUNG CANCER IN PATIENTS WITH DIFFERENT TYPES OF HISTOLOGICAL CHANGES TO THE BRONCHIAL EPITHELIUM

Zavyalova MV[1,2], Loos DM[1], Pismenny DS[1,2] ✉, Durova AA[1], Pankova OV[2], Rodionov EO[2], Tuzikov SA[1,2], Tashireva LA[2], Perelmuter VM[2]

[1] Siberian State Medical University, Tomsk, Russia

[2] Cancer Research Institute, Tomsk National Research Medical Center, Tomsk, Russia

Lung cancer occupies the leading position in the global structure of oncological diseases. Despite significant advances in its treatment, the survival remains low. Morphological changes to the bronchial epithelium outside the tumor may provide important cues on progression of the disease in patients with lung cancer. This study aimed to identify associations between morphological and clinical features of non-small cell lung cancer and morphological changes to the epithelium in small bronchi outside the tumor. The study encompassed tumor specimens collected from 90 patients, 75 (83%) men and 15 (17%) women, diagnosed with non-small cell lung cancer. The average age of the patients was $67.8 \pm 7.4$ years. The results indicate higher frequency of lymphogenous metastasis in patients with combined basal cell hyperplasia and squamous metaplasia (BCH+SM+ group) compared to patients with isolated basal cell hyperplasia (BCH+SM– group, $p = 0.05$). The BCH+SM– group presented with higher rates of hematogenous metastasis compared to BCH+SM+ and BCH–SM– groups ($p = 0.004$ and $p = 0.0019$, respectively), as well as increased representation of low-differentiated structures in the primary tumors. The results suggest a commonality of parenchymal-stromal interactions in non-small cell lung cancers and their surroundings and a significant impact of these interactions on differentiation status and progression of the tumors.

**Keywords:** non-small cell lung cancer, tumor heterogeneity, basal cell hyperplasia, squamous cell metaplasia, metastasis

# КЛИНИКО-МОРФОЛОГИЧЕСКИЕ ОСОБЕННОСТИ НЕМЕЛКОКЛЕТОЧНОГО РАКА ЛЕГКОГО У БОЛЬНЫХ С РАЗНЫМИ ВАРИАНТАМИ ГИСТОЛОГИЧЕСКИХ ИЗМЕНЕНИЙ БРОНХИАЛЬНОГО ЭПИТЕЛИЯ

М. В. Завьялова[1,2], Д. М. Лоос[1], Д. С. Письменный[1,2] ✉, А. А. Дурова[1], О. В. Панкова[2], Е. О. Родионов[2], С. А. Тузиков[1,2], Л. А. Таширева[2], В. М. Перельмутер[2]

[1] Сибирский государственный медицинский университет, Томск, Россия

[2] Научно-исследовательский институт онкологии Томского научно-исследовательского медицинского центра, Томск, Россия

По данным мировой статистики рак легких занимает ведущие позиии в структуре онкологических заболеваний. Несмотря на значительные достижения в лечении, выживаемость остается низкой. Изучение ассоциации морфологических изменений бронхиального эпителия смежных с опухолью у пациентов с раком легкого, может привнести значимый вклад в понимание прогрессии опухоли. Целью работы было выявить особенности морфологического строения и прогрессии немелкоклеточного рака легких, ассоциированные с характером изменений эпителия в мелких бронхах, смежных с опухолью. В исследование был включен операционный материал от 90 пациентов с диагнозом немелкоклеточный рак легкого. Средний возраст пациентов составил $67,8 \pm 7,4$ лет. Мужчин было 75 (83%), женщин — 15 (17%). Выявлена высокая частота развития лимфогенного метастазирования в группе пациентов с сочетанием базальноклеточной гиперплазии и плоскоклеточной метаплазии (БКГ+ПМ+) по сравнению с группой, где выявлена только базальноклеточная гиперплазия (БКГ+ПМ–) ($p = 0,05$). Частота встречаемости гематогенных метастазов была выше группе с БКГ+ПМ– по сравнению с БКГ+ПМ+ ($p = 0,004$) и БКГ–ПМ– ($p = 0,0019$). В то же время в группе высокого риска гематогенного метастазирования (БКГ+ПМ–) в первичных опухолях чаще встречаются низкодифференцированные структуры. Результаты исследования позволяют предполагать о наличии ассоциации паренхиматозно-стромальных отношений в мелких бронхах опухоленосителей и в опухоли и их связь со степенью дифференцировки НМРЛ и с его прогрессией.

**Ключевые слова:** немелкоклеточный рак легкого, опухолевая гетерогенность, базальноклеточная гиперплазия, плоскоклеточная метаплазия, метастазирование.

Lung cancer occupies the first place in the structure of cancer mortality, both globally and in Russia [1].

The continued search for additional prognostic indicators in lung cancer is accompanied by extensive mechanistic studies on lung carcinogenesis. With bronchial epithelium being the main substratum and cell source of lung tumors, the condition of the bronchial epithelium outside the tumor foci in patients with lung cancer is given close consideration.

Earlier reports emphasized the relevance of research into hyperplastic processes in small bronchi located at some distance from the primary tumor. The hyperplastic lesions of the bronchial epithelium may already harbor the minute genetic changes that subsequently direct neoplastic processes and become fully actualized in carcinogenesis [2, 3].

The development of squamous cell lung carcinomas from pre-existing hyperplastic lesions in the bronchial epithelium has been largely attributed to the influence of inflammatory factors that interfere with normal cell cycle while inhibiting apoptosis and cell differentiation [4].

Basal cell hyperplasia (BCH), the first morphologically identifiable step of pathogenic alterations in the bronchial epithelium, is caused by accelerated regeneration with a simultaneous constraint on cell differentiation under chronic inflammatory conditions [5]. In BCH, the number of cell rows reaches three [6]. The cells present with no atypia, intercellular cytoplasmic bridges or keratinization while preserving the cilia at their surface [7, 8]. Nevertheless, the altered expression of proliferation and apoptosis markers (Ki67, Bcl-2, p53) is noted already in BCH [5, 9].

Squamous cell metaplasia (squamous metaplasia, SM) is defined as replacement of the columnar ciliated respiratory epithelium with mature squamous epithelium. In SM, the surface layer of the epithelium is formed by cells lying in parallel to the basement membrane, showing minimal or zero signs of atypia and connected by intercellular bridges. Maturation of the basal layer cells and preservation of the intermediate cell zone are also characteristic of SM [10].

BCH and SM frequently progress into neoplasia and/or invasive squamous cell cancer [6, 11]. Particular changes to the bronchial epithelium have been positively or negatively associated with various dysplastic and carcinogenic processes in the lung. For example, combinations of bronchial epithelial dysplasia with BCH are rare, independently of the presence or absence of SM, whereas BCH and SM are seldom found in patients with lung adenocarcinoma [2].

Apart from their role in the primary tumor pathogenesis, BCH and SM have been characterized as candidate predictors of tumor progression in non-small cell lung cancer. For example, a combination of BCH and SM without dysplasia in small bronchi correlates with higher probability of recurrence [12], whereas isolated BCH has been associated with higher risks of hematogenous metastasis [13].

Such associations can be explained by a variety of stromal immune reactions defined genetically and playing a key role in various types of epithelial-stromal interactions. The stromal immune reactions in the bronchi presumably reflect specific features of the tumor microenvironment [14].

This study aimed to identify associations between morphological and clinical features of non-small cell lung cancer and morphological changes to the epithelium in small bronchi outside the tumor.

METHODS

The study encompassed tumor specimens collected from 90 patients with non-small cell lung cancer T1-3N0-2M0 receiving treatment in the Thoracoabdominal Surgery Department at the Research Institute of Oncology of the Tomsk National Research Medical Center in 2009–2017. The inclusion criteria for the study encompassed the availability of written informed consent and the diagnosis of malignant epithelial tumor of the lung (squamous cell cancer or adenocarcinoma). The exclusion criteria encompassed refusal to participate, chronic comorbidities (tuberculosis, hepatitis C) and small-cell lung cancer. The spread of the disease was determined in accordance with the TNM staging system [15]. The pulmonary surgery amounted to lobectomy with ipsilateral mediastinal lymphadenectomy without neoadjuvant chemotherapy or intraoperative radiotherapy. The adjuvant chemotherapy was administered if indicated in accordance with the schemes: vinorelbine, cisplatin (25–30 mg/m$^2$ on days one and eight, 75–80 mg/m$^2$ i/v on day one, in 21 day cycles) or paclitaxel, carboplatin (200 mg/m$^2$ i/v on day one, AUC 6 i/v on day one, in 21 day cycles).

The morphological examination was conducted with an Axio Lab.A1 light microscope (Zeiss; Germany) and a Mirax Midi slide scanning system (Zeiss; Germany). The specimens were fixed in 10–12% solution of neutral formalin. Histological processing and subsequent sectioning of the formalin-fixed paraffin-embedded tissues were carried out by standard techniques. The sections were stained with hematoxylin and eosin (H&E).

Histological type of the tumor was determined based on the current WHO classification [16]. Only cases of squamous cell carcinoma or adenocarcinoma of the lung were selected for the study. The diagnoses were verified by immunohistochemical assessment using specific antibodies to TTF (clone SPT24, Novocastra; Leica Biosystems, UK), Napsin A (clone NCL-L, Novocastra; Leica Biosystems, UK), p63 (клон 7JUL, Novocastra; Leica Biosystems, UK), Cytokeratine 7 (clone OV-TL 12/30, Novocastra; Leica Biosystems, UK) and Cytokeratine 5/6 (clone D5/16, Dako; Agilent, Denmark). Immunostaining on slides was carried out by standard protocols. Adenocarcinomas stained positively for Cytokeratine 7, TTF and Napsin A and negatively for p63 and Cytokeratine 5/6. Squamous cell carcinomas stained positively for p63 and Cytokeratine 5/6 and negatively for Cytokeratine 7, TTF and Napsin A.

In adenocarcinoma, the parenchymal component was represented by lepidic, acinar, papillary, micropapillary or solid architectures, and occasionally by solitary tumor cells. Lepidic patterns were recognized by atypical cuboidal cells lining the alveoli from inside. Acinar patterns comprised rounded or oval glandular clusters of atypical cells. Papillary patterns comprised papillae with fibrovascular core and epithelial lining composed of atypical cuboidal or columnar cells. Micropapillary patterns comprised diminutive papillae without fibrovascular cores. Solid patterns comprised large sheets and nests of tumor cells.

In squamous cell carcinoma, the parenchymal component was represented by five types of structures: I) keratinized; II) composed of atypical non-keratinized spinous cells; III) composed of atypical basaloid cells; IV) composed of atypical, distinctly polymorphous cells; V) solitary tumor cells [17]. The analysis involved identification of these structures and determination of their abundance in a tumor (Fig. 1).

The analysis also accounted for the degree of tumor differentiation (high, medium or low) and condition of the stroma within the neoplasm. The degree of stromal development across the tumor, as well as in the vicinity of each particular type of parenchymal architecture within the neoplasm, was determined using a three-point scale (1 point — sparse stroma, less than 30% of the tumor bulk; 2 points — moderately
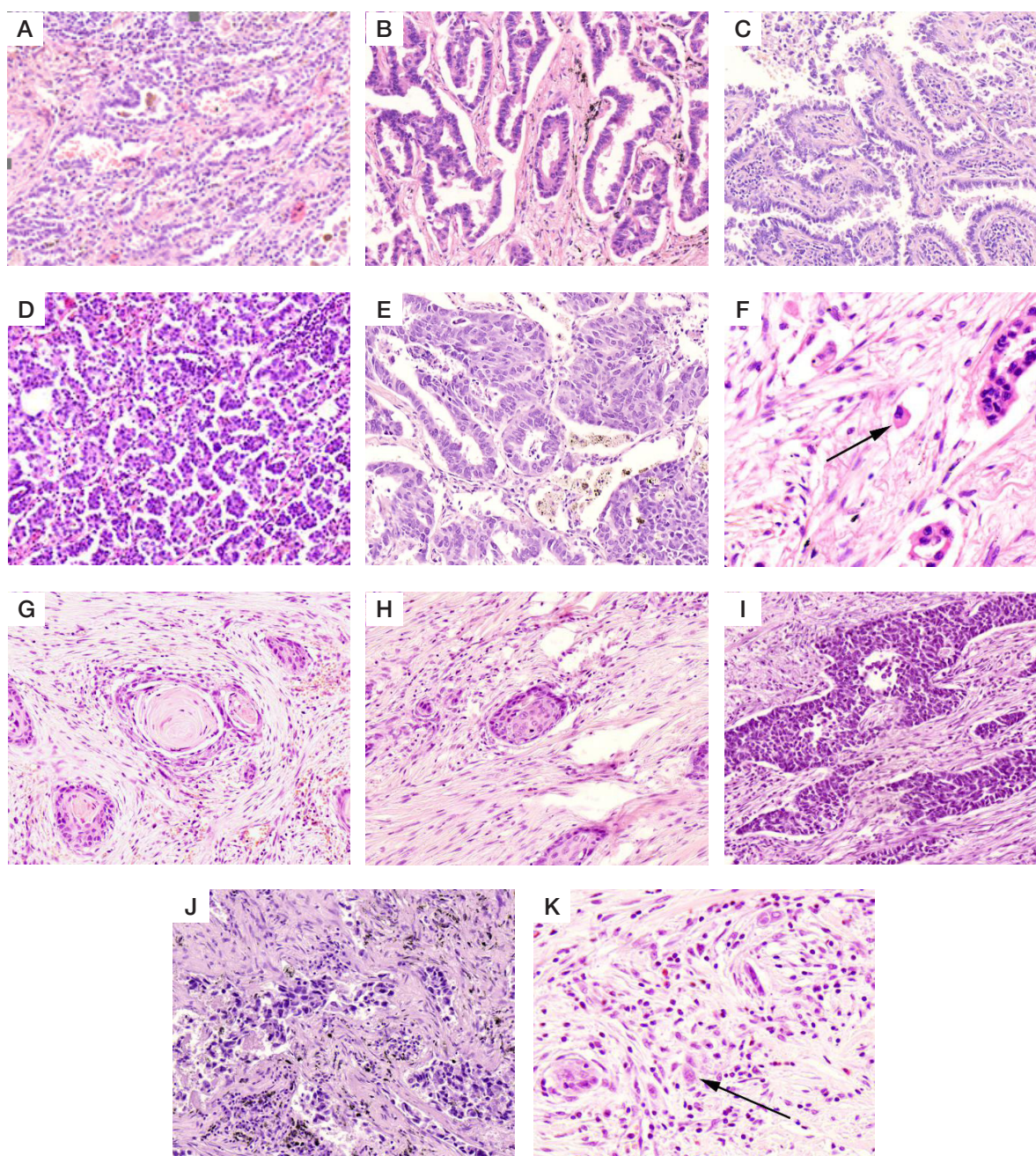
**Fig. 1.** Morphological subtypes of the parenchymal component of primary tumors in adenocarcinoma (**A**, lepidic; **B**, acinar; **C**, papillary; **D**, micropapillary; **E**, solid; **F**, solitary tumor cells) and squamous cell carcinoma (**G**, type I; **H**, type II; **I**, type III; **J**, type IV; **K**, type V). Staining H & E, magnification ×200

developed stroma, 30–70% of the tumor bulk; 3 points — abundant stroma, over 70% of the tumor bulk). The degree of inflammatory infiltration of the stroma across the tumor, as well as in the vicinity of each particular type of parenchymal architecture within the neoplasm, was quantified in percentages as described by Salgado et al [18]. To rule out a possible subjective bias, all examinations were carried out by two pathologists independently.

The mucosa of small bronchi located at a 3–4 cm distance from the tumor boundary was assessed for the presence of BCH and SM separately or in combination (Fig. 2).

The patients were distributed into three groups on the basis of histological changes to the bronchial epithelium: neither basal cell hyperplasia nor squamous metaplasia encountered (group a, BCH–SM–) — 17 pts; isolated basal cell hyperplasia (group b, BCH+SM–) — 45 pts; basal cell hyperplasia combined to squamous metaplasia (group c, BCH+SM+) — 28 pts. The

lymph nodes were examined for the presence of metastatic lesions and the counts of lymph nodes with metastases were recorded. The follow-up period was 5 years. The medical histories and outpatient records were analyzed to retrieve information about the incidence, time-points and localization of hematogenous metastases and relapses.

Statistical processing of the data was carried out in the Statistica 10.0 program package for Windows (Dell; USA). The comparisons involved standard methods of descriptive statistics and the Mann–Whitney test for two independent samples. Correction for multiple comparisons was not applied. The differences were considered significant at $p < 0.05$.

RESULTS

The age of patients in the three groups of the study was similar. In all groups, most of the patients were men and the non-small
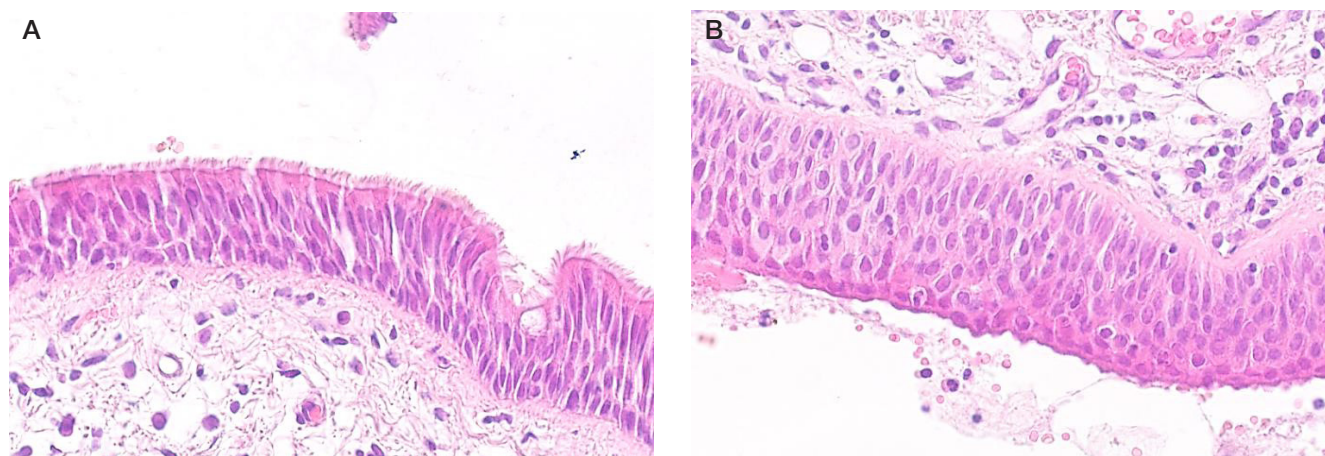
**Fig. 2.** Morphological changes to the bronchial epithelium outside the tumor: basal cell hyperplasia, BCH (**A**) and squamous cell metaplasia, SM (**B**). Staining H&E, magnification ×200

cell primary lung tumors had predominantly central localization (Table 1).

No significant differences in tumor size (T1, T2 or T3) were observed among the three groups of the study (Fig. 3).

The incidence of lymphogenous metastasis was significantly higher in patients with combined basal cell hyperplasia and squamous metaplasia (BCH+SM+, 57%) compared to patients with isolated basal cell hyperplasia (BCH+SM–, 38%; $p = 0.05$) while being similar to the frequency of lymphogenous metastasis in patients with neither (BCH–SM–, 47%) (Fig. 3).

Hematogenous metastases were significantly more typical in patients with isolated basal cell hyperplasia (BCH+SM–, 22%) compared to BCH–SM– (0%; $p = 0.019$) and BCH+SM+ (0%; $p = 0.004$) groups (Fig. 3).

Relapses were significantly more typical in patients with combined basal cell hyperplasia and squamous metaplasia (14%) compared to BCH–SM– (0%; $p = 0.05$) and BCH+SM– (2%; $p = 0.02$) groups (Fig. 3).

In the group of patients with neither basal cell hyperplasia nor squamous metaplasia (BCH–SM–, group a), histological type of the tumor was significantly skewed towards adenocarcinoma (65%) as opposed to squamous cell carcinoma (35%; $p = 0.04$). A reciprocal trend was observed for patients with combined basal cell hyperplasia and squamous metaplasia (BCH+SM+, group c) with the prevalence of squamous cell carcinoma (64%) over adenocarcinoma (36%; $p = 0.01$). In patients with isolated basal cell hyperplasia (BCH+SM–, group b) the two histological

types of non-small cell lung cancer were encountered at similar frequencies.

The degree of tumor differentiation for adenocarcinoma was similar in all groups. At that, the occurrence of acinar structures in the parenchymal component of adenocarcinoma was significantly lower in patients with isolated basal cell hyperplasia (BCH+SM–, 21%) compared to BCH–SM– (91%; $p = 0.0005$) and BCH+SM+ (90%; $p = 0.0007$) groups. By contrast, papillary structures were extremely typical for adenocarcinoma in BCH+SM– group (100%) and much less so in BCH–SM– (18%; $p = 0.0000$) and BCH+SM+ (20%; $p = 0.0000$) groups. The occurrence of solitary cell patterns in the parenchymal component of adenocarcinoma in BCH+SM+ group was significantly lower (20%) than in BCH–SM– (64%; $p = 0.028$) and BCH+SM– (58%; $p = 0.030$) groups.

The degree of tumor differentiation for squamous cell carcinoma was also similar in all groups. At the same time, architecture of the parenchymal component in squamous cell carcinoma revealed significant associations with morphological changes to the bronchial epithelium. For instance, type II structures (spinous) in the parenchymal component of squamous cell carcinoma were highly typical in BCH+SM+ group (94%) and less so in BCH–SM– (67%; $p = 0.04$) and BCH+SM– (69%; $p = 0.02$) groups.

The occurrence of type III structures (basaloid) in the parenchymal component of squamous cell carcinoma in patients with combined basal cell hyperplasia and squamous

**Table 1.** Clinical and morphological characterization for the groups of patients with non-small cell lung cancer distinguished on the basis of morphological changes to the bronchial epithelium

| Parameter | | Groups of the study | | |
|---|---|---|---|---|
| | | BCH–SM– ($n = 17$) | BCH+SM– ($n = 45$) | BCH+SM+ ($n = 28$) |
| | | a | b | c |
| 1 | Age, M ± SD | 59.7 ± 5.3 | 58.4 ± 8.3 | 60.5 ± 6.1 |
| 2 | Sex, a.v., % | | | |
| 3 | Men | 14/17 (82%) $p_4 = 0.0001$ | 36/45 (80%) $p_4 = 0.0000$ | 25/28 (89%) $p_4 = 0.0000$ |
| 4 | Women | 3/17 (18%) | 9/45 (20%) | 3/28 (11%) |
| 5 | Localization, a.v., % | | | |
| 6 | Central | 14/17 (82%) $p_7 = 0.0001$ | 30/45 (67%) $p_7 = 0.0006$ | 23/28 (82%) $p_7 = 0.000$ |
| 7 | Peripheral | 3/17 (18%) | 15/45 (33%) | 5/28 (18%) |

**Note:** a.v. — absolute value; $p_4$ measures the consistency of equal morbidity hypothesis for men (row 3) and women (row 4) in a given group; $p_7$ measures the consistency of equal probability hypothesis for central vs peripheral localization (rows 6 and 7, respectively) in a given group.
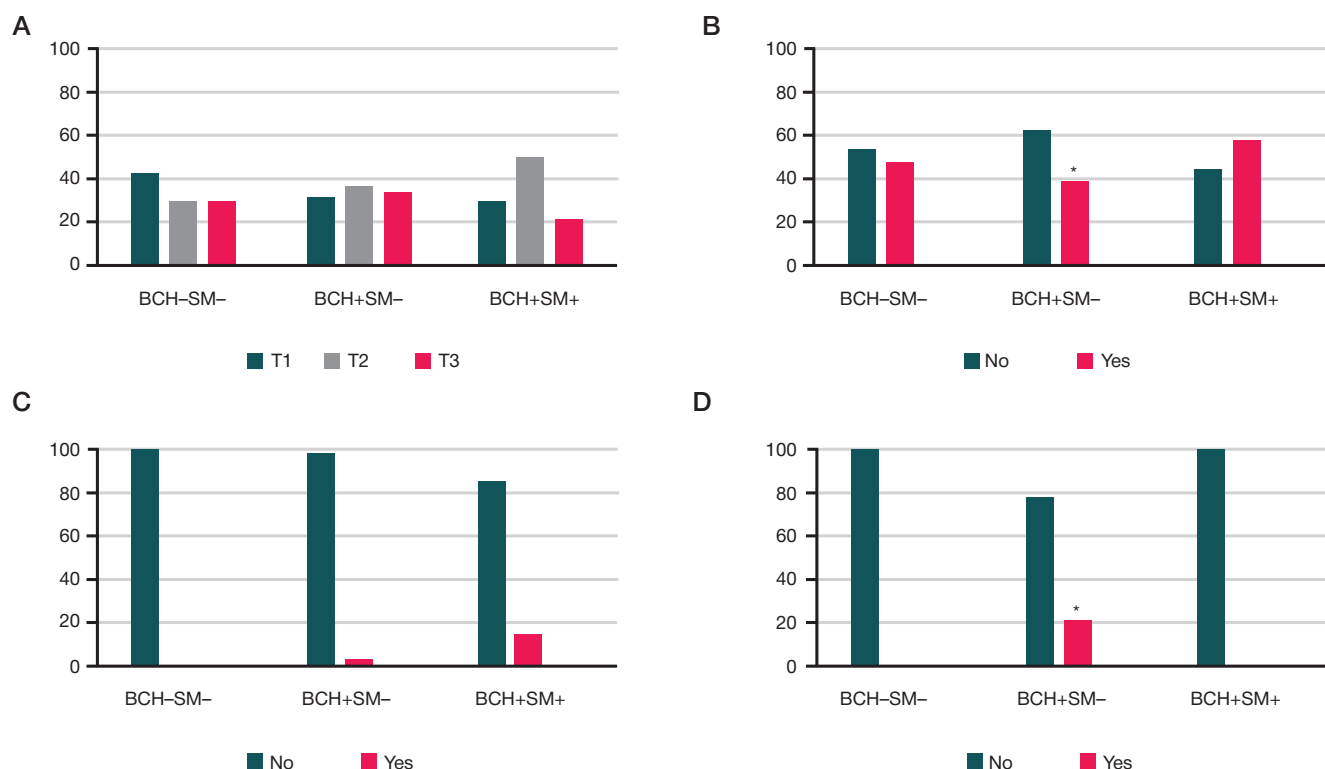
**Fig. 3.** Comparative characterization of the disease progression indicators in the groups of patients with non-small cell lung cancer distinguished on the basis of morphological changes to the bronchial epithelium. **A**. Tumor size (T). **B**. Lymphogenous metastases. **C**. Relapses. **D**. Hematogenous metastases

metaplasia (BCH+SM+, 22%) was significantly lower than in patients with isolated basal cell hyperplasia (BCH+SM–, 50%; $p = 0.025$) while being similar to the occurrence of such structures in patients with neither (BCH–SM–, 50%).

The three groups of patients revealed similar numbers of structural patterns of the parenchymal component combined in a single tumor and similar degrees of stromal development and inflammatory infiltration for both adenocarcinoma and squamous cell carcinoma (Table 2).

DISCUSSION

The study enabled the identification of characteristic clinical and structural features of non-small cell lung carcinoma in patients with particular morphological changes to the bronchial epithelium.

The group of patients with isolated BCH in the respiratory epithelium of small bronchi outside the tumor (BCH+SM–) showed increased rates of hematogenous metastasis and decreased rates of lymphogenous metastasis. In this group, representation of main histological subtypes of epithelial malignancy (adenocarcinoma, squamous cell carcinoma) was balanced. Adenocarcinomas diagnosed in patients with isolated BCH typically presented with low-differentiated papillary structures and, less typically, with higher differentiated acinar structures.

The group of patients with combined BCH and SM in the respiratory epithelium of small bronchi outside the tumor (BCH+SM+) showed increased rates of lymphogenous metastasis and recurrence against the lack of hematogenous metastasis. The prevalent diagnosis in this group was squamous cell carcinoma, most commonly of type II (spinous, higher differentiated) and less commonly of type III (basaloid, lower differentiated).

By contrast, the prevalent diagnosis in patients with neither BCH nor SM (BCH–SM–) was adenocarcinoma. The incidence

of adverse manifestations (lymphogenous and hematogenous metastasis, relapses) and morphological variations of the tumor architecture in this group were regular.

Of note, patients of BCH+SM+ group presented with lymphogenous metastases more frequently than patients of BCH+SM– group. The majority of relapses in non-small cell lung cancers are due to metachronous lymphogenous metastasis [14]. Our results indicate the existence of intersecting links in the mechanisms of synchronous and metachronous lymphogenous metastasis.

The higher incidence of hematogenous metastasis in BCH+SM– group and the higher incidence of relapses in BCH+SM+ group are consistent with previously reported findings. The data indicate that these groups significantly differ not only by the structure of clinical risks, but also by morphological features of the primary tumors. Interestingly, in BCH+SM+ group, the prevalent histological type was squamous cell carcinoma. The susceptibility to squamous metaplasia under conditions of chronic inflammation augments the development of squamous cell carcinoma, as the metaplastic squamous epithelium provides a favorable site for the pre-cancer dysplasia capable of progression into carcinoma. The associated differences in morphological architecture of primary tumors, reported for the first time herein, appear even more relevant. Consistently with the higher risks of hematogenous metastasis, BCH+SM– group shows increased occurrence of low-differentiated structures in both adenocarcinoma and squamous cell carcinoma. The differential character of epithelial changes in small bronchi most likely reflects some essential, constitutive differences in the stromal-parenchymal relationships inextricably linked to the parenchymal-stromal interactions in the adjacent carcinomas [13, 14].

The observed among-the-group differences in the condition of the stroma are obviously based on the features of immune and inflammatory reactions. The results allow us to assume that the mode of inflammatory response delivered by microenvironment of non-small cell lung cancer with isolated basal cell hyperplasia

**Table 2.** Histological characterization of the primary tumors for the groups of patients with non-small cell lung cancer distinguished on the basis of morphological changes to the bronchial epithelium

| Parameter | | Group of the study | | |
|---|---|---|---|---|
| | | BCH–SM– ($n$ = 17) | BCH+SM– ($n$ = 45) | BCH+SM+ ($n$ = 28) |
| | | a | b | c |
| 1 | Histological type, a.v., % | | | |
| 2 | Adenocarcinoma | 11/17 (65%) $p_3$ = 0.04 | 19/45 (42%) | 10/28 (36%) $p_3$ = 0.01 |
| 3 | Squamous cell carcinoma | 6/17 (35%) | 26/45 (58%) | 18/28 (64%) |
| 4 | Degree of tumor differentiation in adenocarcinoma, a.v., % | | | |
| 5 | High | 3/11 (27%) | 7/19 (37%) | 2/10 (20%) |
| 6 | Medium | 5/11 (46%) | 7/19 (37%) | 5/10 (50%) |
| 7 | Low | 3/11 (27%) | 5/19 (26%) | 3/10 (30%) |
| 8 | Structural patterns in adenocarcinoma, a.v., % | | | |
| 9 | Lepidic | 2/11 (18%) | 7/19 (37%) | 2/10 (20%) |
| 10 | Acinar | 10/11 (91%) | "4/19 (21%) pa = 0,0005 pc = 0,0005" | 9/10 (90%) |
| 11 | Papillary | 2/11 (18%) | 19/19 (100%) | 2/10 (20%) |
| 12 | Micropapillary | 3/11 (27%) | 7/19 (37%) | 1/10 (10%) |
| 13 | Solid | 6/11 (54%) | 6/19 (32%) | 5/10 (50%) |
| 14 | Solitary cells | 7/11 (64%) | 11/19 (58%) | 2/10 (20%) |
| 15 | Number of structural patterns combined in a single tumor for adenocarcinoma, Me ($Q_1 \div Q_3$) | 3.0 (2.0÷3.0) ($n$ = 11) | 3.0 (2.0÷4.0) ($n$ = 19) | 2.0 (1.0÷3.0) ($n$ = 10) |
| 16 | Overall representation of stromal component in adenocarcinoma, points, Me ($Q_1 \div Q_3$) | 1.0 (1.0÷2.0) ($n$ = 11) | 1.0 (1.0÷2.0) ($n$ = 19) | 2.0 (1.0÷2.0) ($n$ = 10) |
| 17 | Overall degree of inflammatory stromal infiltration in adenocarcinoma, %, Me ($Q_1 \div Q_3$) | 20.0 (10.0÷90.0) ($n$ = 11) | 20.0 (10.0÷60.0) ($n$ = 19) | 15.0 (10.0÷60.0) ($n$ = 10) |
| 18 | Degree of tumor differentiation in squamous cell carcinoma, a.v., % | | | |
| 19 | High | 0/6 (0%) | 2/26 (8%) | 0/18 (0%) |
| 20 | Medium | 4/6 (67%) | 17/26 (65%) | 12/18 (67%) |
| 21 | Low | 2/6 (33%) | 7/26 (27%) | 6/18 (33%) |
| | Structural patterns in squamous cell carcinoma, a.v., % | | | |
| 22 | Type I (keratinized) | 0/6 (0%) | 6/26 (23%) | 2/18 (11%) |
| 23 | Type II (spinous) | 4/6 (67%) | 18/26 (69%) | 17/18 (94%) $p_a$ = 0.04 $p_b$ = 0.02 |
| 24 | Type III (basaloid) | 3/6 (50%) | 13/26 (50%) $p_c$ = 0.025 | 4/18 (22%) |
| 25 | Type IV (polymorphous) | 2/6 (33%) | 14/26 (54%) | 11/18 (61%) |
| 26 | Solitary cells | 3/6 (50%) | 17/26 (65%) | 9/18 (50%) |
| 27 | Number of structural patterns combined in a single tumor for squamous cell carcinoma, Me ($Q_1 \div Q_3$) | 2.0 (1.0÷3.0) ($n$ = 6) | 3.0 (1.0÷4.0) ($n$ = 26) | 2.5 (1.0÷3.0) ($n$ = 18) |
| 28 | Overall representation of stromal component in squamous cell carcinoma, points, Me ($Q_1 \div Q_3$) | 1.5 (1.0÷2.0) ($n$ = 6) | 2.0 (1.0÷2.0) ($n$ = 26) | 1.0 (1.0÷2.0) ($n$ = 18) |
| 29 | Overall degree of inflammatory stromal infiltration for squamous cell carcinoma, %, Me ($Q_1 \div Q_3$) | 40.0 (20.0÷70.0) ($n$ = 6) | 20.0 (10.0÷70.0) ($n$ = 26) | 20,0 (5.0÷70.0) ($n$ = 18) |

**Note:** $p_3$ measures the consistency of equal probability hypothesis for squamous cell carcinoma (row 3) and adenocarcinoma (row 2) in a given group; $p_a$ measures the consistency of differences in a given parameter with group a (BCH–SM–); $p_b$ measures the consistency of differences in a given parameter with group b (BCH+SM–); $p_c$ measures the consistency of differences in a given parameter with group c (BCH+SM+).

of the bronchial epithelium outside the tumor (BCH+SM–) facilitates not only hematogenous metastasis but also dedifferentiation of the tumor elements. The latter effect may act as an autonomous factor contributing to hematogenous metastasis. Deciphering the mechanisms of this contribution will require further research activities.

CONCLUSIONS

The study evaluates the condition of lung parenchyma in the vicinity of malignant epithelial tumors. The results confirm the association of specific morphological changes to the epithelium in small bronchi with the risks of metastasis

and recurrence, while further associating these changes with the degree of tumor differentiation. The identified trends may reflect some universal, constitutive features of stromal-parenchymal interactions that equally apply to pulmonary chronic inflammation and tumorigenesis. Detailed examination of histochemical and molecular genetic mechanisms that define and elaborate these interactions is a matter of further research.

## References

1. Kaprin AD, Starinskij VV, Petrova GV, redaktory. Sostoyanie onkologicheskoj pomoshhi naseleniyu Rossii v 2017 g. M.: MNIOI im. PA Gercena — filial FGBU «NMIC radiologii» Minzdrava Rossii, 2018. Russian.
2. Pankova OV, Perelmuter VM, Litvyakov NV, Denisov EV, Gerdt LV. Vzaimosvyaz' neoplasticheskix izmenenij s bazal'nokletochnoj giperplaziej bronxial'nogo ehpiteliya pri ploskokletochnom rake i adenokarcinome legkogo. Sibirskij onkologicheskij zhurnal. 2011; 5: 57–60. Russian.
3. Pankova OV, Perelmuter VM, Tuzikov SA, Denisov EV. Pre- i neoplasticheskie izmeneniya bronxial'nogo ehpiteliya pri ploskokletochnom rake i adenokarcinome legkogo. Byulleten' sibirskoj mediciny. 2014; 13 (3): 100–10. Russian.
4. Pankova OV, Perelmuter VM, Savenkova OV, Denisov EV, Vasilev SA, Skryabin NA, i dr. Osobennosti vospalitel'noj reakcii v slizistoj bronxa v uchastkax bazal'nokletochnoj giperplazii i ploskokletochnoj metaplazii na fone ploskokletochnogo raka legkogo. Sibirskij onkologicheskij zhurnal. 2012; 5: 28–33. Russian.
5. Pankova OV, Perelmuter VM, Savenkova OV. Xarakteristika ehkspressii markerov proliferacii i regulyacii apoptoza v zavisimosti ot xaraktera disregeneratornyx izmenenij v ehpitelii bronxov pri ploskokletochnom rake legkogo. Sibirskij onkologicheskij zhurnal. 2010; 5: 36–41. Russian.
6. Kerr KM. Preneoplastic and Preinvasive Lesions.Diagnostic Pulmonary Pathology. In: Cagle PT, Allen TC, Beasley MB editors. 2008; 519–26.
7. Kerr KM, Popper HH. Pre-invasive lung lesions. Europen Respiratory Monograph. 2007; 12 (39): 37–63.
8. Dacic S. Pulmonary Preneoplasia. Archives of pathology & laboratory medicine. 2008; 132 (7): 1073–8.
9. Greenberg A, Yee H, Rom W. Preneoplastic lesions of the lung. Respiratory research. 2002; 3 (1): 1–10.
10. Lantuejoul S, Salameire D, Salon C, Brambilla E. Pulmonary preneoplasia — sequential molecular carcinogenetic events. Histopathology. 2009; 54 (1): 43–54.
11. Denisov EV, Schegoleva AA, Gervas PA, Ponomaryova AA, Tashireva LA, Boyarko VV, et al. Premalignant lesions of squamous cell carcinoma of the lung: The molecular make-up and factors affecting their progression. Lung Cancer. 2019; 135: 21–28.
12. Pankova OV, Denisov EV, Ponomaryova AA, Gerashchenko TS, Tuzikov SA, Perelmuter, VM. Recurrence of squamous cell lung carcinoma is associated with the co-presence of reactive lesions in tumor-adjacent bronchial epithelium. Tumor Biology. 2016; 37 (3): 3599–607.
13. Pankova OV, Tashireva LA, Rodionov EO, Miller SV, Tuzikov SA, Pismenny DS, et al. Premalignant changes in the bronchial epithelium are prognostic factors of distant metastasis in non-small cell lung cancer patients. Frontiers in Oncology. 2021; 11: 771802. DOI: 10.3389/fonc.2021.771802.
14. Pankova OV, Rodionov EO, Miller SV, Tuzikov SA, Tashireva LA, Gerashchenko TS, et al. Neoadjuvant chemotherapy combined with intraoperative radiotherapy is effective to prevent recurrence in high-risk non-small cell lung cancer (NSCLC) patients. Translational Lung Cancer Research. 2020; 9 (4): 988–99. DOI: 10.21037/tlcr-19-719.
15. Hortobagyi GN, Connolly JL, D'Orsi CJ, Edge SB, Mittendorf EA, Rugo HS. The AJCC Cancer staging manual. Eight Edition: Springer Nature. 2017.
16. Travis WD, Brambilla E, Burke AP, Marx A, Nicholson AG. WHO classification of tumours of the lung, pleura, thymus and heart. International Agency for Research on Cancer. Journal of Thoracic Oncology. 2015; 10 (9): 1243–60.
17. Savenkova OV, Zavyalova MV, Bychkov VA, Choinzonov EL, Perelmuter VM. Svyaz' ehkspressii matriksnyx metalloproteinaz s morfologicheskoj geterogennost'yu, differencirovkoj opuxoli i limfogennym metastazirovaniem ploskokletochnoj karcinomy gortani. Sibirskij onkologicheskij zhurnal. 2015; 1: 51–58. Russian.
18. Salgado R, Denkert C, Demaria S, Sirtaine N, Klauschen F, Pruneri G, et al. The evaluation of tumor-infiltrating lymphocytes (TILs) in breast cancer: recommendations by an International TILs Working Group 2014. Annals of oncology. 2015; 26 (2): 259–71.

## Литература

1. Каприн А. Д., Старинский В. В., Петрова Г. В., редакторы. Состояние онкологической помощи населению России в 2017 г. М.: МНИОИ им. П. А. Герцена — филиал ФГБУ «НМИЦ радиологии» Минздрава России, 2018.
2. Панкова О. В., Перельмутер В. М., Литвяков Н. В., Денисов Е. В., Гердт Л. В. Взаимосвязь неопластических изменений с базальноклеточной гиперплазией бронхиального эпителия при плоскоклеточном раке и аденокарциноме легкого. Сибирский онкологический журнал. 2011; 5: 57–60.
3. Панкова О. В., Перельмутер В. М., Тузиков С. А., Денисов Е. В. Пре- и неопластические изменения бронхиального эпителия при плоскоклеточном раке и аденокарциноме легкого. Бюллетень сибирской медицины. 2014; 13 (3): 100–10.
4. Панкова О. В., Перельмутер В. М., Савенкова О. В., Денисов Е. В., Васильев С. А., Скрябин Н. А., и др. Особенности воспалительной реакции в слизистой бронха в участках базальноклеточной гиперплазии и плоскоклеточной метаплазии на фоне плоскоклеточного рака легкого. Сибирский онкологический журнал. 2012; 5: 28–33.
5. Панкова О. В., Перельмутер В. М., Савенкова О. В. Характеристика экспрессии маркеров пролиферации и регуляции апоптоза в зависимости от характера дисрегенераторных изменений в эпителии бронхов при плоскоклеточном раке легкого. Сибирский онкологический журнал. 2010; 5: 36–41.
6. Kerr KM. Preneoplastic and Preinvasive Lesions.Diagnostic Pulmonary Pathology. In: Cagle PT, Allen TC, Beasley MB editors. 2008; 519–26.
7. Kerr KM, Popper HH. Pre-invasive lung lesions. Europen Respiratory Monograph. 2007; 12 (39): 37–63.
8. Dacic S. Pulmonary Preneoplasia. Archives of pathology & laboratory medicine. 2008; 132 (7): 1073–8.
9. Greenberg A, Yee H, Rom W. Preneoplastic lesions of the lung. Respiratory research. 2002; 3 (1): 1–10.
10. Lantuejoul S, Salameire D, Salon C, Brambilla E. Pulmonary preneoplasia — sequential molecular carcinogenetic events. Histopathology. 2009; 54 (1): 43–54.
11. Denisov EV, Schegoleva AA, Gervas PA, Ponomaryova AA, Tashireva LA, Boyarko VV, et al. Premalignant lesions of squamous cell carcinoma of the lung: The molecular make-up and factors affecting their progression. Lung Cancer. 2019; 135: 21–28.
12. Pankova OV, Denisov EV, Ponomaryova AA, Gerashchenko TS, Tuzikov SA, Perelmuter, VM. Recurrence of squamous cell lung carcinoma is associated with the co-presence of reactive lesions

in tumor-adjacent bronchial epithelium. Tumor Biology. 2016; 37 (3): 3599–607.

13. Pankova OV, Tashireva LA, Rodionov EO, Miller SV, Tuzikov SA, Pismenny DS, et al. Premalignant changes in the bronchial epithelium are prognostic factors of distant metastasis in non-small cell lung cancer patients. Frontiers in Oncology. 2021; 11: 771802. DOI: 10.3389/fonc.2021.771802.

14. Pankova OV, Rodionov EO, Miller SV, Tuzikov SA, Tashireva LA, Gerashchenko TS, et al. Neoadjuvant chemotherapy combined with intraoperative radiotherapy is effective to prevent recurrence in high-risk non-small cell lung cancer (NSCLC) patients. Translational Lung Cancer Research. 2020; 9 (4): 988–99. DOI: 10.21037/tlcr-19-719.

15. Hortobagyi GN, Connolly JL, D'Orsi CJ, Edge SB, Mittendorf EA, Rugo HS. The AJCC Cancer staging manual. Eight Edition: Springer Nature. 2017.

16. Travis WD, Brambilla E, Burke AP, Marx A, Nicholson AG. WHO classification of tumours of the lung, pleura, thymus and heart. International Agency for Research on Cancer. Journal of Thoracic Oncology. 2015; 10 (9): 1243–60.

17. Савенкова О. В., Завьялова М. В., Бычков В. А., Чойнзонов Е. Л., Перельмутер В. М. Связь экспрессии матриксных металлопротеиназ с морфологической гетерогенностью, дифференцировкой опухоли и лимфогенным метастазированием плоскоклеточной карциномы гортани. Сибирский онкологический журнал. 2015; 1: 51–58.

18. Salgado R, Denkert C, Demaria S, Sirtaine N, Klauschen F, Pruneri G, et al. The evaluation of tumor-infiltrating lymphocytes (TILs) in breast cancer: recommendations by an International TILs Working Group 2014. Annals of oncology. 2015; 26 (2): 259–71.

# STUDY OF THE HUMAN BRAIN POTENTIALS VARIABILITY EFFECTS IN P300 BASED BRAIN–COMPUTER INTERFACE

Ganin IP ✉, Kaplan AYa

Lomonosov Moscow State University, Moscow, Russia

The P300-based brain–computer interfaces (P300 BCI) allow the user to select commands by focusing on them. The technology involves electroencephalographic (EEG) representation of the event-related potentials (ERP) that arise in response to repetitive external stimulation. Conventional procedures for ERP extraction and analysis imply that identical stimuli produce identical responses. However, the floating onset of EEG reactions is a known neurophysiological phenomenon. A failure to account for this source of variability may considerably skew the output and undermine the overall accuracy of the interface. This study aimed to analyze the effects of ERP variability in EEG reactions in order to minimize their influence on P300 BCI command classification accuracy. Healthy subjects aged 21–22 years ($n$ = 12) were presented with a modified P300 BCI matrix moving with specified parameters within the working area. The results strongly support the inherent significance of ERP variability in P300 BCI environments. The correction of peak latencies in single EEG reactions provided a 1.5–2 fold increase in ERP amplitude with a concomitant enhancement of classification accuracy (from 71–78% to 92–95%, $p < 0.0005$). These effects were particularly pronounced in attention-demanding tasks with the highest matrix velocities. The findings underscore the importance of accounting for ERP variability in advanced BCI systems.

✉ Correspondence should be addressed: Ilya P. Ganin
Leninskie Gory, 1, str. 12, k. 246, Moscow, 119234, Russia; ipganin@mail.ru

# ИЗУЧЕНИЕ ЭФФЕКТОВ ВАРИАТИВНОСТИ ПОТЕНЦИАЛОВ МОЗГА ЧЕЛОВЕКА В ИНТЕРФЕЙСЕ МОЗГ–КОМПЬЮТЕР НА ВОЛНЕ Р300

И. П. Ганин ✉, А. Я. Каплан

Московский государственный университет имени М. В. Ломоносова, Москва, Россия

Технология интерфейс мозг–компьютер на волне Р300 (ИМК-Р300) позволяет пользователю выбирать команды при фокусировании на них внимания. Это возможно за счет регистрации в ЭЭГ потенциалов, связанных с событиями (ПСС), возникающих в ответ на многократно повторяемые внешние стимулы. Традиционно при выделении и анализе ПСС полагают, что реакции на отдельные стимулы идентичны, хотя в нейрофизиологии известен феномен вариативности во времени возникновения таких реакций. Поэтому есть предпосылки считать, что непринятие во внимание вариативности ПСС в ряде случаев может снижать наблюдаемые в эксперименте эффекты, а также точность работы ИМК. Целью работы было изучить эффекты вариативности ЭЭГ-реакций внимания пользователя к стимульным командам в ИМК-Р300 и выявить возможности учета этих эффектов при классификации команд в интерфейсе. Здоровым испытуемым 21–22 лет ($n$ = 12) необходимо было реагировать на целевые стимулы в модифицированной нами стимульной матрице ИМК-Р300, которая могла двигаться с различными параметрами в пределах рабочего поля. В исследовании показано, что эффект вариативности ПСС присутствует в технологии ИМК-Р300, а использованный метод коррекции латентности пиков в единичных реакциях привел к увеличению амплитуды компонентов ПСС в 1,5–2 раза, а также повышению точности классификации с 71–78% до 92–95% ($p$ < 0,0005). Вариативность и повышение классификации после коррекции латентности были выше в более требовательном по ресурсам внимания режиме с наибольшей скоростью движения стимульной матрицы. В целом результаты показывают важность учета вариативности компонентов ПСС в ИМК-Р300 для создания более эффективных систем нейроуправления.

✉ Для корреспонденции: Илья Петрович Ганин
Ленинские горы, д. 1, стр. 12, к. 246, Москва, 119234, Россия; ipganin@mail.ru

The brain–computer interfaces (BCI) enable the use of executive devices without mediation of peripheral nerves and muscles. The technology involves recording and transformation of the electrical activity of the brain, most commonly by means of electroencephalography (EEG) [1]. The conventional scope of applications for BCI includes neurorehabilitation and replacement of speech and locomotion output in patients with severe motor impairments [2]. Other applications of BCI include their use as accessory means of instrumental diagnostics, e.g. in autism [3] or anorexia nervosa [4], as well as in cognitive training devices [5].

BCI systems based on exposure to external stimuli and detection of event-related potentials (ERP) by EEG are considered the most efficient in terms of communication and control [6]. A pioneering interface for text typing termed P300 BCI was firstly published in 1988 [7]. The user is presented with a letter matrix and receives the stimuli in the form of sequential highlighting of the letters. The mental response to the highlighting of target letters is accompanied by enhancement of certain ERP components, notably the P300 wave. Based on ERP analysis, the interface identifies the letter on which the user's attention is focused at the moment (target stimulus) [8].

The general classification principle in BCI (subdivision of EEG reactions into target and non-target classes) is based on the fundamental technique of ERP extraction and analysis. The technique employs the accumulation of epochs corresponding to identical repetitive stimuli as a substrate for ERP extraction. The averaging of these 'identical' epochs reveals a coherent ERP signal against the background noise which is incoherent to the moment of stimulation [6].

The variability of latency of individual EEG reactions from the moment of stimulation is a well-known neurophysiological phenomenon [9]. A failure to account for this source of variance can substantially distort the output of individual ERP components [10]. This effect involves both early and late components of EEG reactions [11, 12], with the averaged P300 wave being particularly vulnerable [13]. As a consequence, the amplitude of the component decreases and the width increases [14]. Beyond its fundamental interest, the temporal variability of ERP should be regarded as a major hindrance for P300 BCI classification accuracy.

The latency of ERP components, notably P300, is known to correlate with the age, cognitive status of the subject and other parameters [15, 16]. Deviations in characteristics of isolated responses to external stimuli can be observed in the divided attention tasks; the variability positively correlates with the complexity of the second task (i.e. its competitiveness for perception resources) [16]. The process of achieving a final goal with BCI (text typing) and execution of immediate instructions (reacting to stimuli) may be competing tasks themselves. In addition, the practical use of BCI technology in real-world settings is usually accompanied by collateral tasks and events that promote continuous variations in attention and perception [17]. It should be noted that additional source of multidirectional destabilization of ERP characteristics, including variability, involves the stimulation parameters per se: in BCI, the presentation rate is usually high, up to 4–5 stimuli per second [8], whereas the majority of standard protocols for ERP acquisition use presentation of one stimulus in 1–2 seconds [18].

From a neurophysiological perspective, variations in the brain output are rooted in the hierarchical complexity of the nervous system organization, so that these variations are generally considered inherent for the brain [19]. However, the elevated overall levels of such variation have been associated with certain pathologies. The abnormally high levels of neuronal noise and plasticity may interfere with the integrity of external stimuli processing and production of adequate behavioral responses, e.g. in autism [19, 20]. The increased variability of ERP was also demonstrated in patients with attention deficit hyperactivity disorder, especially under conditions of cognitive challenge [19, 21].

The cognitive fatigue of the user, a major cause of variability in EEG reactions [22], may negatively affect the neurocontrol efficacy in healthy users and even more so in patients. People with locomotion and speech impairments often have reduced attention capacities possibly accompanied by cognitive deficits. Such users tend to quickly get tired and may experience difficulties upon sustaining the control in BCI [23, 24].

Therefore, the effects of ERP variability in P300 BCI should be given immense consideration. On the one hand, proper understanding of the variability patterns will allow enhancement and optimization of the stimulus environment in terms of efficiency; on the other hand, it will mitigate the undesirable effects of variability to facilitate mastering of this technology by healthy users and notably by patients with neurocognitive impairments. This study aimed to analyze the effects of ERP variability in EEG reactions in order to minimize their influence on P300 BCI command classification accuracy.

METHODS

The study used EEG data obtained earlier in a modified version of P300 BCI with a stimulus matrix moving freely within the visual field. The details of this modification and some results obtained with its use were described by us previously [25]. The current study deals with identification and evaluation of ERP variability effects possibly encountered by users of such interfaces.

The recording was carried out at the Faculty of Biology, Lomonosov Moscow State University, and enrolled 12 participants (four men and eight women) aged 21–22 years. Inclusion criteria: healthy volunteers of both sexes, aged 18–35 years. Exclusion criteria: diagnosed neurological and/or mental conditions, a history of convulsive seizures episodes or diagnosed status epilepticus. The study initially intended to test the feasibility of ERP-based monitoring of the subject's attention to continuously moving target stimuli [25].

The participants (subjects) were presented with a $3 \times 3$ icon matrix, angular dimensions $7.4° \times 7.4°$, single stimulus size $2.2° \times 2.2°$. The stimulation was performed by highlighting (125 ms in every 500 ms) of the rows and columns of the matrix in random order.

The subjects were tasked with focusing their attention on a target stimulus within the matrix, carefully follow this stimulus, and mentally count the number of highlights encompassing this stimulus.

The study used various modes and velocities of matrix motion within the screen limits. The matrix moved at a constant speed in a straight direction inverted upon reaching the edge of the screen. A total of six modes were used in the study:
– 'static matrix' (motionless, positioned at the center of the screen);
– 'horizontal movement' (at 5°/s);
– 'vertical movement' (at 5°/s);
– 'random movement' (at 5°/s, the direction could change at random moments of time);
– 'velocity 10°/s' (horizontal movement);
– 'velocity 20°/s' (horizontal movement).

Each participant was exposed to all modes succeeding in random order. Each mode encompassed presentations of 120 target and 240 non-target stimuli.

The EEG recordings were carried out with six scalp electrodes (Cz, Pz, PO7, PO8, O1 and O2) and a common reference electrode attached to ear lobule, using an NVX 24 electroencephalograph (Medical Computer Systems; Zelenograd, Russia) at 250 Hz discretization frequency. We used the CONAN-NVX software for the recording and original software written in Python 2.6 for the stimuli presentation. Synchronization of EEG recording with the highlightings involved a photodiode sensor. Simultaneously with the
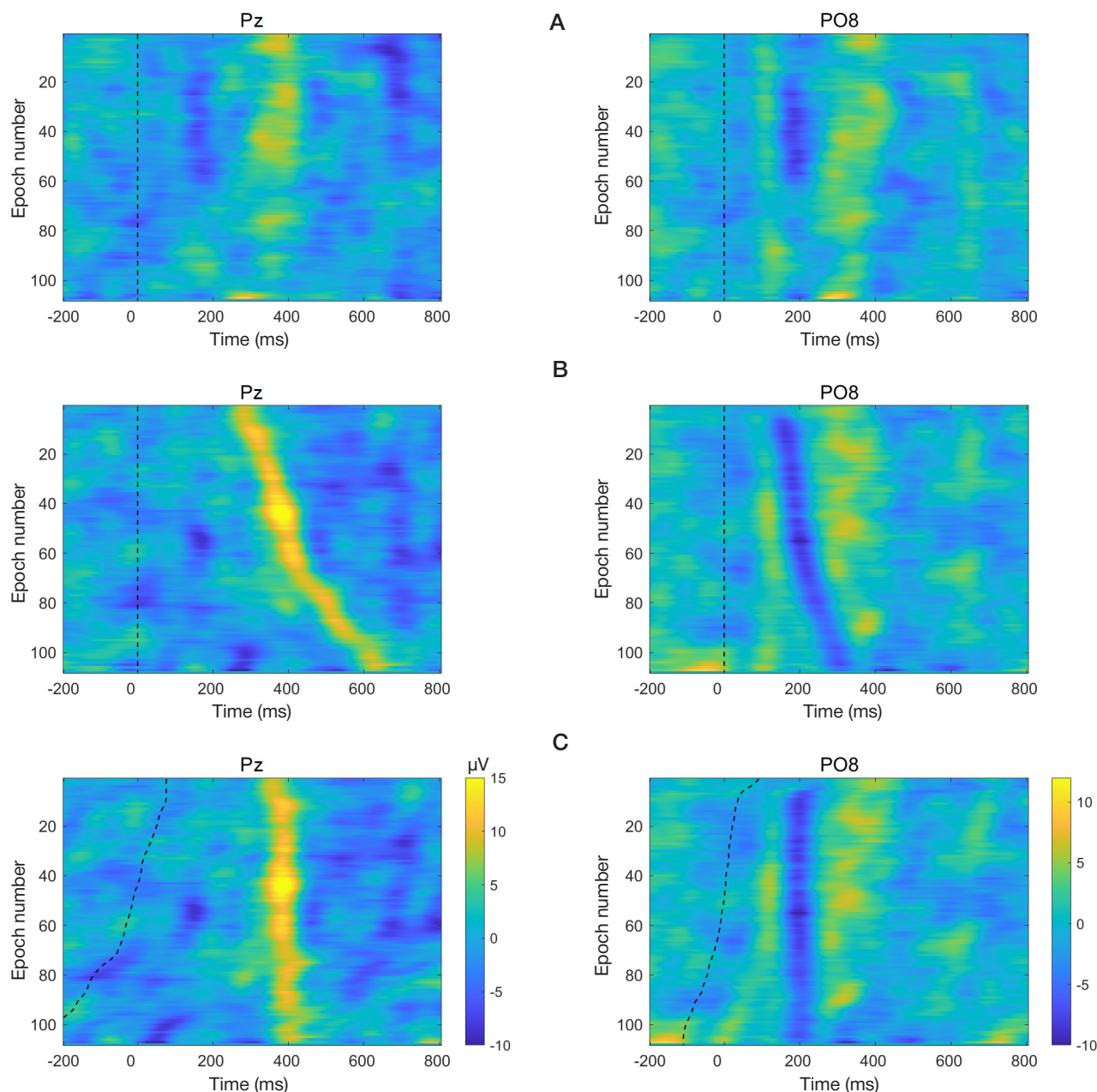
**Fig. 1.** Color maps of single target EEG epochs for subject #1, 'static matrix' mode, leads Pz and PO8. Horizontal axis represents time, ms; vertical axis represents individual epochs numbered and sorted by the number from top to bottom, with the moving average-based vertical smoothing applied in series of 10. **A.** The epochs are sorted in chronological order (as recorded). **B.** The epochs are sorted by peak latency for P300 (Pz) or N1 (PO8). In charts **A** and **B** the epochs are synchronized by the moment of stimulus presentation (vertical *dashed lines*). **C.** Peak latency-corrected epochs with *dashed lines* indicating the moment of stimulus presentation

appearance of the target/non-target stimulus, a small white/black square appeared in the upper right corner of the screen exactly beneath the sensor. The signal from the sensor was recorded along with the EEG data in a separate channel, and the change in brightness beneath the sensor made it possible to accurately determine the actual moments of presentation.

The signal processing including ERP extraction and analysis was carried out in MATLAB 9.11 (R2021b) (MathWorks; USA). The EEG signal was band-pass filtered within 0.5–20 Hz range (0.5–10 Hz for working with single epochs and calculating classification) using a fourth-order Butterworth filter and split into epochs from –400 to 1200 ms time-locked to the stimulus onset. The artifact epochs containing +/– 50 μV excess of signal amplitude in any of the channels were excluded. The percentage of excluded epochs was usually within 10%.

The epochs were classified into target and non-target and averaged within each class, subject and mode. The procedure

yielded target and non-target ERP in a reduced –200 to 800 ms window. The amplitude of P300 was determined as the maximum signal value in Pz lead within a 300–600 ms window. The amplitude of N1 component was determined as the minimum signal value in PO7, PO8, O1 and O2 leads within a 100–300 ms window. Peak latencies were measured from the stimulus onset.

To analyze the component variability, P300 and N1 peak latencies were calculated similarly in the same channels and windows, albeit using single, non-averaged epochs. The epochs within each lead, mode and subject were sorted (ordered) based on these latencies. To analyze the variability of latencies, the median absolute deviation (MAD) value was calculated within each mode for each subject individually. To analyze the effect of component variability on calculated ERP, all epochs were centered on the peak time prior to averaging: each epoch was shifted by the subtracted difference between
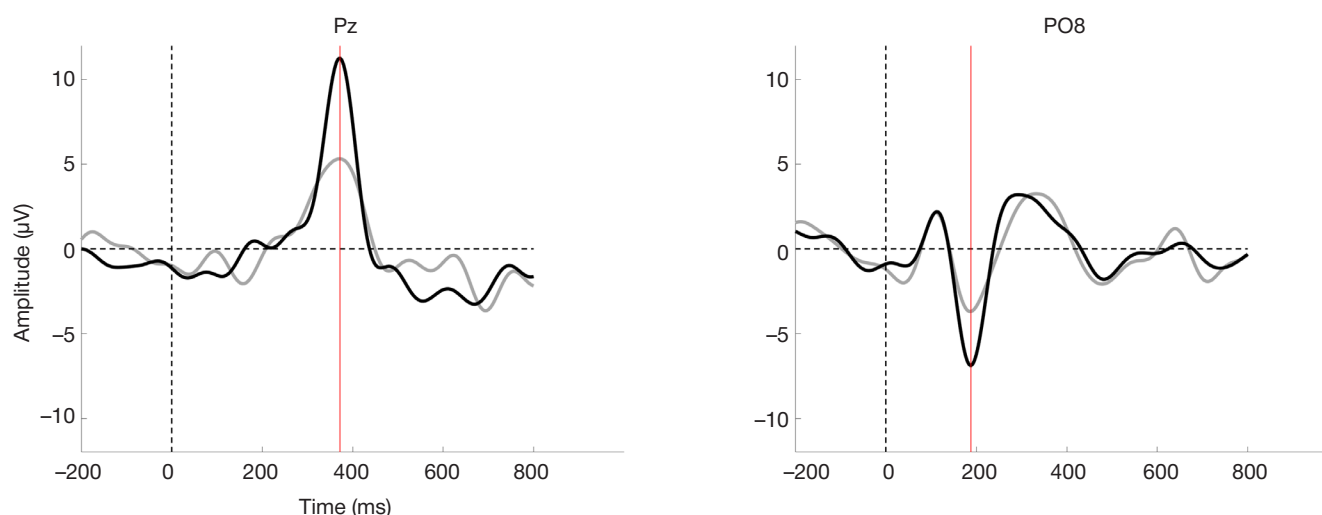
**Fig. 2.** An example of averaged target ERP (subject #1) acquired in the 'static matrix' mode. *Gray curves* correspond to standard method of ERP averaging (no latency correction applied), *black curves* correspond to the use of peak latency-corrected epochs for P300 (Pz) and N1 (PO8). Vertical *dashed lines* (0 ms) indicate the moment of stimulus presentation; *red lines* indicate the latency of particular component in a given lead

the latency in the averaged ERP and its own specific latency, forward or backward along the time axis, after which the epochs were averaged conventionally in a −200 to 800 ms window. In Cz and Pz leads the epochs were corrected by P300 and in occipital leads the epochs were corrected by N1. The peak amplitudes were subsequently calculated for the averaged corrected ERP. For the group analysis of N1 amplitudes, the values were calculated using the curves averaged over four occipital leads (PO7, PO8, O1 and O2).

To assess the variability of the ERP components subject-wise, the amplitudes were calculated for individual EEG epochs (raw and latency-corrected); in each epoch, the average signal value was calculated in a 52 ms window centered on the peak latency for a particular lead and mode.

To identify the effects of ERP variability on the command classification accuracy in P300 BCI, offline classification scores were calculated for all subjects in each mode, separately for the initial averaged ERP and for the latency-corrected epochs. The feature vectors for the linear Fisher discriminant analysis in each mode were built based on signal amplitudes in all EEG channels, spanning 600 ms post-stimulation (one point per 50 ms). The classification accuracy was assessed by cross-validation (leave-one-out) with sequential testing of each epoch with a classifier trained on all other epochs of the same mode. The procedure was repeated for all epochs, and the classification accuracy was assessed as the percentage of

correctly identified epochs (two classes: target and non-target). To correctly calculate the accuracy before classification, the quantities of target and non-target epochs were equalized by randomly deleting a subset of non-target epochs. To exclude sampling-related variations, this classification process was repeated 100 times with random elimination of non-target epochs and the accuracy values obtained over 100 iterations were averaged.

All quantitative data (amplitudes, latencies and classification accuracy values) were analyzed using STATISTICA 7.0 package. One- or two-way analysis of variance (ANOVA) was used for group analysis. The Tukey's or Benjamini–Hochberg's post-hoc tests were applied in cases of significant main effects in pairwise comparisons. The analysis of component amplitudes within subjects involved the normality check by $\chi^2$ (Chi-square) test followed by paired Student's t-test.

## RESULTS

To visualize the accumulations of single EEG epochs (before ERP averaging), the time was plotted horizontally, the epochs were plotted vertically one by one and the amplitude values were color-coded [11]. This method allows representation of different grouping options for individual epochs and accentuates the effects of their variability. Fig. 1 shows an example of such representation of target epochs for a single
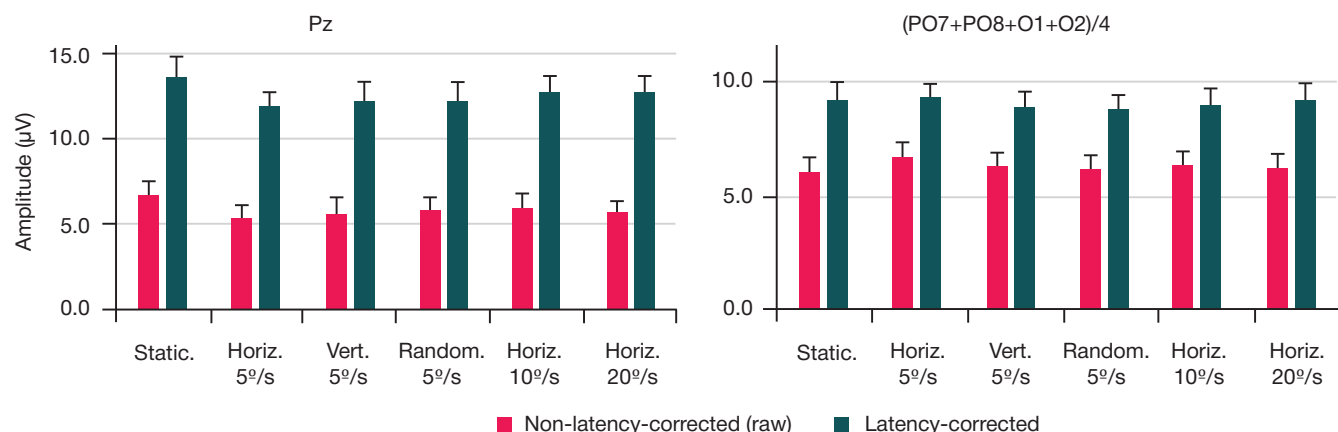


**Fig. 3.** The amplitudes of P300 and N1 components (by modulus) for different modes, calculated by the standard method (no latency correction applied) as opposed to the use of peak latency-corrected epochs for P300 (Pz, *right* chart) and N1 (*left* chart). Heights and error bars correspond to means and standard errors of the mean, respectively (*n* = 12)
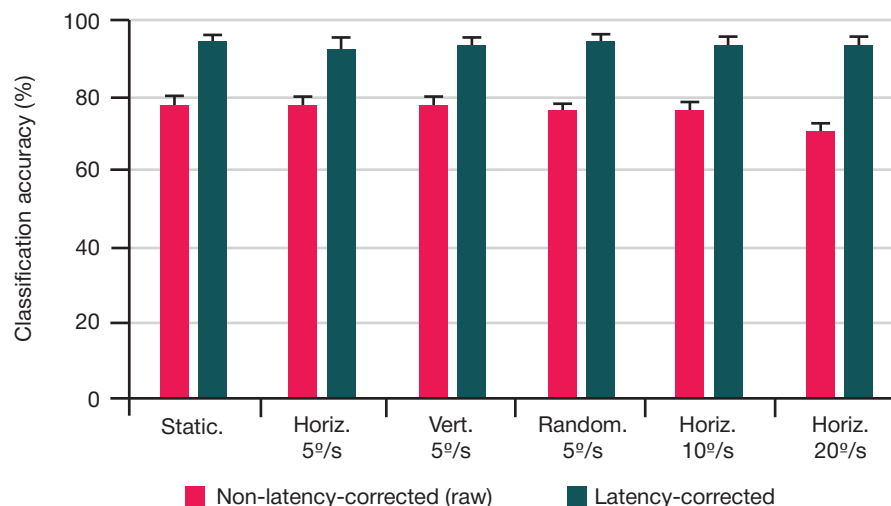
**Fig. 4.** The offline classification accuracy for different modes, calculated by the standard method (no latency correction applied) as opposed to the use of peak latency-corrected epochs for P300 and N1. Heights and error bars correspond to means and standard errors of the mean, respectively ($n = 12$)

participant, acquired in Pz and PO8 using the 'static matrix' mode. In Fig. 1A, arrangement of the epochs from top to bottom corresponds to their actual chronological order. In Fig. 1B, the epochs are sorted by latency so that epochs with earlier peaks of P300 (in Pz) or N1 (in PO8) are located at the top. Fig. 1C shows the latency-corrected epochs, i.e. adjusted with the use of averaged latency value for particular mode and channel. For better clarity, we applied vertical smoothing by the 'moving average' in 10 epoch series.

Fig. 2 shows ERP obtained by averaging of raw and latency-corrected epochs for the same participant (subject). The latency-corrected amplitudes of both components significantly exceeded the initial values obtained by raw averaging without correction for the peak latency. These differences were significant for all subjects in all modes ($p < 0.001$, paired Student's $t$-test).

We further analyzed the influence of latency correction procedure on the calculated amplitudes of P300 and N1 components at the group level; the results are presented in Fig. 3. The amplitudes of P300 and N1 obtained with the latency-corrected epochs were significantly higher compared to those calculated by conventional method. Two-way ANOVA ('latency correction' factor — two levels, 'motion type' factor — four levels including the 'static matrix' mode) revealed significant effect of latency correction on the amplitudes of P300: $F(1,11) = 95.7$ and $\lambda = 0.10$ at $p = 0.000001$, and N1: $F(1,11) = 58.1$ and $\lambda = 0.16$ at $p = 0.00001$. The 'motion type' factor had significant effect on P300: $F(3,9) = 7.5$, $\lambda = 0.29$ at $p = 0.008$ (a lower amplitude for horizontal movement), but not N1.

The analysis of 'latency correction' and 'velocity' factors (comprising, respectively, two and three levels) revealed significant influence of the 'latency correction' factor on the amplitudes of P300: $F(1,11) = 88.5$ and $\lambda = 0.11$ at $p = 0.000001$, and N1: $F(1,11) = 46.6$ and $\lambda = 0.19$ at $p = 0.00003$, despite the lack of significant influence from 'velocity', and significant interaction between the two factors for N1 component: $F(2,10) = 10.4$ and $\lambda = 0.32$ at $p = 0.0036$ (a tendency towards lower amplitude at the highest velocity identified with the use of conventional averaging of the epochs).

The group analysis of ERP variability using MAD indicator of the peak latency revealed certain statistically significant effects. The movement velocity factor (three levels) significantly affected N1 component in PO8, O1 and O2 leads: $F(2,22) = 4.4$ at $p = 0.024$, $F(2,22) = 3.8$ at $p = 0.037$ and $F(2,22) = 4.9$ at $p = 0.017$, respectively. Post-hoc analysis revealed a higher

variability (expressed through MAD) upon using the highest velocity mode compared to slower movement. The effects observed in O1 and O2 leads were significant ($p < 0.05$), whereas in PO8 the differences amounted to a trend ($p < 0.1$). The analysis revealed no significant effects of the 'motion type' factor on N1 component and the 'motion type' and 'velocity' factors on P300 component.

Fig. 4 compares the offline classification accuracy for the standard ERP extraction algorithm as compared to the use of P300 and N1 peak latency-corrected data. Two-way ANOVA ('latency correction' factor — two levels, 'motion type' factor — four levels) revealed significant effect of the latency correction procedure on classification accuracy: $F(1,11) = 102.7$ and $\lambda = 0.09$ at $p = 0.00001$. Post-hoc analysis revealed higher classification accuracies when using latency-corrected epochs in all four modes (94.7, 92.2, 93.2 and 94.8%) compared with the conventional ERP extraction procedure (respectively, 78.3, 78.1, 78.3 and 76.1%; $p < 0.0001$ for all modes). Two-way ANOVA ('latency correction' factor — two levels, 'velocity' factor — three levels) revealed significant effects of both the calculation method and the matrix movement velocity: $F(1,11) = 110.0$ and $\lambda = 0.09$ at $p = 0.00000$; $F(2,10) = 6.0$ and $\lambda = 0.46$ at $p = 0.0196$, as well as significant interaction between these factors: $F(2,10) = 11.5$ and $\lambda = 0.30$ at $p = 0.0026$. Post-hoc analysis revealed higher classification accuracy when using latency-corrected epochs in all three modes (92.2, 93.7 and 94.0%) compared with the conventional ERP extraction procedure (respectively, 78.1, 76.7 and 71.2%; $p < 0.0005$ for all modes). Of note, in the highest velocity mode, the accuracy was significantly lower than in two other modes (71.2% vs 78.1 and 76.7%; $p < 0.05$) unless the latency correction was applied.

DISCUSSION

Overall, the obtained results confirm that ERP variability is inherent to P300 BCI and should be considered as a major influence on the shapes of ERP components; the exact impact depends on the degree of attention involvement. Correction of such variability at the level of single EEG reactions can substantially improve the command interpretation accuracy.

Despite the fact that ERP approach relies on the averaging of multiple EEG reactions to a stimulus, at certain signal processing parameters the detection of individual reaction peaks is quite feasible. This statement is illustrated well by our data (Fig. 1) along with other studies [9, 10, 12]. Importantly,

the analysis of single epochs allows correction for the variable peak latency in individual realizations of the response to ultimately afford a better extraction quality and enhanced amplitude for the components of interest (Fig. 2). Despite the well-established phenomenon of variable latency, prediction of its specific impact in P300 BCI is nontrivial, as the conventional BCI stimulation rates are considerably higher compared with those typically used in psychophysiological studies. One one hand, this difference can mitigate the variability and stabilize the temporal heterogeneity of the reactions; on the other hand, it might also augment the heterogeneity and complicate correct interpretation of the stimulus at higher rates of presentation, as the suboptimal conditions for the attention/concentration activity may promote a concomitant increase in ERP variability [20]. The variable latency has been attributed to the inherent variance of time required for perception and categorization of the stimulus in every single presentation event [26]. We show that accounting for the variability effects allows significant enhancement of the amplitude for components that represent attention to target stimuli at both individual and group levels (Figs. 2 and 3).

Despite the lack of significant effects of different matrix motion modes on the amplitudes, MAD index showed increased variability of N1 component at higher velocities of the matrix. The decrease in visual acuity upon increase in the speed of tracked objects [27] has been associated with a concomitant increase in attention costs. Given the profound association of ERP components with specific features of oculomotor functionality [28], the observed increase in N1 component variability at higher velocities can be explained by the inherent attention variance combined to the pressing demand for tracking the matrix cells. The observation is also consistent with the decreased amplitude of N1 component in the difference (target — non-target) waveforms reported by us previously [25]. Noteworthy, the effect is characteristic of this earlier component, sensitive to target events at the eye fixation point [29], but not of the later P300 component.

Apart from its fundamental relevance, the developed correction procedure is of clear applied interest. The accounting for the latency factor in ERP components significantly rescued the accuracy of target stimuli classification in the modified P300 BCI environment used by us in this study (Fig. 4). The temporal variability of ERP has been already featured as a putative cause of poor individual performance in BCI [17]. However, the authors suggested to improve the accuracy by using the amplitude values of the classifier output instead of the raw peaks in EEG epochs, which may seem less consistent and efficient, as the classifier output is more prone to external influences (noise, etc.). Another study has indeed succeeded in increasing the accuracy of P300 BCI output by means of latency correction for P300, albeit in a narrow window; overall, the method provided no classification benefits compared with the conventional approach [26]. Besides, the authors themselves emphasize irrelevance of their algorithm for online use, since it requires the explicit target/non-target labeling of each epoch. By contrast, our setting significantly enhances the classification accuracy through correction of the latency for both P300 and N1 components known to provide comparable contributions [30] and is equally suitable for the online mode as the correction is applied to both target and non-target epochs. It should be noted that the initial accuracy at the highest velocity was lower (71%) than in other modes (76–78%) and that introducing the latency correction rendered the accuracy ubiquitously high (92–95%) in all modes. This result underscores the utility of the developed correction approach in similar and even more attention-demanding BCI operation modes.

CONCLUSIONS

The dedicated analysis at the level of single EEG epochs enables overall correction for the variable latencies in a modified P300 BCI environment. Correction for this major source of variability refines the target ERP components with a concomitant improvement in the command classification accuracy. By using a movable stimulus matrix, we demonstrate particular relevance of the developed correction procedure under conditions of increased cognitive demand modeled by higher movement velocity. Taken together, our findings underscore the importance of accounting for ERP variability in the development of P300 BCI environments and provide the basis for creation of advanced ERP-based systems of neurocontrol, particularly those intended for people with reduced attention capacities.

### References

1. Abiri R, Borhani S, Sellers EW, Jiang Y, Zhao X. A comprehensive review of EEG-based brain-computer interface paradigms. J Neural Eng. 2019; 16 (1): 011001.
2. Yang S, Li R, Li H, Xu K, Shi Y, Wang Q, et al. Exploring the Use of Brain-Computer Interfaces in Stroke Neurorehabilitation. Biomed Res Int. 2021: 9967348.
3. Eldeeb S, Susam BT, Akcakaya M, Conner CM, White SW, Mazefsky CA. Trial by trial EEG based BCI for distress versus non distress classification in individuals with ASD. Sci Rep. 2021; 11 (1): 6000.
4. Ganin IP, Kosichenko EA, Sokolov AV, Ioannisyanc OM, Arefev IM, Basova AYa, Kaplan AYa. Adaptation of the p300-based brain-computer interface for anorexia nervosa patients state evaluation. Bulletin of RSMU. 2019; 2: 32-38.
5. Carelli L, Solca F, Faini A, Meriggi P, Sangalli D, Cipresso P, Riva G, Ticozzi N, Ciammola A, Silani V, Poletti B. Brain-Computer Interface for Clinical Purposes: Cognitive Assessment and Rehabilitation. Biomed Res Int. 2017; 2017: 1695290.
6. Luck SJ. An introduction to the event related potential technique. MIT Press, Cambridge, MA, 2014.
7. Farwell LA, Donchin E. Talking off the top of your head: toward a mental prosthesis utilizing event-related brain potentials. Electroencephalography and Clinical Neurophysiology. 1988; 70: 510–23.
8. Rezeika A, Benda M, Stawicki P, Gembler F, Saboor A, Volosyak I. Brain–Computer Interface Spellers: A Review. Brain Sciences. 2018; 8 (4): 57.
9. Zang S, Zhou C, Chao F. Estimation of Event-Related Potentials from Single-Trial EEG. UK Workshop on Computational Intelligence. Springer, Cham. 2021; 1409: 415–27.
10. Ouyang G, Hildebrandt A, Sommer W, Zhou C. Exploiting the intra-subject latency variability from single-trial event-related potentials in the P3 time range: A review and comparative evaluation of methods. Neurosci Biobehav Rev. 2017; 75: 1–21.
11. Burwell SJ, Makeig S, Iacono WG, Malone SM. Reduced premovement positivity during the stimulus-response interval precedes errors: Using single-trial and regression ERPs to understand performance deficits in ADHD. Psychophysiology. 2019; 56 (9): e13392.
12. Dowdall JR, Luczak A, Tata MS. Temporal variability of the N2pc during efficient and inefficient visual search. Neuropsychologia. 2012; 50 (10): 2442–53.

13. Kutas M, McCarthy G and Donchin E. Augmenting mental chronometry: the P300 as a measure of stimulus evaluation time. Science. 1977; 197 (4305): 792–5.

14. Zisk AH, Borgheai SB, McLinden J, Hosni SM, Deligani RJ, Shahriari Y. P300 latency jitter and its correlates in people with amyotrophic lateral sclerosis. Clinical Neurophysiology. 2021; 132 (2): 632–42.

15. Kim JS, Lee YJ, Shim SH. What Event-Related Potential Tells Us about Brain Function: Child-Adolescent Psychiatric Perspectives. Soa Chongsonyon Chongsin Uihak. 2021; 32 (3): 93–98.

16. Riggins T, Scott LS. P300 development from infancy to adolescence. Psychophysiology. 2020; 57 (7): e13346.

17. Thompson DE, Warschausky S, Huggins JE. Classifier-based latency estimation: a novel way to estimate and predict BCI accuracy. Journal of neural engineering. 2013; 10 (1): 016006.

18. Picton TW, Bentin S, Berg P, Donchin E, Hillyard SA, Johnson R, et al. Guidelines for using human event-related potentials to study cognition: recording standards and publication criteria. Psychophysiology. 2000; 37 (2): 127–52.

19. Dinstein I, Heeger DJ, Behrmann M. Neural variability: friend or foe? Trends Cogn Sci. 2015; 19 (6): 322–28.

20. Kovarski K, Malvy J, Khanna RK, Arsène S, Batty M, Latinus M. Reduced visual evoked potential amplitude in autism spectrum disorder, a variability effect? Translational Psychiatry. 2019; 9 (1): 1–9.

21. Gonen-Yaacovi G, Arazi A, Shahar N, Karmo A, Haar S, Meiran N, et al. Increased ongoing neural variability in ADHD. Cortex. 2016; 81: 50–63.

22. Zeba MZ, Friganović K, Palmović M, Išgum V, Cifrek M. Assessment of mental fatigue during examination period with P300 oddball paradigm. In 2019 42nd International Convention on Information and Communication Technology, Electronics and Microelectronics (MIPRO), IEEE. 2019: 1479–84.

23. McFarland DJ, Vaughan TM. BCI in practice. Progress in brain research. 2016; 228: 389–404.

24. Ganin IP, Kim SA, Liburkina SP, Galkina NV, Luzhin AO, Majorova LA, et al. Nabor teksta pacientami s postinsul'tnoj afaziej v komplekse «NejroChat» na osnove texnologii interfejsov mozg-komp'yuter na volne P300. Zhurn. vyssh. nerv. deyat. 2020; 70 (4): 435–45. Russian.

25. Shishkin SL, Ganin IP, Kaplan AY. Event-related potentials in a moving matrix modification of the P300 brain–computer interface paradigm. Neuroscience letters. 2011; 496 (2): 95–99.

26. Aricò P, Aloise F, Schettini F, Salinari S, Mattia D, Cincotti F. Influence of P300 latency jitter on event related potential-based brain–computer interface performance. Journal of neural engineering. 2014; 11 (3): 035008.

27. Schütz AC, Delipetkos E, Braun DI, Kerzel D, Gegenfurtner KR. Temporal contrast sensitivity during smooth pursuit eye movements. Journal of Vision. 2007; 7 (13): 3–3.

28. Zhang B, Stevenson SS, Cheng H, Laron M, Kumar G, Tong J, et al. Effects of fixation instability on multifocal VEP (mfVEP) responses in amblyopes. Journal of Vision. 2008; 8 (3): 16.

29. Aloise F, Aricò P, Schettini F, Riccio A, Salinari S, Mattia D, et al. A covert attention P300-based brain–computer interface: Geospell. Ergonomics. 2012; 55 (5): 538–51.

30. McCane LM, Sellers EW, McFarland DJ, Mak JN, Carmack CS, Zeitlin D, et al. Brain-computer interface (BCI) evaluation in people with amyotrophic lateral sclerosis. Amyotroph Lateral Scler Frontotemporal Degener. 2014; 15 (3–4): 207–15.

## Литература

1. Abiri R, Borhani S, Sellers EW, Jiang Y, Zhao X. A comprehensive review of EEG-based brain-computer interface paradigms. J Neural Eng. 2019; 16 (1): 011001.

2. Yang S, Li R, Li H, Xu K, Shi Y, Wang Q, et al. Exploring the Use of Brain-Computer Interfaces in Stroke Neurorehabilitation. Biomed Res Int. 2021: 9967348.

3. Eldeeb S, Susam BT, Akcakaya M, Conner CM, White SW, Mazefsky CA. Trial by trial EEG based BCI for distress versus non distress classification in individuals with ASD. Sci Rep. 2021; 11 (1): 6000.

4. Ганин И. П., Косиченко Е. А., Соколов А. В., Иоаннисянц О. М., Арефьев И. М., Басова А. Я., и др. Адаптация технологии интерфейсов мозг-компьютер на волне Р300 для оценивания состояния больных нервной анорексией. Вестник Российского государственного медицинского университета. 2019; 2: 36–43.

5. Carelli L, Solca F, Faini A, Meriggi P, Sangalli D, Cipresso P, Riva G, Ticozzi N, Ciammola A, Silani V, Poletti B. Brain-Computer Interface for Clinical Purposes: Cognitive Assessment and Rehabilitation. Biomed Res Int. 2017; 2017: 1695290.

6. Luck SJ. An introduction to the event related potential technique. MIT Press, Cambridge, MA, 2014.

7. Farwell LA, Donchin E. Talking off the top of your head: toward a mental prosthesis utilizing event-related brain potentials. Electroencephalography and Clinical Neurophysiology. 1988; 70: 510–23.

8. Rezeika A, Benda M, Stawicki P, Gembler F, Saboor A, Volosyak I. Brain–Computer Interface Spellers: A Review. Brain Sciences. 2018; 8 (4): 57.

9. Zang S, Zhou C, Chao F. Estimation of Event-Related Potentials from Single-Trial EEG. UK Workshop on Computational Intelligence. Springer, Cham. 2021; 1409: 415–27.

10. Ouyang G, Hildebrandt A, Sommer W, Zhou C. Exploiting the intra-subject latency variability from single-trial event-related potentials in the P3 time range: A review and comparative evaluation of methods. Neurosci Biobehav Rev. 2017; 75: 1–21.

11. Burwell SJ, Makeig S, Iacono WG, Malone SM. Reduced premovement positivity during the stimulus-response interval precedes errors: Using single-trial and regression ERPs to understand performance deficits in ADHD. Psychophysiology. 2019; 56 (9): e13392.

12. Dowdall JR, Luczak A, Tata MS. Temporal variability of the N2pc during efficient and inefficient visual search. Neuropsychologia. 2012; 50 (10): 2442–53.

13. Kutas M, McCarthy G and Donchin E. Augmenting mental chronometry: the P300 as a measure of stimulus evaluation time. Science. 1977; 197 (4305): 792–5.

14. Zisk AH, Borgheai SB, McLinden J, Hosni SM, Deligani RJ, Shahriari Y. P300 latency jitter and its correlates in people with amyotrophic lateral sclerosis. Clinical Neurophysiology. 2021; 132 (2): 632–42.

15. Kim JS, Lee YJ, Shim SH. What Event-Related Potential Tells Us about Brain Function: Child-Adolescent Psychiatric Perspectives. Soa Chongsonyon Chongsin Uihak. 2021; 32 (3): 93–98.

16. Riggins T, Scott LS. P300 development from infancy to adolescence. Psychophysiology. 2020; 57 (7): e13346.

17. Thompson DE, Warschausky S, Huggins JE. Classifier-based latency estimation: a novel way to estimate and predict BCI accuracy. Journal of neural engineering. 2013; 10 (1): 016006.

18. Picton TW, Bentin S, Berg P, Donchin E, Hillyard SA, Johnson R, et al. Guidelines for using human event-related potentials to study cognition: recording standards and publication criteria. Psychophysiology. 2000; 37 (2): 127–52.

19. Dinstein I, Heeger DJ, Behrmann M. Neural variability: friend or foe? Trends Cogn Sci. 2015; 19 (6): 322–28.

20. Kovarski K, Malvy J, Khanna RK, Arsène S, Batty M, Latinus M. Reduced visual evoked potential amplitude in autism spectrum disorder, a variability effect? Translational Psychiatry. 2019; 9 (1): 1–9.

21. Gonen-Yaacovi G, Arazi A, Shahar N, Karmo A, Haar S, Meiran N, et al. Increased ongoing neural variability in ADHD. Cortex. 2016; 81: 50–63.

22. Zeba MZ, Friganović K, Palmović M, Išgum V, Cifrek M. Assessment of mental fatigue during examination period with P300 oddball paradigm. In 2019 42nd International Convention on Information and Communication Technology, Electronics and Microelectronics (MIPRO), IEEE. 2019: 1479–84.

23. McFarland DJ, Vaughan TM. BCI in practice. Progress in brain research. 2016; 228: 389–404.

24. Ганин И. П., Ким С. А., Либуркина С. П., Галкина Н. В., Лужин А. О.,

Майорова Л. А., et al. Набор текста пациентами с постинсультной афазией в комплексе «НейроЧат» на основе технологии интерфейсов мозг-компьютер на волне Р300. Журн. высш. нерв. деят. 2020; 70 (4): 435–45.

25. Shishkin SL, Ganin IP, Kaplan AY. Event-related potentials in a moving matrix modification of the P300 brain–computer interface paradigm. Neuroscience letters. 2011; 496 (2): 95–99.

26. Aricò P, Aloise F, Schettini F, Salinari S, Mattia D, Cincotti F. Influence of P300 latency jitter on event related potential-based brain–computer interface performance. Journal of neural engineering. 2014; 11 (3): 035008.

27. Schütz AC, Delipetkos E, Braun DI, Kerzel D, Gegenfurtner KR. Temporal contrast sensitivity during smooth pursuit eye movements. Journal of Vision. 2007; 7 (13): 3–3.

28. Zhang B, Stevenson SS, Cheng H, Laron M, Kumar G, Tong J, et al. Effects of fixation instability on multifocal VEP (mfVEP) responses in amblyopes. Journal of Vision. 2008; 8 (3): 16.

29. Aloise F, Aricò P, Schettini F, Riccio A, Salinari S, Mattia D, et al. A covert attention P300-based brain–computer interface: Geospell. Ergonomics. 2012; 55 (5): 538–51.

30. McCane LM, Sellers EW, McFarland DJ, Mak JN, Carmack CS, Zeitlin D, et al. Brain-computer interface (BCI) evaluation in people with amyotrophic lateral sclerosis. Amyotroph Lateral Scler Frontotemporal Degener. 2014; 15 (3–4): 207–15.

# ASSESSMENT OF OCULAR MANIFESTATION FREQUENCY AND QUALITY OF LIFE IN CHRONIC MYELOPROLIFERATIVE DISORDERS

Yunusova EM ✉, Mukhamadeev TR, Bakirov BA

Bashkir State Medical University, Ufa, Russia

Chronic myeloproliferative disorders (CMPD) include hemoblastoses with abnormal proliferation of myeloid lineages and concomitant alterations in the peripheral blood indicators. The aim of this study was to assess the frequency and structure of ophthalmic complications as a quality of life factor in patients with CMPD. A group of patients with hemoblastoses of this type ($n = 41$) were surveyed using National Eye Institute Visual Function Questionnaire-25 along with a comprehensive examination by noninvasive ophthalmological techniques. The patients typically reported impaired visual acuity, visual discomfort and foreign body sensation in the eyes. Though many of the patients assessed their general health and vision as satisfactory, the vast majority (68.3%) expressed serious concerns about their visual abilities. The ophthalmological examination revealed various defects including refractive errors (61%), corkscrew dilation and tortuosity of conjunctival and retinal vessels (77.9%), recurrent subconjunctival hemorrhages (39%) and dilated optic nerve sheaths (36.6%). The survey data indicate that visual impairments significantly affect quality of life in patients with CMPD. Overall, the results underscore the importance of interdisciplinary approach in the management of patients with CMPD to enable early diagnosis and feasible correction of the ophthalmic component.

**Keywords:** chronic myeloproliferative disorders, ocular manifestations, quality of life

✉ **Correspondence should be addressed:** Elvira M. Yunusova
Lenina, 3, 450008, Ufa, Russia; zainullina16@mail.ru

# ОЦЕНКА ЧАСТОТЫ ГЛАЗНЫХ ИЗМЕНЕНИЙ И КАЧЕСТВА ЖИЗНИ ПАЦИЕНТОВ ПРИ ХРОНИЧЕСКИХ МИЕЛОПРОЛИФЕРАТИВНЫХ ЗАБОЛЕВАНИЯХ

Э. М. Юнусова ✉, Т. Р. Мухамадеев, Б. А. Бакиров

Башкирский государственный медицинский университет, Уфа, Россия

К хроническим миелопролиферативным заболеваниям относят группу гемобластозов, характеризующуюся разрастанием миелоидных линий гемопоэза и изменением показателей периферической крови. Целью работы было оценить частоту офтальмологических нарушений и качество жизни вследствие изменений зрительных функций у пациентов с хроническими миелопролиферативными заболеваниями. Пациенты с данной группой гемобластозов ($n = 41$) для оценки качества жизни были проанкетированы при помощи специализированного медицинского опросника «National eye institute visual function questionnaire-25», обследованы стандартными и специальными неинвазивными методами. Большинство из них предъявляли жалобы на ухудшение зрения, дискомфорт, ощущение инородного тела в глазах. По данным анкетирования, многие больные оценивают свое общее состояние здоровья и зрения как удовлетворительное, подавляющая часть опрошенных (68,3%) испытывают беспокойство по поводу зрения. По результатам объективного офтальмологического обследования, у большинства пациентов выявлены различные виды патологий рефракции (61%), штопорообразное расширение и извитость сосудов конъюнктивы и сетчатки (77,9%), частые субконъюнктивальные кровоизлияния (39%), расширение периневрального пространства зрительных нервов (36,6%). При хронических миелопролиферативных заболеваниях ухудшается качество жизни пациентов, возможно поражение различных структур глаза. Крайне важен междисциплинарный подход к ведению таких больных с целью ранней диагностики и коррекции офтальмологических нарушений.

**Ключевые слова:** хронические миелопролиферативные заболевания, глазные проявления, качество жизни

✉ **Для корреспонденции:** Эльвира Маратовна Юнусова
ул. Ленина, д. 3, 450008, г. Уфа, Россия; zainullina16@mail.ru

Chronic myeloproliferative disorders (CMPD) result from defects of clonal proliferation of the bone marrow pluripotent stem cells leading to the excessively increased numbers of blood cells with sustained differentiation capacity [1]. The most common types of CMPD are chronic myeloid leukemia (CML), essential thrombocythemia (ET) and true polycythemia (TP). CMPD is known to confer multiple organ complications. The ophthalmic component in CMPD largely results from the abnormal hemodynamics and blood rheology that reflect the altered content of formed elements in peripheral blood due to the inhibition of normal hemopoiesis. Another important clinical factor in CMPD is the imbalance in blood coagulation and anticoagulation systems due to the release of coagulants by circulating blast cells [2]. The abnormal hemodynamics leads to increased vascular permeability, endothelial dysfunction and hypoperfusion of ocular tissues. An additional source of ophthalmic damage in CMPD is provided by anti-hemoblastosis drugs that may be oculotoxic per se. For instance, conjunctival hemorrhages, bilateral periorbital edema and dry eye syndrome have been described in patients receiving tyrosine kinase

inhibitors as a treatment for CML [3, 4]. In this study we aimed to assess the frequency and structure of ocular manifestations and their impact on quality of life in patients with CMPD.

## METHODS

A total of 41 patients with CMPD, 29 women (70.7%) and and 12 men (29.3%) aged $51 \pm 14$ years, participated in the study during the period from October 2020 to November 2021. The inclusion criteria were (1) age over 18 and (2) verified diagnosis of the CMPD spectrum. The exclusion criteria were (1) pregnancy or breastfeeding at the time of surveying/ examination and (2) verified diagnoses of diabetes mellitus and/ or arterial hypertension. The diagnostic structure of the cohort was as follows: 32 patients with CML (78%), five patients with ET (12.2%) and four patients with TP (9.8%). The disease length constituted $11 \pm 6$ years. In terms of treatment for CMPD, 32 patients received first- and second-generation tyrosine kinase inhibitors (78%), five patients received hydroxycarbamide (12.2%), three patients received interferon α-2b (7.3%) and one patient was newly diagnosed and received no specific treatment (2.4%).

It is widely recognized that visual impairments may negatively affect the general health status, as well as social functioning and quality of life. The medical term "quality of life" (QL) reflects the capability to engage in normal daily activities in spite of particular medical condition. The study used the self-report National Eye Institute Visual Function Questionnaire-25 (NEI VFQ-25) encompassing 25 questions and reflecting the general health status and various aspects of visual performance, with the scores structured in 12 subscales termed General Health, General Vision, Ocular Pain, Distance Vision, Near Vision, Peripheral Vision, Color Vision, Driving, Social Functioning, Mental Health, Role Difficulties and Dependency. The scores were calculated using the standard Likert scaling algorithm within the range from 0 (extremely poor) to 100 (perfectly normal). The control group included 30 volunteers without CMPD and matching by sex and age to the main group. The questionnaire scores were subject to descriptive statistical characterization; the distributions were assessed for normality using the Shapiro–Wilk test. Given the non-normality of distributions for the studied indicators, the comparisons used nonparametric Mann–Whitney test. The statistical analysis was carried out in the Microsoft Excel 2204 spreadsheet software (Microsoft Corporation; USA). The differences were considered significant at $p < 0.05$.

In addition to the survey, all patients underwent a standard ophthalmological examination including visometry, autorefractometry, tonometry, perimetry, biomicroscopy and ophthalmoscopy, as well as advanced non-invasive examinations including optical coherence tomography (OCT) of the macular area and optic nerve disc, OCT angiography of the macular area and optic nerve disc in an Avanti RTVue XR tomograph (Optovue; USA), fundus photography with a VISUCAM 524/224 fundus camera (Carl Zeiss; Germany) and ultrasound examination of the eyeball and orbital tissues by vascular dopplerography with a MySono U5 ultrasound system (Samsung-Medison; South Korea).

## RESULTS

Remarkably, 36 (88%) of the patients included in the study had never been comprehensively examined by an ophthalmologist. The prevalent ocular manifestations included impaired visual acuity (28 pts, 68.3%); visual discomfort and foreign body

sensation (12 pts, 29.3%); tearing (10 pts, 24.4%); dry eyes (8 pts, 19.5%); blurred vision (7 pts, 17%) and object shape distortion (2 pts, 4.9%). Upon surveying, patients with CMPD ($n = 41$) rated their vision as good (12 pts, 29.3%), satisfactory (20 pts, 48.8%) or poor (9 pts, 22%); at that, 26 pts (63.4%) rated their general health as satisfactory. The vast majority of the group (28 pts, 68.3%) "felt frustrated because of eyesight" i.e. experienced serious concerns about their visual abilities, 13 of them constantly (31.7%). Statistical processing of the data for different subscales of the questionnaire revealed significantly lower General Health, General Vision and Driving scores (respectively, $34.1 \pm 1.9$ vs. $50.9 \pm 3.8$, $p < 0.001$; $61.5 \pm 2.3$ vs. $77.2 \pm 2.8$, $p < 0.001$; and $47 \pm 12.7$ vs. $163 \pm 23.7$; $p < 0.001$) along with significantly higher Ocular Pain scores (respectively, $109.8 \pm 4.1$ vs. $95.9 \pm 3.5$; $p < 0.05$) in patients with CMPD compared with the control. Other subscales revealed no significant differences between patients with CMPD and the control group.

The physical eye examination revealed ophthalmological defects in 38 pts with CMPD (92.7%). Refractive errors were diagnosed in 25 pts (61%); these included myopia in 9 pts (36%), hyperopia in 6 pts (24%), presbiopia in 5 pts (20%)
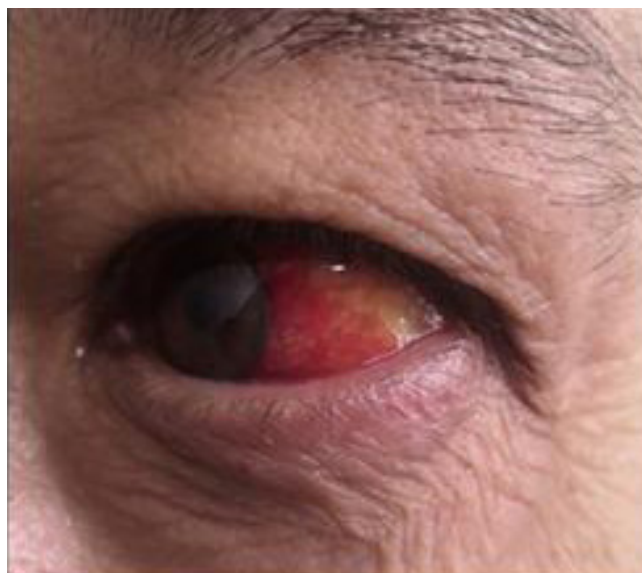


**Fig. 1.** Subconjunctival hemorrhage in male patient N. with CML



**Fig. 2.** Corkscrew dilation and tortuosity of conjunctival vessels in male patient A. with CML

and astigmatism in 5 pts (20%). Bilateral non-inflammatory periorbital edema and dry eye syndrome were diagnosed in 3 pts (7.3%) and 6 pts (14.6%), respectively. In addition, 10 pts (24.3%) manifested irregularity and corkscrew dilation of conjunctival vessels with intermittent blood flow. Other defects included recurrent subconjunctival hemorrhages in 16 pts (39%) and corkscrew dilation and tortuosity of retinal vessels in 22 pts (53.6%). Ultrasound scans of the eyeball and orbital tissues with vascular dopplerography revealed dilated perineural spaces of the optic nerves in 15 pts (36.6%) and reduced velocity of blood flow in ophthalmic arteries in 7 pts (17%). OCT of the macular area revealed serous detachment of the retinal neuroepithelium in 2 pts (4.9%). OCT angiography of the macular area revealed retinal neovascularization in 2 pts (4.9%). Primary open-angle glaucoma was diagnosed in 2 pts (4.9%); for one of them, our OCT examination of the optic disc identified this complication for the first time. Keratoconus, immature cataract, destruction of the vitreous body, lamellar macular hole, macular edema and ischemic optic nerve atrophy were represented by single cases (2.4% each) in the studied group of patients with CMPD.

DISCUSSION

QL in CMPD may progressively decline for multiple reasons linked in some manner with the main diagnosis, including the characteristic damage to eye structures. The estimated frequency of the ophthalmic component in hemoblastoses is 14–53 %. Its manifestations are subdivided into primary (direct leukemic infiltrations of the eye) and secondary (resulting from the altered rheological properties of the blood and the ongoing therapy) [5]. Direct involvement of the eyes is characteristic of acute leukemia [6]. Comparative studies on the incidence of ocular damage in acute and chronic hemopoietic malignancies are few and most of them argue that ocular manifestations are more common in acute than in chronic leukemia [7]. Thus, relative prevalence of leukemic ophthalmopathy constituted 68% for acute myeloid leukemia, 42% for acute lymphoid leukemia, 33% for chronic lymphoid leukemia and 13% for chronic myeloid leukemia, whereas such formidable complications as subhyaloid hemorrhage involving the posterior pole (20%) and vitreous hemorrhage (10%) were observed exclusively in patients with acute leukemia [8]. At the same time, a number of studies emphasize the high prevalence of ocular manifestations of variable severity in chronic leukemia [7].

A considerable number of our patients presented with recurrent spontaneous subconjunctival hemorrhages approximately every 2–3 months (Fig. 1). It should be noted that the hemorrhagic syndrome, which often provides the basis for other ocular manifestations in hemoblastoses, reflects the increased vascular permeability resulting from abnormal hemopoiesis. The higher incidence of ocular bleeding may also be a consequence of targeted therapies for CMPD [3].

The corkscrew-type lumina dilation and tortuosity of conjunctival and retinal vessels observed in most of the patients (Figs. 2 and 3) might result from the increased blood viscosity [9] confirmed by laboratory tests.

The blood hyperviscosity typical in patients with hematological malignancies may also lead to intracranial hypertension (ICH) as a consequence of the impaired drainage of cerebrospinal fluid into dural venous sinuses [10]. Dilation of the optic perineural space, considered a direct sign of ICH, was observed in ultrasound scans of the eyeball and orbital tissues with vascular dopplerography in more than one-third of the cases (Fig. 4). All patients exhibiting dilated optic nerve sheaths

underwent magnetic resonance imaging of the brain revealing signs of ICH without focal pathology in all cases.

Another possible consequence of the hemoblastosis-associated damage to microcirculation in ocular tissues is exudative (serous) detachment of the retinal neuroepithelium and secondary dysfunction of the retinal pigment epithelium (Fig. 5) [11]. The pathogenesis of such conditions has been related to partial occlusion of choriocapillaries and impaired choroidal hemoperfusion [12]. The resulting ischemic effect on the retina observed in myeloproliferative disorders may cause microaneurysms, arteriovenous anastomoses and pathological retinal neovascularization (Fig. 6) [13].

The identified ocular manifestations may eventually lead to critical visual impairments up to a complete loss of vision. Importantly, an ophthalmologist may be the first physician to suspect a proliferative blood disease based on the results of an eye examination and refer the patient to a hematologist in a timely manner. In turn, hematologists and therapists should be explicitly aware that hemoblastoses present with severe ocular manifestations. Therefore, it is pivotal to ensure an interdisciplinary framework in the management



**Fig. 3.** Corkscrew dilation and tortuosity of retinal vessels in male patient M. with CML
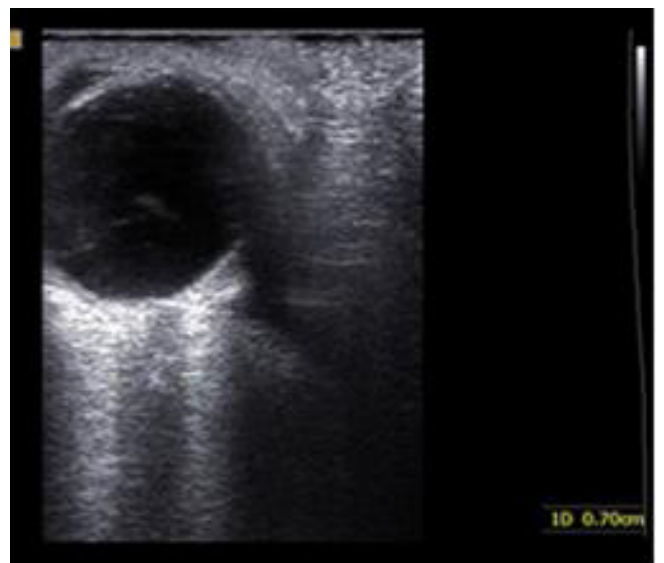


**Fig. 4.** Dilation of the optic perineural space in male patient M. (main diagnosis — CML; ultrasound scan of the eyeball and orbital tissues with vascular dopplerography)

of such patients, enabling joint participation of hematologists and ophthalmologists for the purpose of early diagnosis and treatment of the ophthalmic complications in CMPD.

Visual impairments, which most certainly affect daily routines and the ability to choose a desired lifestyle, are likely to affect psychological comfort and social adaptation of the patients thereby reducing QL. The beginning of this century was marked by a significant increase in the number of medical studies with a special focus on QL. The assessment is carried out to account for the treatment efficacy and the success of preventive and rehabilitation protocols, as well as to provide a means for personalized monitoring of the patient's condition. The NEI VFQ-25 questionnaire has been widely applied in patients with cataracts, glaucoma, retinopathy and age-related macular degeneration. QL assessment using this method provided a substantive contribution to a number of large studies. QL is severely impacted by visual impairments, with a consistent decrease in multiple subscale scores of the questionnaire [14, 15]. QL measurements in visually affected patients provide important indicators for the socio-psychological outcome in a wide spectrum of disorders including primary ocular conditions as well as chronic systemic disorders with ophthalmic component. The QL scores allow differential determination of the disease influence on the patient's condition with regard to both disease-related and disease-unrelated factors.

Our survey suggests that the decrease in QL values largely reflects the underlying chronic disease and ongoing drug therapy complemented by various ametropias and other ophthalmic disorders revealed by physical examination.

CONCLUSIONS

The data indicate that the vast majority of the patients with CMPD (92.7%) present with ophthalmic component which
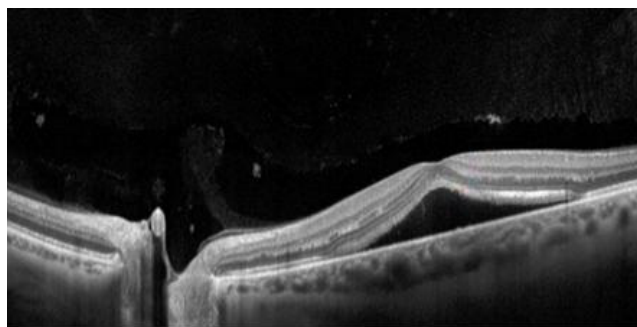


**Fig. 5.** Serous detachment of the retinal neuroepithelium in female patient S. (main diagnosis — TP; OCT of the macular area)
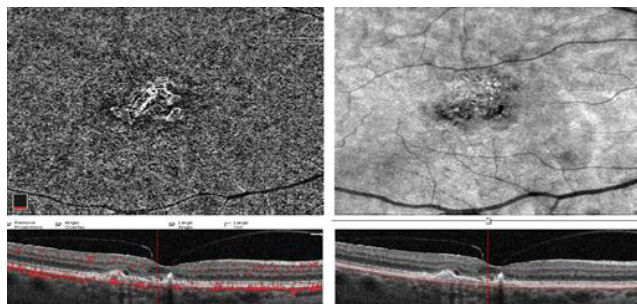


**Fig. 6.** Choroidal neovascular membrane in the macular area visualized in female patient T. (main diagnosis — CML; OCT angiography of the macular area)

significantly affects the life quality as indicated by the General Vision, Ocular Pain, General Health and Driving subscales of NEI VFQ-25. Though the study has fully achieved its goal in terms of primary characterizaton, the clinical picture of ocular manifestations that occur in CMPD and related hematological diseases is not finished. The origin of visual impairments in CMPD and their clinical dynamics require further dedicated analysis.

### References

1. Lacerda JF, Oliveira SN, Ferro JM. Chronic myeloproliferative diseases. Chronic myeloproliferative diseases. Handb Clin Neurol. 2014; 120: 1073–81. DOI: 10.1016/B978-0-7020-4087-0.00072-3.

2. Rumyanceva YuV, Karachunskij AI. Optimizaciya terapii ostrogo limfoblastnogo lejkoza u detej v Rossii i Belorussii. Voprosy gematologii/onkologii i immunopatologii v pediatrii. 2007; 6 (4): 13. Russian.

3. Breccia M, Gentilini F, Cannella L, Latagliata R, Carmosino I, Frustaci A, Alimena G. Ocular side effects in chronic myeloid leukemia patients treated with imatinib. Leuk Res. 2008; 32 (7): 1022–5. DOI: 10.1016/j.leukres. 2007.10.016.

4. Wahab A, Rafae A, Mushtaq K, asood A, Ehsan H, Khakwani M, Khan A. Ocular Toxicity of Belantamab Mafodotin, an Oncological Perspective of Management in Relapsed and Refractory Multiple Myeloma. Front Oncol. 2021; 11: 678634. DOI: 10.3389/fonc.2021.678634.

5. Rudneva LF, Ponomareva MN. Strategiya lecheniya glaz pri gemoblastozax. Medicinskaya nauka i obrazovanie Urala. 2019; 20 (2): 205–8. Russian.

6. Chistyakova NV, Shadrichev FE, Kuznecova TI. Sluchaj izolirovannogo vnutriglaznogo recidiva ostrogo limfoblastnogo lejkoza. Oftal'mologicheskie vedomosti. 2017; 10 (3): 74–84. Russian.

7. Dhasmana R, Prakash A, Gupta N, Verma SK. Ocular manifestations in leukemia and myeloproliferative disorders and their association with hematological parameters. Ann Afr Med. 2016; 15 (3): 97–103. DOI: 10.4103/1596-3519.188887.

8. Soman S, Kasturi N, Srinivasan R, Vinod KV. Ocular Manifestations in Leukemias and Their Correlation with Hematologic Parameters at a Tertiary Care Setting in South India. Ophthalmol. Retina. 2018; 2 (1): 17–23. DOI: 10.1016/j.oret.2017.05.009.

9. Grishina EE, Mamontov AO. Oftal'mologicheskie proyavleniya lejkoza. Al'manax klinicheskoj mediciny. 2016; 44 (5): 587–91. Russian.

10. Sharma PV, Ilyas O, Jobanputra Y, Casanova T, Kalidindi V, Santos N. Is it always cancer? A curious case of benign intracranial hypertension in chronic myeloid leukemia. Intractable Rare Dis. Res. 2018; 7 (3): 182–4. DOI: 10.5582/irdr.2018.01045.

11. Chinta S, Rani PK, Manusani U. Bilateral exudative retinal detachment as a presenting sign of acute lymphoblastic leukemia. Middle East Afr J. 2012; 19 (4): 410–2. DOI: 10.4103/0974-9233.102762.

12. Rudneva LF, Vasilkova TN, Petrov IM., Ponomareva MN. Gemoblastozy. Osobennosti porazheniya glaz. Tyumen': Konovalov IS, 2020; 90 s. Russian.

13. Mohamed SF, Qatami A, Nashwan A, Abdulla MA, Yassin MA. Ophthalmologic Manifestations as Initial Presentation of Patients with Chronic Myeloid Leukemia: Report of Two Cases. Case Rep Oncol. 2020; 13 (1): 7–11. DOI: 10.1159/000504928.

14. Igonina IA. Osnovnye metody ocenki kachestva zhizni oftal'mologicheskix bol'nyx. Smolenskij medicinskij al'manax. 2017; 1: 152–6. Russian.

15. Gabdrakhmanova AF, Kurbanov SA. Kliniko-funkcional'noe znachenie pokazatelej kachestva zhizni pri pervichnoj otkrytougol'noj glaukome. Nacional'nyj zhurnal glaukoma. 2015; 14 (4): 29–35. Russian.

### Литература

1. Lacerda JF, Oliveira SN, Ferro JM. Chronic myeloproliferative diseases. Chronic myeloproliferative diseases. Handb Clin Neurol. 2014; 120: 1073–81. DOI: 10.1016/B978-0-7020-4087-0.00072-3.
2. Румянцева Ю. В., Карачунский А. И. Оптимизация терапии острого лимфобластного лейкоза у детей в России и Белоруссии. Вопросы гематологии/онкологии и иммунопатологии в педиатрии. 2007; 6 (4): 13.
3. Breccia M, Gentilini F, Cannella L, Latagliata R, Carmosino I, Frustaci A, Alimena G. Ocular side effects in chronic myeloid leukemia patients treated with imatinib. Leuk Res. 2008; 32 (7): 1022–5. DOI: 10.1016/j.leukres. 2007.10.016.
4. Wahab A, Rafae A, Mushtaq K, asood A, Ehsan H, Khakwani M, Khan A. Ocular Toxicity of Belantamab Mafodotin, an Oncological Perspective of Management in Relapsed and Refractory Multiple Myeloma. Front Oncol. 2021; 11: 678634. DOI: 10.3389/fonc.2021.678634.
5. Руднева Л. Ф., Пономарева М. Н. Стратегия лечения глаз при гемобластозах. Медицинская наука и образование Урала. 2019; 20 (2): 205–8.
6. Чистякова Н. В., Шадричев Ф. Е., Кузнецова Т. И. Случай изолированного внутриглазного рецидива острого лимфобластного лейкоза. Офтальмологические ведомости. 2017; 10 (3): 74–84.
7. Dhasmana R, Prakash A, Gupta N, Verma SK. Ocular manifestations in leukemia and myeloproliferative disorders and their association with hematological parameters. Ann Afr Med. 2016; 15 (3): 97–103. DOI: 10.4103/1596-3519.188887.
8. Soman S, Kasturi N, Srinivasan R, Vinod KV. Ocular Manifestations in Leukemias and Their Correlation with Hematologic Parameters at a Tertiary Care Setting in South India. Ophthalmol. Retina. 2018; 2 (1): 17–23. DOI: 10.1016/j.oret.2017.05.009.
9. Гришина Е. Е., Мамонтов А. О. Офтальмологические проявления лейкоза. Альманах клинической медицины. 2016; 44 (5): 587–91.
10. Sharma PV, Ilyas O, Jobanputra Y, Casanova T, Kalidindi V, Santos N. Is it always cancer? A curious case of benign intracranial hypertension in chronic myeloid leukemia. Intractable Rare Dis. Res. 2018; 7 (3): 182–4. DOI: 10.5582/irdr.2018.01045.
11. Chinta S, Rani PK, Manusani U. Bilateral exudative retinal detachment as a presenting sign of acute lymphoblastic leukemia. Middle East Afr J. 2012; 19 (4): 410–2. DOI: 10.4103/0974-9233.102762.
12. Руднева Л. Ф., Василькова Т. Н., Петров И. М., Пономарева М. Н. Гемобластозы. Особенности поражения глаз. Тюмень: Коновалов И. С., 2020; 90 с.
13. Mohamed SF, Qatami A, Nashwan A, Abdulla MA, Yassin MA. Ophthalmologic Manifestations as Initial Presentation of Patients with Chronic Myeloid Leukemia: Report of Two Cases. Case Rep Oncol. 2020; 13 (1): 7–11. DOI: 10.1159/000504928.
14. Игонина И. А. Основные методы оценки качества жизни офтальмологических больных. Смоленский медицинский альманах. 2017; 1: 152–6.
15. Габдрахманова А. Ф., Курбанов С. А. Клинико-функциональное значение показателей качества жизни при первичной открытоугольной глаукоме. Национальный журнал глаукома. 2015; 14 (4): 29–35.

# ALLEVIATION OF NEUROLOGICAL AND COGNITIVE IMPAIRMENTS IN RAT MODEL OF ISCHEMIC STROKE BY 0.5 MAC XENON EXPOSURE

Krukov IA[1], Ershov AV[2,3], Cherpakov RA[2,4] ✉, Grebenchikov OA[2]

[1] Dmitry Rogachev National Medical Research Center of Pediatric Hematology, Oncology and Immunology, Moscow, Russia

[2] Negovsky Research Institute of General Reanimatology, Federal Research and Clinical Center of Intensive Care Medicine and Rehabilitology, Moscow, Russia

[3] Sechenov First Moscow State Medical University, Moscow, Russia

[4] Sklifosovsky Institute for Emergency Medicine, Moscow, Russia

The majority of stroke patients have cognitive symptoms and about 50% of them live with neurological deficits that critically limit social adaptation capacities even in the absence of significant motor impairments. The aim of this study was to select the optimal length of 0.5 MAC xenon exposure in order to alleviate the neurological and cognitive impairments in experimental stroke. The focal ischemia-reperfusion injury was modeled in rats ($n = 70$) ising Longa method. The intervention was immediately followed by inhalation of 0.5 MAC xenon for 30, 60 or 120 min. The neurological deficit was assessed using a 'Limb placement' seven-test battery and the cognitive functionalities were assessed by the Morris water maze test. A 30 min 0.5 MAC xenon exposure provided a 40% increase in the limb placement scores and a 17.6% decrease in the Morris water maze test latency compared with the control group ($p = 0.055$ and $p = 0.08$, respectively). With a longer 60 min exposure, the trends became significant, the scores improving 2-fold and by 44.4% compared with the control group ($p = 0.01$ and $p = 0.04$, respectively), whereas 120 min exposures afforded 2-fold improvements in both tests ($p = 0.01$). We conclude that, although 30 min post-stroke inhalations provide negligible benefits in terms of neurological status and learning capacity, prolonged exposure times of 60–120 min afford significant improvement in neurological and cognitive indicators and largely alleviate the deteriorating ischemic damage.

**Keywords:** xenon, stroke, neurological deficiency, cognitive impairment

# ВЫРАЖЕННОСТЬ КОГНИТИВНЫХ И НЕВРОЛОГИЧЕСКИХ НАРУШЕНИЙ У КРЫС ПОСЛЕ ИШЕМИЧЕСКОГО ИНСУЛЬТА НА ФОНЕ ПРИМЕНЕНИЯ КСЕНОНА 0,5 МАК

И. А. Крюков[1], А. В. Ершов[2,3], Р. А. Черпаков[2,4] ✉, О. А. Гребенчиков[2]

[1] Национальный медицинский исследовательский центр детской гематологии, онкологии и иммунологии имени Д. Рогачева, Москва, Россия

[2] Научно-исследовательский институт общей реаниматологии имени В. А. Неговского Федерального научно-клинического центра реаниматологии и реабилитологии, Москва, Россия

[3] Первый Московский государственный медицинский университет имени И. М. Сеченова (Сеченовский университет), Москва, Россия

[4] Научно-исследовательский институт скорой помощи имени Н. В. Склифосовского, Москва, Россия

У подавляющего числа пациентов, перенесших острое нарушение мозгового кровообращения, выявляются остаточные явления, из них у 50% — когнитивные нарушения, ограничивающие самообслуживание в быту, трудовую деятельность и социальную адаптацию в целом и приводящие к инвалидности даже при отсутствии значительных двигательных нарушений. Целью исследования было подобрать наиболее эффективную продолжительность ингаляции ксенона с 0,5 МАК (максимальной альвеолярной концентрацией) для снижения выраженности неврологических и когнитивных нарушений при экспериментальном инсульте. На 70 крысах смоделирована фокальная ишемия-реперфузия по методу Лонга с последующей ингаляцией ксенона 0,5 МАК в течение 30, 60 или 120 мин. Неврологический дефицит оценивали с помощью серии из семи тестов «Постановка конечности на опору», когнитивные функции — тестом «Водный лабиринт Морриса». Экспозиция ксенона 0,5 МАК в течение 30 мин приводила к росту числа баллов в тесте «Постановка конечности на опору» на 40% ($p = 0,055$) и уменьшению латентного времени в тесте «Водный лабиринт Морриса» на 17,6% ($p = 0,08$) по сравнению с контрольной группой, экспозиция в течение 60 мин — в 2 раза ($p = 0,01$) и на 44,4% ($p = 0,04$), в течение 120 мин — тоже в 2 раза ($p = 0,01$) в обоих тестах соответственно. Сделан вывод, что ингаляция ксенона 0,5 МАК при экспозиции 30 мин не приводит к значительному улучшению состояния животных и их способности к обучению, о чем свидетельствует отсутствие статистически значимых различий. Экспозиция же ксенона в течение 60 мин значительно уменьшает неврологический и когнитивный дефицит в группе исследования, а увеличение времени экспозиции ксенона до 120 мин оказывает сопоставимый эффект.

**Ключевые слова:** ксенон, инсульт, неврологический дефицит, когнитивные нарушения

According to the World Health Organization, about 1/3 of all diseases in developed countries are brain disorders, which are also the major cause of disability [1]. The contribution of brain disorders to the general structure of morbidity and invalidization is further boosted by the growing prevalence of neurodegenerative and cerebrovascular pathologies, as well as the increasing burden of risk factors: the incidence of diabetes mellitus, arterial hypertension, kidney pathology, environmental degradation, population ageing, car accidents and man-made disasters.

The leading place among the causes of disability is occupied by strokes. According to various sources, 40–60% of stroke patients become disabled and need medical and social support throughout their lives, which has a substantial social and economic impact [2, 3]. Moreover, stroke patients frequently present with cognitive impairments in the form of dementia, which dramatically undermines the quality of life for themselves and their families. Only 15% of the patients manage a return to their labor activities and daily routines, whereas 25% have pronounced dementia symptoms [4, 5].

The post-stroke cognitive impairments encompass the higher mental performance deficiencies that manifest and progress over the course of one year after the accident. The early post-stroke cognitive impairments evident within three months (the acute phase) are encountered in 70% of the patients. The manifestations can be focal (aphasia, apraxia) or generalized; the latter may include disorientation in time and space, absent-mindedness and inability to hold attention for a long time, difficulty in choosing words, increased forgetfulness, decreased ability to switch between different types of activity, deterioration of reasoning, difficulties in performing ordinary actions and impaired abstract thinking [2, 3, 6].

Brain damage from ischemic or hemorrhagic stroke, as well as from cardiac arrest or traumatic brain injury, initiates a cascade of pathophysiological reactions based on NMDA receptor-mediated excitotoxicity implicated in pathogenesis of diverse acute and chronic neurodegenerative conditions including Alzheimer's, Huntington's and Parkinson's diseases [7].

The inert gas xenon, which acts as antagonist of NMDA receptors located on the postsynaptic membrane of neurons and also expressed by glial cells, monocytes, macrophages and neutrophils [8, 9], has been used in psychiatry for over 15 years. NMDA-receptors, which participate in memorization, learning and pain perception, have been implicated in acute and chronic neurological conditions, mental disorders and neuropathic pain syndrome. These receptors also contribute to hyperactivation of neurons under the influence of excitatory amino acids and development of the addiction to psychoactive substances [10, 11]. Xenon is known to exert an anti-stress effect and reduce anxiety levels at sub-narcotic concentrations. The use of xenon in the treatment of borderline mental disorders leads to a reduction in psychopathological and somato-vegetative symptoms [12].

The post-stroke cognitive impairments are difficult to manage and even more so to treat, since they are multifactorial in nature and apart from the direct devastating ischemic damage may involve aggravation of cognitive deficits already in place before the acute episode. Neuroprotective therapies are highly relevant in both pathogenetic and symptomatic treatment of the post-stroke cognitive impairments [13, 14]; however, no unified theoretical basis for the use of neuroprotective drugs and other modalities is available so far, with the efficiencies being studied. In recent years, noble gases and xenon in particular receive increased attention due to accumulating evidence of their neuroprotective effects [15–20]. At the same time, no established protocols for modes and doses of xenon administration in different clinical situations are available, and the impact of xenon on the cognitive sphere and restoration of neurological status after stroke is largely obscure.

This study aimed at selecting the optimal length of 0.5 minimum alveolar concentration (0.5 MAC) xenon exposure to alleviate the neurological and cognitive impairments that arise in experimental ischemic stroke.

## METHODS

The experiments involved 70 male rats, 300–350 g body weight, purchased from breeding facilities (Krolinfo Ltd.; Russia). Before and after the intervention, the animals were housed under standard conditions with ad libitum access to food and water. Focal ischemia within the tree of the right middle cerebral artery was modeled as described by Longa et al. [21] in animals pre-anesthetized by intraperitoneal injection of 12% chloral hydrate solution at a dose of 300 mg/kg. The lethality constituted 14.3% (10 animals). Sham-operated animals ($n$ = 10) were subject to the same procedures (chloral hydrate anesthesia, surgical access) except the artery occlusion; the sham interventions were performed to account for the bias of narcosis and surgical manipulations. The interventions lasted 7–10 min on average; upon completion the animals were transferred to an air-tight chamber where they received either oxygen-air mix (30% oxygen, control groups) or 0.5 MAC xenon (70% xenon + 30% oxygen, main groups) for 30, 60 or 120 min. The neurological deficiency status was assessed on day 3 of the experiment: the motor functionalities of fore- and hind limbs contralateral to the affected hemisphere were checked by the 'Limb placement on a support' battery of seven tests performed using a 'Staircase test' setup (OpenScience; Russia) [22]. Completion of the task earned 2 points, completion with delay (more than 2 s) and/or partially earned 1 point and a failure to complete the task brought 0 points.

The preservation of cognitive functionalities including learning capacity and spatial memory was assessed by the Morris water maze test. The setup involved a circular pool 150 cm in diameter and 60 cm in height, half-filled with water, and containing a 28 cm high submerged platform in one of the sectors [23, 24]. The training was conducted on days 7–10 of the experiment; each animal was given four attempts, 120 s long and starting from different points, to find and memorize the location of the platform. The times of mounting the platform in each attempt were recorded. The tests were conducted on day 14 of the experiment: the animal was given 60 s to determine the location of the platform when starting from a new position and the latent period of entering the sector where the platform was located at the training stage was recorded. After completion of the tests the animals were withdrawn from the experiment by chloral hydrate overdose.

### Statistical analysis

Statistical processing of the data used Statistica 10.0 software (StatSoft Inc.; USA). The data are presented in the 'median (lower quartile; upper quartile)' Me (LQ; HQ) format. Between-the-group differences were assessed by Mann–Whitney U-test, the critical level of significance was $p < 0.05$.

## RESULTS

Sham-operated animals presented with zero neurological deficit and invariably got the highest scores (14 points) in the

**Table.** Alleviation of neurological and cognitive impairments by 0.5 MAC xenon exposure of varying time length, Me (LQ; HQ)

| Parameter | SO (n = 10) | Exposure time 30 min | | Exposure time 60 min | | Exposure time 120 min | |
|---|---|---|---|---|---|---|---|
| | | Control (n = 10) | Xenon (n = 10) | Control (n = 10) | Xenon (n = 10) | Control (n = 10) | Xenon (n = 10) |
| Neurological deficit, points | 14 | 5 (3; 7)^ | 7 (5; 10)^ | 6 (3; 8)^ | 12 (8;13)* | 6 (3; 7)^ | 12 (8;13)* |
| Latent period of finding the platform, s | 8 (7; 9) | 17 (14; 19)^ | 14 (8; 20)^ | 18 (15; 20)^ | 10 (5; 15)* | 18 (16; 20)^ | 9 (5; 13)* |

**Note:** SO — sham-operated animals; ^ — significant differences compared to sham-operated animals ($p < 0.05$; Mann–Whitney test); * — significant differences compared to the control group ($p < 0.05$; Mann–Whitney test).

'Limb placement' tests. The control group with 30 min exposure to air-oxygen mixture presented with apparent neurological deficit and 64.3% lower scores in the 'Limb placement' tests compared to sham-operated animals ($p = 0.005$). For 30 min 0.5 MAC xenon exposure, the scores were 40% higher compared to the control group ($p = 0.055$; Table), but 2-fold lower compared to sham-operated animals ($p = 0.0001$), indicating sustained neurological deficit.

The control group with 60 min exposure to air-oxygen mixture also presented with apparent neurological deficits. The total score in the 'Limb placement' tests for this group was 57.1% lower compared to sham-operated animals ($p = 0.004$). The animals exposed to 0.5 MAC xenon for 60 min scored 2-fold higher than the control group ($p = 0.01$) and only 14.3% lower than sham-operated animals ($p = 0.08$), thus showing minimal neurological changes. It should be noted that the total score obtained with 60 min exposure was 71.4% higher than corresponding value obtained with 30 min exposure ($p = 0.0002$), confirming the higher benefits of 60 min 0.5 MAC xenon inhalations compared to 30 min inhalations of the same composition.

The control group with 120 min exposure to air-oxygen mixture presented with neurological deficits very similar to those obtained with 60 min exposure to air-oxygen mixture, with the total scores 57.1% lower compared to sham-operated animals ($p = 0.004$). The animals exposed to 0.5 MAC xenon for 120 min scored 2-fold higher than the control group ($p = 0.01$) and only 14.3% lower than sham-operated animals ($p = 0.08$), which was identical to the corresponding results obtained with 60 min exposure.

In the Morris water maze test, the latent period of finding the platform by sham-operated animals was 8 (7; 9) s. For the control group with 30 min exposure to air-oxygen mixture the latent period was 2.1 times longer ($p = 0.007$), which indicates significant deterioration of learning and spatial recognition capacities in the aftermath of ischemic injury to the brain. For 30 min exposure to 0.5 MAC xenon, the latent period was 17.6% shorter compared to the control group ($p = 0.08$; Table), but 75% longer compared to sham-operated animals ($p = 0.001$).

For the control group with 60 min exposure to air-oxygen mixture the latent period was 2.25 times longer compared to sham-operated animals ($p = 0.006$). When using 60 min exposure to 0.5 MAC xenon, the latent period was reduced by 44.4% compared to the corresponding control group ($p = 0.04$) while being 25% longer compared to sham-operated animals ($p = 0.57$).

For the control group with 120 min exposure to air-oxygen mixture the latent period was also 2.25 times longer compared to sham-operated animals ($p = 0.005$). When using 120 min exposure to 0.5 MAC xenon, the latent period was reduced 2-fold compared to the corresponding control group ($p = 0.01$) while being only 12.5% longer compared to sham-operated animals ($p = 0.74$).

Taken together, the data demonstrate that modeling of cerebrovascular ischemic stroke in rats by the chosen method causes pronounced neurological and cognitive deficits. The 30 min 0.5 MAC xenon inhalations, applied as a rescue measure immediately post-intervention, provide negligible benefits in terms of neurological status and learning capacity, as demonstrated by the lack of statistical differences between the corresponding groups. Most notably, the prolongation of xenon exposure to 60–120 min largely alleviates the deteriorating ischemic damage as indicated by significant improvement in neurological and cognitive outcomes.

DISCUSSION

Two-thirds of the patients after acute cerebrovascular episodes present with residual effects often associated with primary disability. About 50% of them have cognitive impairments that limit self-help abilities, as well as participation in labor activities and social adaptation in general, even in the absence of significant motor impairments. With a reported 25% increase in the incidence of stroke among people of young and middle working age over the past 20 years, these figures are particularly appalling [1, 2]. The frequency of post-stroke dementia varies from 7.4 to 41.3%, according to different studies, and the condition tends to aggravate [2]. For instance, one study identifies cognitive impairments in 68% of patients in the acute phase of ischemic stroke (days 1–3), growing to 83% within 1 month follow-up, including 52% of moderate cognitive impairment and 30% of dementia cases [3]. Another study reveals cognitive impairments in 84% of the patients in a four years follow-up [25].

The problem of cognitive impairment in ischemic brain damage requires active multidisciplinary attitude fueling the quest for drugs and other modalities that will possibly reduce the rates of post-stroke disability. The use of xenon endowed with neurotrophic and neuroprotective properties as a component of such therapy is of particular interest. According to the published evidence, xenon has a positive psychotropic effect, which manifests itself in improving attention and intellectual performance, while also reducing anxiety and improving sleep [8, 26–29].

The use of subnarcotic doses of xenon in a course of 5–10 procedures contributed to the reduction of anxiety in patients with various forms of anxiety-phobic disorder without organic brain pathology [10]. A positive effect of oxygen-xenon mixture inhalations (5–10% Xe, 95–90% $O_2$) was demonstrated against the background of stabilization of systemic hemodynamic parameters in patients with Parkinson's disease and age-related cerebral atrophy [30].

Administration of the oxygen-xenon mixture (50% Xe, 50% $O_2$) inhalation courses to patients with acute encephalopathy against the background of alcohol, drug and mixed forms

of addiction promoted substantial reduction in severity of mental and somato-neurological manifestations. The patients reported reduced anxiety, better mood, vivacity, a need for communication and an expansion of active vocabulary. They also presented with enhanced memorization, improvement of short-term memory and attention switching indicators, faster rates of thinking and better self-help skills. Thus, xenon therapy outdid standard regimens in terms of both psychosomatic correction and cognitive and intellectual improvement [31].

Still, no unified method for the use of xenon under various pathological conditions is available. In experimental settings, the agent can be delivered in the form of xenon liposomes [32]. The authors demonstrate a positive effect of intravenous infusions of such liposomes in the aftermath of focal cerebral ischemia in rat model: alleviation of neurological deficit as measured by forelimb placement tests on days 3 and 5, as well as increased swimming time compared to animals with modeled stroke unaccompanied by xenon therapy (interpreted as reduced depressiveness). The majority of studies use xenon in the form of inhalations of varying length. A neuroprotective effect of xenon inhaled as a mixture of 50% xenon, 25% argon and 25% oxygen for 6 h or 3 h was demonstrated in rodent models of traumatic brain injury [33, 34]. Similarly, inhalations of 70% xenon for 1 h or 5 h improved cognitive and neurological indicators by days 1–3 in pig model of cardiac arrest followed by cardiopulmonary resuscitation [35]. Inhalations of 70% xenon reduced the total infarction volume and improve the 24 h neurological outcomes after transient focal cerebral ischemia in mice as compared with 70% nitrogen, whereas the effect of 35% xenon was intermediate [36]. We considered it important

to study the effects of subanesthetic doses of xenon (0.5 MAC) at short exposures on the severity of neurological disorders and cognitive functions in experimental ischemic brain damage modeled by occlusion of the middle cerebral artery; to the best of our knowledge, no such experiments have been published so far. Incidentally, the use of 0.5 MAC xenon allows combining the treatment with oxygen supplementation often required in patients with acute ischemic brain injury. The inhalations were started immediately after modeling the middle cerebral artery stroke and lasted a relatively short time (30, 60 and 120 min) in spontaneously breathing animals, simulating a scenario in which the emergency treatment is started by a visiting medical team to be continued in a hospital setting.

CONCLUSIONS

The experimental use of 30 min 0.5 MAC xenon inhalations provided no significant improvement of neurological status and learning capacity of animals i.e. showed negligible therapeutic efficiency. The prolongation of exposure to 60 min provided significant alleviation of the neurological and cognitive deficits during the recovery as indicated by significant increase in the relevant behavioral test scores (2-fold on average), whereas 120 min inhalations had a comparable effect. Thus, 1–2-hour xenon inhalations represent a promising therapeutic option when administered on the 'as soon as possible' basis after cerebrovascular accident. Alleviation and correction of the neurological and cognitive sequelae of ischemic brain injury by this method requires further clinical evaluation.

### References

1. Bejot Y, Bailly H, Durier J, Giroud M. Epidemiology of stroke in Europe and trends for the 21st century. Presse Medicale. 2016; 45 (12): 391–8. DOI: 10.1016/j.lpm.2016.10.003.

2. Preobrazhenskaya IS. Kognitivnye narusheniya posle insul'ta: rasprostranennost', prichiny i podxody k terapii. Ehffektivnaya farmakoterapiya. 2013; 45: 50–57. Russian.

3. Parfenov VA, Verbickaya SV. Postinsul'tnye kognitivnye narusheniya. Medicinskij sovet. 2018; 18: 11–15. DOI: 10.21518/2079-701X-2018-18-10-15. Russian.

4. Piradov MA, Krylov VV, Belkin AA, Petrikov SS. Insulty. V knige: Gelfand BR, Zabolotskij IB, redaktory. Intensivnaya terapiya. Nacional'noe rukovodstvo. 2-e izd., Moskva: GEhO-TAR-Media, 2017; c. 288–309. Russian.

5. Shevchenko EV, Ramazanov GR, Petrikov SS. Prichiny golovokruzheniya u bol'nyx s podozreniem na ostroe narushenie mozgovogo krovoobrashheniya. Zhurnal im. N. V. Sklifosovskogo «Neotlozhnaya medicinskaya pomoshh'». 2018; 7 (3): 217–21. Russian.

6. Douglas-Escobar M, Weiss MD. Hypoxic-ischemic encephalopathy: a review for the clinician. JAMA Pediatr. 2015;169 (4): 397–403. DOI: 10.1001/jamapediatrics.2014.3269. PMID: 25685948.

7. Wong TP, Howland JG, Wang YT. NMDA Receptors and Disease+C464. Encyclopedia of Neuroscience. 2009: 1177–82. DOI: 10.1016/b978-008045046-9.01223-7.

8. Bubeev YuA, Kotrovskaya TI, Kalmanov AS. Ksenon-kislorodnaya gazovaya ingalyaciya dlya korrekcii negativnyx posledstvij stressa. V sb.: Ksenon i inertnye gazy v medicine: Materialy konferencii anesteziologov-reanimatologov medicinskix uchrezhdenij MO RF. M.: GVKG im. N. N. Burdenko, 2008; c. 4–9. Russian.

9. Goto T. Xenon anesthesia — results from human studies. Applied Cardiopulmonary Pathophysiology. 2000; 9: 129–31. Available from: https: //academic.naver.com/article.naver?doc_id=194615041.

10. Gerasimova YuYu, Ermakova MA. Nejroprotektivnye ehffekty subnarkoticheskix i narkoticheskix koncentracij medicinskogo ksenona. Vestnik soveta molodyx uchenyx i specialistov chelyabinskoj oblasti. 2017; 3 (18). Dostupno po ssylke: https://www.elibrary.ru/download/elibrary_30672509_99990060.pdf. Russian.

11. Burov NE, Makeev GN, Potapov VN. Applying xenon technologies in Russia. Applied Cardiopulmonary Pathophysiology. 2000; 9: 132–3. Available from: https://www.researchgate.net/publication/297793098_Applying_xenon_technologies_in_Russian.

12. de Sousa SL, Dickinson R, Lieb WR, Franks NP. Contrasting synaptic actions of the inhalational general anesthetics isoflurane and xenon. Anesthesiology. 2000; 92 (4): 1055–66. DOI: 10.1097/00000542-200004000-00024. PMID: 10754626.

13. Kuzovlev AN, Shpichko AI, Ryzhkov IA, Grebenchikov OA, Shabanov AK, Xusainov ShZh, Cokolaeva ZI, Lobanov AV. Vliyanie ksenona na fosforilirovanie kinazy glikogensintazy-3ß i antioksidantnye fermenty v mozge krys. Zhurnal im. N. V. Sklifosovskogo «Neotlozhnaya medicinskaya pomoshh'». 2020; 9 (4): 564–572. DOI: 10.23934/2223-9022-2020-9-4-564-572. Russan.

14. Grebenchikov OA, Molchanov IV, Shpichko AI, Evseev AK, Shabanov AK, Xusainov ShZh, Petrikov SS. Nejroprotektivnye svojstva ksenona po dannym ehksperimental'nyx issledovanij. Zhurnal im. N. V. Sklifosovskogo «Neotlozhnaya medicinskaya pomoshh'». 2020; 9 (1): 85–95. DOI: 10.23934/2223-9022-2020-9-1-85-95. Russan.

15. Zhang J, Liu W, Bi M, Xu J, Yang H, Zhang Y. Noble gases therapy in cardiocerebrovascular diseases: the novel stars? Front Cardiovasc Med. 2022; 9: 802783. DOI: 10.3389/fcvm.2022.802783.

16. Tetorou K, Sisa C, Iqbal A, Dhillon K, Hristova M. Current Therapies for Neonatal Hypoxic–Ischaemic and Infection-Sensitised Hypoxic–Ischaemic Brain Damage. Front Synaptic

Neurosci. 2021; 13: 709301. DOI: 10.3389/fnsyn.2021.709301.

17. Zhao C-S, Li H, Wan Z, Chen G. Potential application value of xenon in stroke treatment. Med Gas Res. 2018; 8 (3): 116–20. DOI: 10.4103/ 2045-9912.241077.

18. Roehl A, Rolf R, Mark C. Update of the organoprotective properties of xenon and argon: from bench to beside. ICMx. 2020; 11. DOI: 10.1186/s40635-020-0294-6.

19. Koziakova M, Harris K, Edge CJ, Franks NP, White IL, Dickinson R. Noble gas neuroprotection: xenon and argon protect against hypoxic-ischaemic injury in rat hippocampus in vitro via distinct mechanisms. Br J Anaesth. 2019; 123 (5): 601–9. DOI: 10.1016/j.bja.2019.07.010.

20. Maze, M, Laitio T. Neuroprotective Properties of Xenon. Mol Neurobiol. 2020; 57: 118–24. DOI: 10.1007/s12035-019-01761-z.

21. Longa EZ, Weinstein PR, Carlson S, Cummins R. Reversible middle cerebral artery occlusion without craniectomy in rats. Stroke. 1989; 20 (1): 84–91. DOI: 10.1161/01.str.20.1.84.

22. Silachyov DN, Shubina MI, Yankauskas SS, Mkrtchyan VP, Manskix VN, Gulyaev MV, Zorov DB. Ocenka sensomotornogo deficita v otdalennom periode posle ishemii/gipoksii golovnogo mozga neonatal'nyx krys. Zhurnal vysshej nervnoj deyatel'nosti. 2013; 63 (3): 405–16. DOI: 10.7868/S0044467713030131. Russian.

23. Iptyshev AM, Gorina YaV, Lopatina OL, Komleva YuK, Chernyx AI, Belova OA, et al. Sravnenie testov «Vos'mirukavnyj radial'nyj labirint» i «Vodnyj labirint Morrisa» pri ocenke prostranstvennoj pamyati u ehksperimental'nyx zhivotnyx v xode nejropovedencheskogo testirovaniya. Fundamental'naya i klinicheskaya medicina. 2017; 2 (2): 62–69. DOI: 10.23946/2500-0764-2017-2-2-62-69. Russian. 2017; 2 (2): 62–69. DOI: 10.23946/2500-0764-2017-2-2-62-69.

24. Notova SV, Kazakova TV, Marshinskaya OV. Sovremennye metody i oborudovanie dlya ocenki povedeniya laboratornyx zhivotnyx. Zhivotnovodstvo i kormoproizvodstvo. 2018; 101 (1): 106–15. Russian.

25. Mahon S, Parmar P, Barker-Collo S. Determinants, prevalence, and trajectory of long-term post-stroke cognitive impairment. Results from a 4-year follow-up of the ARCOS-IV study. Neuroepidemiology. 2017; 49 (3–4): 129–34. DOI: 10.1159/000484606 PMID: 29145207.

26. Vasilev SV, Vladimirov SA. Vozmozhnosti klinicheskogo ispol'zovaniya subnarkoticheskix doz ksenona. Journal of Siberian Medical Sciences. 2012; 6. Dostupno po ssylke: https://docplayer.com/68328413-Vozmozhnosti-klinicheskogo-ispolzovaniya-subnarkoticheskih-doz-ksenona.html. Russan.

27. Igoshina TV. Korrekciya svyazannyx so stressom nevroticheskix rasstrojstv metodom ingalyacii subnarkoticheskix doz ksenona v usloviyax sanatoriya. Kremlevskaya medicina. 2013; 4: 37–42. http://kremlin-medicine.ru/index.php/km/article/view/10/9. Russian.

28. Bogomolov IS, Pavlova RA, Fedorov SS, Xabibulin RF. Vliyanie ksenona na kognitivnuyu sferu terapevticheskix pacientov s soputstvuyushhej ehncefalopatiej razlichnogo geneza. Materialy tret'ej konferencii. 2012; s. 107–12. Russian.

29. Kornetov NA, Shpisman MN, Naumov SA. Primenenie lechebnogo ksenonovogo narkoza v kompleksnoj terapii abstinentnogo sindroma pri opiatnoj narkomanii. M.: Medicina, 2001. Russan.

30. Perov AYu, Ovchinnikov BM. Vnedrenie v shirokuyu medicinskuyu praktiku texnologii lecheniya smesyami blagorodnyx gazov s kislorodom. Birzha intellektual'noj sobstvennosti. 2010; 9 (5): 35–36. Russian.

31. Davletov LA. Primenenie ksenona v kompleksnoj terapii psixicheskix i somatonevrologicheskix rasstrojstv v strukture ostroj ehncefalopatii u pacientov s zavisimost'yu ot psixoaktivnyx veshhestv: dissertaciya na zvanie kand. med. nauk. Moskva, 2007: 27. Russian.

32. Dandekar MP, Yin X, Peng T, Devaraj S, Morales R, McPherson D, et al. Repetitive xenon treatment improves post-stroke sensorimotor and neuropsychiatric dysfunction Journal of Affective Disorders 2022; 301: 315–30. DOI: 10.1016/j.jad.2022.01.025.

33. Campos-Pires R, Hirnet T, Valeo F, Ong BE, Radyushkin K, Aldhoun J, et al. Xenon improves long-term cognitive function, reduces neuronal loss and chronic neuroinflammation, and improves survival after traumatic brain injury in mice. Br J Anaesth. 2019; 123 (1): 60–73. DOI: 10.1016/j.bja.2019.02.032.

34. Campos-Pires R, Ongradito H, Ujvari E, Karimi S, Valeo F, Aldhoun J, et al. Xenon treatment after severe traumatic brain injury improves locomotor outcome, reduces acute neuronal loss and enhances early beneficial neuroinflammation: a randomized, blinded, controlled animal study. Crit Care. 2020; 24 (1): 667. DOI: 10.1186/ s13054-020-03373-9.

35. Fries M, Nolte KW, Coburn M, Rex S, Timper A, Kottmann K, et al. Xenon reduces neurohistopathological damage and improves the early neurological deficit after cardiac arrest in pigs. Crit Care Med. 2008; 36: 2420–6. DOI: 10.1097 /CCM.0b013e3181802874.

36. Homi HM, Yokoo N, Ma D, Warner DS, Franks NP, Maze M, et al. The neuroprotective effect of xenon administration during transient middle cerebral artery occlusion in mice. Anesthesiology. 2003; 99 (4): 876–81. DOI: 10.1097/00000542-200310000-00020.

## Литература

1. Bejot Y, Bailly H, Durier J, Giroud M. Epidemiology of stroke in Europe and trends for the 21st century. Presse Medicale. 2016; 45 (12): 391–8. DOI: 10.1016/j.lpm.2016.10.003.

2. Преображенская И. С. Когнитивные нарушения после инсульта: распространенность, причины и подходы к терапии. Эффективная фармакотерапия. 2013; 45: 50–57.

3. Парфенов В. А., Вербицкая С. В. Постинсультные когнитивные нарушения. Медицинский совет. 2018; 18: 11–15. DOI: 10.21518/2079-701X-2018-18-10-15.

4. Пирадов М. А., Крылов В. В., Белкин А. А., Петриков С. С. Инсульты. В книге: Гельфанд Б. Р., Заболотский И. Б., редакторы. Интенсивная терапия. Национальное руководство. 2-е изд., Москва: ГЭО-ТАР-Медиа, 2017; с. 288–309.

5. Шевченко Е. В., Рамазанов Г. Р., Петриков С. С. Причины головокружения у больных с подозрением на острое нарушение мозгового кровообращения. Журнал им. Н. В. Склифосовского «Неотложная медицинская помощь». 2018; 7 (3): 217–21. DOI: 10.23934/2223-9022-2018-7-3-217-221.

6. Douglas-Escobar M, Weiss MD. Hypoxic-ischemic encephalopathy: a review for the clinician. JAMA Pediatr. 2015;169 (4): 397–403. DOI: 10.1001/jamapediatrics.2014.3269. PMID: 25685948.

7. Wong TP, Howland JG, Wang YT. NMDA Receptors and Disease+C464. Encyclopedia of Neuroscience. 2009: 1177–82. DOI: 10.1016/b978-008045046-9.01223-7.

8. Бубеев Ю. А., Котровская Т. И., Кальманов А. С. Ксенон-кислородная газовая ингаляция для коррекции негативных последствий стресса. В сб.: Ксенон и инертные газы в медицине: Материалы конференции анестезиологов-реаниматологов медицинских учреждений МО РФ. М.: ГВКГ им. Н. Н. Бурденко, 2008; с. 4–9.

9. Goto T. Xenon anesthesia — results from human studies. Applied Cardiopulmonary Pathophysiology. 2000; 9: 129–31. Available from: https: //academic.naver.com/article.naver?doc_id=194615041.

10. Герасимова Ю. Ю., Ермакова М. А. Нейропротективные эффекты субнаркотических и наркотических концентраций медицинского ксенона. Вестник совета молодых ученых и специалистов челябинской области. 2017; 3 (18). Доступно по ссылке: https://www.elibrary.ru/download/elibrary_30672509_99990060.pdf.

11. Burov NE, Makeev GN, Potapov VN. Applying xenon technologies in Russia. Applied Cardiopulmonary Pathophysiology. 2000; 9: 132–3. Available from: https://www.researchgate.net/publication/297793098_Applying_xenon_technologies_in_Russia.

12. de Sousa SL, Dickinson R, Lieb WR, Franks NP. Contrasting synaptic actions of the inhalational general anesthetics isoflurane and xenon. Anesthesiology. 2000; 92 (4): 1055–66. DOI: 10.1097/00000542-200004000-00024. PMID: 10754626.

13. Кузовлев А. Н., Шпичко А. И., Рыжков И. А., Гребенчиков О. А.,

Шабанов А. К., Хусаинов Ш. Ж., Цоколаева З. И., Лобанов А. В. Влияние ксенона на фосфорилирование киназы гликогенсинтазы-3ß и антиоксидантные ферменты в мозге крыс. Журнал им. Н. В. Склифосовского «Неотложная медицинская помощь». 2020; 9 (4): 564–572. DOI: 10.23934/2223-9022-2020-9-4-564-572.

14. Гребенчиков О. А., Молчанов И. В., Шпичко А. И., Евсеев А. К., Шабанов А. К., Хусаинов Ш. Ж., Петриков С. С. Нейропротективные свойства ксенона по данным экспериментальных исследований. Журнал им. Н. В. Склифосовского «Неотложная медицинская помощь». 2020; 9 (1): 85–95. DOI: 10.23934/2223-9022-2020-9-1-85-95.

15. Zhang J, Liu W, Bi M, Xu J, Yang H, Zhang Y. Noble gases therapy in cardiocerebrovascular diseases: the novel stars? Front Cardiovasc Med. 2022; 9: 802783. DOI: 10.3389/fcvm.2022.802783.

16. Tetorou K, Sisa C, Iqbal A, Dhillon K, Hristova M. Current Therapies for Neonatal Hypoxic–Ischaemic and Infection-Sensitised Hypoxic–Ischaemic Brain Damage. Front Synaptic Neurosci. 2021; 13: 709301. DOI: 10.3389/fnsyn.2021.709301.

17. Zhao C-S, Li H, Wan Z, Chen G. Potential application value of xenon in stroke treatment. Med Gas Res. 2018; 8 (3): 116–20. DOI: 10.4103/ 2045-9912.241077.

18. Roehl A, Rolf R, Mark C. Update of the organoprotective properties of xenon and argon: from bench to beside. ICMx. 2020; 11. DOI: 10.1186/s40635-020-0294-6.

19. Koziakova M, Harris K, Edge CJ, Franks NP, White IL, Dickinson R. Noble gas neuroprotection: xenon and argon protect against hypoxic-ischaemic injury in rat hippocampus in vitro via distinct mechanisms. Br J Anaesth. 2019; 123 (5): 601–9. DOI: 10.1016/j.bja.2019.07.010.

20. Maze M, Laitio T. Neuroprotective Properties of Xenon. Mol Neurobiol. 2020; 57: 118–24. DOI: 10.1007/s12035-019-01761-z.

21. Longa EZ, Weinstein PR, Carlson S, Cummins R. Reversible middle cerebral artery occlusion without craniectomy in rats. Stroke. 1989; 20 (1): 84–91. DOI: 10.1161/01.str.20.1.84.

22. Силачёв Д. Н., Шубина М. И., Янкаускас С. С., Мкртчян В. П., Манских В. Н., Гуляев М. В., Зоров Д. Б. Оценка сенсомоторного дефицита в отдаленном периоде после ишемии/гипоксии головного мозга неонатальных крыс. Журнал высшей нервной деятельности. 2013; 63 (3): 405–16. DOI: 10.7868/S0044467713030131.

23. Иптышев А. М., Горина Я. В., Лопатина О. Л., Комлева Ю. К., Черных А. И., Белова О. А., Салмина А. Б. Сравнение тестов «Восьмирукавный радиальный лабиринт» и «Водный лабиринт Морриса» при оценке пространственной памяти у экспериментальных животных в ходе нейроповеденческого тестирования. Фундаментальная и клиническая медицина. 2017; 2 (2): 62–69. DOI: 10.23946/2500-0764-2017-2-2-62-69.

24. Нотова С. В., Казакова Т. В., Маршинская О. В. Современные методы и оборудование для оценки поведения лабораторных животных. Животноводство и кормопроизводство. 2018; 101 (1): 106–15.

25. Mahon S, Parmar P, Barker-Collo S. Determinants, prevalence, and trajectory of long-term post-stroke cognitive impairment. Results from a 4-year follow-up of the ARCOS-IV study. Neuroepidemiology. 2017; 49 (3–4): 129–34. DOI: 10.1159/000484606 PMID: 29145207.

26. Васильев С. В., Владимиров С. А. Возможности клинического использования субнаркотических доз ксенона. Journal of Siberian Medical Sciences. 2012; 6. Доступно по ссылке: https: //docplayer.com/68328413-Vozmozhnosti-klinicheskogo-ispolzovaniya-subnarkoticeskih-doz-ksenona.html.

27. Игошина Т. В. Коррекция связанных со стрессом невротических расстройств методом ингаляции субнаркотических доз ксенона в условиях санатория. Кремлевская медицина. 2013; 4: 37–42. http://kremlin-medicine.ru/index.php/km/article/view/10/9

28. Богомолов И. С., Павлова Р. А., Федоров С. С., Хабибулин Р. Ф. Влияние ксенона на когнитивную сферу терапевтических пациентов с сопутствующей энцефалопатией различного генеза. Материалы третьей конференции. 2012; с. 107–12.

29. Корнетов Н. А., Шписман М. Н., Наумов С. А. Применение лечебного ксенонового наркоза в комплексной терапии абстинентного синдрома при опиатной наркомании. М.: Медицина, 2001.

30. Перов А. Ю., Овчинников Б. М. Внедрение в широкую медицинскую практику технологии лечения смесями благородных газов с кислородом. Биржа интеллектуальной собственности. 2010; 9 (5): 35–36.

31. Давлетов Л. А. Применение ксенона в комплексной терапии психических и соматоневрологических расстройств в структуре острой энцефалопатии у пациентов с зависимостью от психоактивных веществ: диссертация на звание канд. мед. наук. Москва, 2007: 27.

32. Dandekar MP, Yin X, Peng T, Devaraj S, Morales R, McPherson D, et al. Repetitive xenon treatment improves post-stroke sensorimotor and neuropsychiatric dysfunction Journal of Affective Disorders 2022; 301: 315–30. DOI: 10.1016/j.jad.2022.01.025.

33. Campos-Pires R, Hirnet T, Valeo F, Ong BE, Radyushkin K, Aldhoun J, et al. Xenon improves long-term cognitive function, reduces neuronal loss and chronic neuroinflammation, and improves survival after traumatic brain injury in mice. Br J Anaesth. 2019; 123 (1): 60–73. DOI: 10.1016/j.bja.2019.02.032.

34. Campos-Pires R, Ongradito H, Ujvari E, Karimi S, Valeo F, Aldhoun J, et al. Xenon treatment after severe traumatic brain injury improves locomotor outcome, reduces acute neuronal loss and enhances early beneficial neuroinflammation: a randomized, blinded, controlled animal study. Crit Care. 2020; 24 (1): 667. DOI: 10.1186/ s13054-020-03373-9.

35. Fries M, Nolte KW, Coburn M, Rex S, Timper A, Kottmann K, et al. Xenon reduces neurohistopathological damage and improves the early neurological deficit after cardiac arrest in pigs. Crit Care Med. 2008; 36: 2420–6. DOI: 10.1097 /CCM.0b013e3181802874.

36. Homi HM, Yokoo N, Ma D, Warner DS, Franks NP, Maze M, et al. The neuroprotective effect of xenon administration during transient middle cerebral artery occlusion in mice. Anesthesiology. 2003; 99 (4): 876–81. DOI: 10.1097/00000542-200310000-00020.